

Durham E-Theses

N-Phosphino-pyridyl Imines: Flexible, Multi-functional Reagents

SMITH, DAN,ANDREW

How to cite:

SMITH, DAN,ANDREW (2009) *N-Phosphino-pyridyl Imines: Flexible, Multi-functional Reagents*, Durham theses, Durham University. Available at Durham E-Theses Online:
<http://etheses.dur.ac.uk/42/>

Use policy

The full-text may be used and/or reproduced, and given to third parties in any format or medium, without prior permission or charge, for personal research or study, educational, or not-for-profit purposes provided that:

- a full bibliographic reference is made to the original source
- a [link](#) is made to the metadata record in Durham E-Theses
- the full-text is not changed in any way

The full-text must not be sold in any format or medium without the formal permission of the copyright holders.

Please consult the [full Durham E-Theses policy](#) for further details.



*N-Phosphino-pyridyl Imines: Flexible,
Multi-functional Reagents*

Thesis submitted for the Degree of Doctor of
Philosophy

By

Daniel A. Smith, M.Chem. (Durham)

In the Department of Chemistry
Durham University

October 2009

Abstract

Chapter I includes a summary of the chemistry of phosphines and bidentate phosphorus-nitrogen ligands of relevance to this thesis, and highlights their application in transition metal-based catalysis. In addition, a review of the characteristic properties and reactivity of iminophosphanes and phosphonium cations is presented in preparation for work outlined later in this manuscript.

The synthesis and coordination studies of a range of *N*-phosphino-pyridyl imines with the general structure $(C_5H_5N)(Ar)C=NPR_2$ (**1**) {R = alkyl or aryl and Ar = aryl} are reported in chapter II. The molecular structures of their palladium dichloride complexes are presented, highlighting the effect of differing substituents on framework **1** upon the geometry of the complexes.

The chemistry surrounding a novel equilibrium between two valence tautomers prepared from reaction of *N*-lithio pyridyl imine with bis(diisopropylamino)chlorophosphine is presented in chapters III and IV. The tautomers 1,1-bis(diisopropylamino)-3-phenyl- $1\lambda^5$ -[1,3,2]diazaphospholo [1,5-*a*]pyridine (**2c**) and bis(diisopropylamino)phosphino(phenyl-pyridin-2-yl methylene)amine (**2o**) exist in a ratio of 95 : 5, respectively, at ambient temperature. Investigations of the thermodynamic properties, the rate of interconversion and the possible mechanistic pathways of interconversion for **2o/2c** have been conducted. The synthesis and characterisation of another equilibrium mixture, that of the tautomers 1,1-bis(diisopropylamino)-3-anthracenyl- $1\lambda^5$ -[1,3,2]diazaphospholo [1,5-*a*]pyridine (**3c**) and bis(diisopropylamino)phosphino(anthracenyl-pyridin-2-yl methylene)amine (**3o**), which exist in a ratio of 30 : 70, respectively, at ambient temperature is reported.

Chapter V describes the reaction of bis(diisopropylamino)phosphenium triflate with 1,1-bis(diisopropylamino)-3-phenyl- $1\lambda^5$ -[1,3,2]diazaphospholo[1,5-*a*]pyridine, which affords 1,1,1',1'-tetrakis(diisopropylamino)-3,3'-diphenyl-1*H*,1'*H*-[5,5'-bi- $1\lambda^5$ -[1,3,2]diazaphospholo[1,5-*a*]pyridinylidene]-1,1'-diium bis(triflate) (**4**) *via* a homo-bimolecular coupling process. This apparent 'oxidative' coupling by a phosphenium cation has no literature precedent and hence a detailed exploration of the possible mechanism of the reaction is outlined. Comparative reactions involving established oxidants, for example ferrocenium triflate, are examined and also give the diphosponium salt **4**.

Chapter VI outlines an exploration of the behaviour of *N*-dialkyl- and diaryl-phosphino-pyridyl imines in the coordination sphere of low valent palladium species. The isolation and characterisation of a novel dimeric palladium(I) complex is reported, which is found to undergo reactions with chlorobenzene and triphenylphosphine, acting as a source of 'masked' palladium(0). These reactions are consistent with redox processes occurring to give palladium(0) or palladium(II) species.

Statement

This thesis is based on work conducted by the author, in the Department of Chemistry at Durham University, during the period October 2006 to September 2009.

All work described in this thesis is original, unless otherwise acknowledged in the text or in the references. None of this work has been submitted for another degree in this or any other University.

Signed: _____

Date: _____

Daniel Smith

Acknowledgements

Firstly, I would like to thank my supervisor Dr Phil Dyer for his enthusiastic approach, his help and guidance throughout the three years. I do actually mean it ☺

My thanks must also go to Dr Mark Fox for his help and patience with calculations, CV and spectroelectrochemistry. In addition, Prof. Todd Marder, Dr P. J. Low and Dr K. B. Dillon are thanked for their advice.

SASOL Tech. UK are warmly acknowledged for funding with thanks extended to Dr. Kenny Tenza, Dr David Smith and Prof. Bob Tooze. Also Dr Martin Hanton is thanked for his input, encouragement and helpful comments about the usefulness of THF as a solvent for catalysis.

I also must thank the solution-state NMR spectroscopy (Dr Alan Kenwright, Catherine Heffernan, Ian McKeag), elemental analysis (Judith Magee), solid-state NMR (Dr David Appleby, Fraser Markwell) and crystallographic services at Durham (Dr Andrei Batsanov) and the EPR spectroscopy service (Prof. David Collison, Dr Ruth Edge) at Manchester. Calculations conducted by Dr K. Miqueu and Dr. J.-M. Stiropoulos (Pau) and Prof. J.-F. Halet and Dr. K. Costous (Rennes) are also appreciated.

I also greatly indebted to Dr Will “Pie Magic” Wright and Dr Lise Baiget for their helpful guidance, experience with aluminium reagents and most of all light relief.

I wish to thank all those I’ve worked with in Durham but a special mention is required for Dr Carly Anderson, Dr Pippa Monks, “BuLi” Pete, Graeme “Will Jr.” Jorgenson, Antonis Messinis, Dr. Helene Dubarle and Prof. Regis Reau. I’d also like to thank those in Lab 100 for their help (and chemicals). There are too many to thank but a few more include Scott, Helena, Khairul and “Piglet”.

Perhaps most importantly I’d like to thank my Mum, Dad, Grandad, Grandma, Kay, Casey and Fred for their support and Louise for her help throughout.

Chapter I

1	Literature Review	1
1.1	Phosphines	1
1.1.1	Binding of phosphines to metal centres	2
1.1.2	Quantifying the steric effect of phosphines	3
1.1.3	Quantifying the electronic effect of phosphines	4
1.1.4	The “ <i>trans</i> effect” of phosphines	6
1.1.5	The “ <i>trans</i> influence” of phosphines	7
1.2	Bidentate phosphorus-nitrogen ligands	7
1.2.1	Examples and applications of bidentate P ^N ligands	8
1.2.1.1	Carbonylation of alkynes	9
1.2.1.2	Decarbonylation	11
1.3	Iminophosphoranes	12
1.3.1	Rearrangements of iminophosphoranes	12
1.3.2	Alkylation of iminophosphoranes	13
1.3.3	Cycloaddition reactions of alkynes with iminophosphoranes	14
1.4	Phosphenium cations	15
1.4.1	Crystallographic studies of phosphenium cations	16
1.4.2	³¹ P NMR spectroscopic studies of phosphenium cations	17
1.4.3	Reactions of phosphenium cations	18
1.4.3.1	Reactions of phosphenium cations with Lewis bases	18
1.4.3.2	Insertion of phosphenium cations into C-H bonds	19
1.4.3.3	Reactions of phosphenium cations with alkynes	20
1.4.3.4	Reactions of phosphenium cations with alkenes	21
1.4.3.4.1	The McBride synthesis	21
1.4.3.4.2	Reactions of phosphenium cations with cyclic dienes	22
1.4.3.4.3	Reactions of phosphenium cations with acyclic dienes	24
1.4.3.4.4	Reactions of phosphenium cations with strained saturated rings	26
1.4.4	Phosphirenylium cations	27
1.4.5	Diazaphosphenium salts	28
1.5	Intramolecular rearrangements of phosphino-substituted azobenzenes	30
1.6	Summary	32

Chapter II

2	Synthesis and coordination of <i>N</i>-phosphino-pyridyl imines	36
2.1	Introduction: <i>N</i> -Diphenylphosphino-pyridyl imine, 2IP-PPh₂	36
2.1.1	Synthesis of 2IP-PPh₂ and coordination studies	37
2.1.2	The application of as a 2IP-PPh₂ scaffold in methoxycarbonylation studies	38

2.2	Synthesis of diphenylphosphino(phenyl pyridin-2-yl)amine variants	39
2.2.1	Variation of the pyridyl ring of 2IP-PPh₂	39
2.2.2	Variation of the P-substituents of 2IP-PPh₂	40
2.2.3	Variation of the phenyl ring of 2IP-PPh₂	42
2.3	Complexation of the diphenylphosphino(phenyl pyridin-2-yl)amine variants to palladium dichloride	43
2.3.1	Coordination of the ligands 1o-6o , to give the palladium dichloride complexes 7-12	43
2.3.2	Solution state NMR spectroscopic studies of complexes 7-12	44
2.3.3	Crystallographic studies of palladium dichloride complexes 7, 10-12	46
2.3.3.1	X-ray diffraction study of complex 7	46
2.3.3.2	X-ray diffraction studies of complexes 10 and 12	48
2.3.4	X-ray diffraction study of complex 11	51
2.4	Summary	52

Chapter III

3	1,1-bis(Diisopropylamino)-3-phenyl-1λ^5-[1,3,2]diazaphospholo [1,5-α]pyridine – synthesis, dual tautomeric forms and reactivity towards main group and transition metal compounds	54
3.1	Introduction	54
3.2	Synthesis and characterisation of equilibrium mixture 13c/13o	55
3.2.1	Introduction	55
3.2.2	Synthesis of 13c/13o	56
3.2.3	X-ray crystallographic study of 13c	57
3.2.4	Solution-state NMR spectroscopic studies of 13c/13o	58
3.2.5	Solid-state NMR spectroscopic studies of 13c/13o	60
3.2.6	Variable-temperature NMR spectroscopic studies on 13c/13o	62
3.2.7	Possible mechanisms of interconversion of 13c/13o	64
3.2.8	Determination of the rate of interconversion between 13c and 13o	66
3.3	Synthesis and properties of bis(diisopropylamino) phosphino (phenyl 6-methylpyridin-2-yl methylene)amine, 14o	67
3.3.1	Investigation of the factors controlling the lack of cyclisation of 14o	68
3.4	Reactivity of 13o/13c	69
3.4.1	Reaction of 13c/13o with Rh(I) to give complex 15	69
3.4.2	Reaction of 13c/13o with trimethylaluminium to give complex 16	72
3.4.3	Reaction of 13c/13o with dimethylacetylene dicarboxylate (DMAD) to give compound 17	74
3.4.4	Reaction of 13c/13o with selenium to give compound 13o.Se	77
3.5	Summary	79

Chapter IV

4	Synthesis, reactivity, and equilibrium studies of 1,1-bis(diamino)-3-aryl-1λ^5-[1,3,2]diazaphospholo[1,5-<i>a</i>]pyridines and related species	81
4.1	Introduction	81
4.2	1,1-bis(Diisopropylamino)-3-anthracenyl-1 λ^5 -[1,3,2]-diazaphospholo[1,5- <i>a</i>] pyridine (18)	82
4.2.1	Synthesis of the equilibrium mixture 18c/18o	82
4.2.2	Solution-state NMR spectroscopic studies of the tautomers 18c and 18o	83
4.2.3	Solid-state NMR spectroscopic studies of the tautomers 18c and 18o	84
4.2.4	X-ray diffraction studies of the tautomer 18c	85
4.3	The attempted synthesis and isolation of 3-phenyl- <i>spiro</i> -[1 λ^5 -[1,3,2]diazaphospholo[1,5- <i>a</i>] pyridine-1,2'-[1,3,2]dioxaphospholane] (19)	86
4.3.1	Attempted synthesis of 19	87
4.3.2	X-ray molecular structure of the diazadiphosphetane <i>trans</i> - 20	88
4.3.3	Solution-state NMR spectroscopic studies of the diazadiphosphetane 20	91
4.4	The attempted synthesis of a sterically unencumbered variant of 13c	92
4.4.1	Synthesis and isolation of 1',3'-dimethyl-3-phenyl- <i>spiro</i> -[1 λ^5 -[1,3,2]diazaphospholo[1,5- <i>a</i>]pyridine-1,2'-[1,3,2] diazaphospholane] (21c)	94
4.4.2	Attempts to detect an 'open' tautomer 21o	95
4.4.3	Reaction of 21 with selenium	96
4.4.4	Reaction of compound 21 with DMAD to give 22	97
4.4.4.1	Solution-state NMR spectroscopic studies of 22	98
4.4.4.2	The mechanism of formation of compound 22	100
4.5	Summary	101

Chapter V

5	Synthesis of a viologen-containing diphosphonium salt by a phosphonium-mediated oxidative coupling	103
5.1	Introduction	103
5.2	Reaction of 13c/13o with [(i-Pr ₂ N) ₂ P][OTf] to give 23	105
5.2.1	X-ray diffraction study of <i>trans</i> - 23	106
5.2.2	Analysis of 23 by solution-state ¹ H and ³¹ P NMR spectroscopies	109
5.2.3	Analysis of 23 by 2D NMR spectroscopy	110
5.3	Possible mechanisms of formation of 23	111
5.3.1	The loss of a hydrogen atom from 13c/13o	111

5.3.2	Assessment of the formal oxidation state changes in the reaction of 13c/13o with [(i-Pr ₂ N) ₂ P][OTf] to give 23	112
5.3.3	The fate of the phosphonium cation in its reaction with 13c/13o	114
5.4	The 'Scholl coupling' of aryl rings	116
5.5	Formation of compound 23 by use of ferrocenium salts as the oxidant	120
5.5.1	Reaction of ferrocenium salts with 13c/13o	120
5.5.2	Possible mechanisms for the formation of compound 23 from reaction of ferrocenium salts with 13c/13o	122
5.6	Electrochemical study of 13c/13o	123
5.7	Reaction of 14o with [(i-Pr ₂ N) ₂ P][OTf]	124
5.8	Spectroscopic and electrochemical studies of 23	126
5.8.1	UV/visible spectrum of 23	126
5.8.2	Comparison of the calculated MOs of <i>trans</i> - 23 and doubly-reduced methylviologen	128
5.8.3	Assessment of the composition of the electronic transitions of compound 23	131
5.8.4	Electrochemistry of 23	133
5.8.5	Spectroelectrochemistry of 23	136
5.8.5.1	Spectroelectrochemical observation of 25	137
5.8.5.2	Chemical generation of 25	139
5.8.5.3	Spectroelectrochemical observation of 24	140
5.8.6	Near-IR emission	141
5.9	Summary	142

Chapter VI

6	Investigations into <i>N</i>-phosphino-pyridyl imines in the coordination sphere of palladium(0)	145
6.1	Introduction	145
6.2	Investigation into the synthesis and thermolysis of [PdMe ₂ (κ ² - <i>N,P</i> -2IP-PPh ₂)] (26)	146
6.2.1	Synthesis and characterisation of complex 26	146
6.2.2	Thermolysis of [PdMe ₂ (κ ² - <i>N,P</i> -2IP-PPh ₂)] (26)	148
6.3	Synthesis and characterisation of the dimeric complex 27	148
6.3.1	Reaction of [PdMe ₂ (TMEDA)] with ligand 2o	148
6.3.2	X-ray molecular structure of complex 27	149
6.3.2.1	Comparison of the <i>N</i> -phosphino-pyridyl imine framework in complex 27 to known coordinated pyridyl imine scaffolds	151
6.3.2.2	Examination of palladium(I)-palladium(I) bond distance of complex 27	153
6.3.2.3	Summary of the crystallographic data of complex 27	154
6.3.3	Computational investigations into the structure of complex 27	154
6.3.4	Solid-state NMR spectroscopic studies of complex 27	158

6.3.5	Electron paramagnetic resonance (EPR) and solid state magnetic studies of complex 27	159
6.4	Reactivity of palladium dimer 27	161
6.4.1	Reactivity of complex 27 towards aryl halides	161
6.4.1.1	Introduction to oxidative addition of aryl halides in palladium(0)-mediated catalytic cross-coupling	161
6.4.1.2	Reactivity of complex 27 towards chlorobenzene	162
6.4.2	Reactivity of complex 27 towards donor molecules	164
6.5	Summary	166

Chapter VII

7	Experimental procedures and preparations	168
7.1	General considerations	168
7.2	<i>N</i> -Phosphino-pyridyl imines	171
7.3	Palladium dichloride complexes of <i>N</i> -phosphino-pyridyl imines	177
7.4	Diazaphosphole synthesis and reactivity	183
7.5	Further reactions exploring the open P ^{AN} ligand / closed diazaphosphole equilibrium	192
7.6	Investigations into the 'Scholl-like' coupling of 13o/13c	200
7.7	Synthesis and reactivity of palladium dimethyl and palladium(0) species	203
7.8	Additional reactions	207

Appendices

Appendix I: Crystallographic data	212
Appendix II: Postgraduate first year modules	217
Appendix III: Colloquia attended	217
Appendix IV: Presentations and publications	220
Appendix V: Magnetic susceptibility measurements and analyses	222
Appendix VI: Molecular orbital nature of the UV/visible light transitions for compound <i>cis</i> - 23 and <i>trans</i> - 23	225

Abbreviations

(2-IP)H: (phenyl pyridin-2-yl methylene) amine

Ar: aryl

B3LYP: Becke's three parameter exchange functional and the Lee-Yang-Parr correlation functional

BP86: Becke's exchange functional with Perdew's correlation functional

Bu: butyl

COSY: correlated spectroscopy

CP: cross-polarisation

CV: cyclic voltammogram

Cy: cyclohexyl

DCM: dichloromethane

DFT: density functional theory

DMAD: dimethoxyacetylene dicarboxylate

DME: dimethoxyethane

dppp: diphenylphosphinopropane

EI: electron ionisation

EPR: electron paramagnetic resonance

EPSRC: Engineering and physical sciences research council

ES: electrospray

esd: estimated standard deviation

Et: ethyl

eV: electron volt

FAB: fast atom bombardment

Fc: ferrocene

Fc⁺: ferrocenium

FTIR: Fourier-transform infra red

HMBC: heteronuclear multiple bond correlation

HOMO: highest occupied molecular orbital

HSAB: hard soft acid base

HSQC: heteronuclear single quantum coherence

IR: infra red

LUMO: lowest unoccupied molecular orbital

MAS: magic angle spinning
Me: methyl
Mes: 2,4,6-trimethylphenyl (mesityl)
MMA: methyl methacrylate
MO: molecular orbital
NIR: near-infra red
NMR: nuclear magnetic resonance
NOESY: nuclear overhauser effect spectroscopy
OTf: triflate
OTTLE: optically transparent thin-layer electrochemical
Ph: phenyl
PIFA: phenyliodine bis(trifluoroacetate)
ppm: parts per million
Pr: propyl
Py: pyridine
R: alkyl unless specified otherwise
RT: room temperature, unless specified otherwise
TD-DFT: time dependent density functional theory
TEMPO: 2,2,6,6-tetramethylpiperidine 1-oxyl
THF: tetrahydrofuran
TMEDA: tetramethylethylenediamine
TMS: trimethylsilyl
TZP: triple-zeta with polarisation
UV/vis: ultra-violet and visible light
UV: ultra-violet
VT: variable-temperature
WHO: world health organisation
ZORA: zeroth-order regular approximation

NMR Abbreviations

δ = chemical shift (in ppm)

(s) = singlet

(d) = doublet

(t) = triplet

(q) = quartet

(quin) = quintet

(sept) = septet

(m) = complex multiplet

Chapter I

1. Literature Review

This literature review aims to introduce the basic aspects of phosphorus chemistry relevant to the work presented in the following chapters of this thesis. The aim is to give an overview of phosphines, phosphorus-nitrogen ligands and phosphonium cations, including their synthesis and reactivity.

1.1. Phosphines

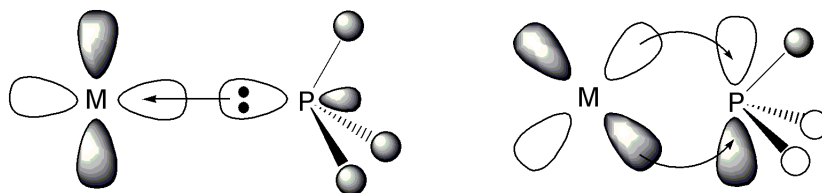
Phosphine ligands (PR_3) are crucial components in a vast number of metal-catalysed processes, controlling key reaction factors such as activity and selectivity. The influence of a phosphine upon a metal to which it is bound can be primarily divided into steric and electronic effects. These properties have been quantified by a number of methods, with perhaps the most established being those reported by Tolman, and these are addressed in detail later.¹

The steric and electronic effects of phosphines are apparent in their phosphine-ligated metal complexes, affecting the strength of metal- PR_3 binding and the rate of dissociation which frequently play decisive roles in metal-catalysed processes. Phosphine donors are often incorporated into multidentate and pincer scaffolds, which allow greater control of the coordination number and possible aggregation of metal species, much better than monodentate ligands. The chemistry of phosphines is indispensable in rationalising the properties of multidentate scaffolds and their corresponding metal-ligated species. Therefore the basic chemistry of metal-phosphine bonding is addressed to aid in the later discussion of heteroditopic ligands.

1.1.1. Binding of phosphines to metal centres

A simple Lewis acid – Lewis base approach is sufficient to explain the bonding of amines to metals, with the nitrogen lone pair donating into a vacant metal orbital of suitable symmetry; such ligands may be regarded as being pure σ -donors due to the comparatively high energy of the π -acceptor orbitals. For phosphines the situation is more complex. The lone pair of the phosphine still donates to the metal in a classical σ -bond fashion, however, 'back-donation' from the metal to the phosphine also occurs. This 'back-donation' is from an appropriate d orbital on the metal into the antibonding P-R σ^* orbitals. Confirmation of such a bonding arrangement was first revealed by Orpen who performed a crystallographic analysis of a range of metal-phosphine complexes that revealed the lengthening of P-R bonds with stronger metal coordination.² This is a direct result of donation into the antibonding P-R σ^* orbital. In terms of the molecular orbital (MO) diagram of a phosphine this 'back-donation' is often described as involving one of the two antibonding orbitals of the phosphine of the appropriate symmetry (see Figure 1), which are predominantly phosphorus p-orbital in character.³

Figure 1: Molecular orbital description of σ -bonding (left) and π -bonding (right) in phosphine-metal complexes



The extent of the 'back-donation' from a metal to a phosphine is dependent upon the π -acceptor or π -acid character of the phosphine, which decreases in the following order:



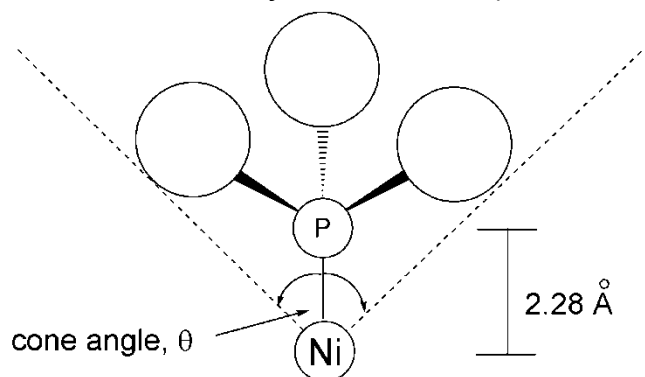
The rationale behind the trend is that the energy of the phosphine antibonding orbital lowers as the electronegativity of the substituents increases, and therefore the orbital is more available for 'back-donation'. However, this is a somewhat oversimplified view since, in many heteroatom-substituted phosphines there is competition for the vacant P-R σ^* orbitals from

both the filled metal d-orbital of appropriate symmetry and the lone pair(s) residing on the heteroatom itself.⁴

1.1.2. Quantifying the steric effect of phosphines

The steric bulk of a phosphine directly affects the metal complex to which it is bound by determining the size and/or number of species that can bind to the metal-phosphine fragment. This factor has been quantified by the cone angle, θ , devised by Tolman.¹ If a bound phosphine was to be rotated about an axis defined by the metal-phosphorus bond, then its substituents would carve out a section of space in the shape of a cone with its point at the metal. The larger the phosphine, the larger the cone and, therefore, the greater the space that is unavailable for other metal-bound species to occupy. Tolman used the van der Waals radii of the phosphorus substituents to define the limits of the cone created with a fixed metal-phosphorus length of 2.28 Å.^{1*} The size of the cone is easily defined for symmetrical phosphines (PR₃) by the angle from its edge to its central axis, which is doubled to give the cone angle, θ (see Figure 2).

Figure 2: Visual description of the cone angle of a phosphine (the circles represent the van der Waals radii of the substituents)¹



This steric parameter θ can be used to explain the decreased binding constants observed for phosphines on nickel(0), $\text{PMe}_3 > \text{PPh}_3 > \text{PCy}_3 > \text{P}(\text{t-Bu})_3$, with the cone angle

* Tolman chose nickel as the metal to base the metal-phosphorus distance on due to the inability of solely electronic factors to explain the order of preferential binding of phosphines to nickel(0) complexes.

increasing as binding constant decreases.¹ Steric factors alone, however, cannot explain all the observed properties of metal-phosphine complexes, making the assessment of the electronic nature of phosphine ligands also necessary.

Table 1: A selection of phosphine cone angles¹

PR ₃	Cone angle, θ / °	PR ₃	Cone angle, θ / °
PH ₃	87	PPh ₃	145
PF ₃	104	P(NMe ₂) ₃	157
PMe ₃	118	PCy ₃	170
PCl ₃	124	P(t-Bu) ₃	182

1.1.3. Quantifying the electronic effect of phosphines

As discussed earlier, the binding of phosphines to metals involves both σ - and π -bonding components and there is no direct correlation between the magnitudes of σ -donation and π -acceptance. Often, only an overall net electronic contribution of a phosphine to a metal is determined, something traditionally achieved by coordination of PR₃ to the Ni(CO)₃ fragment and measurement of the A₁ CO stretching frequency for the resultant complex of C_{3v} symmetry. The greater the electron donating character of a phosphine, the higher the electron density at the metal centre and hence, the greater the degree of back donation into the CO π^* orbital. This orbital is antibonding in nature, so its population weakens the CO bond and the carbonyl stretching frequency is observed to decrease. The electronic parameters for a representative selection of symmetric phosphines are provided in Table 2.^{1,5}

Table 2: A selection of phosphine electronic parameters ($\nu = A_1$ band) for $[\text{Ni}(\text{CO})_3\text{PR}_3]^1$

PR ₃	ν / cm^{-1}	PR ₃	ν / cm^{-1}
PF ₃	2111	PPh ₃	2069
PCl ₃	2097	PMe ₃	2064
P(OPh) ₃	2085	P(NMe ₂) ₃	2062
PH ₃	2083	PCy ₃	2056
P(OMe) ₃	2080	P(t-Bu) ₃	2056

The carbonyl stretching frequencies in the $\text{Ni}(\text{CO})_3$ fragment, however, only reflect the electron density at the metal centre resulting from both σ -donation and π -withdrawal. In response to this, Allen demonstrated the use of the corresponding phosphorus(V) selenides (R_3PSe) to gain insight into the relative σ -donor strength of phosphines.⁶ For a phosphorus selenide two resonance forms can be drawn, a double bonded canonical and a polarised canonical (Figure 3). It has been shown that the nature of the bond most resembles the latter form with little π -contribution and is therefore mainly s in character.³ The relative magnitude of the s character of the bond can be measured by ^{31}P NMR spectroscopic analysis due to the natural abundance (7.5 %) of the ^{77}Se isotope giving rise to a $^1J_{\text{SeP}}$ coupling constant. It is observed that the larger the $|^1J_{\text{SeP}}|$ coupling, the greater the s character, and therefore the lower the basicity of the phosphine.⁷ Hence, a poorly σ -donating phosphine will exhibit a greater $|^1J_{\text{SeP}}|$ coupling than a strongly σ -donating phosphine. The $|^1J_{\text{SeP}}|$ coupling constants for a selection of phosphines are presented in Table 3.

Figure 3: Resonance canonical forms of the phosphorus selenium double bond

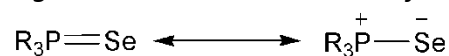


Table 3: A selection of $|^1J_{\text{SeP}}|$ coupling constants^{7,8,9}

PR ₃	$ ^1J_{\text{SeP}} / \text{Hz}$	PR ₃	$ ^1J_{\text{SeP}} / \text{Hz}$
P(OPh) ₃	1027	P(NEt ₂) ₃	794
P(OMe) ₃	963	PPh ₃	732
P(NMe ₂) ₃	805	PMe ₃	684

1.1.4. The “*trans* effect” of phosphines

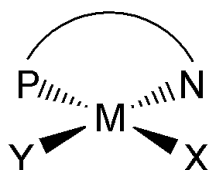
In square planar complexes the rate of substitution of a ligand is directly affected by the identity of the ligand in the *trans* position.¹⁰ Ligands that are strong σ -donors or strong π -acceptors cause faster rates of substitution by reducing the strength of the bonding of the *trans* group. This is known as the “*trans* effect” and is kinetic in nature.^{11,12} A strong σ -donor destabilises the bonding of its *trans* counterpart by donating electron density into a metal d orbital that is shared by the *trans* group, thus weakening its binding to the metal. In contrast, good π -acceptor ligands reduce the electron density at the metal, predominantly at the site opposite (*trans*), therefore lowering the energy of activation for nucleophilic attack by an incoming ligand. This accelerates the rate of exchange at the *trans* site. Consequently, the rate of substitution for σ -donors and π -acceptors decreases in the order:¹⁰

σ -donor: $\text{H}^- > \text{PR}_3 > \text{SCN}^- > \text{I}^- > \text{CH}_3^-$, CO , CN^- , $\text{Br}^- > \text{Cl}^- > \text{NH}_3 > \text{OH}^-$

π -acceptor: CO , $\text{C}_2\text{H}_4 > \text{CN}^- > \text{NO}_2^- > \text{NCS}^- > \text{I}^- > \text{Br}^-$

From these trends it can be seen that phosphines have a strong “*trans* effect”, whereas amines have a weaker “*trans* effect”.¹⁰ This difference can be utilised in the design of heteroditopic ligands; for example in Figure 4 the phosphine donor will cause substituent X to be labilised in preference to substituent Y. This is important in catalytic processes, where controlling the site of coordination of a substrate at a metal complex can affect the stereochemistry of the resultant product. In addition, a metal complex possessing a stronger *trans* donor would be envisaged to give rise to faster rates of substitution at the *trans* position, relative to a complex containing a weaker “*trans* effect” donor. This could potentially result in a quicker rate of reaction for a metal-catalysed process.

Figure 4: Pictorial representation of a heteroditopic phosphorus-nitrogen ligand



1.1.5. The “*trans* influence” of phosphines

The relative magnitude of σ -donation and π -acceptance of a ligand to a metal are also indicated by changes in the bond length *trans* to the ligand, known as “*trans* influence”, which is thermodynamic in origin.^{11,13} For strong *trans*-influencing ligands, such as phosphines, bond weakening is commonly observed for those groups in the *trans* position and is usually, but not always, noticeable in X-ray molecular structure determinations.¹¹ In addition, a lower observed stretching frequency is generally regarded to be concurrent with weakening of a bond and therefore can act as a measure of *trans* influence as well. For the complex $[\text{Pt}(\text{Cl})(\text{X})\text{L}_2]$, where X and Cl are *trans*, the stretching frequencies for the Pt-Cl bond are presented in Table 4, where the decreasing magnitude of the stretching frequency reflects the increasing *trans* influence of X.¹³

Table 4: Reported stretching frequencies for the Pt-Cl bond for $[\text{Pt}(\text{Cl})(\text{X})\text{L}_2]$ where Cl and X are *trans* to each other¹³

X	Cl ⁻	Py	P(OPh) ₃	PPh ₃	PEt ₃	H ⁻
$\nu_{\text{Pt-Cl}}$ (cm ⁻¹)	340	337	316	298	295	269

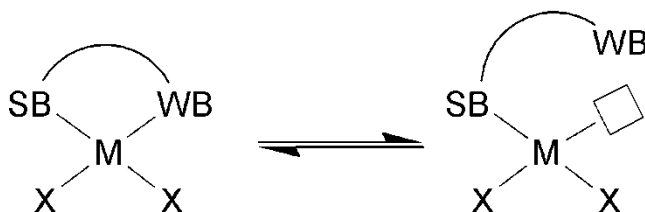
1.2. Bidentate phosphorus-nitrogen ligands

Bidentate ligands have been widely developed in inorganic chemistry. In particular, they have found extensive use in homogenous catalysis, where their ability to confer a specific electronic and steric environment at a metal centre has allowed a wealth of catalysts to emerge. Furthermore, the entropic advantage provided by the chelate effect disfavours ligand dissociation, resulting in stabilised metal complexes sufficiently robust to survive often challenging catalytic process conditions. As a result, a vast array of bidentate ligands have been described, for example homoditopic P[^]P,¹⁴ N[^]N^{15,16} and S[^]S systems¹⁷ and

heteroditopic P[^]O,¹⁸ P[^]S,¹⁹ N[^]O¹⁵ and N[^]S¹⁹ scaffolds, each of which has been exploited in a range of applications. For brevity, this review will focus on heteroditopic P[^]N ligands only.²⁰

Bidentate phosphorus-nitrogen ligands (P[^]N) are heteroditopic in nature with their two different donor atoms providing electronic asymmetry to the metal to which they are bonded.²⁰ As a consequence, with the 'softer' d-block metals (*e.g.* Pd, Pt, and Rh) it is found that the 'softer' phosphorus donor binds more strongly than the 'harder' nitrogen donor atom.²¹ As expected, the preference for binding reverses if more electropositive, earlier transition metals are considered. With this in mind, it can be envisaged that the weaker bound donor atom could potentially be 'hemilabile', and its dissociation would yield a vacant coordination site, whilst the ligand as a whole remains in the coordination sphere of the metal under consideration.²² Binding sites are, of course, necessary for incoming substrates in catalytic pathways, but their existence must be balanced against need to stabilise reactive metal species that are susceptible to degradation reactions. Therefore 'hemilabile' chelates can potentially provide the best properties of both mono- and bi-dentate ligands.²²

Scheme 1: Proposed hemilability of a heteroditopic ligand on a metal complex, where SB is a strongly binding donor atom, WB is a weakly binding donor atom and the square denotes a vacant coordination site.



1.2.1. Examples and applications of bidentate P[^]N ligands

There have been many recent reviews describing catalysis facilitated by P[^]N scaffolds often involving relatively simple frameworks, where slight modifications in structure can have a significant impact in catalytic function.²³⁻²⁵ A few representative examples of the benefits of

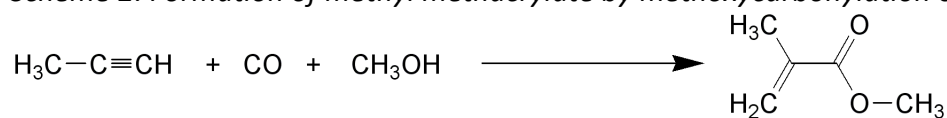
bidentate P^N ligands versus monodentate phosphines and bidentate phosphines are presented below.

1.2.1.1. Carbonylation of alkynes

Metal-catalysed carbonylation of unsaturated hydrocarbons in the presence of a nucleophile, typically an aqueous or alcoholic solvent medium, has been studied in detail.²⁶ A wide range of alkenes and alkynes are suitable as substrates, with the products generated often highly dependent upon the nature of the ligands involved in the catalytic process. Although these ligands are frequently monodentate or bidentate phosphines, many heteroditopic ligands have been explored.²⁷

In the early 1990s Drent and co-workers investigated a set of bidentate pyridyl-phosphine ligands in the palladium-mediated methoxycarbonylation of propyne (Scheme 2) comparing their rate and selectivity for the production of methyl methacrylate (MMA) against that of triphenylphosphine.²⁸ The use of PPh₃ as the palladium scaffold was found to give a poor rate of carbonylation with a regioselectivity for MMA of 89 %. In contrast, the 2-pyridyl-diphenylphosphine ligand gave unprecedented activities for the methoxycarbonylation of propyne, several orders of magnitude greater than those observed with PPh₃ (Table 5). In addition, a higher selectivity (98.9 %) was noted and the catalytic process was possible at milder temperatures (45 °C relative to 115 °C).²⁸

Scheme 2: Formation of methyl methacrylate by methoxycarbonylation of propyne²⁸



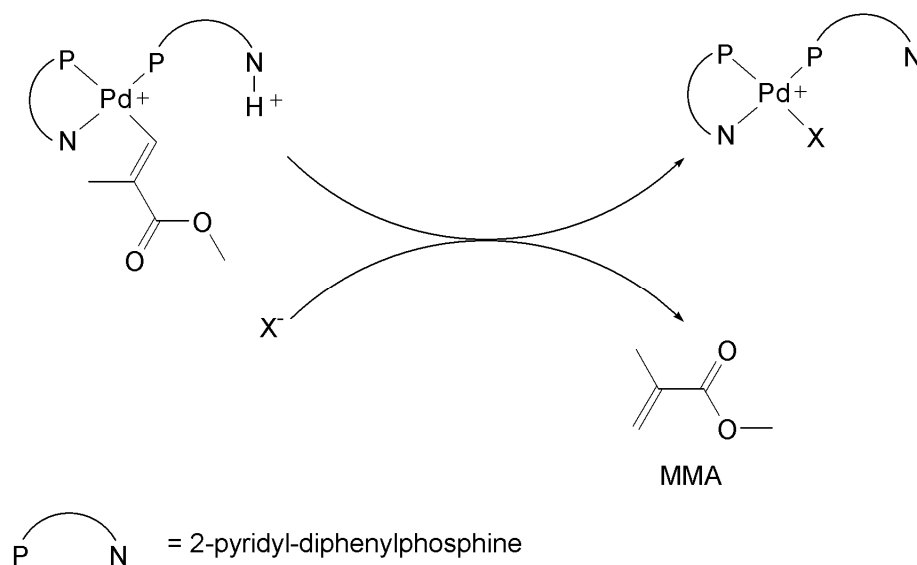
The highly efficient nature of the 2-pyridyl-diphenylphosphine ligand is proposed by Drent to result from the nitrogen atom of the pyridine acting as a 'proton messenger' in the catalytic cycle. It can be envisaged that fast delivery of a proton to the palladium coordination sphere would allow an increased rate of cleavage of the alkenyl-palladium bond to give MMA (Scheme 3).²⁸

Table 5: Palladium-catalysed methoxycarbonylation of propyne. Conditions: 60 bar CO, 3.0 mmol ligand, 2.0 mmol $\text{CH}_3\text{SO}_3\text{OH}$, Py = pyridyl²⁸

Ligand	Palladium acetate (mmol)	Temperature (° C)	Average rate (mol (mol Pd) ⁻¹ h ⁻¹)	Selectivity (% MMA)
PPh_3	0.10	115	~10	89
4-PyPPh ₂	0.10	90	~10	90
3-PyPPh ₂	0.10	70	1000	99.2
2-PyPPh ₂	0.012	45	40000	98.9

Testing of the ligand 4-pyridyl-diphenylphosphine gave results analogous to those obtained using PPh_3 (Table 5), something perhaps to be expected given that the geometry of the former ligand inhibits the presence of both nitrogen and phosphorus in the coordination sphere of palladium at the same time.²⁸ It is therefore unlikely that 4-pyridyl-diphenylphosphine would be able to participate in the proposed ‘proton-messenger’ process where the close proximity of a protonated nitrogen atom to palladium is required.

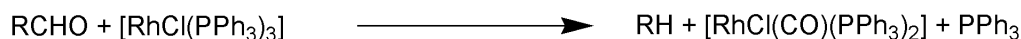
Scheme 3: Proposed ‘proton-messenger’ termination step in the methoxycarbonylation of propyne to methyl methacrylate (MMA)²⁸



1.2.1.2. Decarbonylation

The decarbonylation of aldehydes by stoichiometric quantities of Wilkinson's catalyst, $[\text{RhCl}(\text{PPh}_3)_3]$, was first reported by Tsuji²⁹ with a range of ligated-metal complexes having since been shown to be capable of catalytic decarbonylation.^{30,31} An early study of iridium complexes chelated with bidentate P^P and P^N ligands by Pignolet revealed significant differences in their catalytic activities for decarbonylation.³² A comparison of diphenylphosphinopropane (dppp) and 1-(2-pyridyl)-2-(diphenylphosphino)ethane (**A**) in the coordination sphere of iridium showed the latter to exhibit an increased catalytic activity under decarbonylation conditions (Table 6).³²

*Scheme 4: Stoichiometric decarbonylation of aldehydes by Wilkinson's catalyst*²⁹



Mechanistic studies on the related bidentate phosphine-chelated rhodium carbonylation catalysts suggest that dissociation of a phosphine moiety from the metal is the rate-limiting step in the catalytic cycle.³² Therefore, the increased activity of $[\text{Ir}(\mathbf{A})_2][\text{PF}_6]$, relative to $[\text{Ir}(\text{dppp})_2][\text{PF}_6]$, is consistent with the greater lability of the nitrogen atom, compared to the phosphorus atom, which allows faster metal-donor dissociation.³²

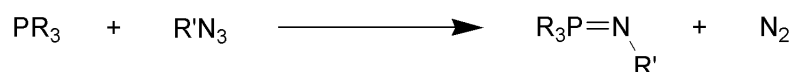
*Table 6: Comparison of catalytic activity of $[\text{Ir}(\mathbf{A})_2][\text{PF}_6]$ and $[\text{Ir}(\text{dppp})_2][\text{PF}_6]$ for decarbonylation of benzaldehyde. **A** = 1-(2-pyridyl)-2-(diphenylphosphino)ethane.*³²

Complex	catalytic activity: (mol of benzene / mol of catalyst) / h esd's are in parenthesis
$[\text{Ir}(\mathbf{A})_2][\text{PF}_6]$	9(2)
$[\text{Ir}(\text{dppp})_2][\text{PF}_6]$	1.5(5)

1.3. Iminophosphoranes

σ^4, λ^5 -Iminophosphoranes ($R_3P=NR'$) are classically the products of the reaction between a phosphine and an azide following loss of dinitrogen, a transformation otherwise known as the Staudinger reaction (Scheme 5).³³ They may be regarded as the *aza* analogues of phosphorus ylides [$R_3PC(R'')R'$], commonly known as Wittig reagents. A wide range of variously-substituted iminophosphoranes may be prepared simply using the Staudinger reaction by changing the initial reagents, although a number of other less flexible methodologies are known.³³ The resulting iminophosphoranes undergo a number of distinctive and synthetically versatile reactions; those that are most relevant to this thesis (rearrangement, alkylation, cycloaddition, and *N*-coordination) are discussed below.

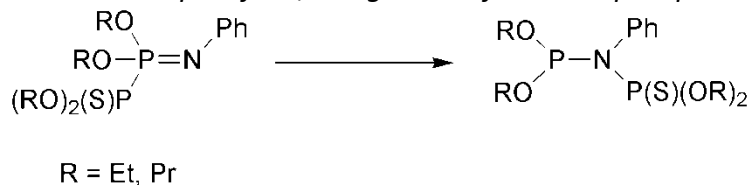
*Scheme 5: The Staudinger reaction*³³



1.3.1. Rearrangements of iminophosphoranes

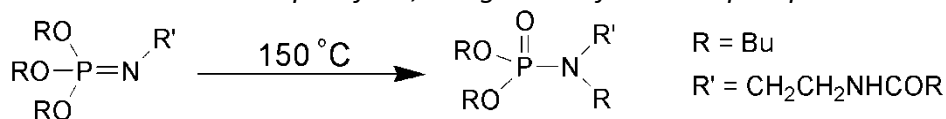
Many iminophosphoranes that are generated by the Staudinger reaction, or other processes, are unstable and are observed to decompose, often by an intramolecular rearrangement. Iminophosphoranes susceptible to decomposition are frequently noted to have singly-bonded heteroatomic substituents at phosphorus, therefore containing either weak P-X bonds (*e.g.* X = P) inclined to bond cleavage, or the potential to form strong P=X double bonds (*e.g.* X = O) and hence are liable to induce rearrangement. An example of the former is a 1,2-migration, in which a group from phosphorus shifts to the imide nitrogen creating an amide with reduction of the iminophosphorane phosphorus atom from + 5 to + 3 (Scheme 6).³³

Scheme 6: Example of a 1,2-migration of an iminophosphorane³³



The rearrangement of an iminophosphorane to give an amidophosphorane, while retaining the P(V) oxidation state, is typical for species with an alkoxy-substituted phosphorus centre (Scheme 7).³⁴ This 1,3-migration results in the formation of a phosphorus-oxygen double bond, which is undoubtedly the driving force for this process.

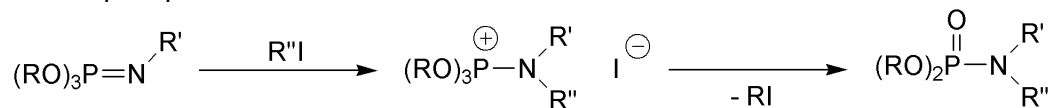
Scheme 7: Example of a 1,3-migration of an iminophosphorane³⁴



1.3.2. Alkylation of iminophosphoranes

For iminophosphoranes the nucleophilicity of the nitrogen lone pair is apparent in reactions with methyl iodide where the alkyl group is transferred to the nitrogen, resulting in the formation of a stable salt, [R₃PNR'₂(Me)][I], when R is alkyl or aryl. In contrast, for imidophosphonates (iminophosphoranes with alkoxy-substituents on phosphorus), the salt formed following reaction with methyl iodide is unstable. This salt undergoes loss of an alkyl group from an alkoxy moiety in the form of an alkyl halide (Scheme 8).³³

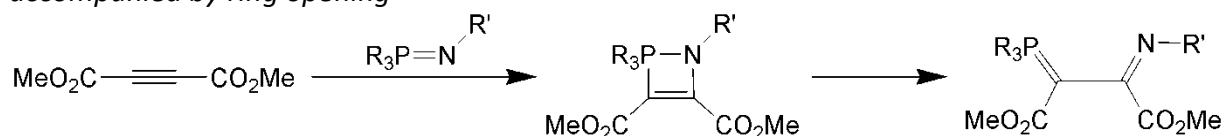
Scheme 8: Alkylation of an iminophosphorane followed by a rearrangement to a N-substituted phosphorus acid amide³³



1.3.3. Cycloaddition reactions of alkynes with iminophosphoranes

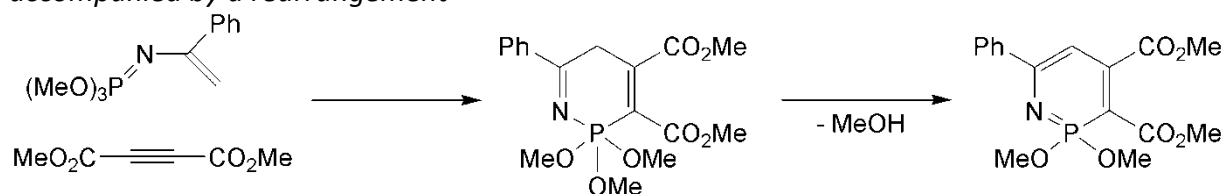
The inherently unsaturated nature of iminophosphoranes allows cycloaddition reactions of the P=N double bond to occur.³³ For example, dimethylacetylene dicarboxylate (DMAD) is an electron deficient alkyne and readily undergoes cyclisations with many double bonds including those of iminophosphoranes. The most common outcome of reactions of DMAD with iminophosphoranes is the expected [2+2] cycloaddition product, namely a four-membered ring. Subsequent ring opening is often observed and gives rise to a P=C-C=N motif; here the overall process can be regarded as an insertion of the alkyne into the P-N bond of the starting iminophosphorane (Scheme 9).³⁵ The addition of iminophosphoranes to more electron rich alkynes (*e.g.* alkyl-substituted) gives similar reactivity pathways.³⁶ Although highly strained, isolated examples of these 4-membered rings formed by this [2+2] cycloaddition are known.³⁷

Scheme 9: Reaction of an iminophosphorane with DMAD via a [2+2] cycloaddition, accompanied by ring opening³⁵



Another, related, mode of reactivity of iminophosphoranes has been reported by Nitta, in which the iminophosphorane, conjugated with an alkene to form a diene, undergoes a [4+2] cycloaddition. A subsequent rearrangement with elimination of methanol then occurs, giving rise to a more stable heterocyclic aromatic system.³⁸

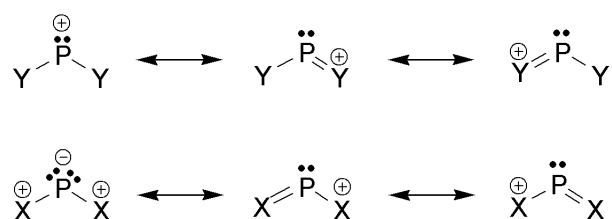
Scheme 10: Reaction of an iminophosphorane with DMAD via a [4+2] cycloaddition, accompanied by a rearrangement³⁸



1.4. Phosphenium cations

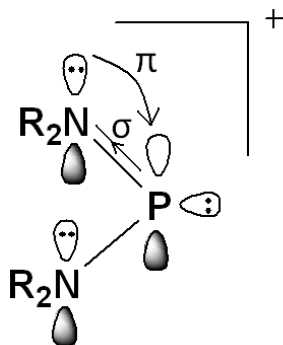
Phosphenium cations $[R_2P]^+$ are formally valence isoelectronic and isolobal with a singlet carbene and share many of the properties and reactivity pathways associated with carbene chemistry.³⁹ Such cations are characterised by the high degree of positive charge on phosphorus and are not to be confused with cations where the positive charge of a species is not localised on phosphorus (see Figure 5).⁴⁰⁻⁴²

Figure 5: Phosphenium cation, $[Y_2P]^+$ (top) and a phosphorus-containing cationic species where the positive charge is not localised on phosphorus $[X_2P]^+$ (lower)⁴²



The phosphorus centre, in phosphenium cations, contains both an empty p orbital and a filled sp^2 hybrid orbital, which inherently makes the species highly reactive. This reactivity can be reduced by the presence of amino substituents on phosphorus, which act in a dual manner. The σ -electron withdrawing effect of the nitrogen atoms lessens the electron density in the sp^2 hybridised orbital on phosphorus, while the filled nitrogen p-orbitals are able to donate into the empty phosphorus p-orbital. The overall effect is a stabilisation of the phosphorus centre and, unsurprisingly, the majority of isolated phosphenium cations contain one or two amino groups.

Figure 6: Pictorial description of the inductive and mesomeric effects stabilising a diaminophosphenium cation



1.4.1. Crystallographic studies of phosphonium cations

In the late seventies Cowley and co-workers synthesised $[(i\text{-Pr}_2\text{N})_2\text{P}][\text{AlCl}_4]$ by addition of AlCl_3 to the corresponding diaminochlorophosphine, and undertook an X-ray diffraction study.⁴³ The structure of $[(i\text{-Pr}_2\text{N})_2\text{P}][\text{AlCl}_4]$ reveals the phosphorus atom to be sp^2 hybridised with the N-P-N bond angle being slightly reduced (114.8°) from an ideal trigonal planar geometry (120°) due to lone pair – bonding pair repulsion.^{43,44} The geometries around both nitrogen atoms are planar allowing full interaction between their full p orbitals and the empty p orbital of phosphorus. Additionally, a slight contraction is observed for the PN bonds ($1.611(4) \text{ \AA}$ and $1.615(4) \text{ \AA}$) relative to non-ionic aminophosphines (typically 1.637 \AA).⁴⁵ This reduction in bond length probably arises from the additional N-to-P π -bonding and the high degree of positive charge on phosphorus.

There are many other examples of acyclic and cyclic phosphonium cations that have been investigated by X-ray diffraction studies. The majority of these species possess one or two amino substituents on the phosphorus centre, which stabilise the system for reasons outlined above, however, a further discussion of the crystallographic studies of these phosphonium cations is beyond the scope of this review.

1.4.2. ^{31}P NMR spectroscopic studies of phosphonium cations

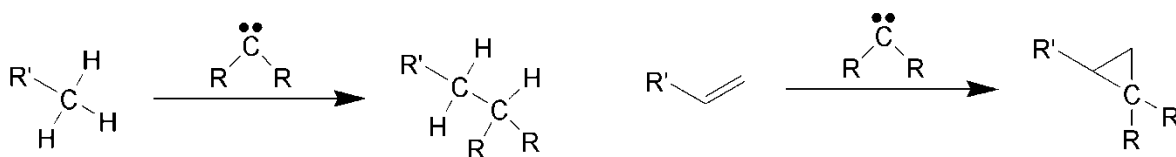
The ^{31}P NMR spectroscopic chemical shift of the phosphorus centre of phosphonium cations is very distinctive, with these ionic species often exhibiting resonances in the range 200 – 500 ppm. This is due to their positively charged nature and their low coordination geometry. Indeed, following the conversion of a chlorophosphine to its corresponding phosphonium cation frequently brings about a shift of approximately 100 ppm according to ^{31}P NMR spectroscopy, consistent with the change from a covalent to a charged species. A notable extreme is the compound $[(\text{t-Bu})(\text{NMe}_2)\text{P}][\text{AlCl}_4]$ where the ^{31}P NMR spectroscopic chemical shift is 513 ppm.⁴⁶ This large shift to high frequency, relative to $[(\text{i-Pr}_2\text{N})_2\text{P}][\text{AlCl}_4]$ (313 ppm), is undoubtedly a reflection of the greater localisation of positive charge on phosphorus. In $[(\text{t-Bu})(\text{NMe}_2)\text{P}][\text{AlCl}_4]$ the phosphonium cation has only one amino group to help delocalise the positive charge from phosphorus. For the alkyl group, however, there is no π -donation, only a degree of σ -electron donation to phosphorus.

Mazieres *et al.* have studied a range of phosphonium cations and the effect of changing the counter anion on the ^{31}P NMR spectroscopic shift.⁴⁷ It was found that for the triflate salt of bis(diisopropylamino)phosphonium a chemical shift of 302 ppm was recorded, whereas with the tetrachloroaluminate counter anion the phosphorus centre displayed a chemical shift of 313 ppm. Alteration of the counter anion causes both electronic and geometric changes at the phosphorus centre and these give rise to the different chemical shifts. However, the effects of changing counteranion are hard to predict as neither $[(\text{Et}_2\text{N})_2\text{P}]^+$ nor the cyclic ion $[(\text{MeNC}_2\text{H}_4\text{NMe})\text{P}]^+$ display a chemical shift difference between their triflate and tetrachloroaluminate salts. It is also worthy of note that Mazieres and co-workers observed that a dynamic exchange of anions occurs if a source of chloride is present in a solution of $[(\text{i-Pr}_2\text{N})_2\text{P}][\text{OTf}]$. The effect of chloride introduction could easily be seen by ^{31}P NMR spectroscopy, where the resonance corresponding to the phosphonium ion was observed to move to lower frequency with the magnitude of the shift being found to be dependent upon the quantity of chloride added.

1.4.3. Reactions of phosphonium cations

The chemistry of carbenes in organic transformations has long been established. Interestingly, the valence isoelectronic and isolobal phosphonium cations exhibit many of the typical reactions associated with their carbon analogues (see Scheme 11).^{39,40} Common unsaturated organic molecules including alkynes, dienes, and strained cyclic alkenes are all susceptible to attack from phosphonium cations, often giving a phosphorus-containing heterocycle as the product, in a manner reminiscent of the cycloadditions known for carbenes.⁴⁸

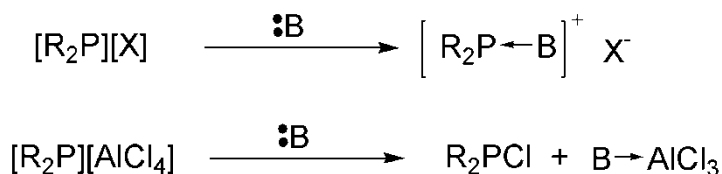
*Scheme 11: Typical reactions of a carbene: insertion into a C-H bond (left) and reaction with a C=C bond (right)*⁴⁹



1.4.3.1. Reactions of phosphonium cations with Lewis bases

Initial work by Parry demonstrated that Lewis bases will bind to phosphonium cations.⁵⁰ Early studies focused on the use of phosphines as the Lewis bases, but a range of acceptor-donor adducts have been synthesised since, including those involving pyridines, amines, and intramolecular donor atoms.^{42,51,52} The nature of the anion is crucial to whether a Lewis acid-Lewis base adduct is formed; in certain cases the anion can dissociate to provide a better acceptor than the phosphonium cation. Use of the tetrachloroaluminate anion is a prime example of where this type of dissociation takes place, and yields aluminium trichloride that scavenges donor molecules and in the process generates the chlorophosphine (Scheme 12).

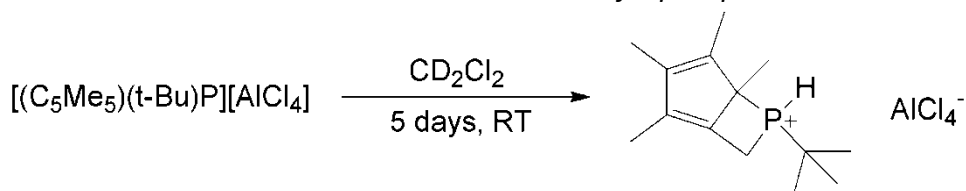
Scheme 12: Reaction to form a base-stabilised phosphonium adduct (upper) and conversion of a phosphonium tetrachloroaluminate salt to a chlorophosphine (lower)⁴²



1.4.3.2. Insertion of phosphonium cations into C-H bonds

Phosphenium cations are inherently reactive species and, as a result, any reduction of the electronic stabilisation provided by the substituent groups increases this reactivity.⁴⁰ However, Cowley and co-workers were able to synthesise and characterise the phosphenium salt $[(\text{C}_5\text{Me}_5)(\text{t-Bu})\text{P}][\text{AlCl}_4]$ despite the absence of stabilising amino substituents.⁵³ The stabilisation instead arises from the cyclopentadienyl fragment, achieved as a result of its η^5 -coordination to the phosphorus centre (as inferred from NMR spectroscopic studies), although lower degrees of hapticity could not be excluded. This phosphenium species slowly, over a period of five days at room temperature, transforms to a phosphonium salt generated by intramolecular C-H activation. The origin of the proton on phosphorus in the phosphonium salt was confirmed as being from the phosphenium cation, by a study conducted in deuterated dichloromethane (Scheme 13), thereby excluding interactions with the solvent during the C-H activation process. This is consistent with an intramolecular insertion of the phosphenium cation into a methyl C-H bond and is comparable with the known C-H insertion reactivity of carbenes.

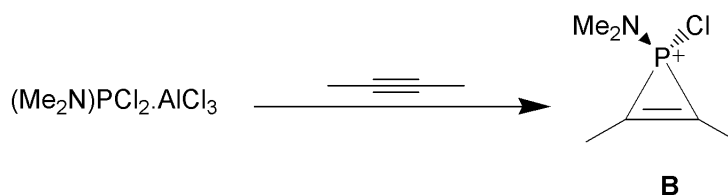
Scheme 13: Intramolecular C-H activation of a phosphenium cation⁵³



1.4.3.3. Reactions of phosphonium cations with alkynes

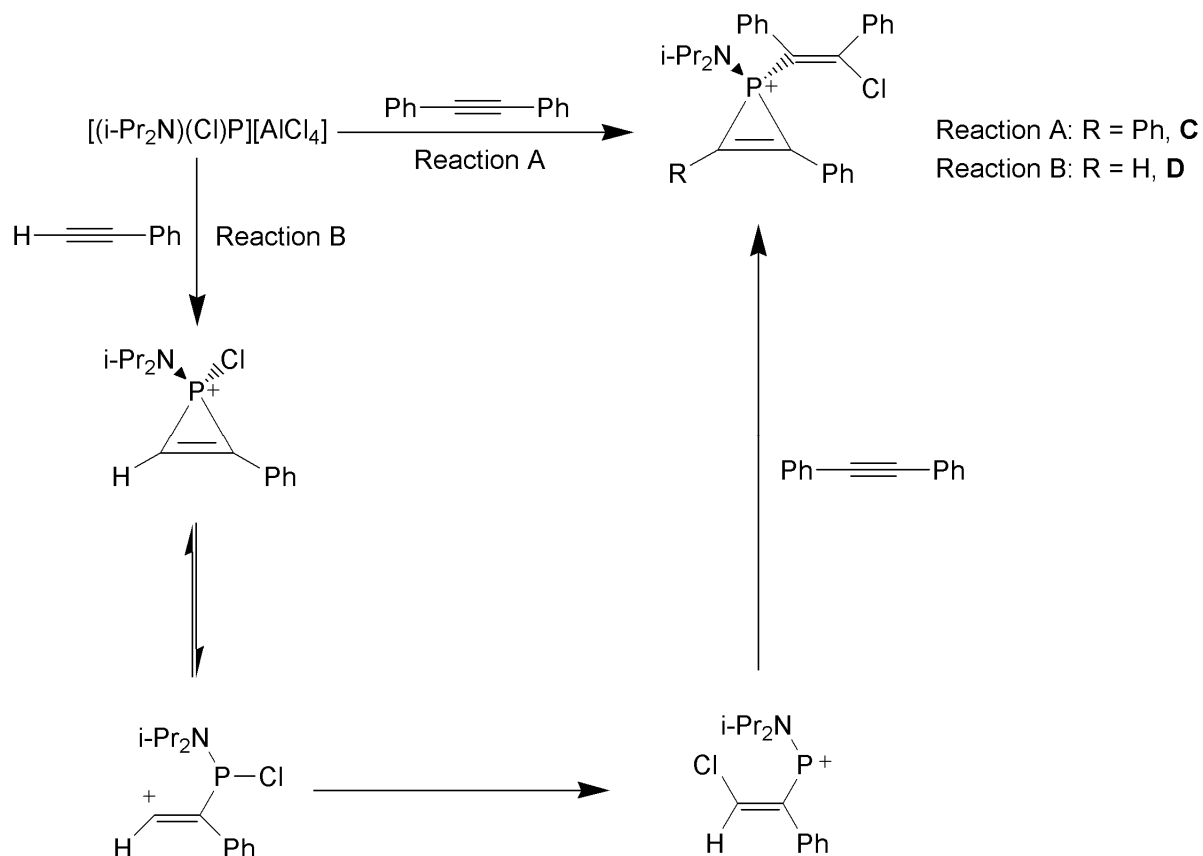
The generation of a phosphonium cation in the presence of dimethylacetylene was found to give a phosphirenium cation, **B**, via a [2+2] cycloaddition (Scheme 14).⁵⁴ A range of aryl-, alkyl- and chloro-substituted chlorophosphines were found to be suitable precursors for this type of transformation, with the addition of AlCl_3 producing the reactive transient phosphonium ion.⁵⁴

Scheme 14: Reaction of a phosphonium cation with dimethylacetylene⁵⁴



Using the methodology of *in situ* phosphonium generation, Baxter and Cowley synthesised phosphirenium salt **C** (Scheme 15: Reaction A), from which they were able to obtain the first X-ray molecular structure of such a heterocyclic ring system.⁵⁵ This compound arises from reaction with two equivalents of diphenylacetylene with the phosphonium cation, but the details of the mechanism were not immediately apparent. Subsequent studies of the addition of $[(i\text{-Pr}_2\text{N})(\text{Cl})\text{P}][\text{AlCl}_4]$ to monophenylacetylene have demonstrated that the initial reaction gives an unstable phosphirenium cation that undergoes rearrangement to a phosphonium cation (Scheme 15: Reaction B). Consequently, addition of diphenylacetylene to this phosphonium salt gives rise to the phosphirenium cation **D**.⁵⁶

Scheme 15: The mechanism of the reaction of $[(i\text{-Pr}_2\text{N})(\text{Cl})\text{P}][\text{AlCl}_4]$ with two equivalents of acetylene⁵⁶



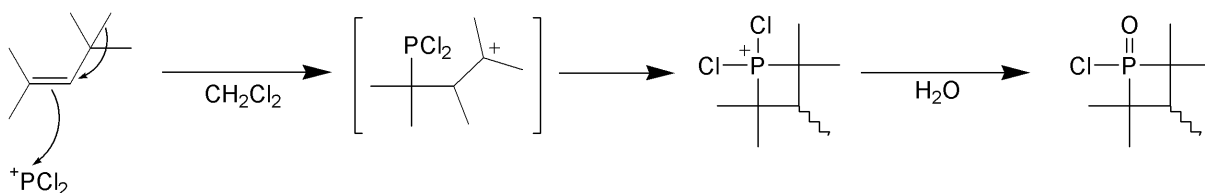
1.4.3.4. Reactions of phosphonium cations with alkenes

1.4.3.4.1. The McBride synthesis

Phosphenium cations are efficient precursors for the synthesis of phosphetanes, partially inorganic cyclobutanes that contain a single phosphorus atom in the ring.⁵⁷ Phosphetanes were first synthesised by McBride using transient phosphenium cations, which when generated in the presence of certain alkenes, will add across the double bond of the alkene and subsequently rearrange (Scheme 16).⁵⁷ The final product is determined by the substitution pattern of the alkene. The McBride synthesis has been expanded to a vast

number of alkenyl substrates, but the method is usually limited to highly-substituted olefins that force the rearrangement to give a four-membered ring.

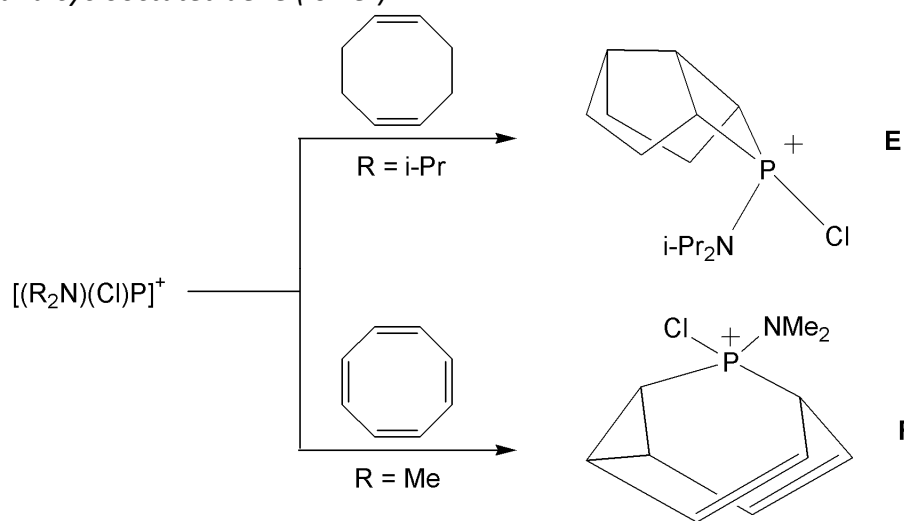
*Scheme 16: Synthesis of a phosphetane by in situ generation of a phosphonium cation with AlCl_3 , the McBride method. A possible mechanism is shown where electrophilic addition occurs in an anti-Markovnikov fashion due to the steric hindrance of the *t*-butyl group.⁵⁷*



1.4.3.4.2. Reactions of phosphonium cations with cyclic dienes

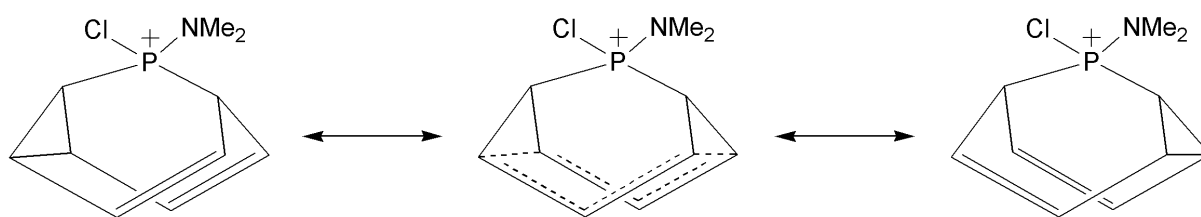
Investigations into the use of stable pre-formed phosphonium cations by the groups of Baxter and Cowley have demonstrated that cyclic unsaturated organic molecules can be used as phosphetane precursors. In a set of collaborative papers, Baxter and Cowley outline the reactivities of 1,5-cyclooctadiene and cyclooctatetraene towards phosphonium cations.^{58,59} In the first case, the phosphetane **E** was generated (Scheme 17), with its formation undoubtedly occurring as a result of an initial reaction with an alkene in a [2+2] cycloaddition and subsequent rearrangements *via* carbocationic intermediates.⁵⁸ Although limited mechanistic information is presented, phosphetane **E** is generated as the major product.

Scheme 17: Reaction of a monohalogeno-phosphenium cation with 1,5-cyclooctadiene (upper)⁵⁸ and cyclooctatetraene (lower)⁵⁹



In the reaction of $[(\text{Me}_2\text{N})(\text{Cl})\text{P}][\text{AlCl}_4]$ with cyclooctatetraene an equally complex phosphorus heterocycle is generated, namely a 9-phosphabarbaralane, **F** (Scheme 17).⁵⁹ Barbaralanes are essentially homotropilidines locked, by a bridging methyldiene, in the appropriate conformation for the Cope rearrangement to occur.⁶⁰ For this phosphorus-bridged barbaralane system the Cope rearrangement occurs at room temperature in solution with an energy barrier calculated to be 12 ± 1.7 kcal/mol (Figure 7).⁵⁹ Structural analysis of the crystalline form of **F** reveals an approach towards the transition state for the Cope rearrangement with a delocalised bonding motif of extended double bonds and shortened single bonds.

Figure 7: Cope rearrangement for the phosphabarbaralane **F** reported by Cowley⁵⁹

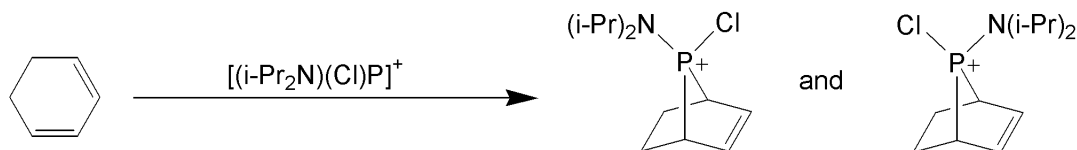


The phosphenium cation of choice in the previous two reactions was a chloro(dialkylamino)phosphenium, since bis(dialkylamino)phosphenium cations showed no

reactivity towards cyclooctadiene.^{58,59} This inactivity is attributed to the reduced positive charge at phosphorus of the $[(R_2N)_2P]^+$ cation, relative to that of $[(R_2N)(Cl)P]^+$, suggesting that the former cation is unable to provide the necessary “carbocation-like behaviour”. This dependence upon the phosphorus substituents mirrors the McBride synthesis, which has been successfully extended to di- and tri-halogenophosphines as the phosphonium source.⁵⁷

The cyclic diene, 1,3-cyclohexadiene, was also found to undergo cycloaddition with $[(i\text{-Pr}_2\text{N})(Cl)P][AlCl_4]$, the resultant products being a mixture of two isomeric phosphanorbornenes (Scheme 18).⁶¹ The two isomers are reported to exist in a ratio of 3:2 with the diisopropylamino group for the predominant species believed to lie on the unsaturated side of the norbornene, minimising the steric interactions.

Scheme 18: Reaction of a monohalogenophosphenium cation, $[(i\text{-Pr}_2\text{N})(Cl)P]^+$, with 1,3-cyclohexadiene giving a mixture of isomeric phosphanorbornenes⁶¹



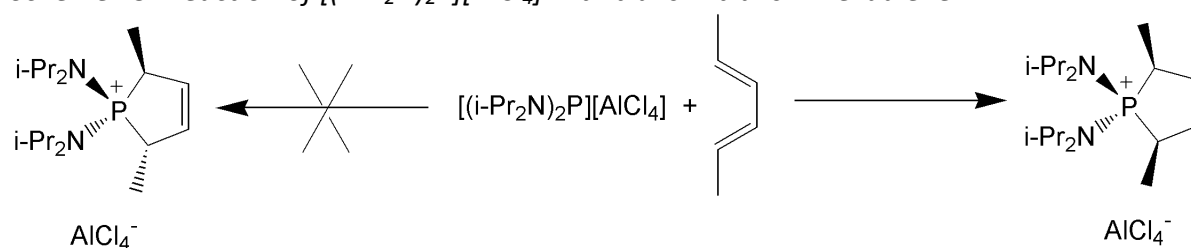
1.4.3.4.3. Reactions of phosphonium cations with acyclic dienes

Acyclic dienes are also capable of reaction with phosphonium cations, often forming positively charged five-membered phosphorus-containing rings with a monounsaturated backbone, known as phospholenium cations.^{40,61} A range of bis(dialkylamino) and chloro(dialkylamino)phosphonium cations are found to be suitable for the synthesis of phospholenium ions from 1,3-dienes.⁶¹ Three potential mechanisms can be envisaged for these types of reaction: a radical process, an initial [2+2] cycloaddition followed by a rearrangement, or a [4+2] cycloaddition. Of these mechanisms, a radical-mediated route was believed to be unlikely since calculations by Harrison predict the singlet electronic configuration for the phosphonium ions to be energetically more stable than the triplet state.⁶² The energy difference was found to widen with the increasing electronegativity of

the substituents of the phosphonium cation, in the order $[\text{H}_2\text{P}]^+ < [\text{HPF}]^+ < [\text{F}_2\text{P}]^+$ with reported energies of 20.4, 42.6, and 84.0 kcal mol⁻¹, respectively.

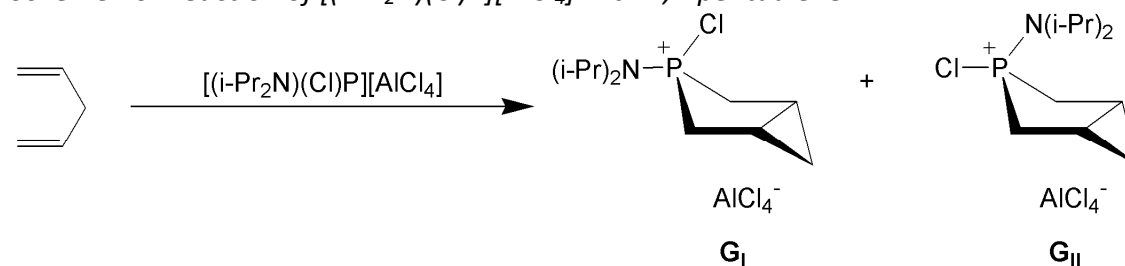
In the majority of reactions between phosphonium cations and acyclic dienes limited mechanistic information is available and therefore distinguishing between the [2+2]- and [4+2]-cycloaddition pathways is not possible. In a study by Cowley, however, the use of *trans*-2-*trans*-4-hexadiene as a reagent generates only one of two possible diastereoisomers (Scheme 19).⁶¹ This indicates that a direct [4+2]-cycloaddition has occurred rather than the two step [2+2]-cycloaddition/rearrangement mechanism, since the latter would not confer any stereospecificity, therefore producing both isomers.

Scheme 19: Reaction of $[(i\text{-Pr}_2\text{N})_2\text{P}][\text{AlCl}_4]$ with *trans*-2-*trans*-4-hexadiene⁶¹



The reaction of 1,4-dienes with phosphonium salts also gives phosphorus-containing heterocycles with the combination of $[(i\text{-Pr}_2\text{N})(\text{Cl})\text{P}][\text{AlCl}_4]$ and 1,4-pentadiene producing two positively charged bicyclic isomers **G_I** and **G_{II}** (Scheme 20).⁶¹ The compounds each consist of a fused cyclopropane and a phosphacyclopentane. The mixture of **G_I** and **G_{II}** was found to contain 77 % of isomer **G_I** where the cyclopropane and the amino group are *trans* each other across the phosphacyclopentane ring, presumably to minimise the unfavourable steric interaction.

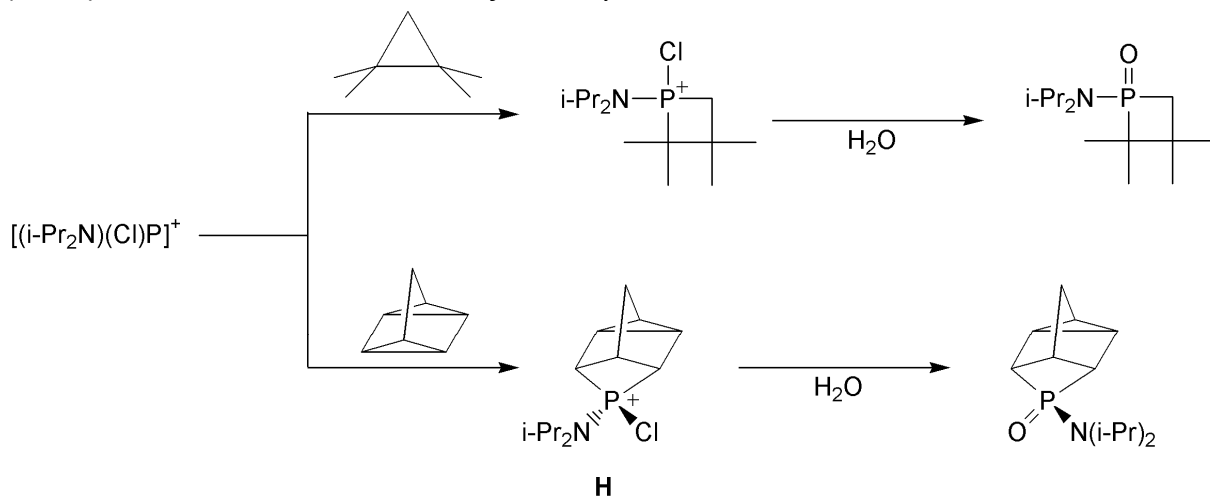
Scheme 20: Reaction of $[(i\text{-Pr}_2\text{N})(\text{Cl})\text{P}][\text{AlCl}_4]$ with 1,4-pentadiene



1.4.3.4.4. Reactions of phosphonium cations with strained saturated rings

Ring-opening of saturated cyclic systems has been observed by Baxter in reactions of phosphonium cations with quadricyclane and other substituted cyclopropanes (Scheme 21).⁶³ Again, the active phosphonium ions for this transformation contain a chloro substituent on phosphorus, implying a related mechanism to that proposed for the McBride synthesis (see section 1.4.3.4.1). The ring-opening reactions both generate phosphetanes, isolable as the corresponding oxides in near quantitative yields for the majority of products.⁶³

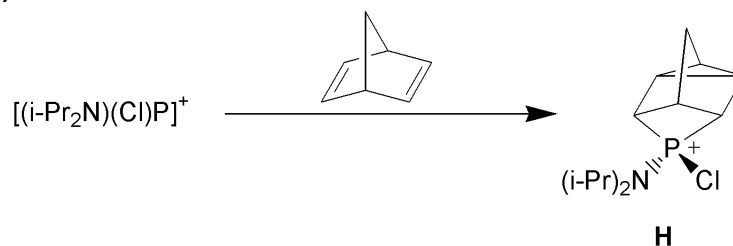
Scheme 21: Reaction of $[(i\text{-Pr}_2\text{N})(\text{Cl})\text{P}][\text{AlCl}_4]$ with a cyclopropane (upper) and quadricyclane (lower). The counter anion is omitted for clarity.⁶³



Norbornadiene also reacts with the chloro(diisopropylamino)phosphonium cation to generate **H**, the quadricyclane adduct (Scheme 22).⁶³ Moreover, norbornadiene is found to react with dialkylaminophosphonium cations generating phosphetanes similar in structure to **H**, however, the rate of reaction is strongly dependent upon the steric size of the alkyl groups, with the recorded rate of reaction decreasing in the order:



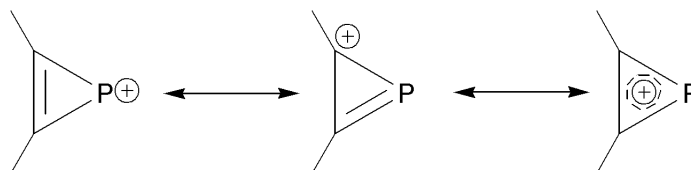
Scheme 22: Reaction of $[(i\text{-Pr}_2\text{N})(\text{Cl})\text{P}][\text{AlCl}_4]$ with norbornadiene with the counter anion omitted for clarity.⁶³



1.4.4. Phosphirenylium cations

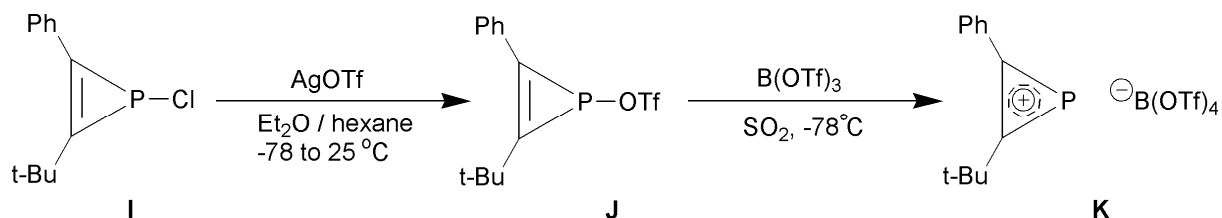
Phosphirenylium cations are a distinctive class of phosphonium cation and are analogues of the cyclopropenium cation.⁶⁴ These cyclic three-membered rings contain a single sp^2 -hybridised phosphorus atom. This arrangement is highly strained, with relief of tension often being achieved by a change in hybridisation at phosphorus to sp^3 upon reaction. Three resonance forms can be drawn for the phosphirenylium ion with the positive charge being either localised solely on phosphorus, localised on carbon, or delocalised (see Figure 8).

Figure 8: Resonance forms of a phosphirenylium⁶⁶



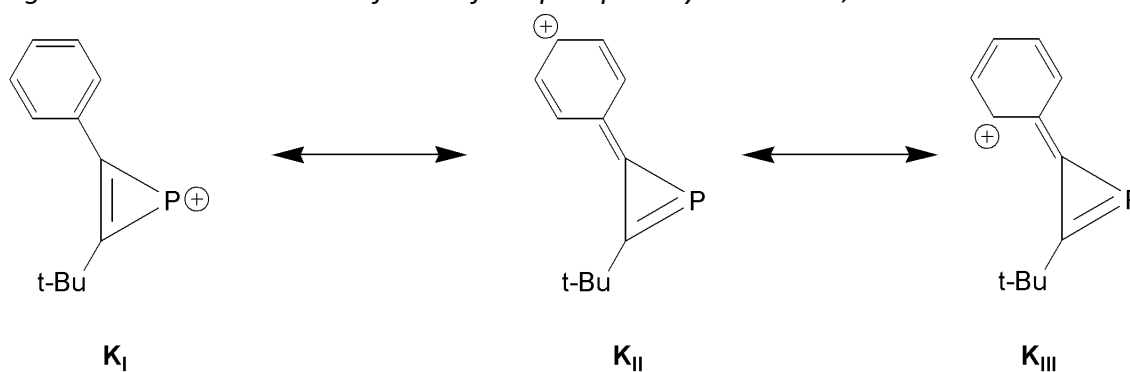
The chlorophosphirene **I**, was synthesised by the group of Regitz as a possible precursor to a phosphirenylium cation.⁶⁵ However, attempts to generate a cation from this compound with either PF_6^- or BPh_4^- as counter anions were unsuccessful and led to fluoride and phenyl abstraction, respectively.⁶⁶ Exchange of chloride for triflate, by use of silver triflate, did give a stable compound **J**, but subsequent analysis by ^{31}P NMR spectroscopy revealed a chemical shift of -3.0 ppm, characteristic of a phosphorus centre with three covalently bound substituents, *i.e.* not a phosphonium cation.

Scheme 23: Synthesis of the first persistent phosphirenylium cation, **K**.⁶⁶



The utilisation of boron tritriflate as the anion abstractor in combination with **I** allowed the synthesis of **K** (see Scheme 23), as the first isolable example of a phosphirenylium cation, which was characterised fully by NMR spectroscopy.⁶⁶ The identity of the cation is evident from the ^{31}P NMR spectroscopic chemical shift of 309.7 ppm, a shift to higher frequency of 313 ppm relative to the covalent triflate. The presence of the phenyl group invites the possibility of delocalisation of positive charge beyond the central three-membered ring (see Figure 9). Although some contribution of the forms **K_{II}** and **K_{III}** is likely, the overall structure is predominantly of **K_I** character with ^{13}C NMR spectroscopy revealing normal phenyl environments. In addition, similar $^1\text{J}_{\text{PC}}$ constants are observed for the carbons t-BuC and PhC of 75 and 66 Hz, respectively, further indication of the symmetrical phosphirenium core of the **K_I** resonance structure.⁶⁶

Figure 9: Possible resonance forms of the phosphirenylium cation, **K**.⁶⁶



1.4.5. Diazaphospholenium salts

Cyclic diaminocarbenes have been studied in extensive detail with the greater stability of imidazol-2-ylidenes over imidazolidin-2-ylidenes being well established.³⁹ The difference in

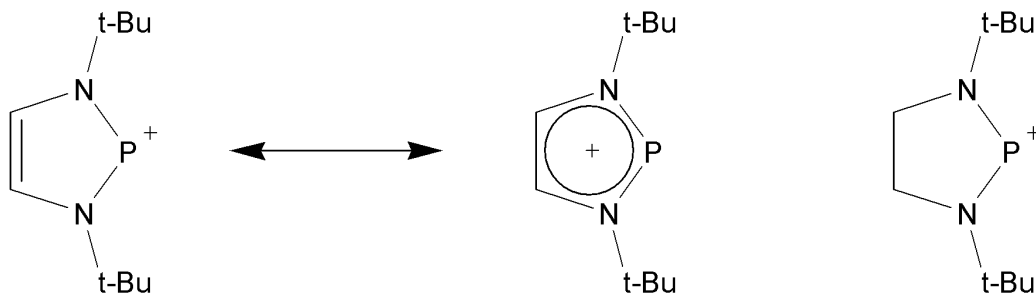
stability arises from the possibility of forming a 6π -aromatic ring and, although the aromatic resonance structure is not predominant, it has been calculated to contribute an additional stabilisation of approximately 25 kcal mol^{-1} to imidazol-2-ylidenes with respect to imidazolidin-2-ylidenes.⁶⁷

Figure 10: An imidazol-2-ylidene (left) and an imidazolidin-2-ylidene (right)³⁹



Similar studies by the groups of Denk and Gudat have been conducted upon diazaphospholenium cations, which are valence isoelectronic to imidazol-2-ylidenes (Figure 11).^{68,69} The diazaphospholenium cations studied were readily synthesised from their *P*-halogenodiazaphospholene analogues by exchange of the halide for a non-coordinating anion. As for imidazol-2-ylidenes, the diazaphospholenium ion has the potential to adopt 6π -aromaticity or a localised bonding arrangement, shown for the example $[(t\text{-BuNCH=CHN}t\text{-Bu})\text{P}][\text{PF}_6]$ in Figure 11.

Figure 11: Resonance forms of a diazaphospholenium cation, $[(t\text{-BuNCH=CHN}t\text{-Bu})\text{P}]^+$, (left) and a cyclic diazaphospholenium cation, $[(t\text{-BuNCH}_2\text{-CH}_2\text{N}t\text{-Bu})\text{P}]^+$, with a saturated carbon framework (right)^{68,69}



The X-ray molecular structure of the diazaphospholenium cation $[(t\text{-BuNCH=CHN}t\text{-Bu})\text{P}][\text{PF}_6]$ has been determined and displays endocyclic bond distances intermediate

between those of formal single and double bonds (see Table 7).⁶⁸ A comparison of the bond lengths of [(*t*-BuNCH=CHN*t*-Bu)P][PF₆] with those for (*t*-BuNCH=CHN*t*-Bu)PF show the partial delocalisation of the positive charge resulting from halide abstraction. The contraction of the C-N and P-N distances with concurrent lengthening of the C-C bonds is a clear reflection of a shift towards 6π-aromaticity.^{68,69}

Table 7: Selected bond distances for a P-halogenodiazaphosphenolene, a diazaphosphenium cation and a cyclic diazaphosphenium cation with a saturated carbon framework.^{68,69}

	P-N / Å	N-C / Å	C-C / Å	Ref
[(<i>t</i> -BuNCH=CHN <i>t</i> -Bu)PF]	1.672(2) 1.6721(19)	1.415(3) 1.415(3)	1.336(3)	69
[(<i>t</i> -BuNCH=CHN <i>t</i> -Bu)P][PF ₆]	1.661(2) 1.662(3)	1.376(3) 1.377(3)	1.341(4)	68
[(<i>t</i> -BuNCH ₂ -CH ₂ N <i>t</i> -Bu)P][PF ₆]	1.613(2) 1.619(2)	1.482(5) 1.389(3)	1.544(7)	68

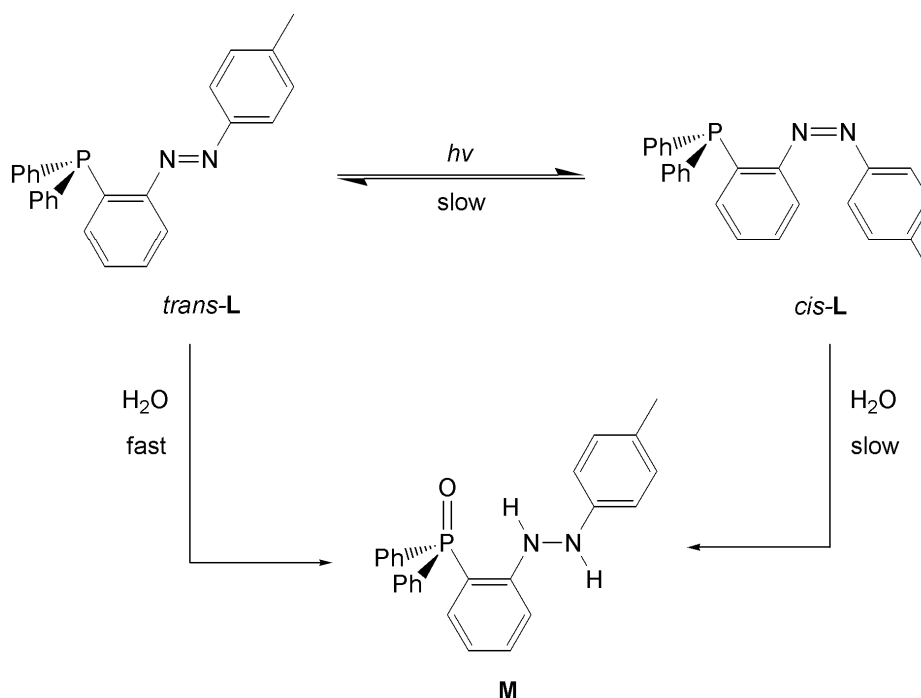
For the cyclic diazaphosphenium cation [(*t*-BuNCH₂-CH₂N*t*-Bu)P][PF₆] a shortening of the P-N bonds lengths is observed relative to those of the phospholenium cation [(*t*-BuNCH=CHN*t*-Bu)P][PF₆], demonstrating the significant aromatic nature of the latter.⁶⁸ The P-N bond distances of [(*t*-BuNCH₂-CH₂N*t*-Bu)P][PF₆] are comparable to those of [(*i*-Pr₂N)₂P][AlCl₄] (1.611(4) Å and 1.615(4) Å) inferring that geometric constraints play a limited role in determining the bonding environment of [(*t*-BuNCH₂-CH₂N*t*-Bu)P][PF₆].^{43,68}

1.5. Intramolecular rearrangements of phosphino-substituted azobenzenes

Kawashima and co-workers have explored the use of azo groups as switches to control the properties of molecules by photoisomerisation.^{70,71} Functionalised azobenzene molecules with silyl groups have been reported, with these substituted compounds shown to be capable of *cis/trans* switching of the N=N double bond. In the case of the 2-tetrafluorosilyl-azobenzene derivative the *cis/trans* conformation was demonstrated to control both the coordination environment of silicon and the overall reactivity of the molecule.⁷² Similar chemistry was investigated for a phosphino-substituted azobenzene.⁷³ Kawashima reports

the synthesis of *trans*-**L** and its partial photochemical conversion to the isomer *cis*-**L** (Scheme 24). The differences in the reactivity of *trans*-**L** and *cis*-**L** were demonstrated by their reactions with water. Compound *trans*-**L** undergoes rapid hydrolysis to generate **M**, whereas *cis*-**L** is effectively inert towards water. Although *cis*-**L** does convert to **M**, the rate of conversion (10^{-3} s^{-1}) is approximately that of the rate of isomerisation to *trans*-**L** (10^{-4} s^{-1} in the dark), suggesting decay to *trans*-**L** and subsequent hydrolysis.⁷³

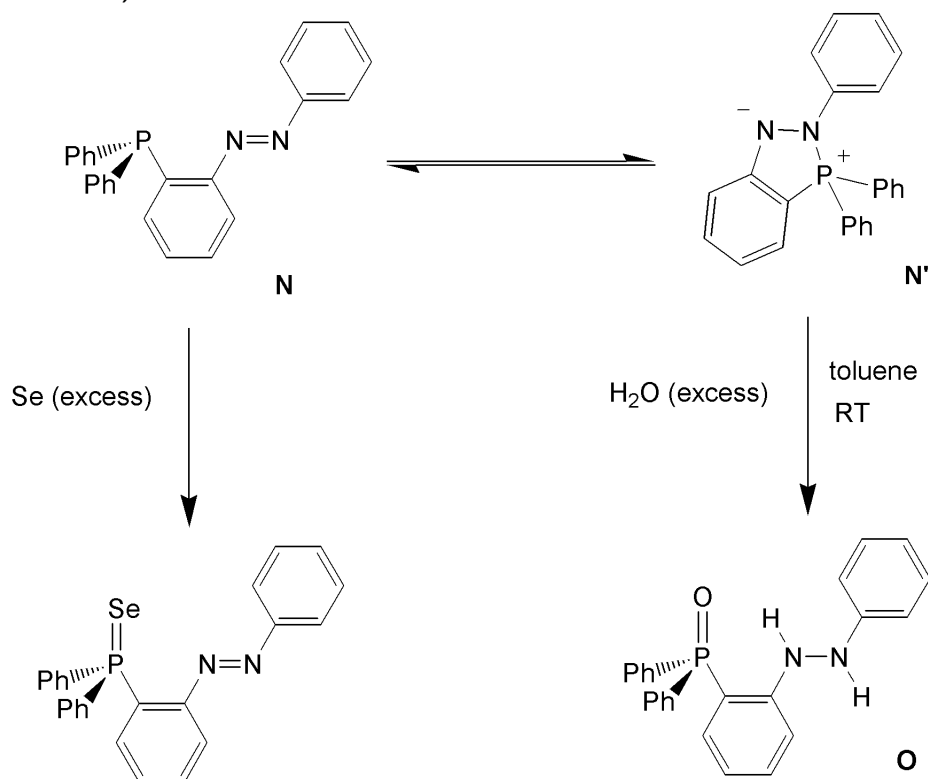
Scheme 24: Photoisomerisation of a phosphino-substituted azobenzene *trans*-**L** to *cis*-**L**, and their reactions with water



This difference in reactivity can be explained by consideration of the related molecule, **N**, reported to be inert towards photoisomerisation (Scheme 25).⁷³ Compound **N** lacks the methyl substituent of *trans*-**L**, but is otherwise structurally analogous. In contrast to compound **L** however, molecule **N** exists in equilibrium with the phosphonium salt **N'**. The reactivity of this equilibrium mixture of **N/N'** can be regarded as being either that of a phosphine or a phosphonium salt depending upon the nature of the other reactant. Addition of selenium to **N/N'** generates the selenide of the phosphine, whereas addition of water generates a hydrolysis adduct **O** with the same form as **M**.⁷³ This multifunctional compound **N/N'** aids the understanding of the reaction of the phosphine *trans*-**L** with water that

generates **M**. The conversion of *trans*-**L** to **M** is fast relative to *cis*-**L** to **M** and the former reaction is likely to proceed by a phosphonium intermediate similar in structure to **N'**. These compounds with their multifunctionality and photochemical switching are expected by the authors to be advantageous in the control of organic reactions.⁷³

*Scheme 25: Equilibrium between two isomers of a phosphino-substituted azobenzene molecule, **N** and **N'***



1.6. Summary

The following chapters of this thesis will build on the chemistry of phosphorus-nitrogen ligands and phosphonium cations described in this review. This will include a development of new variants of a *N*-phosphino-pyridyl imine ligand previously reported by Dyer *et al.* and an exploration of the effect of their substituents upon the geometry of their palladium dichloride complexes.⁷⁴ In addition, a novel intramolecular equilibrium between an 'open'

P⁺N ligand and a 'closed' diazaphosphole is presented. These two compounds can be regarded as valence tautomers of each other and their reactivity towards transition metals, Lewis acids and electron deficient acetylenes is investigated.

-
- ¹ C. A. Tolman, *Chem. Rev.*, 1977, **77**, 313.
- ² A. G. Orpen, N. G. Connelly, *Chem. Commun.*, 1985, 1310.
- ³ D. G. Gilheany, *Chem. Rev.*, 1994, **94**, 1339.
- ⁴ M. L. Clarke, G. L. Holliday, A. M. Z. Slawin, J. D. Woollins, *Dalton Trans.*, 2002, 1093.
- ⁵ C. A. Tolman, *J. Am. Chem. Soc.*, 1970, **92**, 2953.
- ⁶ D. W. Allen, B. F. Taylor, *Dalton Trans.*, 1982, 51.
- ⁷ W. McFarlane, D. S. Rycroft, *Dalton Trans.*, 1973, 2162.
- ⁸ S. M. Godfrey, S. L. Jackson, C. A. McAuliffe, R. G. Pritchard, *Dalton Trans.*, 1998, 4201.
- ⁹ E. Krawczyk, A. Skowronska, J. Michalski, *J. Chem. Soc., Perkin Trans. 2*, 2000, 1135.
- ¹⁰ D. F. Shriver, P. W. Atkins, *'Inorganic Chemistry'*, 3rd ed., Oxford University Press, Oxford, 1999, p. 473.
- ¹¹ B. J. Coe, S. J. Glenwright, *Coord. Chem. Rev.*, 2002, **203**, 5.
- ¹² K. M. Anderson, A. G. Orpen, *Chem. Commun.*, 2001, 2682.
- ¹³ T. G. Appleton, H. C. Clark, L. E. Manzer, *Coord. Chem. Rev.*, 1973, **10**, 335.
- ¹⁴ P. C. Kamer, P. W. N. M. Van Leeuwen, J. N. H. Reek, *Acc. Chem. Res.*, 2001, **34**, 895.
- ¹⁵ M. Gómez, G. Muller, M. Rocamora, *Coord. Chem. Rev.*, 1999, **193**, 769.
- ¹⁶ A. Mederos, S. Domínguez, R. Hernández-Molina, J. Sanchiz, F. Brito, *Coord. Chem. Rev.*, 1999, **193**, 913.
- ¹⁷ A. M. Masdeu-Bultó, M. Diéguez, E. Martin, M. Gómez, *Coord. Chem. Rev.*, 2003, **242**, 159.
- ¹⁸ A. Bader, E. Lindner, *Coord. Chem. Rev.*, 1991, **108**, 27.
- ¹⁹ M. Mellah, A. Voituriez, E. Schulz, *Chem. Rev.*, 2007, **17**, 5133.
- ²⁰ P. Espinet, K. Soulantica, *Coord. Chem. Rev.*, 1999, **293**, 499.
- ²¹ D. F. Shriver, P. W. Atkins, *'Inorganic Chemistry'*, 3rd ed., Oxford University Press, Oxford, 1999, p. 167.
- ²² P. Braunstein, F. Naud, *Angew. Chem. Int. Ed.*, 2001, **40**, 680.
- ²³ F. Speiser, P. Braunstein, L. Saussine, *Acc. Chem. Res.*, 2005, **38**, 784.
- ²⁴ G. Helmchen, A. Pflatz, *Acc. Chem. Res.*, 2000, **33**, 336.

-
- ²⁵ P. J. Guiry, C. P. Saunders, *Adv. Synth. Catal.*, 2004, **346**, 497.
- ²⁶ G. Kiss, *Chem. Rev.*, 2001, **101**, 3435.
- ²⁷ M. Beller, B. Cornils, C D. Frohning, C. W. Kohlpaintner, *J. Mol. Cat. A*, 1995, **104**, 17.
- ²⁸ E. Drent, P. Arnoldy, P. H. M. Budzelaar, *J. Organomet. Chem.*, 1993, **455**, 247.
- ²⁹ J. Tsuji, K. Ohno, *Tetrahedron Lett.*, 1965, **6**, 3969.
- ³⁰ D. H. Dougherty, L. H. Pignolet, *J. Am. Chem. Soc.*, 1978, **100**, 7083.
- ³¹ R. H. Prince, K. A. Rospin, *J. Chem. Soc. A*, 1969, 612.
- ³² M. P. Anderson, A. L. Casalnuovo, B. J. Johnson, B. M. Mattson, A. M. Muetting, L. H. Pignolet, *Inorg. Chem.*, 1988, **27**, 1649.
- ³³ Y. G. Gololobov, L. F. Kasukhin, *Tetrahedron*, 1992, **48**, 1353.
- ³⁴ Y. G. Gololobov, N. I. Gusar, M. P. Chaus, *Tetrahedron*, 1985, **41**, 793.
- ³⁵ J. Barluenga, F. Lopez, F. Palacios, *Chem. Commun.*, 1985, 1681.
- ³⁶ J. Barluenga, I. Merino, F. Palacios, *Tetrahedron. Lett.*, 1989, **30**, 5493.
- ³⁷ N. Kano, A. Kikuchi, T. Kawashima, *Chem. Commun.*, 2001, 2096
- ³⁸ T. Kobayashi, M. Nitta, *Chem. Lett.*, 1985, 1459.
- ³⁹ D. Bourissou, F. Gabbaï, O. Geurret, G. Bertrand, *Chem. Rev.*, 2000, **100**, 39.
- ⁴⁰ A. H. Cowley, R. A. Kemp, *Chem. Rev.*, 1985, **85**, 367.
- ⁴¹ B. D. Ellis, C. L. B. Macdonald, *Coord. Chem. Rev.*, 2007, **251**, 936.
- ⁴² D. Gudat, *Coord. Chem. Rev.*, 1997, **163**, 71.
- ⁴³ A. H. Cowley, M. C. Cushner, J. S. Szobota, *J. Am. Chem. Soc.*, 1978, **100**, 7784.
- ⁴⁴ D. F. Shriver, P. W. Atkins, '*Inorganic Chemistry*', 3rd ed., Oxford University Press, Oxford, 1999, p. 74.
- ⁴⁵ F. H. Allen, O. Kennard, D. G. Watson, L. Brammer, A. G. Orpen, R. Taylor, *J. Chem. Soc., Perkin Trans. 2*, 1987, S1.
- ⁴⁶ A. H. Cowley, M. Lattman, J. C. Wilburn, *Inorg. Chem.*, 1981, **20**, 2916.
- ⁴⁷ M. R. Mazieres, C. Roques, H. Sanchez, J.P. Majoral, R. Wolf, *Tetrahedron*, 1987, **43**, 2109.
- ⁴⁸ S. A. Weissmann, S. G. Baxter, *Tetrahedron Lett.*, 1987, **28**, 603.
- ⁴⁹ J. Clayden, N. Greeves, S. Warren, P. Wothers, '*Organic Chemistry*', Oxford University Press, Oxford, 2001, p. 1055.
- ⁵⁰ C. W. Schultz, R. W. Parry, *Inorg. Chem.*, 1976, **15**, 3046.
- ⁵¹ N. Burford, P. Losier, A. D. Phillips, P. J. Ragogna, T. S. Cameron, *Inorg. Chem.*, 2003, **42**, 1087.
- ⁵² C. Chuit, C. Rey  , *Eur. J. Inorg. Chem.*, 1998, 1847.

-
- ⁵³ A. H. Cowley, S. K. Mehrotra, *J. Am. Chem. Soc.*, 1983, **105**, 2074.
- ⁵⁴ K. A. Fongers, H. Hogveen, R. F. Kingma, *Tetrahedron Lett.*, 1983, **24**, 643.
- ⁵⁵ J. M. Vural, S. A. Weissman, S. G. Baxter, A. H. Cowley, C. M. Nunn, *Chem. Commun.*, 1988, 462.
- ⁵⁶ S. A. Weissmann, S. G. Baxter, *Tetrahedron Lett.*, 1990, **31**, 819.
- ⁵⁷ A. Marinetti, D. Carmichael, *Chem. Rev.*, 2002, **102**, 201.
- ⁵⁸ S. A. Weissman, S. G. Baxter, A. M. Arif, A. H. Cowley, *Chem. Commun.*, 1986, 1081.
- ⁵⁹ S. A. Weissmann, S. G. Baxter, A. M. Arif, A. H. Cowley, *J. Am. Chem. Soc.*, 1986, **108**, 529
- ⁶⁰ R. V. Williams, *Chem. Rev.*, 2001, **101**, 1185.
- ⁶¹ A. H. Cowley, R. A. Kemp, J. G. Lasch, N. C. Norman, C. A. Stewart, B. R. Whittlesey, T. C. Wright, *Inorg. Chem.*, 1986, **25**, 740.
- ⁶² J. F. Harrison, *J. Am. Chem. Soc.*, 1981, **103**, 7406.
- ⁶³ S. A. Weissmann, S. G. Baxter, *Tetrahedron Lett.*, 1988, **29**, 1219.
- ⁶⁴ D. Bourissou, G. Bertrand, *Acc. Chem. Res.*, 1999, **32**, 561.
- ⁶⁵ O. Wagner, M. Ehle, M. Regitz, *Angew. Chem. Int. Ed.*, 1989, **28**, 225.
- ⁶⁶ K. K. Laali, B. Geissler, O. Wagner, J. Hoffmann, R. Armbrust, W. Eisfeld, M. Regitz, *J. Am. Chem. Soc.*, 1994, **116**, 9407.
- ⁶⁷ C. Heinemann, T. Müller, Y. Apeloig, H. Schwarz, *J. Am. Chem. Soc.*, 1996, **118**, 2023.
- ⁶⁸ M. K. Denk, S. Gupta, A. J. Lough, *Eur. J. Inorg. Chem.*, 1999, 41.
- ⁶⁹ D. Gudat, A. Haghverdi, H. Hupfer, M. Nieger, *Chem. Eur. J.*, 2000, **6**, 3414.
- ⁷⁰ N. Kano, F. Komatsu, M. Yamamura, T. Kawashima, *J. Am. Chem. Soc.*, 2006, **128**, 7079.
- ⁷¹ J. Yoshino, N. Kano, T. Kawashima, *Chem. Commun.*, 2007, 559.
- ⁷² N. Kano, F. Komatsu, T. Kawashima, *J. Am. Chem. Soc.*, 2001, **123**, 10778.
- ⁷³ M. Yamamura, N. Kano, T. Kawashima, *J. Am. Chem. Soc.*, 2005, **127**, 11954.
- ⁷⁴ P. W. Dyer, J. Fawcett, M. J. Hanton, *J. Organomet. Chem.*, 2005, **690**, 5264.

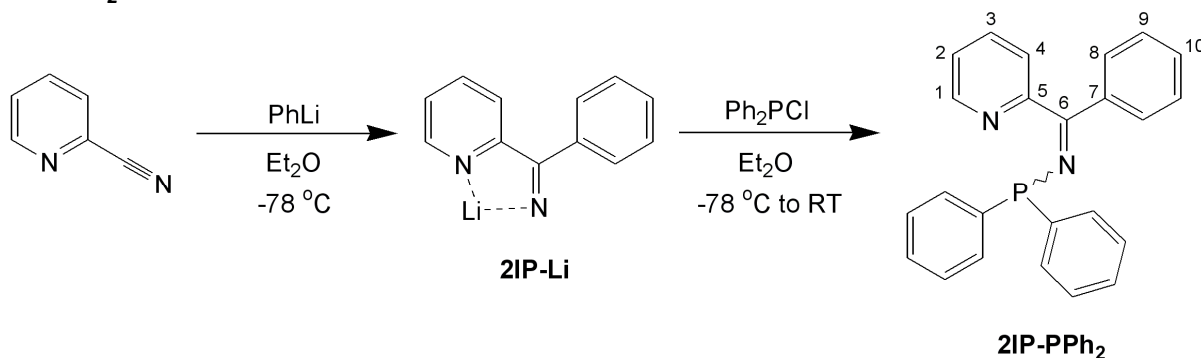
Chapter II

2. Synthesis and coordination of *N*-phosphino-pyridyl imines

2.1. Introduction: *N*-Diphenylphosphino-pyridyl imine, **2IP-PPh₂**

In 2005 Dyer *et al.* reported the synthesis and coordination chemistry of the heteroditopic *N*-diphenylphosphino-pyridyl imine ligand, **2IP-PPh₂** (Scheme 1).¹ The preparation of this chelating phosphorus-nitrogen scaffold was possible in a two-step, one-pot procedure, beginning with the treatment of 2-cyanopyridine with an equimolar quantity of phenyl lithium and gave the proposed reaction intermediate **2IP-Li**. Subsequent addition of the chlorodiphenylphosphine and work-up gave **2IP-PPh₂** as a yellow solid in reasonable yield (45 %).¹

Scheme 1: Synthesis and atom numbering scheme of the N-phosphino-pyridyl imine ligand 2IP-PPh₂.^{1*}

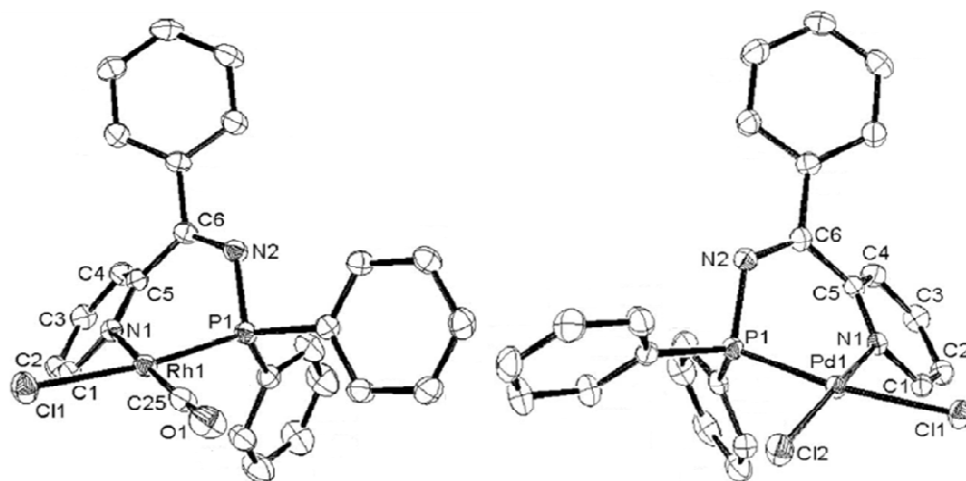


Complexation of the ligand **2IP-PPh₂** to palladium and platinum dichloride fragments resulted in its κ^2 -*P,N* binding coordination to the transition metal, something established by

* The geometry of the imine fragment of the *N*-phosphino-pyridyl imines is arbitrary in all figures

both NMR spectroscopic and X-ray diffraction studies (Figure 1).¹ In addition κ^2 -*P,N*-chelation was also established for the complex $[\text{RhCl}(\text{CO})(\kappa^2\text{-P,N-2IP-PPh}_2)]$, synthesised by combination of the ligand **2IP-PPh₂** with $[\text{RhCl}(\text{CO})_2]_2$ in a 2 : 1 ratio.¹

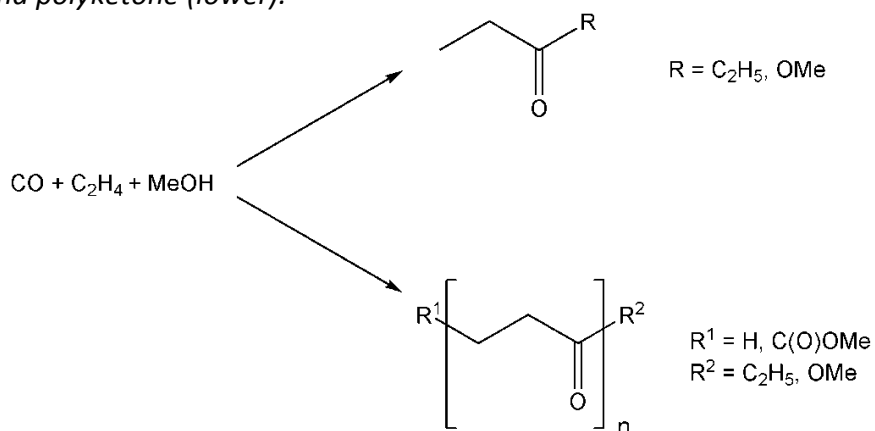
Figure 1: Molecular structures of $[\text{RhCl}(\text{CO})(\kappa^2\text{-P,N-2IP-PPh}_2)]$ (left) and of $[\text{PdCl}_2(\kappa^2\text{-P,N-2IP-PPh}_2)]$ (right) (Thermal ellipsoids set at 50 % level) reported by Dyer et al.¹



2.1.1. The application of **2IP-PPh₂** as a palladium scaffold in methoxycarbonylation studies

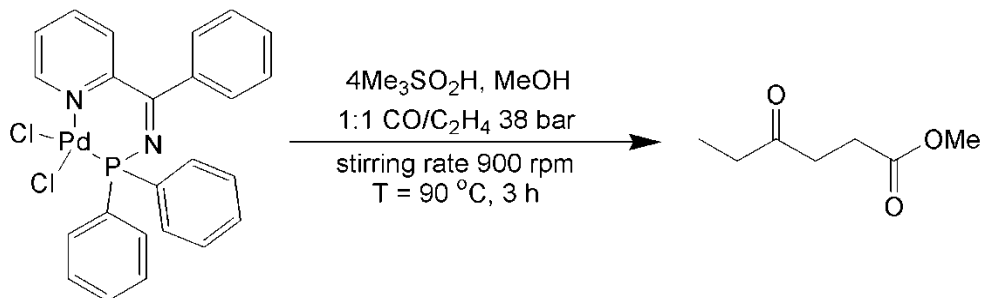
Palladium-catalysed co-oligomerisation of carbon monoxide and ethylene has been studied in detail, primarily with phosphorus ligated species, which produce monomeric, oligomeric and polymeric organic products depending upon the nature of the phosphine ligand (Scheme 2).^{2,3} Of these possible products, the low molecular weight oligomers comprising alternating units of carbon monoxide and ethylene are a common objective of researchers due to their potential as economically and environmentally favourable solvents.²

Scheme 2: The formation of the common methoxycarbonylation products, methyl propanoate (upper) and polyketone (lower).



In spite of extensive research into alkoxycarbonylation reactions the production of low molecular weight oligomers is still a challenge, with the majority of systems studied giving either polyketones or methyl propanoate.^{4,5} For this reason the pro-initiator [PdCl₂(κ²-*P,N*-**2IP-PPh**₂)] is of interest, since this complex exhibits an unprecedented selectivity for a single low molecular weight oligomer.¹ Alkene hydrocarboxylation studies using CO and ethylene (1:1, 30 bar) gave the exclusive formation of the methyl ester of 4-oxo-hexanoic acid with an activity of *ca.* 8–9 g {mol Pd}⁻¹ bar⁻¹ h⁻¹ (Scheme 3).¹ This unusual selectivity is attributed, in part, to the flexible bite angle and framework of the ligand, but the exact relationship between the ligand structure and resultant oligomer formation is unclear.

*Scheme 3: Selective methoxycarbonylation of ethylene in methanol producing the methyl ester of 4-oxo-hexanoic acid by use of the pro-initiator [PdCl₂(κ²-*P,N*-**2IP-PPh**₂)] reported by Dyer et al.¹*



2.2. Synthesis of diphenylphosphino(phenyl pyridin-2-yl)amine variants

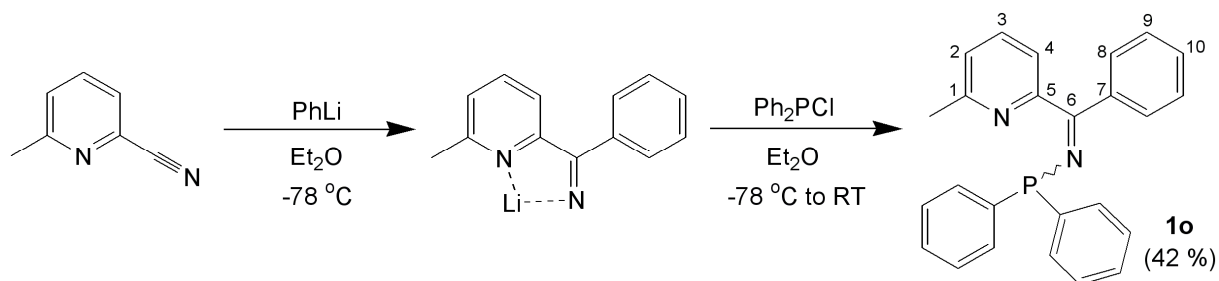
2.2.1. Variation of the pyridyl ring of 2IP-PPh₂

The proposed correlation between the structure of the **2IP-PPh₂** ligand and the selectivity to the single oligomer produced in the methoxycarbonylation catalysis invited further study of the *N*-phosphino-pyridyl imine framework in the coordination sphere of palladium.⁷ Therefore a number of variants of the **2IP-PPh₂** scaffold were synthesised with the aim of investigating their differing properties and also their potential future application in methoxycarbonylation. It was thought that slight variations in the ligand structure could affect the catalytic activity or selectivity and, therefore, aid in the understanding of the production of 4-oxo-hexanoic acid by the pro-initiator [PdCl₂(κ^2 -*P,N*-**2IP-PPh₂**)].¹

With the above objectives in mind, the synthesis of the *N*-phosphino-pyridyl imines **1o-6o**[†] was undertaken, giving a range of bidentate P[^]N scaffolds with differing steric and electronic properties. The first ligand to be synthesised was **1o**, which in comparison to **2IP-PPh₂**, has an *ortho*-methyl group on the heterocyclic ring, something that increases the steric bulk adjacent to this nitrogen donor atom. It was envisaged that this modification may enhance the lability of the pyridyl nitrogen of **1o** relative to that of **2IP-PPh₂**. Target **1o** was prepared using a modification of the original synthesis of **2IP-PPh₂** by the use of the commercially available substrate 6-methyl-2-cyanopyridine. Subsequently, compound **1o** was obtained in moderate yield (42 %) as a viscous oil.

[†] The letter **o** is added to the labelling of the *N*-phosphino-pyridyl imine ligands to denote their 'open' structural motif. This notation is necessary in later Chapters (III, IV and V) and is therefore used throughout this thesis.

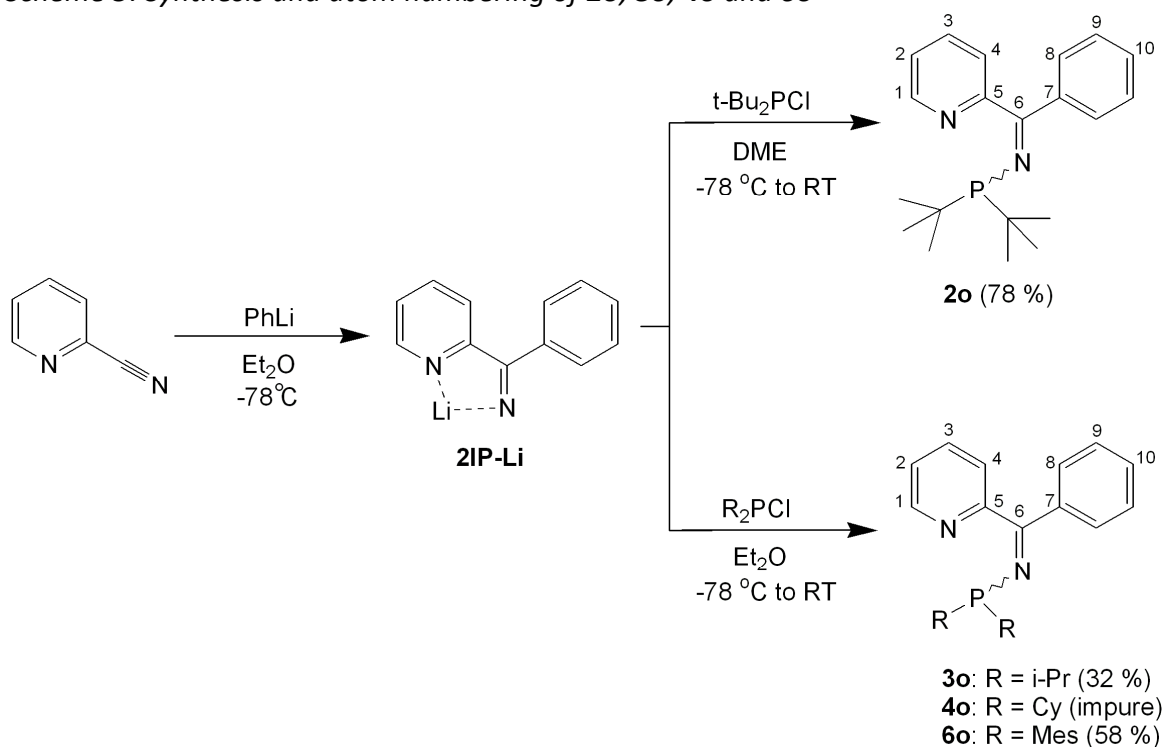
Scheme 4: Synthesis and atom numbering of **1o**



2.2.2. Variation of the P-substituents of 2IP-PPh₂

The use of a different chlorophosphine in the final step allowed various substituents to be introduced at the phosphorus atom of the *N*-phosphino-pyridyl imine. Thus, the compounds **2o**, **3o**, **4o** and **6o** were synthesised in a ‘one-pot’ procedure by a variation of the method for the preparation of **2IP-PPh₂** (Scheme 1 and Scheme 5). The *N*-dialkylphosphino-pyridyl imine ligands (**2o**, **3o** and **4o**) were of particular interest, as the increase in steric bulk and electronic donation should result in a significant deviation in the molecular structures of their palladium dichloride complexes, with respect to [PdCl₂(κ²-*P,N*-**2IP-PPh₂**)].

Scheme 5: Synthesis and atom numbering of **2o**, **3o**, **4o** and **6o**



For the synthesis of the ligands **3o**, **4o**, and **6o** diethyl ether was found to be a suitable solvent, but a change to dimethoxyethane (DME) as the reaction medium was required for compound **2o**. The use of DME as a solvent for promoting the reactivity of lithium reagents by de-aggregation is well documented.⁶ The reaction of t-Bu₂PCl to form **2o** doubtless requires a more reactive lithium species due to the increased steric bulk around the P-Cl fragment, relative to that encountered in the synthesis of **2IP-PPh₂**, *etc.*

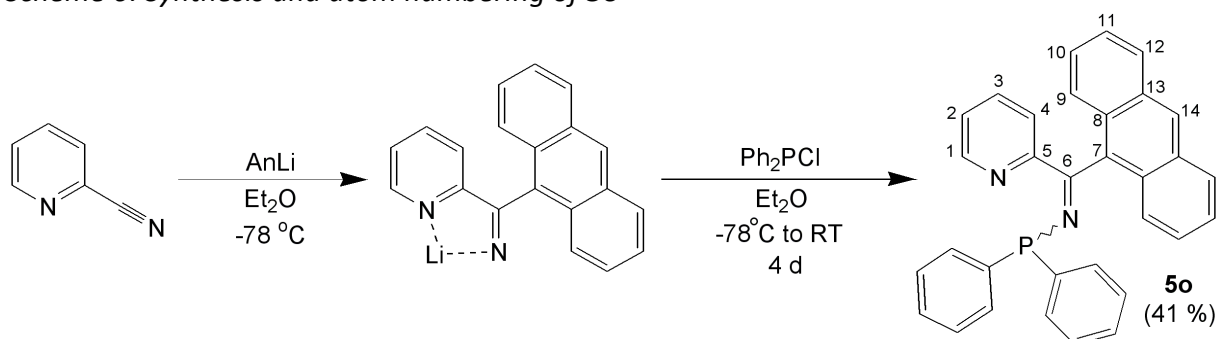
The *N*-dialkylphosphino-pyridyl imines were obtained in notably different forms. The ligand **2o** was isolated as an orange-red semi-crystalline solid in good yield (78 %). In contrast, compound **3o** was isolated as a viscous oil (32 %). The oily nature of **3o** is proposed to arise from the presence of flexible aliphatic groups, combined with the lower molecular weight of the molecule with respect to **2o**. The reaction to form the dicyclohexylphosphino analogue **4o**, was also less successful than that for the synthesis of **2o**, giving only a crude product that was estimated to be of approximately 90 % purity by ³¹P NMR spectroscopy; as a result, full characterization of this compound was not achieved. In spite of this impurity present in samples of ligand **4o**, its complexation to palladium dichloride could be achieved and gave rise to the desired complex (*vide infra*).

The *N*-dimesitylphosphino-pyridyl imine ligand **6o** was synthesised by reaction of dimesitylchlorophosphine, prepared by the method of Bokanov *et al.*⁷ by M. J. Hanton, with **2IP-Li** (Scheme 5). The work-up gave a yellow solid, **6o**, free from dimesitylchlorophosphine oxide, an impurity often present in dimesitylchlorophosphine by virtue of the experimental methodology employed for its preparation. The isolated yield of **6o** was found to be reasonable (58 %) and the compound was predicted to be a good contrast to the bulky, but highly electron rich ligand **2o**.

2.2.3. Variation of the phenyl ring of 2IP-PPh₂

The final variation of the *N*-phosphino-pyridyl imine frame undertaken was the alteration of the backbone phenyl moiety. Such modification is of interest since it has been proposed by Dyer *et al.* that the proximity of this phenyl group to the pyridyl ring is one of the causes of chain termination in the methoxycarbonylation process, which gives rise to 4-oxo-hexanoic acid. The proximity of the two aryl rings results in an unfavourable steric interaction between the pyridyl and phenyl moieties (analogous to the Perri effect) that induce a twisting of the P-N metal scaffold.¹ It was therefore envisaged that increasing the size of the aryl group could induce a greater twisting of the aryl ring relative to the pyridine moiety in the ligand and potentially alter the catalytic results observed. Hence, the introduction of an anthracenyl group in place of a phenyl ring was sought to create a more twisted framework when ligated to palladium.

Scheme 6: Synthesis and atom numbering of **5o**



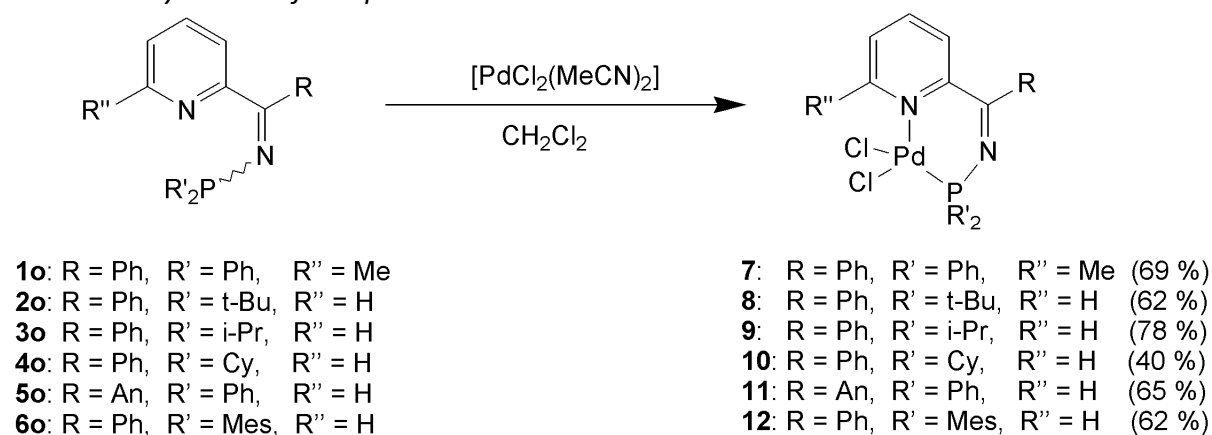
The anthracenyl-containing compound **5o** was synthesised by the addition of anthracenyl lithium⁸ to 2-cyanopyridine to form the lithium intermediate, and subsequent addition of chlorodiphenylphosphine (Scheme 6). It was found that stirring for four days was necessary for the reaction to reach completion, significantly longer than for the synthesis of **2IP-PPh₂** (18 h).¹ This is, in part, attributed to a lower solubility of the anthracenyl-substituted lithium intermediate relative to that of the phenyl derivative, something which slows its reaction with the chlorophosphine. The yield for **5o** was moderate, 41 %, but nevertheless comparable to that reported for **2IP-PPh₂** (45 %).¹

2.3. Complexation of the diphenylphosphino(phenyl pyridin-2-yl)amine variants to palladium dichloride

2.3.1. Coordination of the ligands 1o-6o, to give the palladium dichloride complexes 7-12

The complexes **7-12** were prepared by reaction of the P^N ligands **1o-6o** with bis(acetonitrile) palladium dichloride (Scheme 7). The displacement of coordinated acetonitrile by a bidentate P^N ligand is expected by virtue of the chelate effect and the preference of palladium for a soft donor phosphorus atom. This Pd(II) precursor was chosen in preference to the cyclooctadiene-ligated palladium dichloride complex due to the ease of displacement of the monodentate acetonitrile ligands. The complexes **7-9**, **11**, and **12** were all obtained as yellow or orange solids, in good yields of 60 – 80 %. The preparation of **10**, however, was achieved with a poorer isolated yield (48 %), attributed to the impure nature of the ligand **4o**, something which necessitated the recrystallisation of **10**. The structure of each complex was attributed on the basis of a combination of ^1H , ^{31}P and $^{13}\text{C}\{^1\text{H}\}$ NMR spectroscopies, elemental analysis and, where possible, X-ray structure determination.

Scheme 7: Synthesis of complexes **7-12**

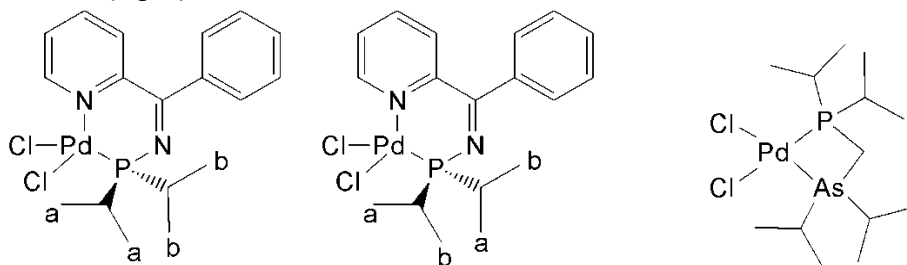


2.3.2. Solution state NMR spectroscopic studies of complexes 7-12

Following coordination of the ligands **10-60** to palladium dichloride their ^{31}P NMR resonances were noted to have shifted to higher frequency by 28 – 37 ppm relative to the free ligand, in agreement with the shift observed for **2IP-PPh₂** when coordinated to the PdCl_2 fragment (from 37.6 ppm to 66.8 ppm in CDCl_3).¹ The ^1H and $^{13}\text{C}\{^1\text{H}\}$ NMR spectra of two complexes, **9** and **10**, revealed that the two substituents at phosphorus were inequivalent in contrast to the equivalent phenyl groups noted for $[\text{PdCl}_2(\kappa^2\text{-P}, N\text{-2IP-PPh}_2)]$ likely due to the increased steric bulk of the substituents.^{1†}

In the ^1H NMR spectrum of complex **9** two sets of doublets of doublets were observed for the methyls of the isopropyl groups. Acquisition of the $^1\text{H}\{^{31}\text{P}\}$ NMR spectrum simplified the resonances to two doublets, and allowed the determination of the $^3J_{\text{PH}}$ coupling constants for the CH_3 protons. These coupling constants were found to be 17 and 19 Hz, which are similar in magnitude to those reported for the $i\text{-Pr}_2\text{P}$ groups of the known complex $[\text{PdCl}_2\{\kappa^2\text{-P,As-}\{(i\text{-Pr})_2\text{PCH}_2\text{As}(i\text{-Pr})_2\}\}]$, which exhibits a $^3J_{\text{PH}}$ coupling of 18 Hz for the methyl protons.⁹ For complex **9**, the $^1\text{H}\{^{31}\text{P}\}$ NMR spectrum displayed two doublets for the methyls of the isopropyl groups, *i.e.* two sets of inequivalent methyl protons. This can result from either two inequivalent isopropyl groups or inequivalent methyl substituents within isopropyl groups (see Figure 2).

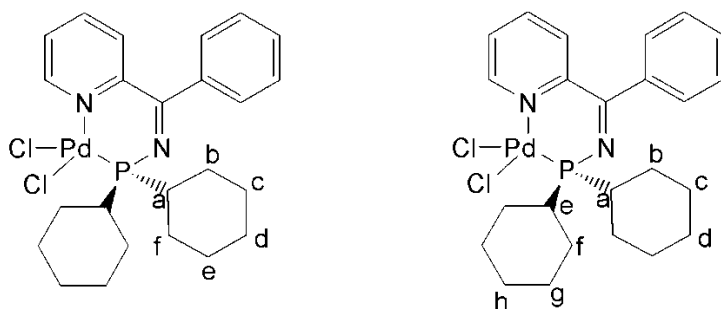
Figure 2: Diagram showing the assignment of the inequivalent methyl resonances in the ^1H NMR spectrum of **9** (left) and the compound $[\text{PdCl}_2\{\kappa^2\text{-P,As-}\{(i\text{-Pr})_2\text{PCH}_2\text{As}(i\text{-Pr})_2\}\}]$ reported by Werner (right)⁹



[†] For complexes **7** and **11** it is unclear whether the phenyl rings are equivalent in the ^1H NMR spectrum due to the complexity of the spectra.

In the $^{13}\text{C}\{^1\text{H}\}$ NMR spectrum of complex **10** the cyclohexyl groups were observed to be inequivalent, and is attributed to their steric bulk that results in slow rotation around the phosphorus-carbon bonds, something not observed for the smaller phenyl rings in $[\text{PdCl}_2(\kappa^2\text{-}P,N\text{-2IP-PPh}_2)]$.¹ The cyclohexyl groups of complex **10** give rise to five doublets and one singlet by $^{13}\text{C}\{^1\text{H}\}$ NMR spectroscopy. This number of resonances cannot be explained by two completely inequivalent cyclohexyl ring environments, something that would give rise to potentially eight signals (see Figure 3).

Figure 3: Possible explanations for the observed inequivalent carbon resonances in the $^{13}\text{C}\{^1\text{H}\}$ NMR spectrum of **10**. ‘Side-side’ inequivalence giving two *ortho* and two *meta* carbon environments within the cyclohexyl ring (left) and inequivalence between each cyclohexyl ring (right).



A possible explanation of the complexity of the recorded $^{13}\text{C}\{^1\text{H}\}$ NMR spectrum of **10** is that the ‘sides’ of the cyclohexyl rings are inequivalent with two chemical environments for each of the *ortho* and *meta* carbons within each ring (see Figure 3), something caused by hindered rotation about the P–C bonds. Only one of the cyclohexyl carbon resonances is recorded as a singlet in the $^{13}\text{C}\{^1\text{H}\}$ NMR spectrum for **10** and is attributed to the *para* carbon, existing in a single chemical environment which is consistent with side-side inequivalence. In addition, a single environment is noted for the *ipso* carbon with a $^1J_{\text{PC}}$ coupling constant of 36 Hz being determined.¹⁰

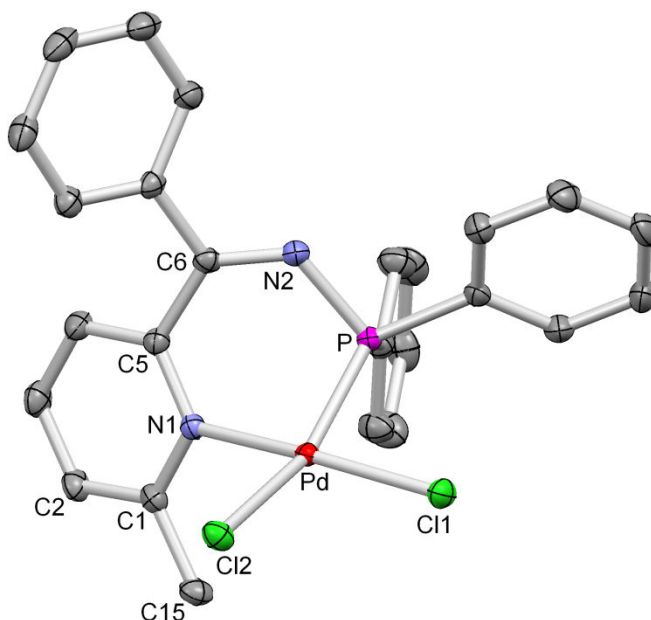
2.3.3. Crystallographic studies of palladium dichloride complexes 7 and 10-12

2.3.3.1. X-ray diffraction study of complex 7

Single crystals of complex **7** suitable for an X-ray crystal structure determination were grown from a cooled, saturated deuteriochloroform solution. As expected, the X-ray molecular structure confirms that the palladium geometry is square planar and that the ligand binds in a bidentate fashion through the phosphorus centre and the pyridyl nitrogen. The electronic asymmetry of the bidentate chelate induces inequivalence in the two Pd–Cl bond distances due to the differing *trans* effect of the phosphorus and nitrogen donors. The two palladium–chloride bond distances of complex **7** differ by 0.13 Å, with the chloride (Cl2) *trans* to phosphorus having the longer bond.

Figure 4: Molecular structure of **7**·4CDCl₃, with selected bond lengths (Å) and angles (°). (Thermal ellipsoids set at 50 % level). Hydrogen atoms and solvent molecules are omitted for clarity.

Pd-P	2.1932(5)
Pd-N1	2.0756(14)
Pd-Cl1	2.2820(5)
Pd-Cl2	2.4147(5)
P-N2	1.6914(16)
N1-C1	1.356(2)
N2-C6	1.287(2)
C5-C6	1.504(2)
N1-C5	1.356(2)
Cl1-Pd-Cl2	91.702(17)
P-Pd-N1	84.45(4)
Cl1-Pd-N1	92.83(4)



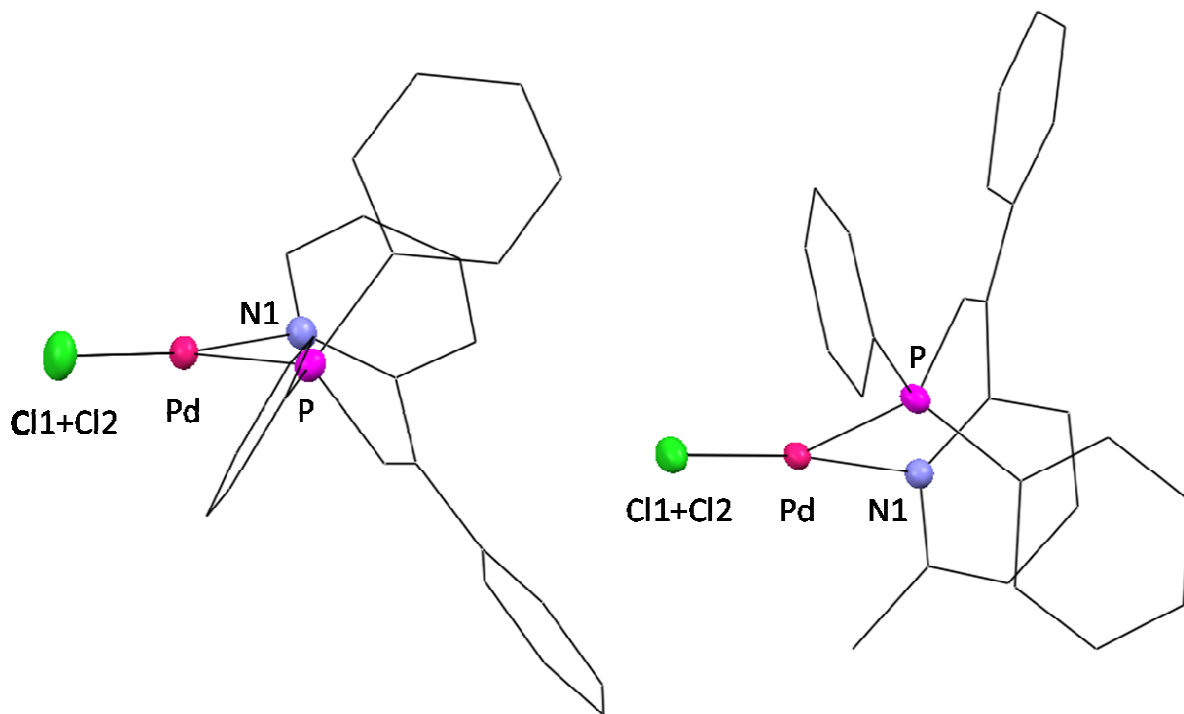
The complexes $[\text{PdCl}_2(\kappa^2\text{-P,N-2IP-PPh}_2)]$ and **7** are differentiated by the presence of an *ortho*-methyl group on the pyridine ring of the latter and it was hoped that the introduction of this substituent would increase the lability of the pyridyl nitrogen in solution. The cause of this greater lability would be an unfavourable steric interaction between the methyl group and the palladium dichloride fragment, something that was expected to be reflected in the X-ray molecular structure.

*Table 1: Comparison of selected bond distances and angles for the complexes $[\text{PdCl}_2(\text{2IP-PPh}_2)]$ and **7**.¹*

	Pd-N1 (Å)	Pd-P (Å)	Cl1-Pd-Cl2 (°)	P-Pd-N1 (°)
$[\text{PdCl}_2(\text{2IP-PPh}_2)]$	2.0610(14)	2.1983(5)	92.021(16)	83.78(4)
7	2.0756(14)	2.1932(5)	91.702(17)	84.45(4)

A comparison of the X-ray molecular structures of $[\text{PdCl}_2(\kappa^2\text{-P,N-2IP-PPh}_2)]$ and **7**, however, reveals only minor differences in the bond lengths, accompanied by a change in the P[^]N bite angle of the *N*-phosphino-pyridyl imine framework of less than one degree (Table 1).¹ In spite of these negligible differences, there is a notable distortion of the square planar geometry of the palladium(II) centre. In an ideal square planar configuration, the atoms bonded *trans* to one another at the palladium centre would be expected to exhibit an atom-Pd-atom angle of 180 °.¹¹ In $[\text{PdCl}_2(\kappa^2\text{-P,N-2IP-PPh}_2)]$ there is little deviation from this ideal square planar configuration with a P-Pd-Cl1 angle of 172.287(17) ° and N2-Pd-Cl1 angle of 173.10(4) ° (Figure 5).¹ This is in marked contrast to complex **7**, which exhibits a P-Pd-Cl1 angle of 159.346(18) °, although the N2-Pd-Cl1 angle is virtually the same as that displayed by $[\text{PdCl}_2(\kappa^2\text{-P,N-2IP-PPh}_2)]$ (172.21(4) °). Defining the PdCl₂ fragment as a plane for both complexes **7** and $[\text{PdCl}_2(\kappa^2\text{-P,N-2IP-PPh}_2)]$ allows the angle between the plane of the PdCl₂ core and the plane of the pyridine ring to be calculated, giving values of 51 ° and 71 ° being obtained for each complex, respectively.¹ From these large differences in the structures of **7** and $[\text{PdCl}_2(\kappa^2\text{-P,N-2IP-PPh}_2)]$ it suggests that there is a significant interaction between the *ortho*-methyl group and the palladium dichloride core.

Figure 5: Comparison of the X-ray molecular structures of $[\text{PdCl}_2(\kappa^2\text{-P,N-2IP-PPh}_2)]$ reported by Dyer¹ and complex **7**. The complexes are drawn with Cl1 and Cl2 eclipsed to present the deviation of P and N1 from the plane of the PdCl_2 fragment.



2.3.3.2. X-ray diffraction studies of complexes **10** and **12**

The determination of the molecular structures of **10** and **12** by X-ray diffraction was undertaken to allow a comparison to be made with that of $[\text{PdCl}_2(\kappa^2\text{-P,N-2IP-PPh}_2)]$. Subsequently, a study can be made to explore the structural impact of the modifications made in the P[^]N-scaffold. In particular, analysis of the Pd-Cl2 bond distances in each of the three complexes $[\text{PdCl}_2(\kappa^2\text{-P,N-2IP-PPh}_2)]$, **10** and **12** allows a qualitative assessment of the strength of donation from the different phosphorus moieties, by virtue of the *trans* influence (see Chapter I).¹² In this series, the Pd-Cl2 bond distance is observed to lengthen in the order $[\text{PdCl}_2(\kappa^2\text{-P,N-2IP-PPh}_2)] < \mathbf{12} < \mathbf{10}$, something that reflects the concurrent increase in the

Lewis basicity of the phosphorus centre (Table 2)¹ and this trend is in agreement with the Tolman electronic parameter (Table 3).¹³

Table 2: Comparison of the Pd-Cl bond lengths that lie trans to phosphorus in the complexes $[\text{PdCl}_2(\kappa^2\text{-P,N-2IP-PPh}_2)]$,¹ **12** and **10**

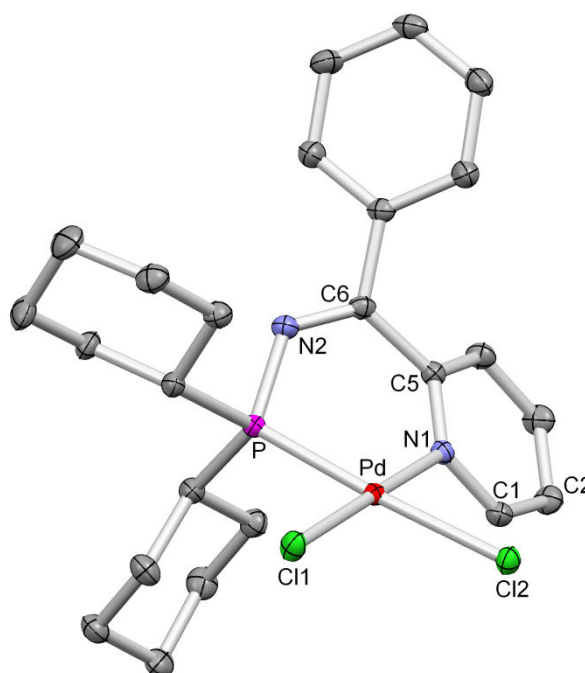
	$[\text{PdCl}_2(\kappa^2\text{-P,N-2IP-PPh}_2)]$	12	10
P-Cl2 (Å) (<i>trans</i> to P)	2.3813(4)	2.3942(10)	2.4042(6)

Table 3: Comparison of the Tolman electronic parameter, CO stretching frequency in $[\text{Ni}(\text{CO})_3(\text{PR}_3)]$, for phosphines analogous to the phosphorus moieties of complexes $[\text{PdCl}_2(\kappa^2\text{-P,N-2IP-PPh}_2)]$, **12**[§] and **10**¹³

	PPh_3	$\text{P}(p\text{-C}_6\text{H}_4\text{Me})_3$	PCy_3
ν (cm^{-1})	2068.9	2066.7	2056.4

Figure 6: Molecular structure of **10**. CH_2Cl_2 , with selected bond lengths (Å) and angles (°). (Thermal ellipsoids set at 50 % level). Hydrogen atoms and solvent molecules are omitted for clarity.

Pd-P	2.2061(6)
Pd-N1	2.0693(17)
Pd-Cl1	2.2984(7)
Pd-Cl2	2.4042(6)
P-N2	1.6895(18)
N1-C1	1.349(3)
N2-C6	1.272(3)
C5-C6	1.500(3)
N1-C5	1.352(3)
Cl1-Pd-Cl2	90.25(3)
P-Pd-N1	88.04(5)
C21-P-C31	107.63(10)

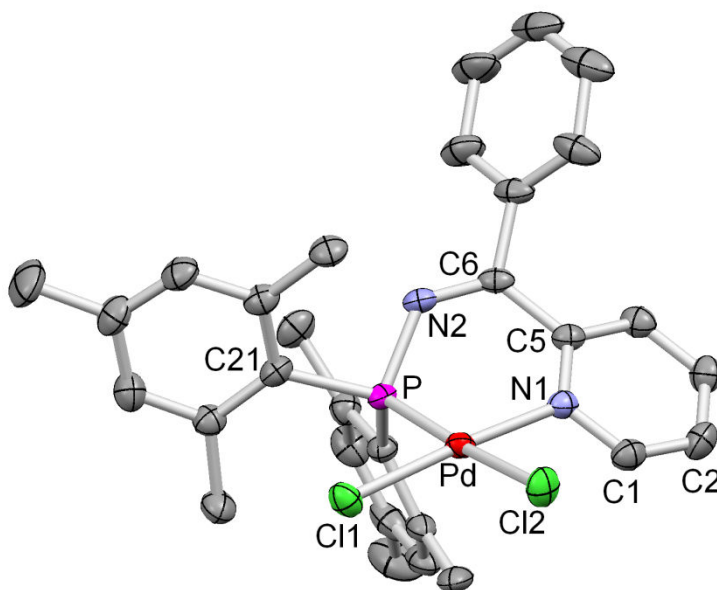


[§] The electronic parameter for $\text{P}(\text{Mes})_3$ is not reported by Tolman, therefore the value for $\text{P}(p\text{-C}_6\text{H}_4\text{Me})_3$ is presented as a reasonable substitute.

It is also worthy of note that replacing the phenyl rings of **2IP-PPh₂** by mesityl and cyclohexyl groups has a significant impact on the P[^]N bite angle in the *N*-phosphino-pyridyl imine chelated palladium dichloride complexes. The complexes **10** and **12** display notably wider P[^]N bite angles of 88.0 ° and 88.5 °, respectively, in comparison to [PdCl₂(κ²-*P,N*-**2IP-PPh₂**)], 83.8 °.¹ This difference is likely to result from the increased size of the mesityl and cyclohexyl substituents relative to that of the phenyl rings.

Figure 7: Molecular structure of **12**·(3.5CH₂Cl₂), with selected bond lengths (Å) and angles (°). (Thermal ellipsoids set at 50 % level). Hydrogen atoms and solvent molecules are omitted for clarity.

Pd-P	2.2072(10)
Pd-N1	2.077(3)
Pd-Cl1	2.2849(10)
Pd-Cl2	2.3942(10)
P-N2	1.695(3)
N1-C1	1.343(5)
N2-C6	1.278(5)
C5-C6	1.502(6)
N1-C5	1.357(5)
Cl1-Pd-Cl2	90.31(4)
P-Pd-N1	88.50(9)
C21-P-C31	109.29(18)



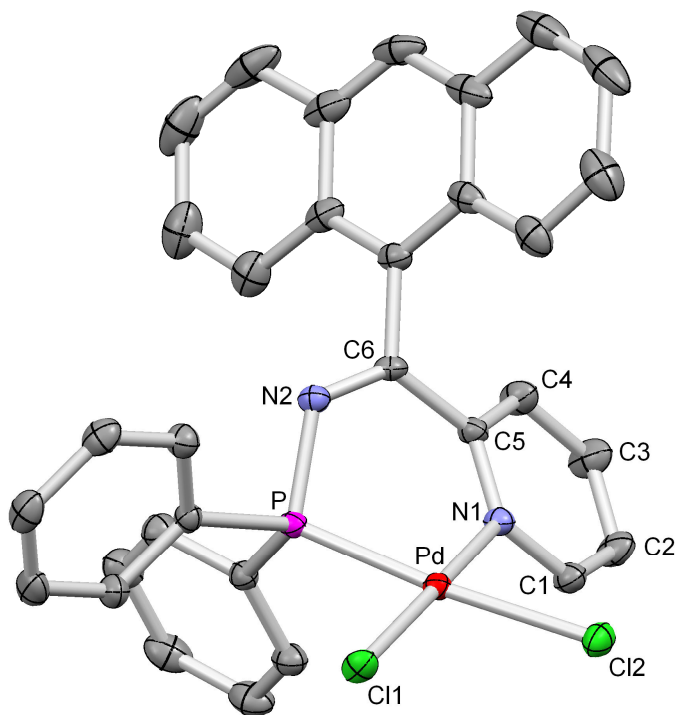
Together, these observations are significant since in methoxycarbonylation the angle between the two neutral donor atoms bound to the active palladium(II) species is believed to be crucial in determining the nature of the organic products obtained from the catalytic cycle.² A diphosphine binding in a *cis* conformation gives alternating ethylene-carbon monoxide copolymers (polyketones) under methoxycarbonylation conditions, whereas two monodentate phosphines, coordinated to palladium in a *trans* geometry, produce methyl propanoate.²

2.3.4. X-ray diffraction study of complex **11**

It was envisaged that the introduction of an anthracenyl group onto the backbone of the *N*-phosphino-pyridyl imine framework would result in greater steric hindrance between the pyridyl group and the aryl substituent compared to that observed in [PdCl₂(κ²-*P,N*-**2IP-PPh**₂)]. Consequently, the greater bulk of the anthracenyl unit should induce a greater twist in the ligand backbone (*cf.* Ph) in order to minimise this unfavourable interaction. Exactly this effect is observed and is reflected in the dihedral angles between the planes of the pyridyl and the aryl rings, which are 61.8 ° for [PdCl₂(κ²-*P,N*-**2IP-PPh**₂)] and 89.1 ° for complex **11**.¹ This increased twisting of 27.3 ° consequently causes the P[^]N bite angle to widen to 86.2 ° for complex **11**, relative to 83.8 ° determined for [PdCl₂(κ²-*P,N*-**2IP-PPh**₂)].¹

*Figure 8: Molecular structure of **11**.3CDCl₃, with selected bond lengths (Å) and angles (°). (Thermal ellipsoids set at 50 % level). Hydrogen atoms and solvent molecules are omitted for clarity.*

Pd-P	2.1905(7)
Pd-N1	2.0749(19)
Pd-Cl1	2.2985(6)
Pd-Cl2	2.3750(7)
P-N2	1.7095(19)
N1-C1	1.351(3)
N2-C6	1.278(3)
C5-C6	1.496(3)
N1-C5	1.362(3)
Cl1-Pd-Cl2	91.22(2)
P-Pd-N1	86.17(5)
P-N2-C6	106.61(7)



2.4. Summary

A range of variously-substituted *N*-phosphino-pyridyl imines have been synthesised and coordinated to palladium dichloride with the molecular structures of **7** and **10-12** having been determined by X-ray diffraction studies. Structural analyses reveal a close relationship between P^{AN} ligand composition and the structure of their complexes, which impacts in terms of P^{AN} bite angle (**10-12**), strength of electron donation from phosphorus (**10** and **12**), and distortion away from the square planar geometry at palladium determined for complex **7**.¹ From this study, it can be seen that the structures of complexes **7-12** differ quite significantly and, as a consequence, it is anticipated that their use as pro-initiators in the methoxycarbonylation of ethylene will potentially give rise to quite different catalytic results. It is envisaged that a range of catalytic results for the ligands **10-60** would allow a greater understanding of the relationship between the structure of the *N*-phosphino-pyridyl imine framework and the selectivity exhibited for the methyl ester of 4-oxo-hexanoic acid by the pro-initiator [PdCl₂(κ²-*P,N*-**2IP-PPh**₂)].¹ Future methoxycarbonylation studies of these *N*-phosphino-pyridyl imine complexes are therefore strongly encouraged.

¹ P. W. Dyer, J. Fawcett, M. J. Hanton, *J. Organomet. Chem.*, 2005, **690**, 5264.

² R. A. M. Robertson, D. J. Cole-Hamilton, *Coord. Chem. Rev.*, 2002, **225**, 67.

³ E. Drent, J. A. M. van Broekhoven, M. J. Doyle, *J. Organomet. Chem.*, 1991, **417**, 235.

⁴ P. Braunstein, M. D. Fryzuk, M. Le Dall, F. Naud, S. J. Rettig, F. Speiser, *Dalton Trans.*, 2000, 1067.

⁵ K. S. Coleman, M. L. H. Green, S. I. Pascu, N. H. Rees, A. R. Cowley, L. H. Rees, *Dalton Trans.*, 2001, 3384.

⁶ J. Claydon, '*Organolithiums: Selectivity for Synthesis*', Elsevier Science Limited, Oxford, 2002, p. 1 – 8.

⁷ A. I. Bokanov, N. A. Rozanel'skaya, B. I. Steanov, *J. Gen. Chem. USSR*, 1978, **48**, 1732.

⁸ J. Wesemann, P. G. Jones, D. Schomburg, L. Heuer, R. Schmutzler, *Chem. Ber.*, 1992, **125**, 2187.

⁹ U. Schmidt, K. Ilg, C. D. Brandt, H. Werner, *Dalton Trans.*, 2002, 2815.

¹⁰ B. F. G. Johnson, T. Khimyak, F. W. Wansel, G. Phillips, S. Hermans, J. R. Adams, *J. Cluster Sci.*, 2004, **15**, 315.

¹¹ D. F. Shriver, P. W. Atkins, '*Inorganic Chemistry*', 3rd ed., Oxford University Press, Oxford, 1999, p. 214.

¹² K. M. Anderson, A. G. Orpen, *Chem. Commun.*, 2001, 2682.

¹³ C. A. Tolman, *Chem. Rev.*, 1977, **77**, 313.

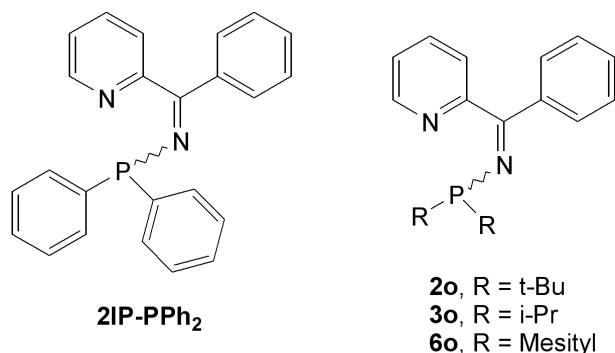
Chapter III

3. 1,1-bis(Diisopropylamino)-3-phenyl-1 λ^5 -[1,3,2]diazaphospholo [1,5-*a*]pyridine – synthesis, dual tautomeric forms and reactivity towards main group and transition metal compounds

3.1. Introduction

Previous work of the Dyer group¹ and subsequent work by this researcher (Chapter II), has shown that the *N*-phosphino-pyridyl imine ligand is an effective scaffold for late transition metals. These investigations focused primarily on diphenylphosphino(phenyl pyridin-2-yl methylene)amine, abbreviated to **2IP-PPh₂** (Figure 1). This compound was found to coordinate in a κ^2 -*P,N* binding mode to the late transition metal fragments Rh(I), Pd(II) and Pt(II). Moreover, it has been demonstrated that this ligand in combination with Pd(II) gives rise to systems that initiate highly chemo- and regio-selective hydroxycarbonylation of ethylene in methanol solvent (Chapter II).¹

Figure 1: The ligand **2IP-PPh₂** reported by Dyer (left)¹ and variants of the 2-iminopyridyl framework synthesised and described in Chapter II (right)



The proposed correlation between the structure of the **2IP-PPh₂** ligand and the selectivity in the methoxycarbonylation catalysis invited further study of the *N*-phosphino-pyridyl imine framework in the coordination sphere of palladium.¹ Therefore, a range of ligands with differing phosphorus substituents on the 2-iminopyridyl framework were synthesised (Figure 1 and Chapter II) and these compounds (**2o**, **3o** and **6o**) bear alkyl and aryl substituents on phosphorus and display an 'open' *N*-phosphino-

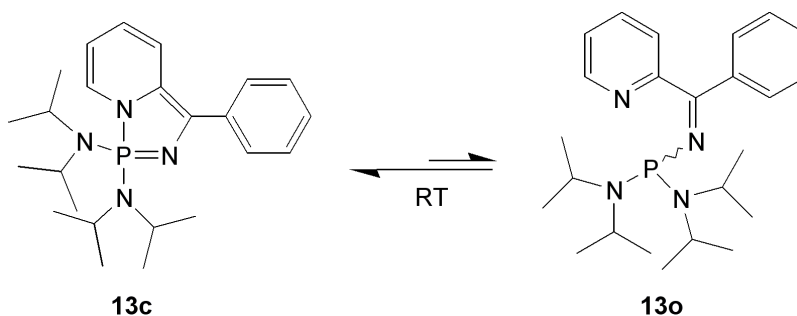
pyridyl imine structure analogous to that of **2IP-PPh₂**. It was of interest to extend this range of ligands to include amino groups on the phosphorus centre to see if this impacted on the outcomes of the hydroxycarbonylation process. The inclusion of amino groups was undertaken since they offer unusual steric and electronic demands, acting jointly as σ -electron-withdrawing and π -electron-donating substituents. Previous researchers have demonstrated the ability of these types of substituents, (R₂N)₂P, to stabilise unusual, often highly reactive systems through a combination of kinetic and electronic effects, for example, Bertrand and co-workers' stabilisation of carbenes by the use of 'push-pull' inductive and mesomeric effects.²

3.2.Synthesis and characterisation of the equilibrium mixture **13c/13o**

3.2.1. Introduction

For the 2-iminopyridyl framework the introduction of bis(diisopropylamino)substituents at the phosphorus centre, however, did not solely give the desired *N*-phosphino-pyridyl imine **13o**, but also the ring-cyclised diazaphosphole, **13c** (Scheme 1).^{*} These compounds are valence tautomers and found to be in dynamic equilibrium with each other by virtue of an intramolecular cyclisation process. Their synthesis and reactivity are described below.

*Scheme 1: Equilibrium between **13c** ('closed') and **13o** ('open')*

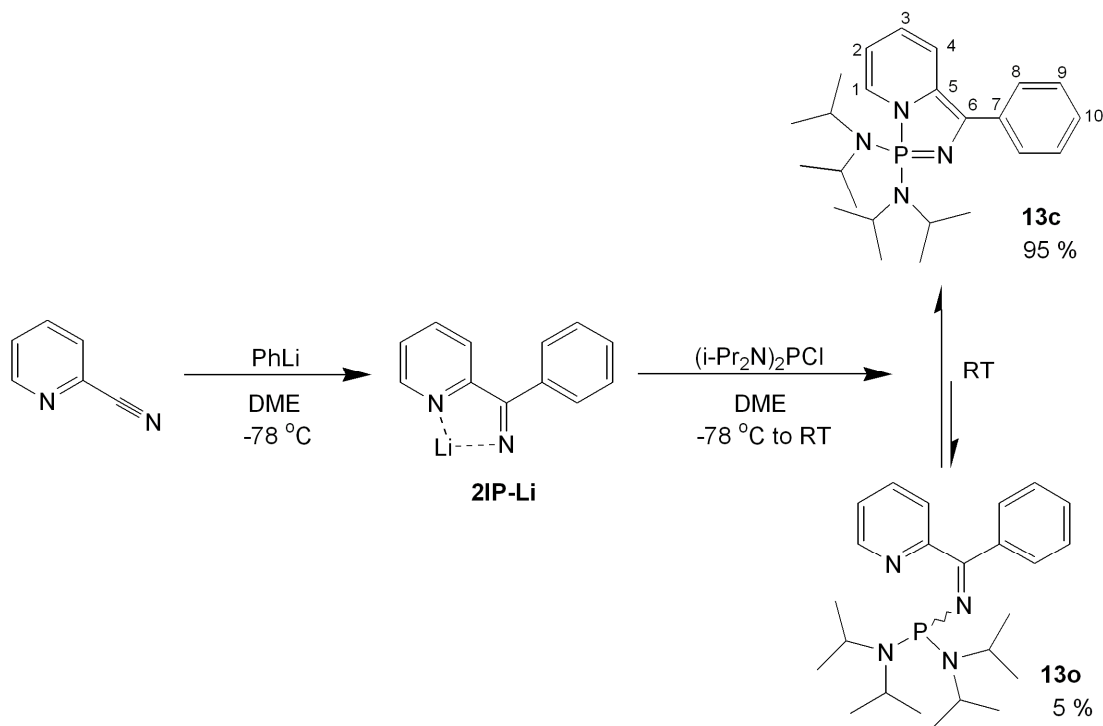


^{*} The tautomeric forms are ascribed the notation **13c** ('closed') and **13o** ('open'), **13c/13o** (equilibrium mixture) and **13** (a molecule in either the 'open' or 'closed' form).

3.2.2. Synthesis of **13c/13o**

The synthesis of the 2-iminopyridyl ligand, **2IP-PPh₂**, has been reported by the Dyer group and involved a two step reaction starting from 2-cyanopyridine, namely addition of phenyllithium across the cyano moiety, followed by electrophilic substitution with diphenylchlorophosphine.¹ This process was found to be a general route for the preparation of *N*-phosphino-pyridyl imines and was successful for the introduction of a variety of alkyl and aromatic groups on phosphorus (Chapter II). Therefore a similar approach was adopted for the attempted synthesis of **13o** (Scheme 2). In the first step 2-cyanopyridine is lithiated with phenyllithium at -78 °C resulting in addition across the triple bond generating a lithium intermediate, **2IP-Li**.

*Scheme 2: Synthesis, equilibrium and atom numbering scheme for **13c/13o***



Upon subsequent addition of bis(diisopropylamino)chlorophosphine to the lithium intermediate, **2IP-Li**, complete consumption of (i-Pr₂N)₂PCl was observed by ³¹P{¹H} NMR spectroscopy to give **13** (Scheme 2). Contrary to the synthesis of **2IP-PPh₂**, the reaction did not proceed in the solvent diethyl ether, something attributed to the less accessible P-

Cl bond, relative to Ph₂PCl, combined with the poor solubility of the chlorophosphine. The use of dimethoxyethane (DME), a well-established solvent and additive for the promotion of the reactivity of lithium compounds,³ was instead required for the generation of **13**. A brown solution was obtained from this attempted synthesis of **13o**, for which the solvent was removed *in vacuo* and resultant residue extracted with hexane giving a red solution. Cooling of this solution gave a crop of red crystals that were isolated in good yield (59 %) and gave elemental analyses consistent with an empirical formula of C₂₄H₃₇N₄P, *i.e.* compound **13**.

3.2.3. X-ray crystallographic study of **13c**

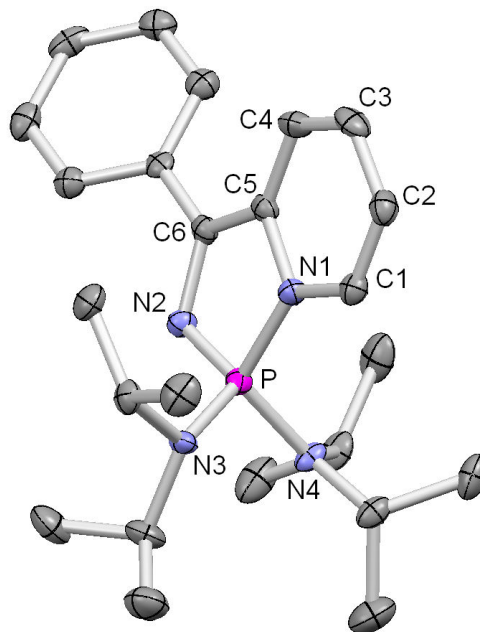
Recrystallisation of **13** from hexane gave deep red cuboidal crystals, from which single crystals suitable for an X-ray diffraction study were selected. The analysis revealed that the structure of the molecule was not the *N*-phosphino-pyridyl imine **13o**, the original target of the reaction. Instead, the crystalline material was revealed to be 1,1-bis(diisopropylamino)-3-phenyl-1λ⁵-[1,3,2]diazaphospholo[1,5-a]pyridine, **13c**, which can be considered to a valence tautomer of **13o** (Figure 2 and Scheme 2). This diazaphosphole **13c** can be considered to be the product of an intramolecular cyclisation of the *N*-phosphino-pyridyl imine **13o** and possible mechanisms for this interconversion are discussed in detail in section 3.2.7.

The diazaphosphole **13c** is shown to be comprised of two heterocyclic rings, which are near-coplanar (Figure 2). Although the central core is not aromatic it can be regarded as a conjugated 10π-system including the lone pair of N1. The bond distances P-N1 and P=N2 are 1.681(3) Å and 1.589(3) Å, respectively, and are consistent with single and double bonds.⁴ Together these data confirm that a true covalent bond does exist between phosphorus and the nitrogen of the six-membered ring (N1) and not just a weak donor-acceptor interaction. The exocyclic PN bond lengths, P-N3 and P-N4, are also consistent with that of single bonds.⁴ The fused rings of **13c** display a localised bonding motif of alternating single and double bonds as a consequence of the loss of the aromaticity of the pyridine.⁶ Bonding in the C4-C5-C6 fragment is partially allylic in

character with a contracted single C4-C5, 1.420(4) Å, and an elongated double bond C5-C6, 1.376(4) Å.

*Figure 2: Molecular structure of **13c**, with selected bond lengths (Å) and angles (°). Thermal ellipsoids set at 50 % level. Hydrogen atoms are omitted for clarity.*

P-N1	1.681(3)
P-N2	1.589(3)
N1-C5	1.442(4)
C5-C6	1.376(4)
C6-N2	1.399(4)
C1-C2	1.336(4)
N1-C1	1.399(4)
C2-C3	1.437(5)
C3-C4	1.353(4)
C4-C5	1.420(4)
P-N3	1.653(3)
P-N4	1.647(3)
N1-P-N2	97.41(14)
P-N1-C5	108.0(2)
N1-C5-C6	109.6(3)
C5-C6-N2	115.2(3)
C6-N2-P	109.6(2)
N3-P-N4	103.11(13)



It is also worthy of note that the phenyl ring of **13c** does not lie in the same plane as the two fused heterocycles in the X-ray molecular structure, orientated with a dihedral angle (C5C6C7C8) of 35.2°. Therefore the phenyl ring is not conjugated to the central core of the molecule, or at least not in the solid-state.

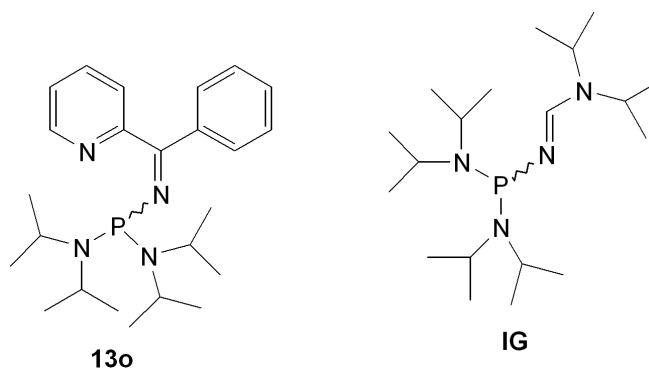
3.2.4. Solution-state NMR spectroscopic studies of **13c**/**13o**

Surprisingly, dissolution of crystalline **13c** and subsequent analysis by ^{31}P NMR spectroscopy revealed the presence of two species at 71.0 and 42.3 ppm (C_6D_6) in a ratio of 5 : 95 at ambient temperature. Further investigation of the ^1H , $^{13}\text{C}\{^1\text{H}\}$ and ^{31}P NMR spectroscopic data for the mixture revealed that the predominant species, giving rise to the singlet resonance at 42.3 ppm by ^{31}P NMR spectroscopy, is that of **13c**.

Unfortunately, the minor species present upon dissolution of **13c** exists as only 5 % of the mixture at ambient temperature, and hence could not be definitively assigned by

^1H and $^{13}\text{C}\{^1\text{H}\}$ NMR spectroscopies since its signals overlapped with the more intense signals of compound **13c**. It is logical, however, to assume that since the ^{31}P NMR spectroscopic chemical shift of the minor species (71.0 ppm) is close to that expected for a comparable *N*-bis(diisopropylamino)phosphino imine (see Figure 3: **IG** ^{31}P δ : 71.3)⁵ that this compound is the ‘open’ *N*-phosphino-pyridyl imine **13o**. From these data, it is therefore likely that open tautomer **13o** exists alongside the predominant **13c** tautomer in solution at ambient temperature.

Figure 3: The structure of compound **13o** (left) and that of a comparable *N*-bis(diisopropylamino)phosphino imine reported by Igau (right)⁵



Examination of the solution-state ^1H NMR spectroscopic data of the diazaphosphole **13c** confirmed the dearomatisation of the pyridine ring observed in the X-ray molecular structure. This was signified by a marked shift in the pyridyl proton resonances (expected 6.5 - 8.5 ppm)¹ to lower frequency (5.2 - 7.2 ppm) - typical of a conjugated alkenyl environment.^{6,7} This change was accompanied by the shift of the attached carbon resonances from 120 - 160 ppm to 107 - 127 ppm in the ^{13}C NMR spectrum of **13c**. The connectivity of the phosphorus to the nitrogen of the dearomatised pyridine was established by a distinctive $^3J_{\text{PH}}$ coupling to the proton of C1 observed in the ^1H NMR spectrum. The magnitude of this $^3J_{\text{PH}}$ coupling constant was revealed to be 5.6 Hz, which is typical for such an arrangement.⁸ Phosphorus couplings are also observed in the $^{13}\text{C}\{^1\text{H}\}$ NMR spectrum for C1 ($^2J_{\text{PC}} = 1.5$ Hz) and C2 ($^3J_{\text{PC}} = 5.8$ Hz). For the methyls of the isopropyl groups two different environments are observed in the ^1H and $^{13}\text{C}\{^1\text{H}\}$ NMR spectra, something which has been attributed to restricted rotation of the diisopropylamino substituents.

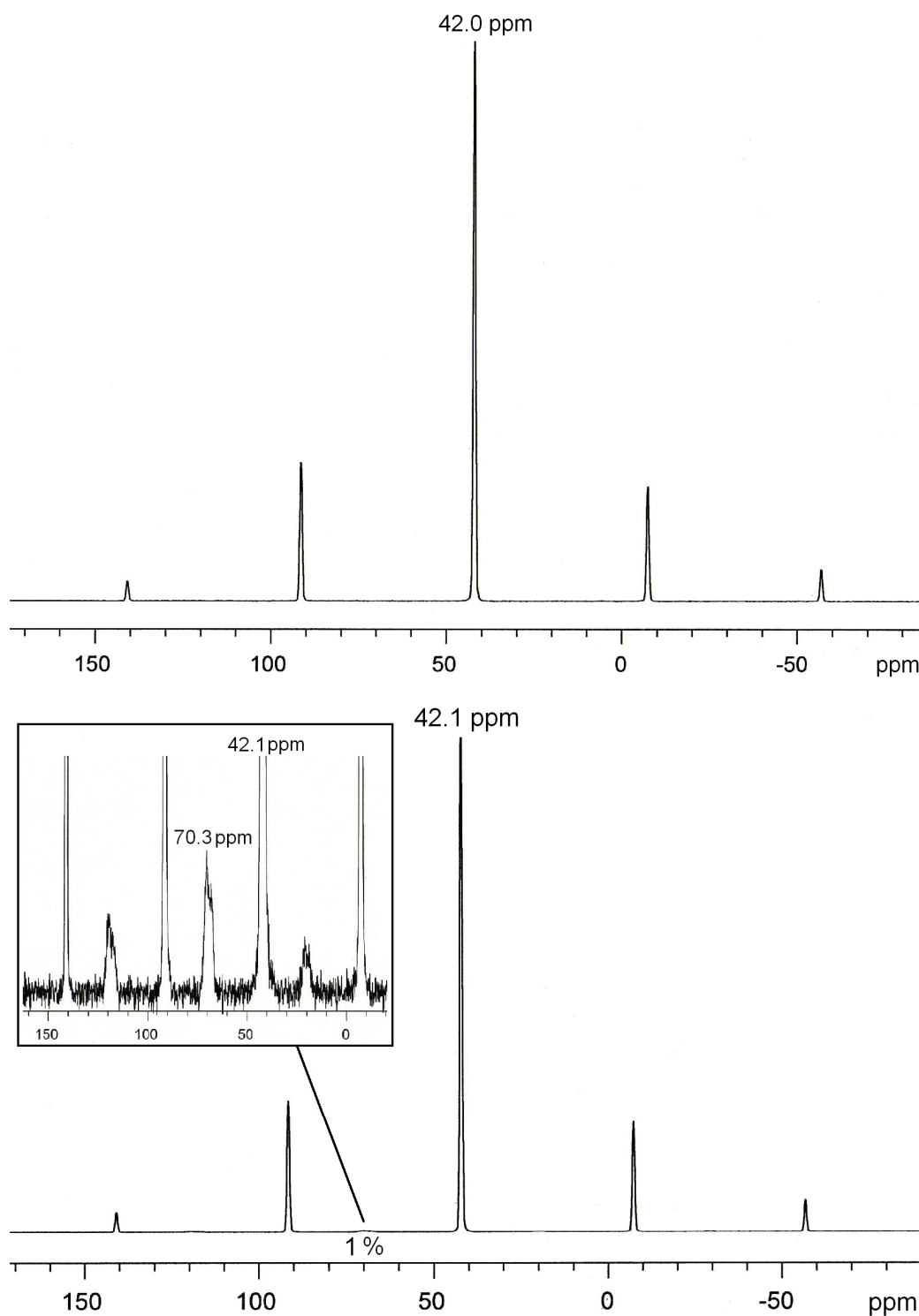
3.2.5. Solid-state NMR spectroscopic studies of **13c**/**13o**

It was next of interest to confirm that the X-ray molecular structure of **13c** was representative of the bulk sample, therefore a quantity (~ 100 mg) of the crystals was ground to a fine powder and the solid-state ^{31}P MAS NMR spectrum recorded using cross-polarisation (CP) (Figure 4).⁹ This approach was necessary as the ^{31}P nuclei, although having 100 % natural abundance with $I = \frac{1}{2}$, are only a minor component of the total sample and therefore spectral acquisition times can be long. The use of cross-polarisation reduces the time needed to acquire spectra with an acceptable signal to noise ratio.⁹ The technique transfers magnetisation from abundant spins (^1H) to the less abundant spins (^{31}P) giving an intensity gain of $\gamma_{\text{H}}/\gamma_{\text{P}}$, ($\gamma_{\text{H}}/\gamma_{\text{P}} = 26.8/10.8$).¹⁰

For the ground sample of crystalline **13c**, a single resonance was observed, with accompanying spinning sidebands, at 42.0 ppm, which corresponds very well to the chemical shift observed in solution for **13c**, 42.3 ppm (C_6D_6). No trace of isomer **13o** was detected, showing the crystalline solid to be pure **13c**. This was further verified by alteration of the spin rate, which moves the position of the spinning sidebands.⁹ Dissolution of crystalline **13c** gives rise to both **13c** and **13o** detected by solution-state NMR spectroscopy. The absence of **13o** in the solid-state ^{31}P NMR spectrum and observation of **13o** upon dissolution of pure **13c** suggests that a conversion of **13c** to **13o** may be occurring in solution.

To further explore this possible equilibrium between **13c** and **13o**, crystals of **13c** were dissolved and the solvent subsequently removed *in vacuo* to give an amorphous solid. Solid-state ^{31}P CP MAS NMR spectroscopy was conducted and the amorphous solid shown to be a mixture of **13c** and the now present **13o** (see Figure 4). Evidently dissolution of the crystals has allowed the regeneration of **13o** in solution. Since the ratio between **13c** and **13o** in solution is always recorded to be 95 : 5 (at 25 °C) respectively, it is necessary that conversion between isomers occurs in both directions (**13o** \rightarrow **13c** and **13c** \rightarrow **13o**), and therefore an equilibrium must exist between these valence tautomers.

Figure 4: Solid-state ^{31}P NMR spectra for recrystallised **13c** (top) and for a solid sample of **13c/13o** obtained from a solution of **13c/13o** by solvent removal in vacuo (bottom)



As stated, isomer **13o** was detected as a weak signal at 70.3 ppm in the ^{31}P NMR solid-state spectrum for a solid sample of **13c/13o**, in an approximate ratio of 1 : 99 (**13o** : **13c**), differing slightly from the ratio recorded in solution at ambient temperature (5 : 95).

This difference is potentially attributable to the temperature drop as solvent is removed resulting in the equilibrium being pushed towards the thermodynamically favoured isomer, **13c**. It is also possible that **13c** is less soluble than **13o** and therefore as **13c** precipitates from the solution the equilibrium is re-established by conversion of **13o** to **13c**.

3.2.6. Variable-temperature NMR spectroscopic studies on **13c/13o**

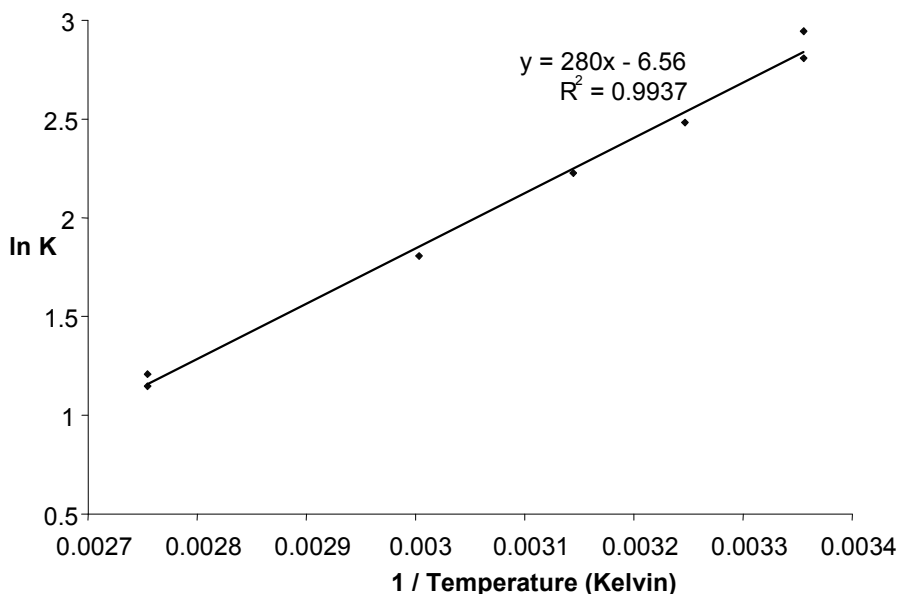
Variable-temperature (VT) solution-state ^{31}P NMR spectroscopy studies were also conducted to further investigate the equilibrium between the two isomers, **13c** and **13o**. These experiments were carried out in toluene over the temperature range 25 °C to 90 °C and show an increase in the proportion of isomer **13o** with increasing temperature. On warming from 25 °C to 90 °C the ratio of **13o:13c** changed from 5:95 to 25:75 illustrating that **13o** is the kinetically-favoured isomer and **13c** is the thermodynamic isomer. Recording the ratio at a range of temperatures (25, 35, 45, 60, 90 °C) allowed the value of K , the equilibrium constant, to be determined at each temperature.

A plot of $\ln K$ against $1/T$ allows the determination of the changes in enthalpy, ΔH , and entropy, ΔS , upon conversion of **13o** (reactant) to **13c** (product) by virtue of the thermodynamic equations in Figure 5. The intercept of this plot is equal to $\Delta S/R$ and gives a value for ΔS of $-51.8 \pm 2.6 \text{ J mol}^{-1} \text{ K}^{-1}$. Thus, isomer **13o** is entropically favoured over **13c**, which can be explained by the extra degrees of freedom gained upon ring opening. The gradient of the plot yields the value of ΔH to be $-22.4 \pm 0.4 \text{ KJ mol}^{-1}$ and in combination with ΔS allows the Gibbs free energy to be calculated by use of equation (2) (Figure 5). The change in the Gibbs free energy is temperature dependent and for the conversion of **13o** (reactant) to **13c** (product), at 298 K, is $-7.0 \pm 0.3 \text{ KJ mol}^{-1}$ reflecting the greater proportion of **13c** relative to **13o** observed at ambient temperature.

Figure 5: Thermodynamic equations (1) – (4) where G = Gibbs free energy, H = enthalpy, S = entropy, R = gas constant and T = temperature

- (1) $\Delta G = -RT \ln K$
- (2) $\Delta G = \Delta H - T\Delta S$
- (3) $-RT \ln K = \Delta H - T\Delta S$
- (4) $\ln K = \frac{\Delta S}{R} - \frac{\Delta H}{RT}$

Figure 6: Plot of $\ln K$ versus $1/\text{temperature}$ for the interconversion between **13c** and **13o**, where the isomer **13o** is considered to be the reactant and **13c** the product

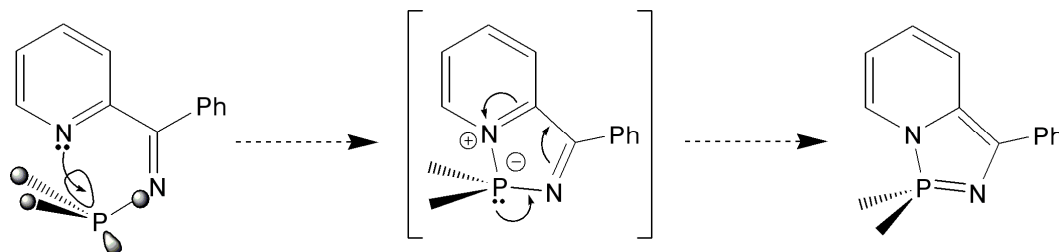


From the values of ΔH and ΔS it is possible to predict the equilibrium constant at different temperatures, and therefore the **13o:13c** ratio, with a calculated ratio of 0.2:99.8 at - 50 °C. In the VT-NMR experiment, however, on cooling to - 50 °C the quantity of **13o** only reduced to approximately 4 %, greater than the value predicted by the thermodynamic calculations. This discrepancy could potentially arise from a dramatic slowing of the exchange rate between **13o** and **13c**, as the temperature decreases, resulting in a ‘freezing out’ of the equilibrium process.

3.2.7. Possible mechanisms of interconversion of **13c**/**13o**

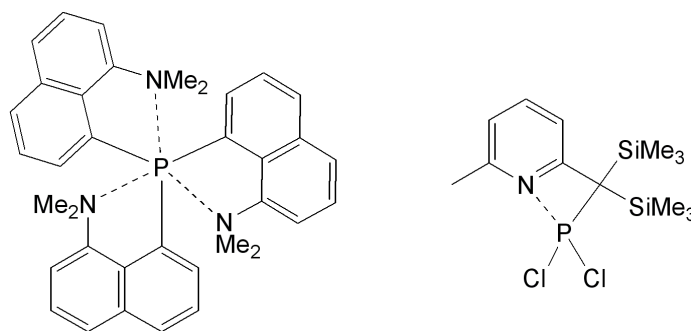
For the closure of **13o** to give **13c**, two possible mechanisms are suggested; step-wise nucleophilic attack (of the nitrogen lone pair on phosphorus) or a concerted 1,5-electrocyclisation-type process. For either mechanism, the reverse processes can be envisaged to regenerate **13o** from **13c**. In the step-wise mechanism, nucleophilic attack of the pyridyl nitrogen lone pair would occur at the LUMO of the phosphine fragment, approaching the more sterically encumbered face, the opposite face to that containing the phosphine lone pair (Scheme 3). Subsequent inversion of the phosphine and re-organisation of electrons would then occur to give the diazaphosphole structure of **13c**.

Scheme 3: The step-wise mechanism. Nucleophilic attack of the pyridyl nitrogen lone pair into the LUMO of the phosphine fragment of a generalised N-phosphino-pyridyl imine is followed by subsequent re-organisation of electrons to give the ‘closed’ diazaphosphole



Dative interactions are known between nitrogen and phosphorus centres with, for example, tris(8-dimethylamino-1-naphthyl)phosphine, synthesised by Corriu *et al.*, displaying weak interactions of ~ 2.83 Å (Figure 7).¹¹ A stronger dative pyridyl N-P(III) interaction, 2.238(1) Å, has been reported by Raston and co-workers which can be regarded as an “arrested” intermediate of a stepwise attack of the pyridyl nitrogen lone pair on phosphorus (Figure 7).¹²

Figure 7: Two examples of intramolecular dative P-N interactions reported by Corriu¹¹ (left) and Raston¹² (right)



An alternative tautomerisation mechanism possible for **13c/13o** is *via* a concerted electrocyclisation, a type of pericyclic reaction where a single new σ bond is generated by the rearrangement of electrons of a conjugated polyene to form a ring, or the reverse process whereby a σ bond is lost.¹³ Since, in **13o** the atoms that are involved in the cyclisation are not connected by a conjugated system this ring closure cannot be considered to be a true electrocyclisation. However, a concerted electrocyclisation-type ring closure involving the phosphorus lone pair and the C=N bonds of **13o** is feasible. In addition, it should be noted that all electrocyclisations are allowed with a thermal 6π -electron reaction predicted to occur in a disrotary fashion.¹³

To further explore the interconversion and possibly determine the existence of a transition state, a computational study was undertaken by researchers at the Université de Pau et des Pays de l'Adour.[†] DFT calculations performed at the B3LYP/6-31G** level closely reproduced the X-ray molecular structure and UV/vis spectrum of **13c**.[‡] However, modelling of the reaction from **13o** to **13c** showed no transition state, disavouring the step-wise nucleophilic attack mechanism, suggesting therefore that a type of electrocyclisation is more probable between **13o** and **13c**.

[†] The calculations in this chapter were carried out by Dr K. Miqueu and Dr J.-M. Sotiropoulos (Université de Pau et des Pays de l'Adour, France).

[‡] For a discussion of the molecular orbitals of **13c** and **13o** see section 3.3.1

3.2.8. Determination of the rate of interconversion between **13c** and **13o**

By solution-state NMR spectroscopy distinct signals for both **13o** and **13c** can be detected and therefore the rate of interconversion is slow on the NMR spectroscopy timescale. If the rate of exchange were to occur faster than the NMR timescale then a single, potentially broad, peak would be expected.

Many methods for determining the rate of exchange between two interconverting isomers are known. In cases where a single isomer can be isolated as a solid, it is possible to reintroduce this isomer into solution and monitor the time it takes for the equilibrium to be re-established. By plotting the decrease in starting material against concentration, the intercept of the resultant straight line is equal to the rate of the backwards reaction. In addition to this technique are two NMR spectroscopic-based experiments, selective inversion and saturation transfer.^{14,15} Since the rate of interconversion between **13o** and **13c** was proposed to be relatively slow at ambient temperature, the selective inversion experiment was chosen as it is generally regarded as more reliable within this regime.^{15§}

By ³¹P NMR spectroscopy the isomers **13o** and **13c** each give rise to a single resonance, 71 and 42 ppm, respectively. In the selective inversion experiment one of the two signals is inverted and, because the two tautomers are interconverting, some of this 'inverted' signal intensity is transferred to the other resonance. This gives an observed reduction in the magnitude of the non-irradiated signal. During this exchange of 'inverted' and 'non-inverted' intensity between the signals of the two isomers, relaxation of the 'irradiated' nuclei to their 'normal' state occurs. For the selective inversion technique to work, the rate of interconversion between isomers must be approximately the same magnitude as the rate of relaxation of the two nuclei. If the rate of interconversion is too slow, no exchange of 'inverted' intensity would be observed before relaxation; if too fast, the rate would not be measurable. In the case of **13c/13o** it was necessary to raise the temperature to quicken the rate of interconversion between the two tautomers.

The selective inversion experiment was applied to **13c/13o** and the data obtained from this technique were analysed using the "cifit" program developed by A. D. Bain at

[§] The selective inversion experiment was conducted by Dr A. M. Kenwright and Mr I. McKeag (Durham University).

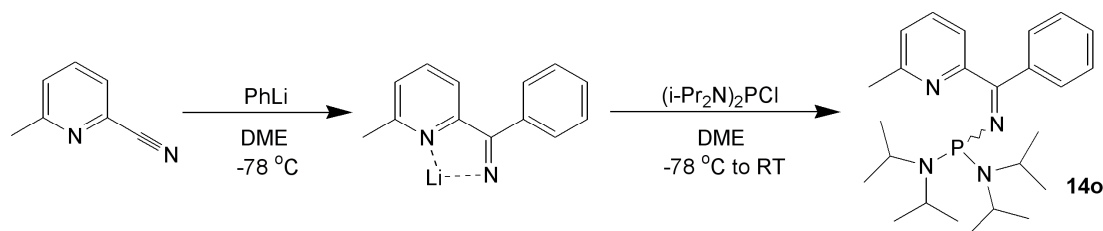
McMaster University to give an approximate rate of 2 s^{-1} at 80°C .¹⁶ The program attempts to fit a rate to the data given by iterative 'guesses' of certain parameters. The best fit gave a rate of $2.03 \text{ s}^{-1} \pm 1.38$ for the conversion of 'open' to 'closed'. In spite of the errors, the magnitude of the rate can be quoted to be of the order of 1 s^{-1} at 80°C .

3.3. Synthesis and properties of bis(diisopropylamino) phosphino (phenyl 6-methylpyridin-2-yl methylene)amine, **14o**

In order to verify the ^{31}P NMR spectroscopic chemical shift of **13o** the preparation of a system that might not ring close was attempted. Logically, the introduction of groups adjacent to the pyridyl nitrogen could block the approach of the phosphine moiety to the pyridine and potentially inhibit ring closure preventing the formation of the diazaphosphole.

The commercially available compound 2-cyano-6-methylpyridine was used to prepare a similar PN compound to **13**, but with a methyl group in the *ortho*-position of the pyridine ring. Indeed, using the same conditions as those used with 2-cyanopyridine, 2-cyano-6-methylpyridine produced **14o** in 46 % yield (Scheme 4), existing in a solely 'open' form.

Scheme 4: Synthesis of 14o



The exclusively 'open' nature of **14o** is evident from both solution-state ^1H and $^{13}\text{C}\{^1\text{H}\}$ NMR spectroscopies, which most characteristically show that the aromaticity of the pyridyl ring is intact. Notably, the phosphorus chemical shift of 71.3 ppm for **14o** agrees well with that assigned to the open isomer **13o** (71.0 ppm), supporting the identity of the latter, which cannot be isolated from the equilibrium, nor directly characterised. It should be noted that despite prolonged heating of compound **14o** at 70°C for 70 h and

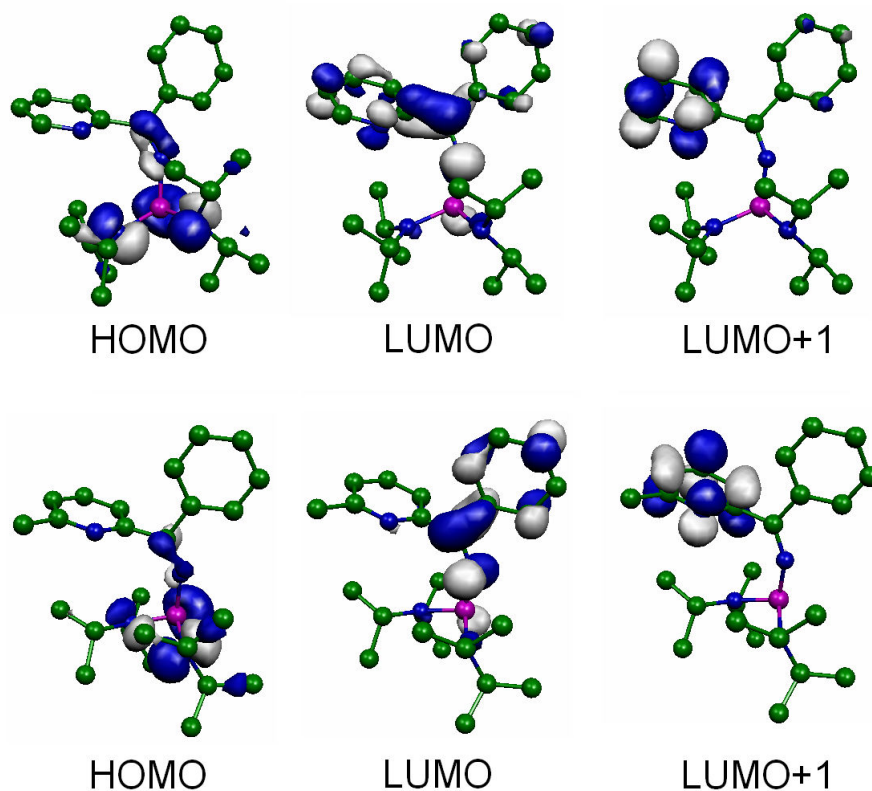
subsequent analysis by ^{31}P NMR spectroscopy, no change or formation of a 'closed' isomer was observed.

3.3.1. Investigation of the factors controlling the lack of cyclisation of **14o**

The lack of cyclisation for **14o** is attributed primarily to steric factors, with the methyl group blocking the approach of the phosphorus centre towards the pyridyl ring. From computed 3D molecular structures it can be seen that the methyl group of **14o** lies in the space that the bis(diisopropylamino) substituents would occupy upon ring closure. Although the electronic influence of the methyl is not discounted, it is believed to be a lesser factor in determining the extent (or lack) of ring closure. DFT calculations at the B3LYP/6-31G** level of theory found both **14o** and the theoretical isomer **14c** to be energy minima, with **14c** being higher in energy by 20.2 kcal/mol (at 25 °C), reflecting the experimental results. This is in stark contrast to the predicted energy difference between **13o** and **13c** calculated to be only 3.0 kcal/mol (at 25 °C), and hence interconversion may be expected. None of the studies, experimental or computational, allows the determination of the energy barrier for the interconversion. To attain this value further work would be needed.

Computational studies to investigate potential differences between the systems **13c/13o** and **14o** were conducted, for which the calculated MOs are shown in Figure 8.[†] Slight differences exist between the MOs of **13o** and **14o**, especially for the LUMOs, where **13o** has a significant amount of pyridyl character, while **14o** does not. It is unclear, however, to what extent these differences arise from geometric or electronic factors.

Figure 8: Selected molecular orbitals of **13o** (upper) and **14o** (lower)



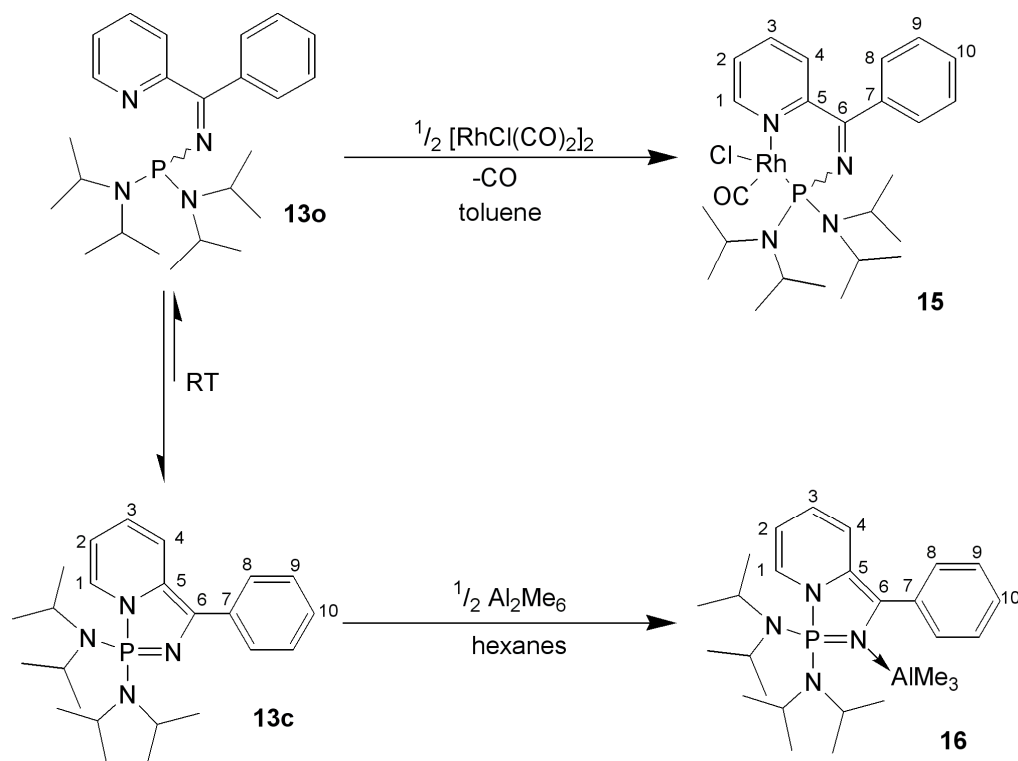
3.4. Reactivity of **13o**/**13c**

3.4.1. Reaction of **13c**/**13o** with Rh(I) to give complex **15**

In the literature both *N*-phosphino-pyridyl imines and iminophosporanes are successful ligands for rhodium(I) and therefore, it was unclear which side of the equilibrium **13c**/**13o** would react preferentially.^{1,17} To answer this question **13c**/**13o** was combined with half an equivalent of $[\text{RhCl}(\text{CO})_2]_2$ yielding a single product according to ^{31}P NMR spectroscopy after 24 h (Scheme 5). The structure of this complex was assigned by ^1H and ^{13}C NMR spectroscopy and confirmed by single crystal X-ray diffraction (*vide infra*) to be $[\text{RhCl}(\text{CO})(\kappa^2\text{-N,P-13o})]$, **15**. This complex is analogous to that obtained from the reaction of **2IP-PPh₂** with $\frac{1}{2}[\text{RhCl}(\text{CO})_2]_2$ namely $[\text{RhCl}(\text{CO})(\kappa^2\text{-N,P-2IP-PPh}_2)]$.¹ The preference for the binding of **13** as a P^ΛN ligand, **13o**, as opposed to an *N*-bound iminophosphorane,

13c, is assumed to be a result of a combination of the chelate effect and the favoured soft-soft phosphorus-rhodium interaction relative to that of nitrogen-rhodium.

*Scheme 5: Synthesis of complexes **15** and **16** with atom numbering scheme*



The solution-state ^1H and $^{13}\text{C}\{^1\text{H}\}$ NMR spectra of **15** clearly show the presence of the **13o** isomeric form and not **13c** in the coordination sphere of rhodium(I). The shift to higher frequency of the protons on the pyridyl ring from 5.2 - 7.2 ppm (**13c**) to 7.3 - 9.7 ppm is in agreement with the presence of an aromatic pyridyl ring, which is also reflected in the $^{13}\text{C}\{^1\text{H}\}$ NMR spectrum. Characteristically C6, in the $^{13}\text{C}\{^1\text{H}\}$ NMR spectrum has a chemical shift of 171.1 ppm, within the range expected for a coordinated *N*-phosphino-pyridyl imine (166 - 177 ppm).¹ The carbonyl carbon was not detected despite increasing the relaxation time and the number of scans. This latter resonance is likely to be broadened by dissociation and reassociation in solution, making the detection difficult by NMR spectroscopy, something compounded by the proximity of the quadrupolar oxygen atom and the absence of proton-mediated relaxation. The observation of the carbonyl will also be hampered by the ^1J coupling to rhodium and the ^2J coupling to phosphorus, which will split the overall intensity of the signal. In the assignment of **15** it is also of note

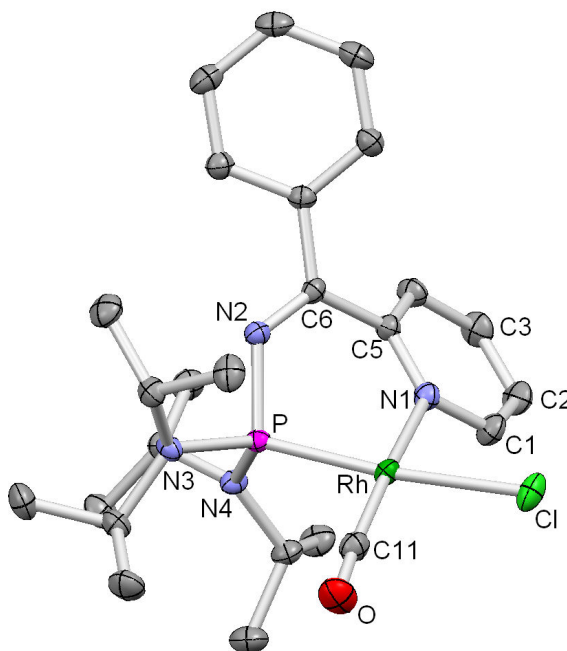
that no $^2J_{\text{RhC}}$ or $^3J_{\text{RhC}}$ couplings are observed for C1, C5 or C6, which is consistent with the lack of similar couplings for $[\text{RhCl}(\text{CO})(\kappa^2\text{-}N,P\text{-}\mathbf{2IP-PPh}_2)]$.¹

The ^{31}P NMR spectrum of complex **15** shows a shift to higher frequency upon coordination of **13o** to rhodium(I) of $\Delta\delta \sim 48$ ppm, a value that agrees well with a shift of $\Delta\delta \sim 43$ ppm found for the coordination of **2IP-PPh₂** to rhodium(I). The rhodium-phosphorus coupling constants displayed by each complex are also of similar magnitudes **15**: $^1J_{\text{RhP}} = 209$ Hz, $[\text{RhCl}(\text{CO})(\kappa^2\text{-}N,P\text{-}\mathbf{2IP-PPh}_2)]$: $^1J_{\text{RhP}} = 167$ Hz.

The infra-red stretch of the carbonyl was recorded at $\nu = 1997\text{ cm}^{-1}$, lower than the corresponding stretch for $[\text{RhCl}(\text{CO})(\kappa^2\text{-}N,P\text{-}\mathbf{2IP-PPh}_2)]$ at 2010 cm^{-1} . This decrease is primarily reflective of the change in the electronic nature of the phosphorus centre with a reduction in the π -acidity of the phosphine. This replicates the trend observed for the phosphines $\text{P}(\text{NMe}_2)_3$ and PPh_3 ; *trans*- $[\text{RhCl}(\text{CO})\{\text{P}(\text{NMe}_2)_3\}_2]$ $\nu_{\text{CO}} = 1959\text{ cm}^{-1}$ and *trans*- $[\text{RhCl}(\text{CO})(\text{PPh}_3)_2]$ $\nu_{\text{CO}} = 1978\text{ cm}^{-1}$.¹⁸

Figure 9: Molecular structure of **15**. C_6H_6 with selected bond lengths (Å) and angles ($^\circ$). Thermal ellipsoids set at 50 % level. Solvent molecules and hydrogen atoms are omitted for clarity.

Rh-P	2.2060(6)
Rh-N1	2.1532(19)
N1-C5	1.354(3)
C5-C6	1.501(3)
C6-N2	1.272(3)
N2-P	1.7085(19)
C1-C2	1.382(3)
C2-C3	1.377(4)
P-N3	1.6823(18)
P-N4	1.6692(18)
Rh-Cl	2.3954(6)
Rh-C11	1.811(2)
C11-O	1.144(3)
P-Rh-N2	84.98(5)
P-N2-C6	125.24(16)
C11-Rh-Cl	90.08(8)



Recrystallisation from a saturated solution of benzene gave single crystals of **15** suitable for an X-ray diffraction study (see Figure 9). The resulting X-ray molecular structure shows a distorted square-planar geometry at the rhodium centre with the phosphorus atom located *trans* to the chloride as expected, because of the greater *trans* influence of a phosphine, relative to a pyridine.¹⁹ The bond lengths Rh-P and Rh-N1 are 2.2060(6) Å and 2.1532(19) Å, respectively, which are both of comparable length to those in [RhCl(CO)(κ^2 -*N,P*-**2IP-PPh₂**)], 2.1905(5) Å and 2.1475(16) Å.¹ The P-N bite angle is slightly less acute in **15** (84.98(5) °) relative to [RhCl(CO)(κ^2 -*N,P*-**2IP-PPh₂**)] (82.71(4) °) with other angles in the structure being as expected.

3.4.2. Reaction of **13c/13o** with trimethylaluminium to give complex **16**

The equilibrium mixture **13c/13o** has been shown to preferentially ‘open’ in the presence of a soft Lewis acid, rhodium(I). Consequently, it was of interest to explore if the same, or different, reactivity would occur with hard Lewis acids. Trimethylaluminium, a simple hard Lewis acid, was chosen and envisaged to bind to the exposed nitrogen lone pair of the P=N double bond. This mode of reactivity would be consistent with the classical behaviour of iminophosphoranes toward Lewis acids,²⁰ where binding at the nitrogen atom occurs, as is observed, for example, in the compound [(Et)₂(Cl)P=NPh)(AlCl₃)] reported by Burford.²¹

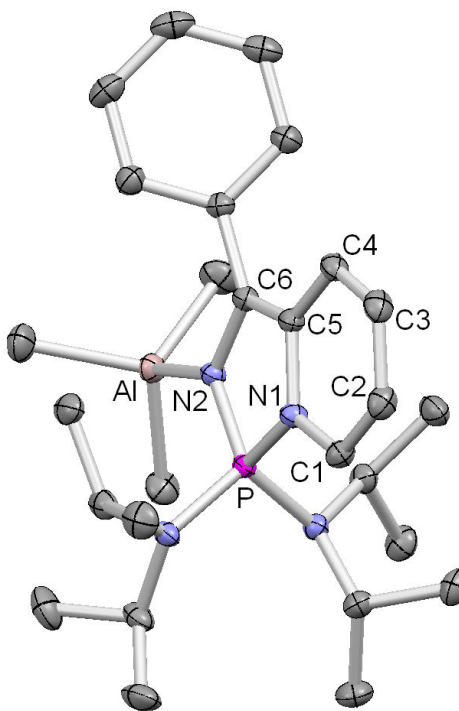
The addition of trimethylaluminium to **13** in a 1:1 ratio immediately yielded **16** as an orange precipitate from a solution of hexane (Scheme 5). Single crystals of **16** suitable for X-ray determination study were grown from a saturated solution in CH₂Cl₂ and, independently by slow addition of AlMe₃ to a concentrated solution of **13c/13o** in hexane. The resulting X-ray molecular structure shows a ring-closed structure with AlMe₃ bound through the nitrogen of the PN double bond of **13c** to aluminium, with an Al-N2 distance of 1.9883(9) Å (Figure 10). This Al-N bond length is in good agreement with that recorded for the compound [{Me₃N}{Al(CH₂SiMe₃)₃}], 2.058(3) Å, reported by Kirss.²² On comparison of the molecular structures of **13c** and **16** a significant change in the bonding of the diazaphosphole framework is noted, the P=N2 bond lengthening by 0.04 Å from 1.589(3) Å in **13c**, to 1.6308(9) Å in **16**. The remaining bond lengths in the heterocyclic

cores of the **13c** and **16**, however, show minimal differences between the two compounds.

In solution complex **16** gives rise to a ^{31}P NMR spectroscopic chemical shift of +46.6 ppm, which is 4.3 ppm higher in frequency than that of **13c**. This small difference in chemical shift indicates only a minor change in the chemical environment of phosphorus, consistent with the binding of trimethylaluminium to the nitrogen atom of the iminophosphorane as displayed in the X-ray molecular structure. Analysis of **16** by ^1H and ^{13}C NMR spectroscopies reveals both a $^3J_{\text{PH}}$ coupling of 6.4 Hz for C^1H and dearomatised pyridyl ring resonances that are characteristic of the 'closed' diazaphosphole structure of **13c**. In addition, the ^{13}C NMR spectroscopic data for **16** are shifted to lower frequency relative to those of **13c**, due to the less electron rich nature of the heterocyclic ring system, a direct result of Lewis acid binding (Scheme 6).

Figure 10: Molecular structure of 16 with selected bond lengths (Å) and angles (°). Thermal ellipsoids set at 50 % level. Hydrogen atoms are omitted for clarity.

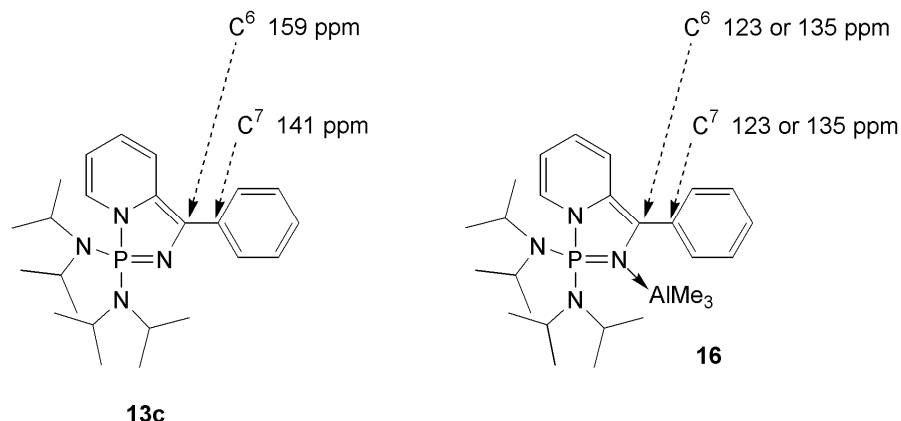
P-N1	1.6745(9)
P-N2	1.6308(9)
N1-C5	1.429(1)
N2-C6	1.436(1)
C5-C6	1.360(1)
C4-C5	1.438(1)
C3-C4	1.358(2)
C2-C3	1.4481(16)
C1-C2	1.3433(15)
Al-N2	1.9883(9)
N1-P-N2	95.70(4)
P-N2-C6	109.46(7)
N2-C6-C5	113.80(9)
C6-C5-N1	110.94(8)
P-N1-C5	109.97(7)
N3-P-N4	107.24(4)
P-N2-Al	125.10(5)



Upon dissolution of crystalline **16** isomerisation to different aluminium binding modes is not observed. Therefore, it is assumed that the Al-N interaction locks the

heterocycle in the 'closed' form, preventing ring opening that would give a trimethylaluminium adduct of **13o**.

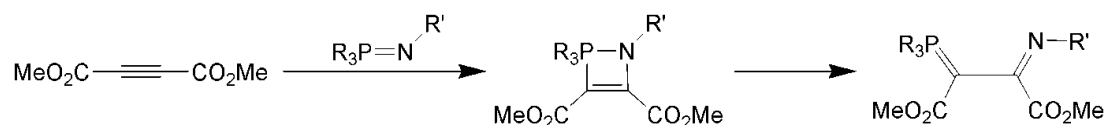
*Scheme 6: Comparison of ^{13}C NMR spectroscopic data for selected carbon atoms of **13c** and **16***



3.4.3. Reaction of **13c/13o** with dimethylacetylene dicarboxylate (DMAD) to give compound **17**

To further investigate the reactivity of the equilibrium mixture **13c/13o**, treatment with an electron deficient alkyne, dimethylacetylene dicarboxylate (DMAD) was undertaken. DMAD readily undergoes cyclisations with many double bonds including those of iminophosphoranes, for which a [2+2] cycloaddition giving a cyclobutene, is the most common mode of reactivity (Scheme 7). Subsequent ring-opening is often observed giving an acyclic $\text{P}=\text{C}-\text{C}=\text{N}$ motif, with the overall process being regarded as an insertion.²³

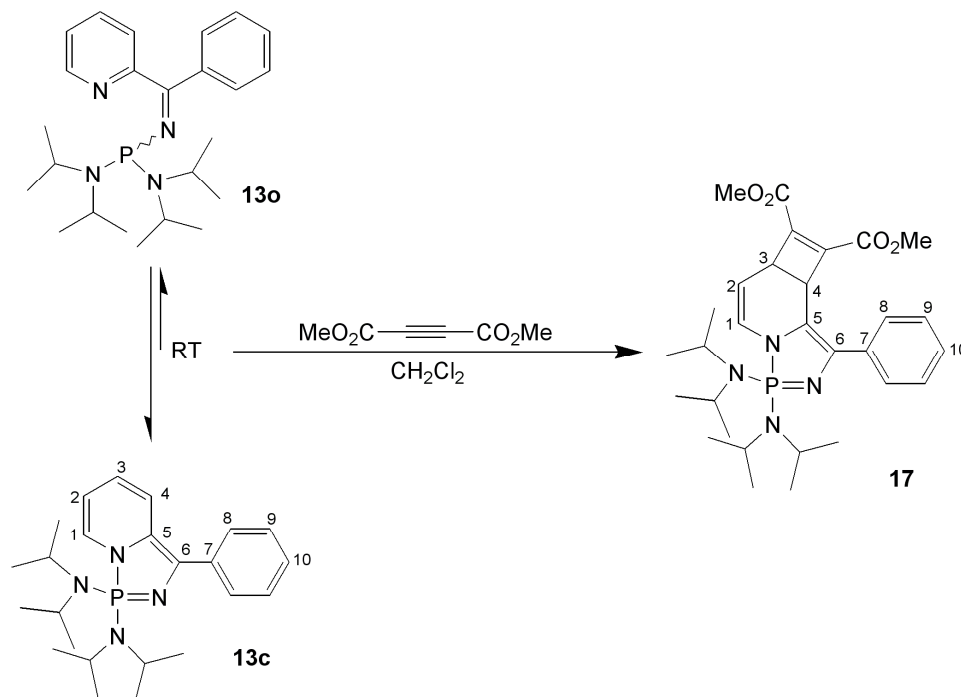
Scheme 7: Reaction of an iminophosphorane with DMAD via a [2+2] cycloaddition, accompanied by ring-opening²³



Combination of **13c/13o** with a stoichiometric quantity of DMAD in dichloromethane was observed by ^{31}P NMR spectroscopy to give a resonance at + 46.6 ppm, corresponding to the formation of a new species **17**, with 95 % conversion after 24 h (Scheme 8). Although compound **17** was not isolated, due to difficulties in purification from excess DMAD and possibly other species, the characterisation of **17** was achieved *in situ*. Mass spectrometric analysis of the reaction mixture by electron impact showed the

ion, M^+ , at m/z : 554, consistent with the molecular weight of a **13**.DMAD adduct. Examination of the ^1H NMR spectrum of **17** showed that the protons C^1H and C^2H exhibit chemical shifts characteristic of a dearomatised pyridyl ring and, in tandem with $^1\text{H}\{^{31}\text{P}\}$ NMR spectroscopy, confirmed the presence of a $^3J_{\text{PH}}$ coupling for C^1H . Hence, these data are consistent with reaction of tautomer **13c** and retention of its diazaphosphole core.

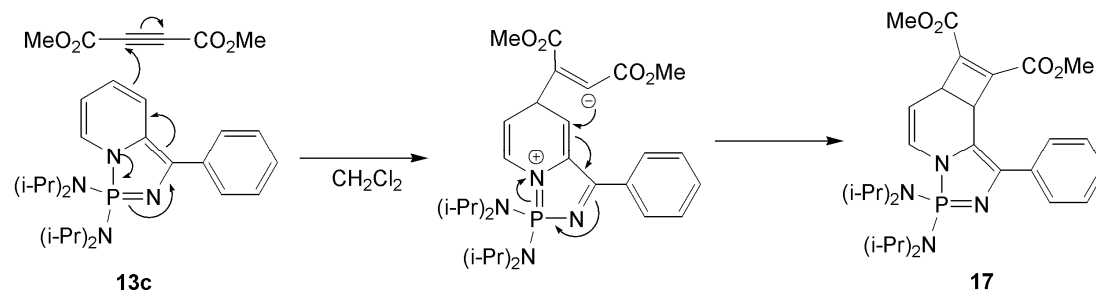
*Scheme 8: Synthesis of compound **17**, with atom numbering scheme*



The assignment of the $^{13}\text{C}\{^1\text{H}\}$ spectrum of **17** revealed the resonances from the carbons CCO_2CH_3 and $\text{C}'\text{CO}_2\text{CH}_3$, formally the alkynyl DMAD carbon atoms, to be singlets. The absence of phosphorus coupling discounted reaction of DMAD at the iminophosphorane of **13c**. Instead, a combination of 2D NMR spectroscopic techniques indicated that the carbons CCO_2CH_3 and $\text{C}'\text{CO}_2\text{CH}_3$ are bonded to those of C3 and C4 (Scheme 8). Two mechanisms are possible for this reaction, either a [2+2] cycloaddition of DMAD across the $\text{C}3=\text{C}4$ double bond or an electrophilic attack of DMAD at the C3 position of **13c**. Although [2+2] cycloaddition is formally forbidden, the presence of an extra pair of p-orbitals at the acetylene, compared to an alkene, allow this pericyclic reaction to occur, albeit *via* a different mechanism.¹³ The alternative mechanism, an electrophilic attack of DMAD upon **13c**, would be a step-wise process generating a quinoidal intermediate (Scheme 9) with the negative charge of the intermediate likely to

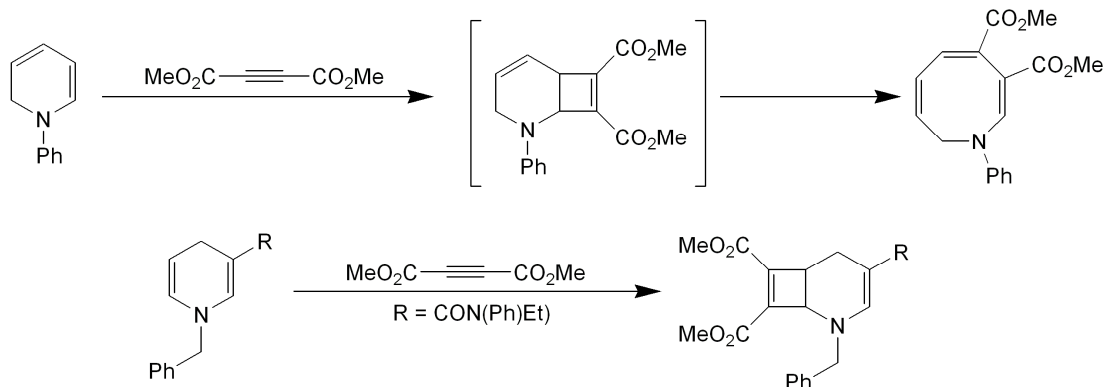
be stabilised by conjugation with the nearby ester functionality. The second step, ring closure, gives the fused cyclobutene-containing ring system **17**.

*Scheme 9: A possible mechanism for the formation of **17** by electrophilic attack of DMAD upon **13c***



Similar [2+2] cycloadditions have been reported by Acheson and co-workers for dihydropyridines, which undergo reaction with DMAD to yield cyclobuta[*b*]pyridines (Scheme 10).²⁴ In the reaction of **13c** the acetylene can attack from either side of the C3=C4 double bond and so two enantiomers must be formed (Figure 11). Since there is no preference for either enantiomer, as both faces of **13c** are identical, a racemic mixture is generated.

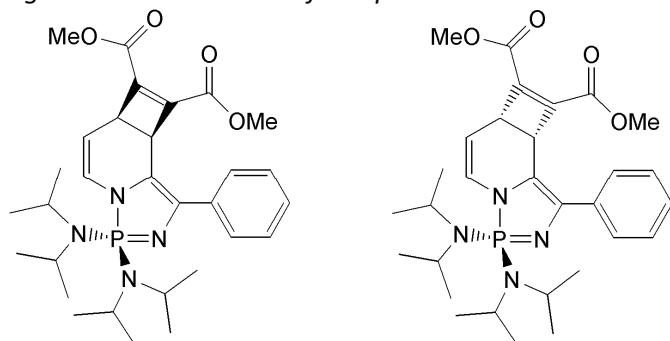
Scheme 10: Reaction of DMAD with 1,2-dihydropyridine (upper) and 1,3-dihydropyridine (lower) reported by Acheson^{7,24}



The preference of DMAD to react at the C=C double bond of **13c** is believed to stem from the steric shielding of the iminophosphorane unit by the bis(diisopropylamino) substituents, which prevents cycloaddition. This hypothesis is supported by results in Chapter IV in which the synthesis of an analogue of **13c** with a more exposed

iminophosphorane functionality showed reactivity with DMAD at the P=N bond exclusively.

Figure 11: Enantiomers of compound **17**



3.4.4. Reaction of **13c/13o** with selenium to give compound **13o.Se**

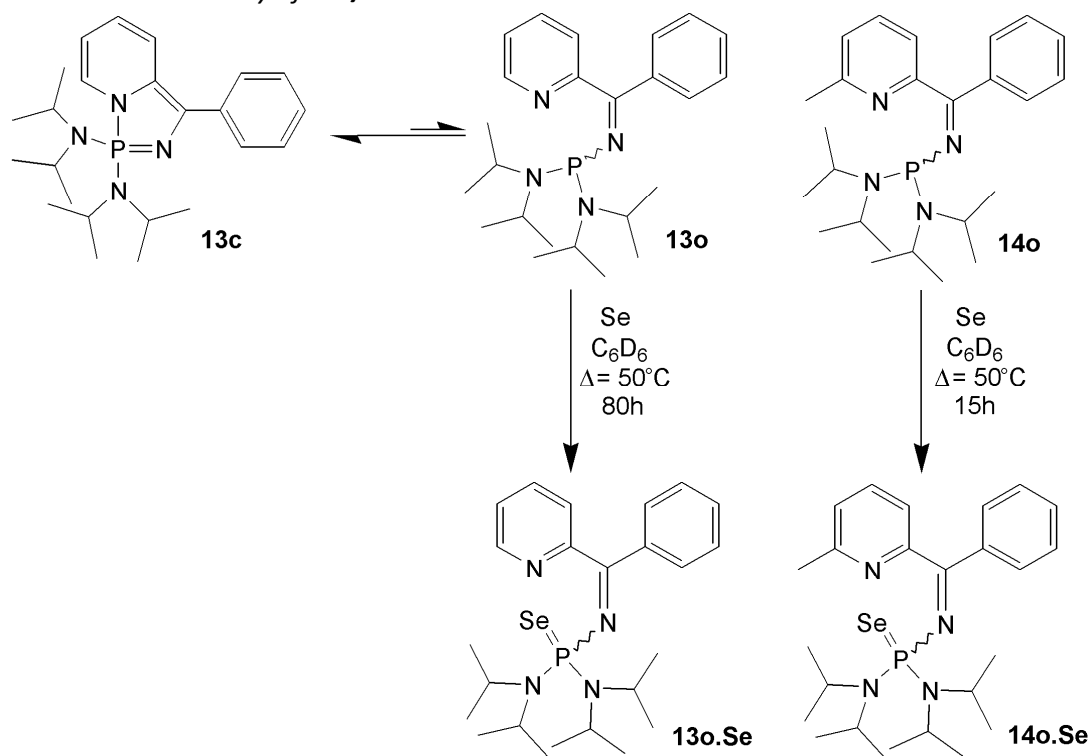
The reaction of elemental chalcogens with unsaturated phosphorus compounds is a well known and defining characteristic of phosphorus(III) centres. In these reactions phosphorus(III) is oxidised to phosphorus(V) with simultaneous reduction of the chalcogen and formation of a formal double bond. In the case of **13**, the compound exists in tautomeric equilibrium between both ‘open’ **13o**, containing an accessible P(III) centre, and a ‘closed’ isomer **13c**, with an unreactive P(V) centre. It was therefore of interest to investigate the influence of this equilibrium on the reactivity of **13** with chalcogens.

Elemental selenium was the reactant of choice, because of the 7 % spin active ^{77}Se isotope, which aids characterisation by ^{31}P NMR spectroscopy. In addition, selenium cannot react by a radical mechanism and therefore, unlike molecular oxygen, can only interact with the ‘open’ form of **13c/13o**.²⁵

The reaction was conducted in a Young’s NMR tube with grey selenium suspended in a solution of **13c/13o** in C_6D_6 and heated to 50 °C (Scheme 11). Complete conversion to the ring-opened selenide compound, **13o.Se**, was found after 80 h. The $^{31}\text{P}\{^1\text{H}\}$ NMR chemical shift of the selenide was + 55.1 ppm, which is in reasonable agreement with the known compound $\text{Se}=\text{P}(\text{NMe}_2)_3$ (+ 81.2, CDCl_3).²⁶ These results support the reaction of the ‘open’ **13o** isomer with selenium and, by virtue of the equilibrium, the concentration of **13o** is replenished until all of **13c/13o** is converted to **13o.Se**. The coupling constant, $|^1J_{\text{SeP}}| = 821 \text{ Hz}$, observed for **13o.Se** reflects the electron deficient nature of the

phosphorus centre of **13o** as there exists an established correlation between basicity and the magnitude of the $^1J_{\text{SeP}}$ coupling constant.²⁷ It is observed that the larger the $^1J_{\text{SeP}}$ coupling, the greater s character, and therefore the lower the basicity of the phosphine.²⁸ The selenide of tris(dimethylamino)phosphine displays a similar coupling constant, $|^1J_{\text{SeP}}| = 805 \text{ Hz}$, to that of **13o.Se** reflecting their comparable basicities as expected.²⁶

*Scheme 11: Reactivity of **13c/13o** and **14o** with selenium*



As a comparison, the reaction of selenium with the fully ‘open’ compound **14o** was carried out under the same conditions as that for **13c/13o**. The corresponding selenide was formed quantitatively after 15 h at 50°C giving rise to a $^{31}\text{P}\{^1\text{H}\}$ NMR spectroscopic chemical shift of + 54.3, very similar to that of **13o.Se** reflecting the now similar chemical and geometric environment of the phosphorus centre. The difference in the rates of oxidation between **13c/13o** and **14o** is undoubtedly due to the presence of the ‘closed’ isomer **13c** in which the phosphorus(V) centre is inherently stable towards oxidation and also geometrically shielded by the bulky bis(diisopropylamino) substituents. This enhanced stability of **13c/13o** relative to **14o** towards oxidants is of interest in catalytic processes. Catalyst lifetime is determined by a number of factors: solvent, degradation pathways, etc., and in many cases limited by the stability of the phosphine

especially if significantly labile. Once a phosphine becomes decoordinated, it is more prone to oxidation as there is far greater access to the phosphorus centre, and if oxidised to P(V) can no longer act as a ligand. Often strict anaerobic conditions are needed to ensure the long-term survival of phosphines. In a hypothetical catalytic cycle if ligand **13o** were to be labile then the dissociated ligand would revert to a **13c/13o** equilibrium, partially protecting the phosphorus centre. Although the equilibrium ratio of **13c:13o** 95:5 % makes this point relatively academic, if the equilibrium could be tuned to 99.9:0.1 % ('closed' : 'open') or better, then the lifetime of the ligand would be presumed to be greatly extended.

3.5. Summary

It has been demonstrated that bis(diisopropylamino)phosphino(phenyl pyridin-2-yl methylene)amine, **13o**, exists in dynamic equilibrium with its ring-cyclised tautomer 1,1-bis(diisopropylamino)-3-phenyl-1 λ^5 -[1,3,2]diazaphospholo[1,5-a]pyridine, **13c**. The presence of both 'open' and 'closed' isomers for compound **13** is in direct contrast to the solely 'open' *N*-phosphino-pyridyl imines (**1o-6o**) presented in Chapter II. This difference arises as a consequence of the nature of the substituents on phosphorus, which for compound **13** are electron withdrawing amino groups, whereas for compounds **1o-6o** more electron rich alkyl or aryl groups are present. Therefore, it was of interest to introduce substituents on phosphorus with an increased π -acceptor character compared to that of diisopropylamino which are envisaged to favour the 'closed' tautomer. This dependence of the intramolecular equilibrium, **13c/13o**, on the identity of the phosphorus substituents and the nature of the *N*-phosphino-pyridyl imine framework is explored in greater depth in Chapter IV.

¹ P. W. Dyer, J. Fawcett, M. J. Hanton, *J. Organomet. Chem.*, 2005, **690**, 5264.

² C. Buron, H. Gornitzka, V. Romanenko, G. Bertrand, *Science*, 2000, **288**, 834.

³ J. Claydon, '*Organolithiums: Selectivity for Synthesis*', Elsevier Science Limited, Oxford, 2002, p. 1

-
- ⁴ F. H. Allen, O. Kennard, D. G. Watson, L. Brammer, A. G. Orpen, R. Taylor, *J. Chem. Soc. Perkin Trans. 2*, 1987, Supplement, S1 – S18.
- ⁵ T. D. Le, D. Arquier, K. Miqueu, J.-M. Sotiropoulos, Y. Coppel, S. Bastin, A. Igau, *J. Organomet. Chem.*, 2009, **694**, 229.
- ⁶ C. D. Entwistle, A. S. Batsanov, J. A. K. Howard, M. A. Fox, T. B. Marder, *Chem. Commun.*, 2004, 702.
- ⁷ R. M. Acheson, N. D. Wright, P. A. Tasker, *J. Chem. Soc. Perkin Trans. 1*, 1972, 2918.
- ⁸ Z. Benkő, S. Burck, D. Gudat, M. Nieger, L. Nyulászi, N. Shore, *Dalton Trans.*, 2008, 4937.
- ⁹ D. D. Laws, H.-M. L. Bitter, A. Jerschow, *Angew. Chem. Int. Ed.*, 2002, **41**, 3096.
- ¹⁰ P. J. Hore, 'Nuclear Magnetic Resonance', Oxford University Press, Oxford, 1995, p. 3.
- ¹¹ F. Carré, C. Chuit, R. J. P. Corriu, P. Monforte, C. Reyé, J. Declercq, A. Dubourg, *Angew. Chem. Int. Ed.*, 1993, **32**, 1430.
- ¹² T. R. van den Ancker, P. C. Andrews, S. J. King, J. E. McGrady, C. L. Raston, B. A. Roberts, B. W. Skelton, A. H. White, *J. Organomet. Chem.*, 2001, **607**, 213.
- ¹³ J. Clayden, N. Greeves, S. Warren, P. Wothers, 'Organic Chemistry', Oxford University Press, Oxford, 2001, p. 905 - 967.
- ¹⁴ P. J. Hore, 'Nuclear Magnetic Resonance', Oxford University Press, Oxford, 1995, p. 44 - 55.
- ¹⁵ J. K. M. Sanders, B. K. Hunter, 'Modern NMR Spectroscopy', Oxford University Press, Oxford, 1987.
- ¹⁶ A. D. Bain, J. A. Cramer, *J. Magn. Reson.*, 1996, **118A**, 21.
- ¹⁷ K. T. K. Chan, L. P. Spencer, J. D. Masuda, J. S. J. McCahill, P. Wei, D. W. Stephan, *Organometallics*, 2004, **23**, 381.
- ¹⁸ P. W. Dyer, J. Fawcett, M. J. Hanton, R. D. W. Kemmitt, R. Padda, N. Singh, *Dalton Trans.*, 2003, 104.
- ¹⁹ T. G. Appleton, H. C. Clark, L. E. Manzer, *Coord. Chem. Rev.*, 1973, **10**, 335.
- ²⁰ Y. G. Gololobov, L. F. Kasukin, *Tetrahedron*, 1992, **48**, 1353.
- ²¹ N. Burford, R. v. H. Spence, J. F. Richardson, *Dalton Trans.*, 1991, 1615.
- ²² W. G. Feighery, R. U. Kirss, C. H. Lake, M. R. Churchill, *Inorg. Chim. Acta.*, 1994, **218**, 47.
- ²³ J. Barluenga, F. Lopez, F. Palacios, *Chem. Commun.*, 1985, 1681.
- ²⁴ R. M. Acheson, G. Pagleitti, P. A. Tasker, *J. Chem. Soc. Perkin Trans. 1*, 1974, 2496.
- ²⁵ D. F. Shriver, P. W. Atkins, 'Inorganic Chemistry', 3rd ed., Oxford University Press, Oxford, 1999, p. 390 - 402.
- ²⁶ E. Krawczyk, A. Skowronska, J. Michalski, *J. Chem. Soc., Perkin Trans. 2*, 2000, 1135.
- ²⁷ D. W. Allen, B. F. Taylor, *Dalton Trans.*, 1982, 51.
- ²⁸ W. McFarlane, D. S. Rycroft, *Dalton Trans.*, 1973, 2162.

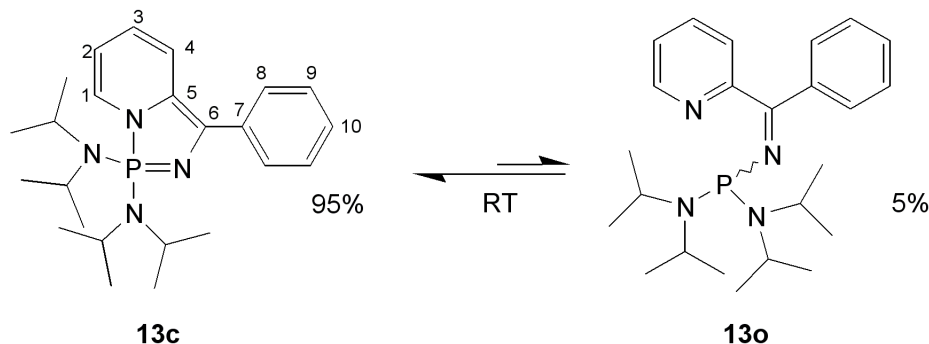
Chapter IV

4. Synthesis, reactivity and equilibrium studies of 1,1-bis(diamino)-3-aryl-1 λ^5 -[1,3,2]diazaphospholo[1,5-*a*]pyridines and related species

4.1. Introduction

It has been demonstrated in Chapter III that an intramolecular equilibrium exists between bis(diisopropylamino)phosphino(phenyl pyridin-2-yl methylene)amine, **13o**, and its valence tautomer 1,1-bis(diisopropylamino)-3-phenyl-1 λ^5 -[1,3,2]diazaphospholo[1,5-*a*]pyridine, **13c** (Scheme 1). The two isomers can be considered to be either ‘open’, **13o**, or ‘closed’, **13c**, towards κ^2 -*P,N* chelation of a metal species. In contrast, related compounds with alkyl or aryl substituents in the place of the diisopropylamino groups on phosphorus (*N*-phosphino-pyridyl imines **1o-6o**) show no evidence of ‘open’/‘closed’ tautomerism (see Chapter II). Similarly, the introduction of a methyl group adjacent to the pyridyl nitrogen of **13c/13o** gives solely compound **14o**, with none of its tautomeric counterpart **14c** being detected. In this latter case, steric repulsion between the methyl and the diisopropylamino groups strongly disfavours the ring closure that would form **14c**, something that is reflected by a computational study (see Chapter III). In contrast, the computed energies of the two isomers **13c/13o** are sufficiently close for a ratio of **13c** : **13o** of 95 : 5 to exist at room temperature.

Scheme 1: Equilibrium between **13c** and **13o**



It was therefore of interest to explore how other minor changes to the pyridyl-imine framework may impact upon the position of the equilibrium between the 'open' and 'closed' tautomers. Since alkyl and aryl substituents on the phosphorus centre (**1o-6o**) and a methyl group on the pyridyl ring (**14o**) do not give an equilibrium, favouring instead solely the 'open' form, it was of interest to investigate the impact of varying the phenyl group on the *N*-phosphino-pyridyl imine framework.

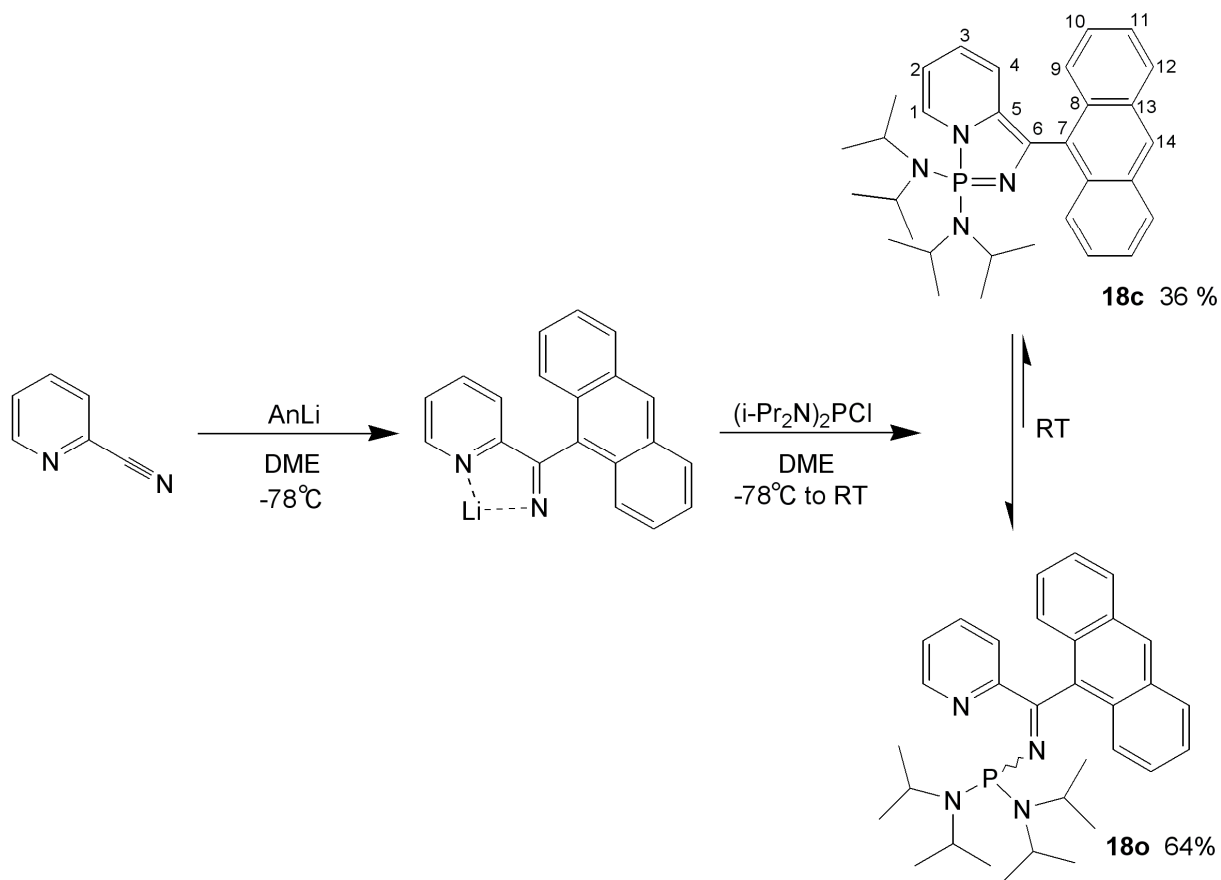
4.2. 1,1-bis(Diisopropylamino)-3-anthracenyl-1 λ^5 -[1,3,2]-diazaphospholo[1,5-*a*]pyridine, **18**

4.2.1. Synthesis of the equilibrium mixture **18c/18o**

Replacement of the phenyl group of compound **13** was synthetically possible by utilisation of a different aryl lithium reagent in the initial metallation of 2-cyanopyridine (Scheme 2). As a starting point, it was of interest to explore how replacing a phenyl group by a related anthracenyl moiety would impact on the equilibrium process. Therefore, synthesis of an anthracenyl-substituted framework, analogous to that of **13c/13o**, was attempted.

Lithiation of 2-cyanopyridine with anthracenyllithium, generated *in situ* by the method of Schmutzler,¹ followed by addition of bis(diisopropylamino)chlorophosphine gave a purple solution (Scheme 2). Following work-up, compound **18** was obtained as a greyish solid in reasonable yield (58 %).

Scheme 2: Synthesis and atom numbering scheme of the equilibrium mixture **18c/18o**



4.2.2. Solution-state NMR spectroscopic studies of the tautomers **18c** and **18o**

Analysis of **18** by solution-state ^{31}P NMR spectroscopy revealed two singlet resonances at 40.5 and 68.9 ppm, closely resembling those observed for **13c**, 42.3 ppm, and **13o**, 71.0 ppm, and hence consistent with the presence of tautomers **18c** and **18o** respectively. This assignment was verified using a combination of ^1H and COSY NMR spectroscopy and confirmed the products to be the 'open' and 'closed' tautomeric forms, **18o** and **18c**, with tautomer **18c** exhibiting the distinctive $^3J_{\text{PH}}$ coupling between C^1H and phosphorus of the expected magnitude (**18c**: $^3J_{\text{PH}} = 5\text{ Hz}$, **13c**: $^3J_{\text{PH}} = 6\text{ Hz}$).²

The ratio of **18c** : **18o** was determined to be 36 : 64 at 25°C . As was the case with **13c/13o**, VT-NMR spectroscopy revealed **18c** to be the thermodynamically more stable

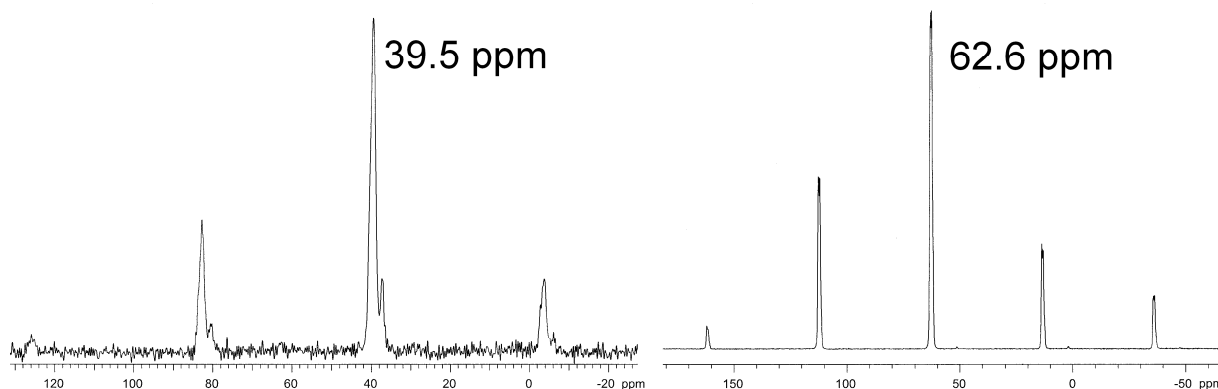
tautomer. Clearly, the change in substituent from phenyl to anthracenyl favours the 'open' form, with a greater proportion of **18o** observed (64 %) in its equilibrium mixture **18c/18o** compared to **13o** (5 % of **13c/13o**) at ambient temperature.

Together the above observations reveal that replacement of the pendant backbone phenyl moiety for an anthracenyl group can affect the stability of the 'open' and 'closed' isomers. The anthracenyl group differs from the phenyl ring in terms of steric bulk and the strength of its electron-withdrawing character and therefore the change in the equilibrium position between **13c/13o** and **18c/18o** could be envisaged to result from a complex combination of steric and electronic factors.

4.2.3. Solid-state NMR spectroscopic studies of the tautomers **18c and 18o**

Rapid cooling of a saturated solution of the equilibrium mixture **18c/18o** gives rise to a mixture of yellow and purple solids. It was found, however, that a slower rate of cooling could be used to obtain solely purple crystals. Of the two possible tautomers, the more thermodynamically stable form will be favoured at lower temperature and therefore the purple solid was proposed to be **18c**. In contrast, slow evaporation of the equilibrium mixture of **18c/18o** gave exclusively yellow cuboidal crystals, proposed to be **18o**. This physical separation of the two isomers **18c** and **18o** was confirmed by solid-state ^{31}P NMR spectroscopic analysis of ground samples of each (Figure 1). The yellow crystalline solid proposed to be **18o** gave rise to a signal at 62.6 ppm, in good agreement with the solution-state value of 68.9 ppm ($\text{C}_6\text{D}_5\text{CD}_3$) for the 'open' isomer. In contrast, the solid-state ^{31}P NMR spectrum of the purple solid gave a signal at 39.5 ppm, consistent with it being **18c** in accordance with the solution-state ^{31}P NMR spectroscopic shift of 40.5 ppm. Dissolution of the yellow crystals of **18o** gave a yellow solution, which slowly became purple within an hour at ambient temperature. Following this conversion by solution-state ^{31}P NMR spectroscopy unambiguously revealed that the colour change mirrored the re-establishment of the equilibrium mixture **18c/18o**.

Figure 1: Solid-state ^{31}P NMR spectra of **18c** (left) and **18o** (right)



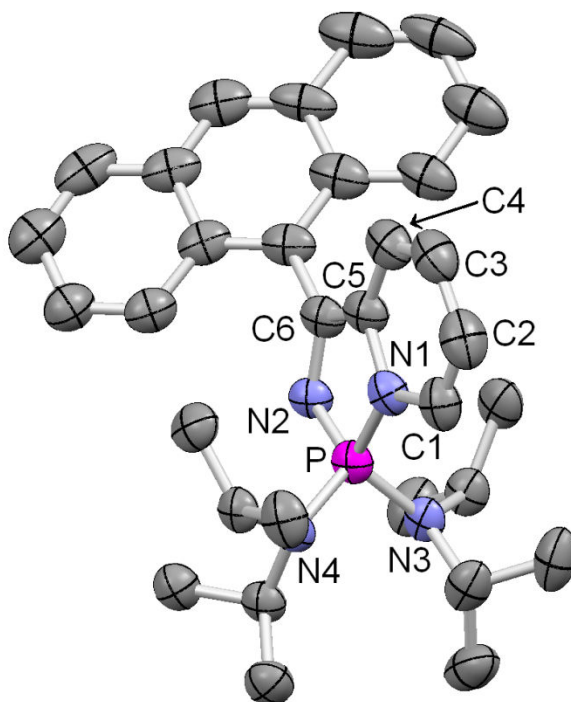
4.2.4. X-Ray diffraction studies of the tautomer **18c** and **18o**

Single crystals, which were purple in colour, were grown by layering a saturated ethereal solution of the equilibrium mixture **18c/18o** with hexane and were found to be suitable for an X-ray diffraction study. The resulting molecular structure confirmed these crystals to be the closed heterocyclic tautomer **18c** (Figure 2), as had been inferred from the solid-state ^{31}P NMR spectroscopic study (*vide supra*). The metric parameters of the phosphole and dearomatised pyridine rings of **18c** closely resemble those of **13c** (P-N1 **18c**: 1.680(2) **13c**: 1.681(3), C5-C6 **18c**: 1.377(3) **13c**: 1.376(4)). The most notable difference between the structures of **13c** and **18c** is in the dihedral angle between the planes of the aryl substituent and of the diazaphosphole ring. In **18c** a larger dihedral angle of 50.9 ° is noted, which compares with an angle of 33.6 ° determined for **13c**, undoubtedly due to the greater steric bulk of the anthracenyl group relative to that of the phenyl moiety.

In contrast, slow evaporation of the equilibrium mixture **18c/18o** gave exclusively yellow cuboidal crystals, of which a small number were found suitable for an X-ray diffraction study. Although, the molecular structure has been confirmed to be **18o** the crystallographic data has not yet been fully refined.

Figure 2: Molecular structure of **18c**, with selected bond lengths (Å) and angles (°). (Thermal ellipsoids set at 50 % level). Hydrogen atoms are omitted for clarity.

P-N1	1.680(2)
P-N2	1.5886(19)
N1-C5	1.437(3)
C5-C6	1.377(3)
C6-N2	1.397(3)
C1-C2	1.337(3)
N1-C1	1.398(3)
C2-C3	1.443(4)
C3-C4	1.342(4)
C4-C5	1.427(3)
P-N3	1.6477(19)
P-N4	1.6504(19)
N1-P-N2	97.25(10)
P-N1-C5	108.11(17)
N1-C5-C6	109.9(2)
C5-C6-N2	114.7(2)
C6-N2-P	109.97(16)
N3-P-N4	103.25(10)



4.3. The attempted synthesis and isolation of 3-phenyl-*spiro*- [1λ⁵-[1,3,2]diazaphospholo[1,5-a]pyridine-1,2'- [1,3,2]dioxaphospholane], **19**

It has been shown that both the compounds **13** and **18** each exist as two tautomers that are in equilibrium, namely as the 'open' and 'closed' forms, something that contrasts to the solely 'open' *N*-phosphino-pyridyl imines **10-60**. The cause of this difference is related to the nature of the substituents on phosphorus, with the more electron-withdrawing diisopropylamino groups allowing ring closure for compounds **13** and **18**. It is therefore logical to assume that increasing the electron deficiency at phosphorus, relative to that for **13c**, would favour the formation of solely the 'closed' tautomer. To explore this hypothesis

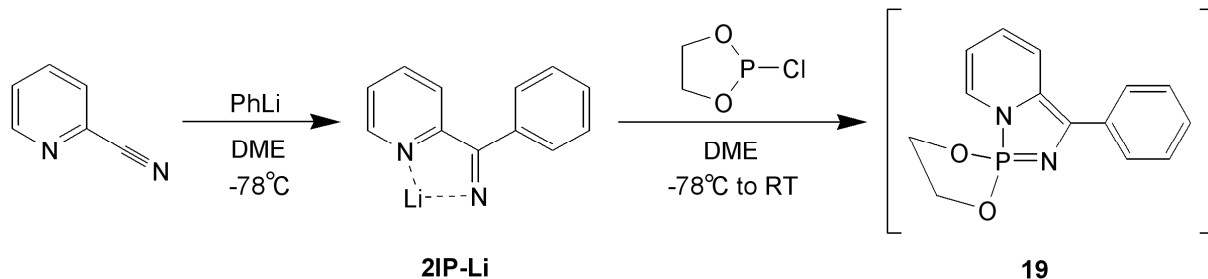
the synthesis of a $1\lambda^5$ -[1,3,2]diazaphospholo[1,5-*a*]pyridine, **19**, with alkoxy-substituents at phosphorus was undertaken.

4.3.1. Attempted synthesis of **19**

The method used for the synthesis of **13c/13o** was adapted to use the commercially available cyclic dialkoxychlorophosphine (OCH₂CH₂O)PCl in the place of (i-Pr₂N)₂PCl (see Scheme 3). The solvent medium chosen was DME in keeping with the synthesis of **13c/13o** to aid the speed of the reaction.

The addition of the dialkoxychlorophosphine to the lithiated intermediate, **2IP-Li**, followed by warming to room temperature gave a yellow-brown solution. Analysis of this reaction mixture by ³¹P NMR spectroscopy (CD₂Cl₂) revealed several resonances at 137.2, 134.5, 130.2, 123.0, 59.5, 13.8, 13.5, - 37.2 and - 43.2 ppm, indicating that a mixture of products was present. The volatile components of the reaction mixture were then removed under reduced pressure, dichloromethane added and the resulting suspension filtered to give an orange solution. The addition of hexane to this solution gave an orange precipitate, which following isolation gave elemental analyses consistent with an empirical formula of (OCH₂CH₂O)P(N)(NC₅H₄)(C₆H₅), **19**, *i.e.* the alkoxy-substituted equivalent of **13c**. Mass spectrometry revealed peaks at (*m/z*;) 272 and 544 indicating the possibility of monomeric (**19**) and dimeric (**20**) structures both being present.

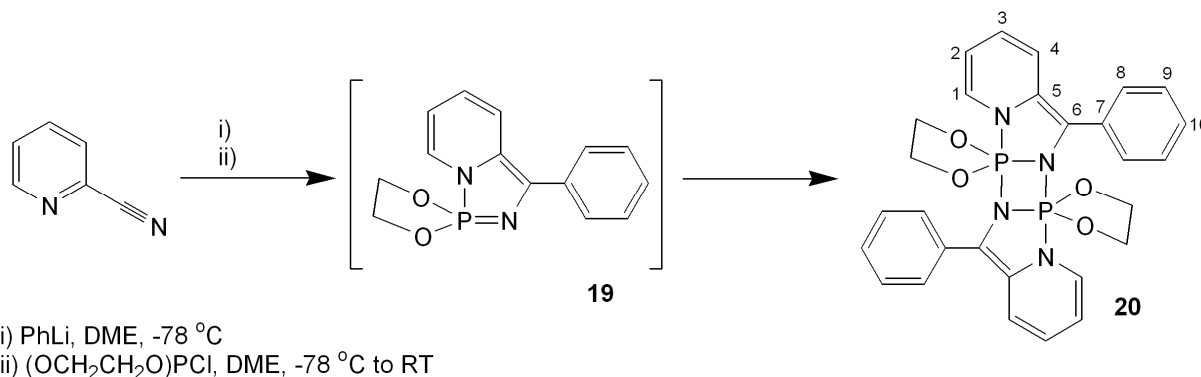
*Scheme 3: Attempted synthesis of compound **19***



4.3.2. X-ray molecular structure of the diazadiphosphetane *trans*-**20**

Recrystallisation of the orange precipitate with an empirical formula consistent with structure **19**, by layering of a dichloromethane solution with hexane, afforded orange single crystals suitable for an X-ray diffraction study. The ensuing molecular structure determination revealed a dimeric species, *trans*-**20**, in which two diazaphosphole molecules are connected by a central four-membered PNPN diazadiphosphetane ring (Scheme 4 and Figure 5).

Scheme 4: Synthesis and atom numbering scheme of compound **20**

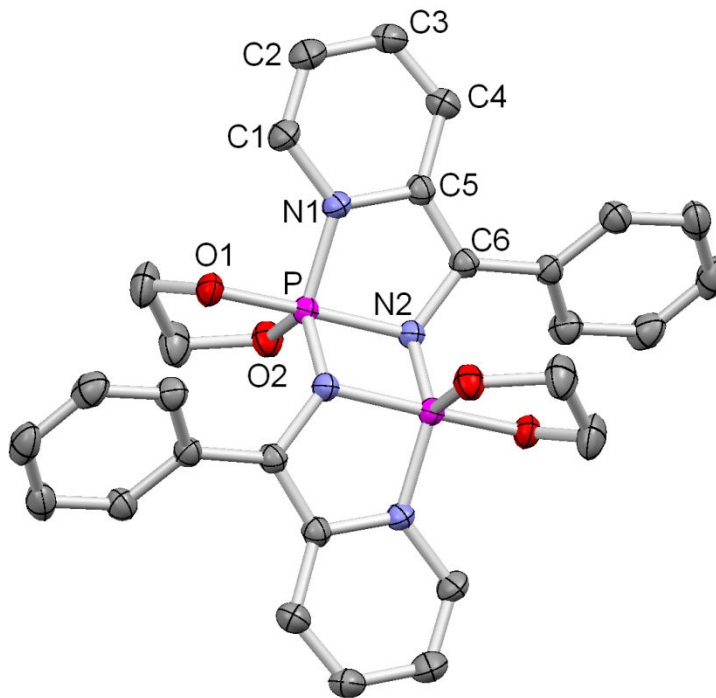


The formation of the dimer *trans*-**20** can be envisaged to result from a cyclodimerisation between two iminophosphorane fragments of the monomer **19**; this type of cyclisation is well documented for iminophosphoranes that possess electron deficient phosphorus centres.³ For example, a similar dimeric species is reported to exist in equilibrium with the corresponding monomeric form (Scheme 5).⁴ The driving force for the cyclodimerisation described for **19** and in Scheme 5 is ascribed to a reduction of ring strain for the dioxaphospholane, which results from the change in geometry about phosphorus from tetrahedral to trigonal bipyramidal. The angles for a tetrahedral geometry are expected to be 109 °, which are significantly larger than the average OPO angle recorded in dioxaphospholanes of 94 °.⁵ In comparison, a trigonal bipyramidal arrangement at

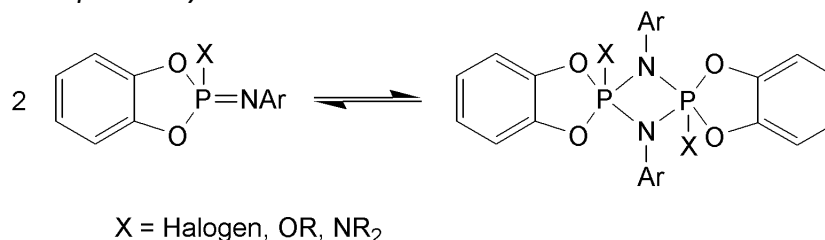
phosphorus allows for a smaller angle of 90 ° to be achieved, far closer to the average OPO angle of dioxaphospholanes.

Figure 3: Molecular structure of *trans*-**20**, with selected bond lengths (Å) and angles (°). (Thermal ellipsoids set at 75 % level). Hydrogen atoms are omitted for clarity.

P-N1	1.7151(9)
P-N2	1.7608(8)
P-N2'	1.6890(9)
N1-C1	1.4046(13)
C2-C3	1.4465(15)
C3-C4	1.3483(15)
C4-C5	1.4403(14)
C5-C6	1.3613(13)
C6-N2	1.4220(12)
P-O1	1.6537(7)
P-O2	1.6225(8)
N1-P-N2	87.10(4)
O1-P-O2	92.84(4)
N2-P-N2'	80.55(4)
P-N2-P'	99.45(4)
O1-P-N1	93.73(4)
O1-P-N2'	93.13(4)
C6-N2-P	115.25(6)



Scheme 5: Reversible cyclodimerisation of an iminophosphorane with alkoxy substituents on phosphorus reported by Kukhar' et al.⁴



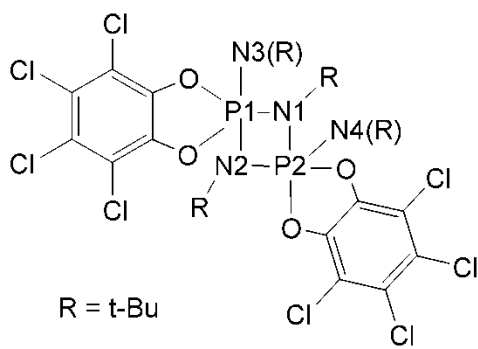
The experimentally-determined P-N bond lengths of *trans*-**20** are consistent with single bonds, with the P-N2' distance of 1.6890(9) Å being in good agreement with the value reported by Allen, 1.652 Å, as the mean average PN bond length for the environment X₂-P(=X)-NX₂ in a survey of crystallographically-characterised compounds.⁶ The two other PN distances of *trans*-**20**, P-N1 1.7151(9) Å and P-N2 1.7608(8) Å, are significantly longer than P-N2'. The mean average distance for the PN distances in P₂N₂ rings reported by Allen is 1.730 Å, which is slightly shorter than the value for P-N2.⁶ Examination of an alkoxy-*P*-substituted

diazadiphosphetane reported by Swamy, **SW**, reveals endocyclic phosphorus-nitrogen bond lengths of 1.645(3) and 1.758(3) Å (Figure 4).⁷ The former distance is comparable to that of P-N2' in *trans*-**20**, differing by only ~0.04 Å, whereas the latter distance of 1.758(3) Å is very close in length to P-N2 in *trans*-**20** with a difference of ~ 0.01 Å. Additionally, a comparison between the PN1 distance of *trans*-**20** and the exocyclic P-N bond of **SW** exposes a significant difference, with the former PN bond distance being ~ 0.07 Å shorter. These disparities are likely to result from the constraints imposed by the diazaphosphole ring of *trans*-**20**, which are absent in the diazadiphosphetane **SW**.

Figure 4: Selected bond lengths of a diazadiphosphetane, **SW**, reported by Swamy with selected bond lengths in Å (left) and structure (right)⁷

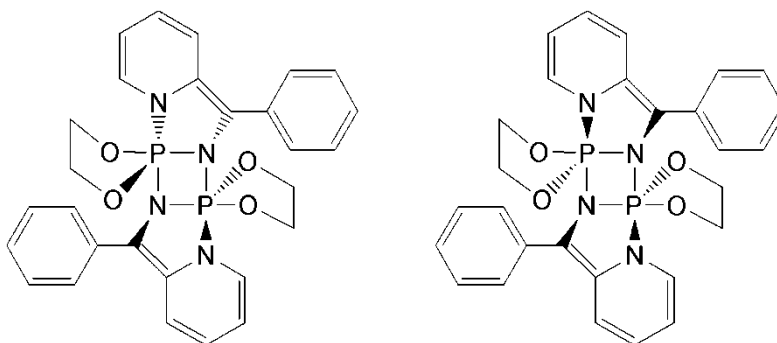
P1-N1	1.645(3)
P1-N2	1.758(3)
P1-N3	1.647(3)
P2-N1	1.758(3)
P2-N2	1.638(3)
P2-N4	1.636(3)

R = t-Bu



The X-ray molecular structure of *trans*-**20** reveals that the two diazaphosphole moieties adopt a *trans* conformation, lying on opposite faces of the diazadiphosphetane ring (Figures 3 and 5). The formation of the alternative isomer where the diazaphosphole rings are *cis* to one another is also possible (see Figure 5), but was not detected by X-ray diffraction studies upon a selection of various crystals of **20**. It is therefore unclear whether compound **20** is comprised of solely the *trans* isomer in the solid state, or a mixture of *cis* and *trans* isomers.

Figure 5: Structure of the crystallographically-characterised isomer *trans*-**20** (left) and possible isomer *cis*-**20** (right)



4.3.3. Solution-state NMR spectroscopic studies of the diazadiphosphetane **20**

Dissolution of crystals of compound **20** gave rise to two singlet resonances by ^{31}P NMR spectroscopy at - 37.8 and - 43.2 ppm, in a ratio of 89 : 11. Signals in this low frequency spectral region are to be expected by comparison with the reported data for the diazadiphosphetane **SW**, (- 51.6 ppm, Figure 4).⁷ However, the origin of the two signals upon dissolution of **20** is less obvious.

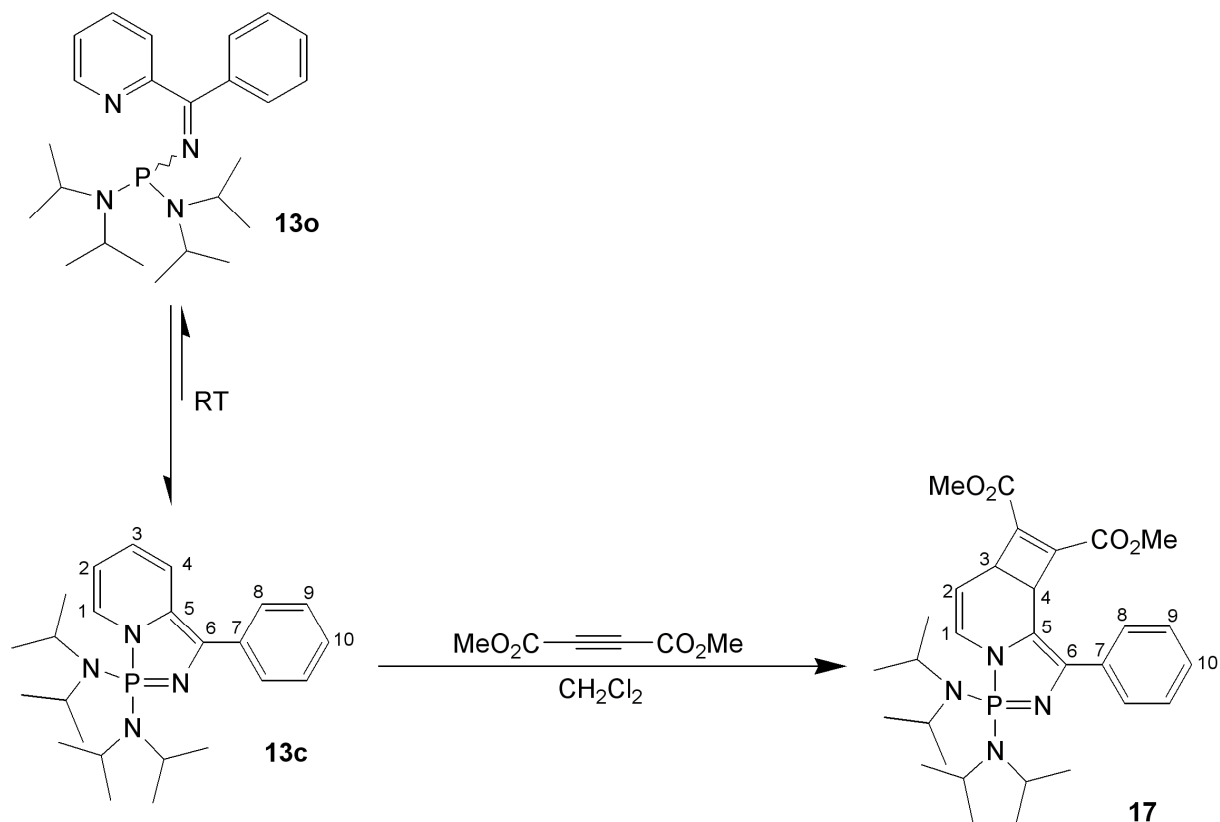
Together the solution-state ^1H and ^{13}C NMR spectra allowed the major component of the mixture of dissolved **20** to be characterised. However, the NMR signals of the minor component overlapped with those of the major species, which prevented acquisition of the ^1H and ^{13}C NMR spectral data for the former. For the major component of **20** a distinctive set of resonances between 5.3 and 6.9 ppm is observed in its ^1H NMR spectra and are attributed to the dearomatised pyridyl ring (Figure 5).^{8,9} In addition, the four protons of the dioxaphospholane moiety are found to be inequivalent with four separate multiplets being observed between 3.0 and 3.9 ppm. These data are suggestive of the major species present in solution is the dimeric structure **20** (Figure 5). Since *trans*-**20** is likely to be more stable than *cis*-**20** on steric grounds, it is logical to assume that the major component in solution is *trans*-**20**. The similarity in the two chemical shifts in the ^{31}P NMR spectrum of **20**, - 37.8 and - 43.2 ppm, implies that the phosphorus atom in the minor component is in a similar chemical

environment to that for the predominant species. This suggests that the minor component of the mixture is *cis*-**20**, although the possibility of the minor component being the monomer **19** cannot be excluded at this time. The presence or absence of the monomer could potentially be determined by an analysis of the molecular weight in solution by use of the Signer method.¹⁰ Unfortunately, the attempt to apply this molecular weight determination technique to compound **20** was unsuccessful, possibly due to air or moisture contamination.

4.4. The attempted synthesis of a sterically unencumbered variant of **13c**

The behaviour of the equilibrium mixture of **13c/13o** towards a variety of reagents has been explored. For example, the electron deficient alkyne, dimethylacetylene dicarboxylate (DMAD), reacts with the C3=C4 bond of isomer **13c** to form a cyclobutene (see Scheme 6 and Chapter III). This observation is intriguing since no reaction at the P=N double bond of **13c** was observed, despite cycloadditions between the multiple bond of iminophosphoranes and DMAD being regarded as facile (Chapter I).^{11,12} This 'inertness' of the iminophosphorane component of **13c** is attributed to the steric shielding imposed by the diisopropylamino groups, which effectively block any interaction with DMAD.

Scheme 6: Reactivity of **13c/13o** (left) with DMAD to give **17** (right)

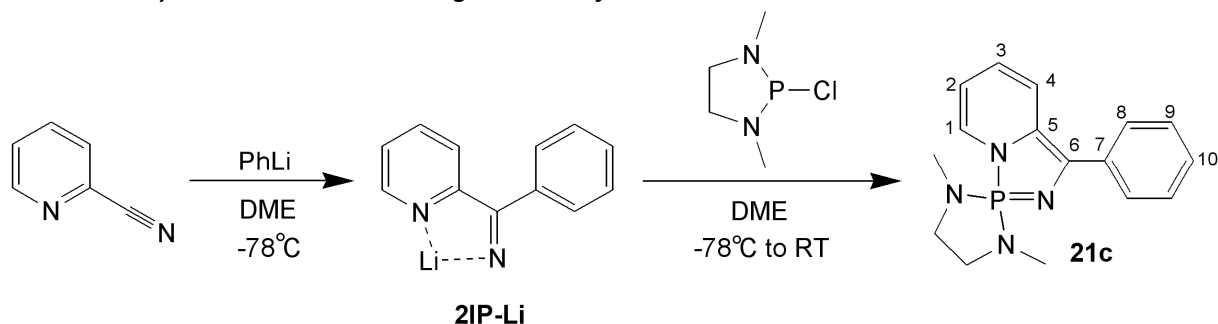


To investigate the extent of the impact of the diisopropylamino groups upon the reactivity of the iminophosphorane a less sterically-encumbered variant of **13c** was needed. Since the attempted synthesis of a heterocyclic system akin to **13c**, but with smaller alkoxy substituents in the place of diisopropylamino groups led to the formation of dimeric species **20**, and hence not directly comparable, an alternative substitution pattern was necessary. Consequently, the synthesis of a system with less sterically demanding dialkylamino substituents, relative to diisopropylamino, was targeted.

4.4.1. Synthesis and isolation of 1',3'-dimethyl-3-phenyl-*spiro*-[1 λ^5 -[1,3,2]diazaphospholo[1,5-a]pyridine-1,2'-[1,3,2]diazaphospholane], **21c**

The method used for the synthesis of **13c/13o** was adapted to use the cyclic diaminochlorophosphine (MeNCH₂CH₂NMe)PCl in place of (i-Pr₂N)₂PCl (see Scheme 7). This heterocyclic diaminochlorophosphine is readily synthesised from reaction of trichlorophosphine and *N,N'*-dimethylethylenediamine in the presence of a suitable base, a methodology first reported by McGuigan.¹³ Subsequent reaction of (MeNCH₂CH₂NMe)PCl with the lithium intermediate, **2IP-Li**, produced a red solution, which upon work-up gave a dark red solid, **21**, in an isolated yield of 81 %. Analysis of **21** by ³¹P NMR spectroscopy in C₆D₆ revealed a single resonance at 40.6 ppm, consistent with the presence of the desired heterocyclic species, **21c**, by comparison with the chemical shift for **13c**, 42.3 ppm (C₆D₆). The identity of **21c** as a closed heterocycle was confirmed by a combination of ¹H and ¹³C NMR spectroscopies. The dearomatisation of the pyridyl ring of **21c** is clearly visible by both ¹H and ¹³C NMR spectroscopy, with the chemical shifts for both protons (5.3 - 7.2 ppm) and carbons (108 – 125 ppm) reflecting an alkenyl environment.^{8,9} In addition, a ³J_{CP} coupling of 6 Hz is observed for C2, further confirmation of the presence of the P-N1 bond.

Scheme 7: Synthesis and numbering scheme of **21c**

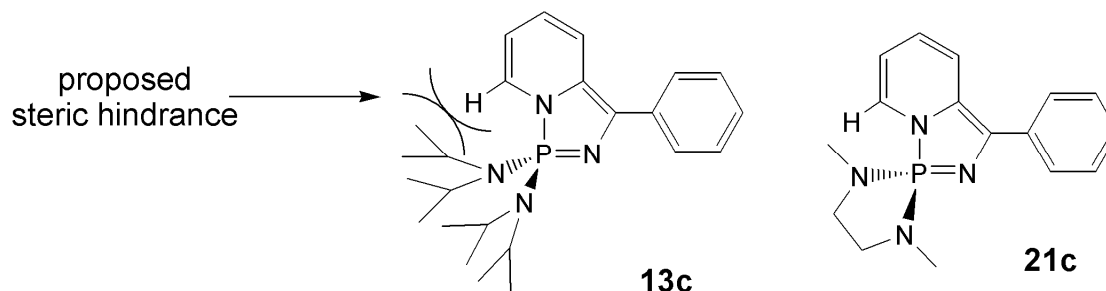


4.4.2. Attempts to detect an 'open' tautomer **21o**

The absence of the open tautomer **21o** in the ambient temperature ^{31}P NMR spectrum of **21** led to variable-temperature NMR spectroscopic experiments being conducted, since it has been demonstrated for the equilibrium mixture **13c/13o** that the proportion of the kinetic isomer **13o** increases, relative to **13c**, as the temperature is increased. However, variable-temperature NMR spectroscopic analysis of a sample of **21** dissolved in deuterated toluene did not reveal the existence of **21o** over the temperature range 20 to 90 °C.

For the equilibrium mixture **13c/13o** the co-existence of both tautomers is a result of the small difference in their Gibbs free energies. The observation of solely the 'closed' tautomer for **21** implies a much larger relative energy difference between **21c** and its **21o** tautomer, than between **13c** and **13o**. This increased energy difference is likely to arise from either destabilisation of **21o** relative to **13o** or stabilisation of **21c** relative to **13c**. For the 'open' isomers the preferred conformation is likely to position the phosphorus group distant from the aryl and pyridyl groups, minimising any unfavourable steric interactions regardless of the size of the phosphorus substituents. With this in mind it is logical to assume that the introduction of smaller substituents at phosphorus will not favour the 'open' isomer **21o**, relative to **13o**, to any significant extent. In **13c** there is the possibility of unfavourable steric interactions between the diisopropylamino groups and the dearomatised pyridyl ring (Figure 6). In contrast, compound **21c** would experience virtually no unfavourable interactions due to the reduced steric demands of the substituents at phosphorus, lowering the energy of the 'closed' form. This potentially accounts for the greater energy difference between the isomers **21o** and **21c**.

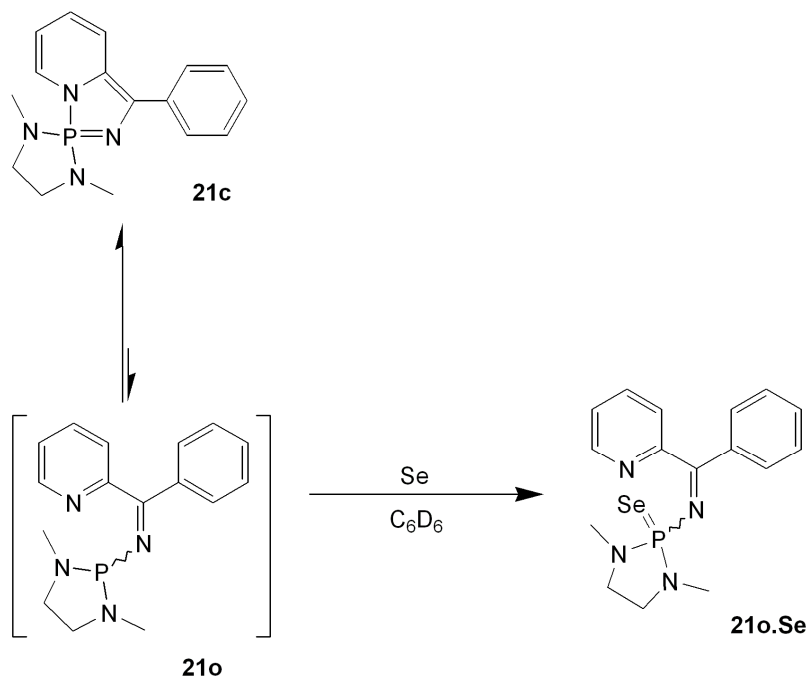
Figure 6: Comparison of **13c** (left) and **21c** (right) showing the proposed steric hindrance between the ortho proton of the pyridyl ring and the substituents on phosphorus of **13c**, relative to **21c**



4.4.3. Reaction of **21** with selenium

In an attempt to establish whether **21c** exists in equilibrium with an extremely small quantity of its 'open' valence tautomer **21o**, the reaction of **21** with selenium was conducted (Scheme 8), since selenium can only react with the phosphorus(III) centre in **21o** and not with the phosphorus(V) centre in **21c**. To this end, a solution of **21** in deuterated benzene was treated with selenium, which resulted in the complete conversion to the selenide **21o.Se**, according to ^{31}P NMR spectroscopy, after 96 h at 50 °C. The ^{31}P NMR chemical shift of 66.7 ppm for the selenide **21o.Se**, and the magnitude of the associated $^1J_{\text{SeP}}$ coupling constant of 842 Hz, are both in good agreement with the values recorded for **13o.Se** (55.5 ppm, $^1J_{\text{SeP}} = 821$ Hz, see Chapter III). Hence, the formation of **21o.Se** is direct evidence for the fact that **21** can exhibit valence tautomerism giving rise to both **21c** and **21o**. The absence of **21o** in the ^{31}P NMR spectroscopic analyses obtained for compound **21** indicates that the proportion of **21o** in the equilibrium mixture is likely to be less than 1 % at ambient temperature.

Scheme 8: Reaction of **21c/21o** with selenium to give **21o.Se**



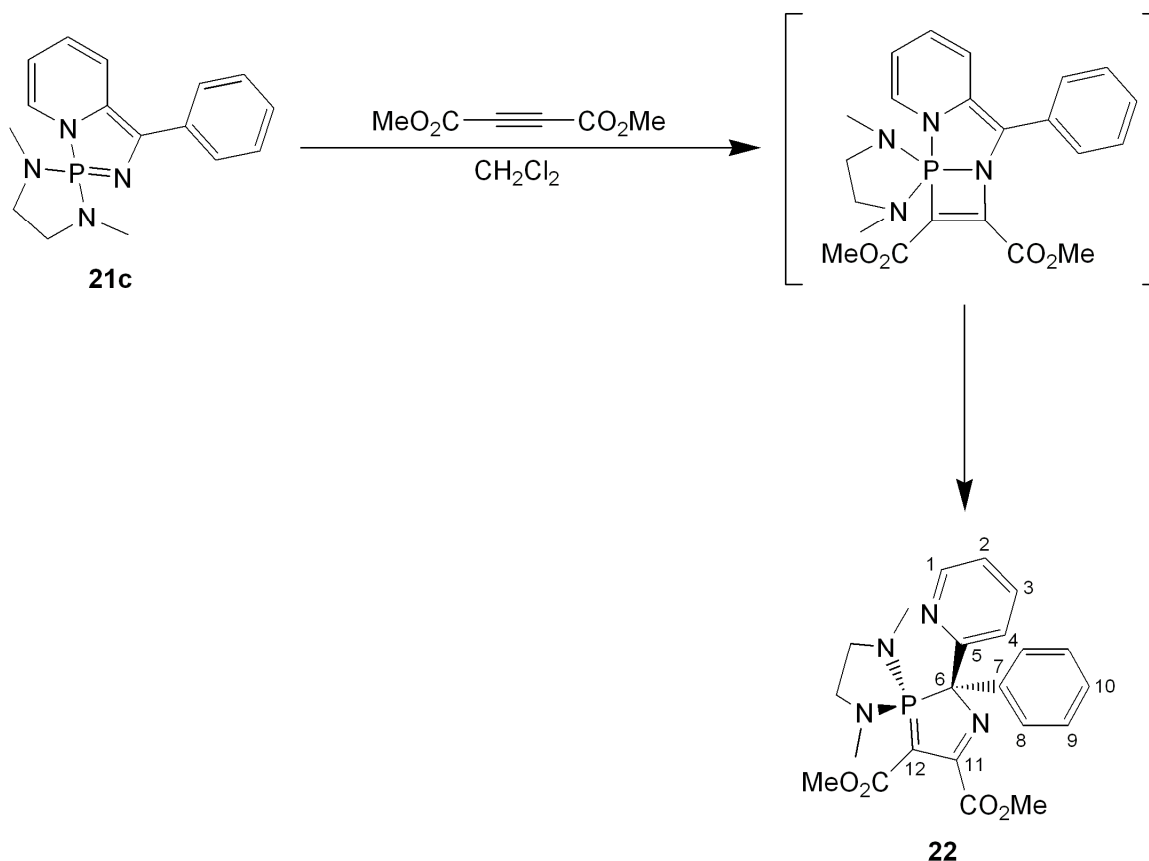
4.4.4. Reaction of compound **21** with DMAD to give **22**

The reaction of DMAD with **13c/13o** was observed to proceed with reaction at the carbon-carbon double bond C3=C4 of **13c** and not at the iminophosphorane component (Scheme 6 and Chapter III). The steric constraints imposed by the bulky diisopropylamino groups were proposed to be the cause of the lack of reaction of the P=N double bond in **13c**. Since the substituents at phosphorus in compound **21c** are far smaller in size, than in **13c**, it was therefore of interest to explore the reactivity of DMAD towards **21**.

Thus, an equimolar reaction between DMAD and **21** was undertaken and gave a new compound, **22**, after 4 h, which presented a single resonance by ^{31}P NMR spectroscopy at 84.3 ppm with no further reaction being observed (Scheme 9). The large difference in ^{31}P NMR chemical shift between **21c** (40.6 ppm) and **22** (84.3 ppm) indicates a significant change in the phosphorus environment. In contrast with the transformation of **21c** to **22**, the reaction of **13c** with DMAD to give the cyclobutene-containing product **17** is accompanied by only a small change in the chemical shift of the phosphorus centre, from 42.3 to 46.6 ppm.

This difference in the magnitudes of $\Delta\delta$ implies that the reaction of **21c** with DMAD occurs at the iminophosphorane and not at the C3=C4 double bond as in **13c** (Scheme 9).

*Scheme 9: The proposed reaction of **21c** with DMAD to give an azaphosphetene and subsequent rearrangement to **22**. The atom numbering scheme is presented.*



4.4.4.1. Solution-state NMR spectroscopic studies of **22**

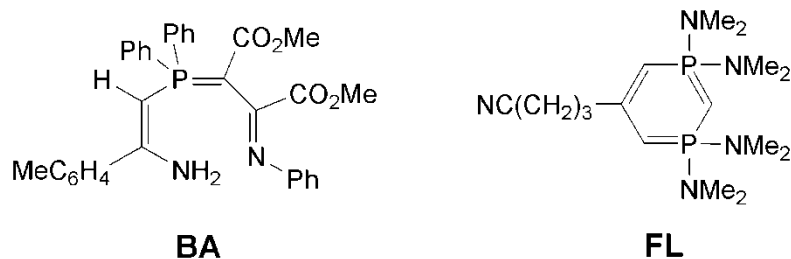
Although compound **22** was not isolated, due to difficulties in purification from DMAD and possibly other species, the characterisation of **22** was achieved *in situ*. Examination of the ^1H NMR spectrum of **22** reveals pyridyl resonances between 7.2 and 8.6 ppm, indicative of an aromatised ring and is suggestive of the structure drawn for **22** in Scheme 9. In addition, the observation of an aromatised pyridyl ring excludes the possible azaphosphetene structure

(Scheme 9) for **22**. Instead, the proposed structure of compound **22** can be described as an azaphosphole with a *spiro* diazaphospholane ring and exocyclic pyridyl and phenyl groups.

The $^{13}\text{C}\{^1\text{H}\}$ NMR spectroscopic analysis of compound **22**, in combination with 2D NMR techniques, allows the assignment of carbon-6 to a doublet resonance at 76.3 ppm, with a J_{PC} coupling constant of 66 Hz.¹⁴ The magnitude of this coupling is suggestive of a one bond coupling between phosphorus and carbon-6, in agreement with the proposed structure (Scheme 9).¹⁵ In addition, a J_{PC} coupling constant of 3 Hz is noted for carbon-8 of the phenyl ring of **22**, inferring the presence of phosphorus within three to four bonds of this carbon.

Consideration of the azaphosphole ring of **22** reveals the chemical shift of carbon-12 (59.3 ppm) to be characteristic of a P=C environment with a similar chemical shift of 60.8 ppm reported for the phospho-alkene carbon of a comparable cycloaddition product synthesised by Barluenga, **BA** (see Figure 7).¹⁴ The J_{PC} coupling constant for the phospho-alkene carbon of **BA** is 110 Hz, which is of the same order of magnitude as that observed for carbon-12 (140 Hz) of **22**. In addition, carbon-11, of compound **22**, exhibits the characteristic high frequency shift of an imine of 170.3 ppm in the ^{13}C NMR spectrum¹⁶ and the proximity of this carbon to phosphorus is evident by the large coupling constant, $J_{\text{PC}} = 53$ Hz.¹⁴ These spectroscopic data are in good agreement with the suggested structure of the compound **22** (Scheme 9).

Figure 7: Examples of phospho-alkenes reported by Barluenga¹⁴ (left) and Fluck¹⁷ (right) with similar phosphorus and carbon chemical environments to those of compound **22**



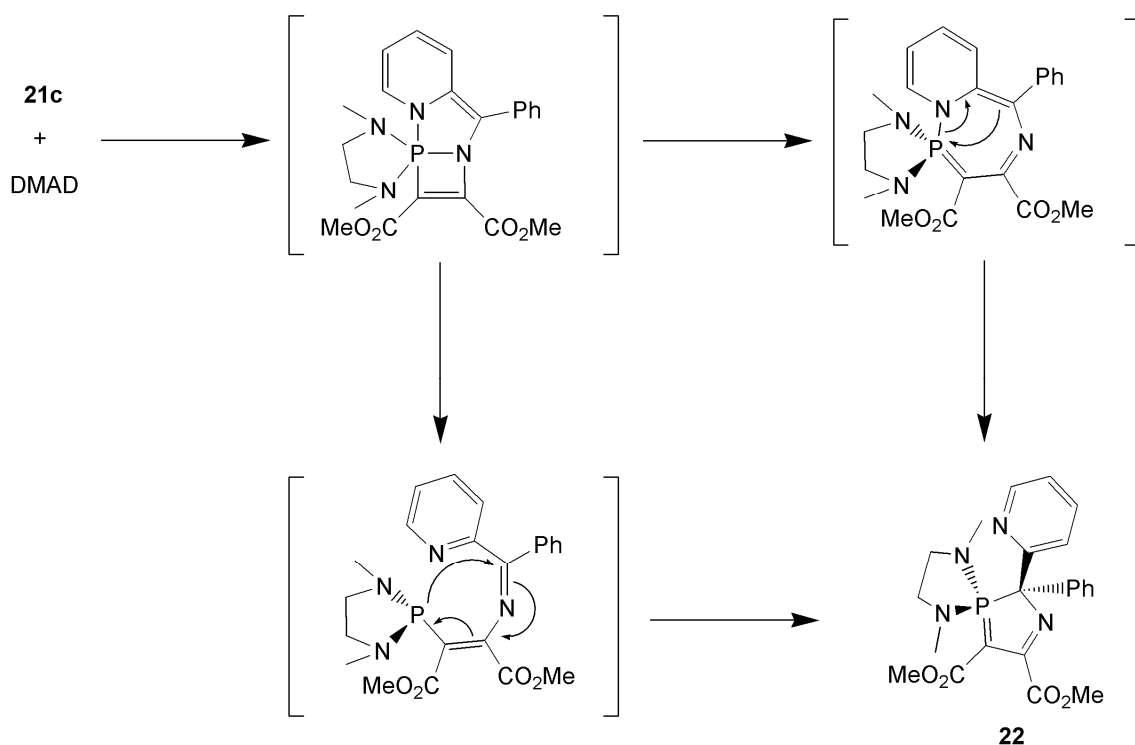
A similar phosphorus environment to that in structure **22** exists in compound **FL** reported by Fluck (see Figure 7).¹⁷ In both cases the ylide is substituted with two dialkylamino groups on phosphorus and exists within a cyclic system. A comparison of the ^{31}P NMR

chemical shift for **FL** and **22** shows a reasonable similarity with signals at 60.3 and 84.3 ppm being recorded, respectively, further supporting the proposed structure of **22**.

4.4.4.2. The mechanism of formation of compound **22**

It can be envisaged that reaction of DMAD with **21c** initially gives an azaphosphetene, which subsequently rearranges to yield azaphosphole **22** (Scheme 9). Although the driving force for the rearrangement of azaphosphetene is undoubtedly the relief of ring strain and the rearomatisation of pyridine, the mechanism is unclear. Two possible mechanisms are described in Scheme 10, where ring opening of the azaphosphetene is necessary in both pathways to give compound **22**. Unfortunately, without further study the mechanism cannot be determined. However, monitoring of the reaction of **21c** with DMAD by ^{31}P NMR spectroscopy, reveals the formation of a broad resonance ($\nu_{1/2} = 81$ Hz) at 76.1 ppm after 15 minutes, which transformed into the resonance corresponding to **22** over the course of 4 h. This broad resonance is attributed to an intermediate species in the formation of **22**.

*Scheme 10: Possible mechanisms of the formation of **22** from the reaction between **21c** and DMAD*



4.5. Summary

An exploration of the chemical factors controlling the equilibrium position for the mixture **13c/13o** has been undertaken. It has been demonstrated that alteration of the back-bone phenyl substituent to an anthracenyl group gives another equilibrium mixture, but in this case a greater proportion of the 'open' tautomer exists at ambient temperature. Physical separation of the two isomers **18o** and **18c** has also been achieved, with the latter characterised by an X-ray diffraction study.

A reduction of the steric demands of the dialkylamino groups of the **13c/13o** framework favours the 'closed' tautomer as shown by compound **21**, for which the 'open' isomer cannot be directly detected. However, indirect evidence for access to the 'open' tautomer is given by the reaction of **21** with selenium to give **21o.Se**. Introduction of alkoxy substituents at phosphorus also favours the 'closed' isomer, which exists not as a monomer, but as a dimeric species **20**.

In conclusion, the compounds **13** and **18** exist as equilibrium mixtures of both 'open' and 'closed' tautomers at ambient temperature, in contrast to the related *N*-phosphino-pyridyl imines (**2IP-PPh₂**, **1o-6o** and **14o**). This is attributed to the energy difference between the 'open' and 'closed' tautomers, which diminishes, and is eventually reversed, upon the introduction of increasingly electron-withdrawing substituents on phosphorus. Steric factors can also affect the energetics of the system as shown by the comparison of **13o/13c** with **21c/21o** and equally prevent ring closure of a *N*-phosphino-pyridyl imine, **14o**, where electronically the diazaphosphole tautomer is favoured.

¹ J. Wesemann, P. G. Jones, D. Schomburg, L. Heuer, R. Schmutzler, *Chem. Ber.*, 1992, **125**, 2187.

² Z. Benkő, S. Burck, D. Gudat, M. Nieger, L. Nyulászi, N. Shore, *Dalton Trans.*, 2008, 4937.

³ Y. G. Gololobov, L. F. Kasukhin, *Tetrahedron*, 1992, **48**, 1353.

⁴ V. P. Kukhar', E. V. Grishkun, V. P. Rudavskii, V. A. Gilyarov, *Russ. J. Gen. Chem.*, 1980, **50**, 1477.

⁵ F. H. Allen, *Acta Cryst.*, 2002, **B58**, 380. Date: October 2009.

-
- ⁶ F. H. Allen, O. Kennard, D. G. Watson, L. Brammer, A. G. Orpen, R. Taylor, *J. Chem. Soc. Perkin Trans. II*, 1987, Supplement, S1 – S18.
- ⁷ K. P. Kumar, M. Chakravarty, K. C. K. Swamy, *Z. Anorg. Allg. Chem.*, 2004, **630**, 2063.
- ⁸ C. D. Entwistle, A. S. Batsanov, J. A. K. Howard, M. A. Fox, T. B. Marder, *Chem. Commun.*, 2004, 702.
- ⁹ R. M. Acheson, N. D. Wright, P. A. Tasker, *J. Chem. Soc. Perkin Trans. I*, 1972, 2918.
- ¹⁰ E. P. Clark, *Ind. Eng. Chem. Anal. Ed.*, 1941, **13**, 820.
- ¹¹ L. R. Falvello, J. C. Gins, J. J. Carb, A. Lleds, R. Navarro, T. Soler, E. P. Urriolabeitia, *Inorg. Chem.*, 2006, **45**, 6803.
- ¹² J. Barluenga, I. Merino, F. Palacios, *Tetrahedron. Lett.*, 1989, **30**, 5493.
- ¹³ M. S. Anson, C. McGuigan, *J. Chem. Soc. Perkin Trans I*, 1989, 715.
- ¹⁴ J. Barluenga, F. Lopez, F. Palacios, *Chem. Commun.*, 1985, 1681.
- ¹⁵ B. F. G. Johnson, T. Khimyak, F. W. Wansel, G. Phillips, S. Hermans, J. R. Adams, *J. Cluster Sci.*, 2004, **15**, 315.
- ¹⁶ A. Baceiredo, G. Bertrand, P. W. Dyer, J. Fawcett, N. Griep-Raming, O. Guerret, M. J. Hanton, D. R. Russell, A.-M. Williamson, *New J. Chem.*, 2001, **25**, 591.
- ¹⁷ G. Heckmann, S. Plank, B. Neumüller, E. Fluck, *Z. Anorg. Allg. Chem.*, 2000, **626**, 1739.

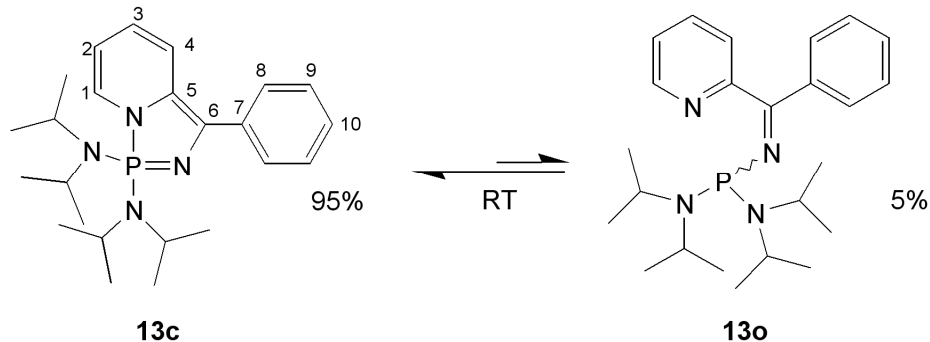
Chapter V

5. Synthesis of a viologen-like diphosphonium salt by a phosphonium-mediated oxidative coupling

5.1. Introduction

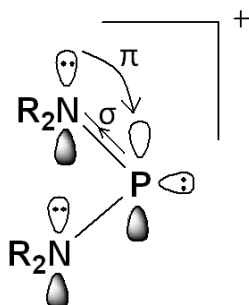
In Chapter III the synthesis and reactivity associated with a novel equilibrium between a P⁺N ligand, **13o**, and a diazaphosphole, **13c**, was described (Scheme 1). The equilibrium mixture **13o/13c** has been demonstrated to react at a variety of different sites around the molecular framework including the phosphorus centre, the imine nitrogen lone pair and the C3=C4 double bond. It was therefore of interest to consider the reactivity of a multi-functional reagent towards **13c/13o**. A suitable choice was deemed to be a phosphonium cation.

*Scheme 1: Equilibrium between **13c** and **13o** with atom numbering scheme*



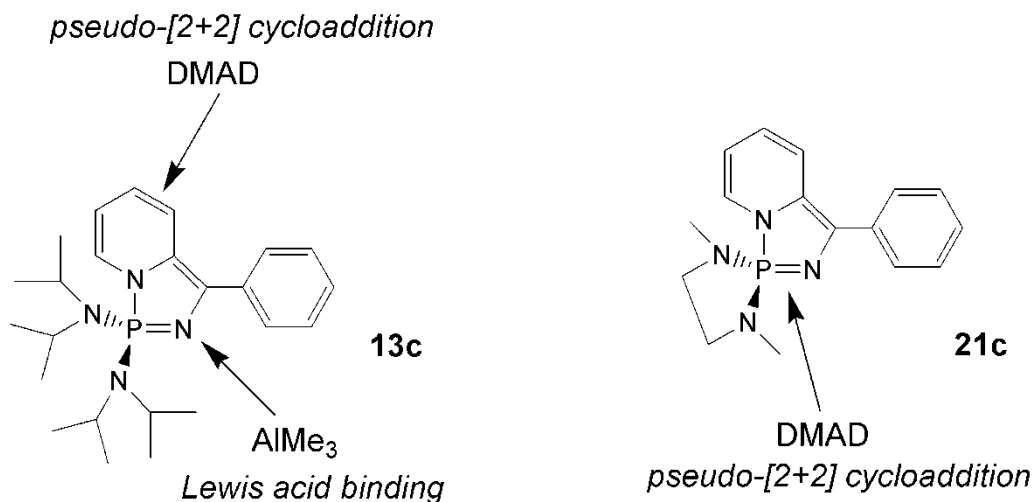
Phosphenium cations are formally valence isoelectronic and isolobal with a singlet carbene.¹ The divalent phosphorus centre is often stabilised by the presence of amino groups, with the σ -electron-withdrawing nitrogen atoms helping to delocalise the phosphorus lone pair in the sp^2 hybridised orbital, while the lone pairs of the nitrogen atoms are able to donate electron density into the empty p-orbital of phosphorus (Figure 1). These ions can be regarded as ambiphilic in nature, functioning as either Lewis acids or bases.¹

Figure 1: Pictorial description of the bonding in a phosphonium cation



In combination with **13c/13o** it was proposed that a phosphonium cation could react either as a Lewis acidic entity and bind to the exposed lone pair of the iminophosphorane in **13c** or, potentially react with the P=N or a localised C=C double bond of **13c** in a cycloaddition-type process (Figure 2 and Chapters III and IV).² The latter reaction would be analogous to the reactivity of **13c** with dimethylacetylene dicarboxylate. Indeed, there is precedent for phosphonium cations undergoing cycloaddition with a wide range of dienes and strained alkenes (see Chapter I).^{1,3,4}

Figure 2: Reactivity observed for **13c** (left) and **21c** (right). Phosphonium cations possess both full and vacant orbitals at phosphorus and so reactivity of $[(i\text{-Pr}_2\text{N})_2\text{P}][\text{OTf}]$ at one of the three sites of the molecular framework was envisaged



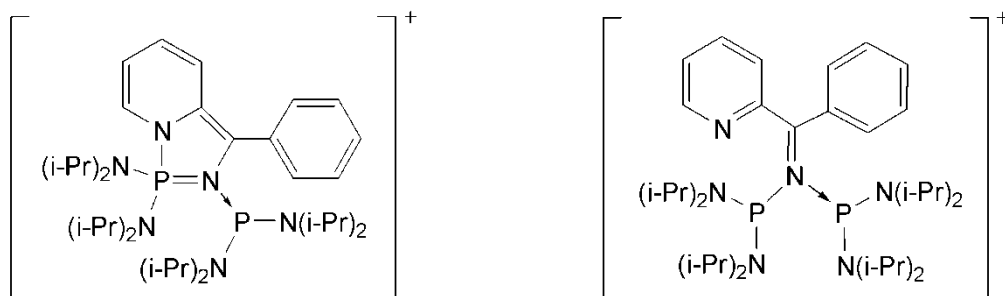
Bis(diisopropylamino)phosphonium triflate was chosen as the phosphonium salt for reaction with **13c/13o** due to its relative stability and ease of synthesis, in comparison to

some phosphonium species (Chapter I). The phosphonium tetrachloroaluminate salt is also known, but in contrast to the triflate, can re-generate AlCl_3 by anion dissociation in the presence of certain bases and so for this study $[(i\text{-Pr}_2\text{N})_2\text{P}][\text{OTf}]$ was used in preference to the $[(i\text{-Pr}_2\text{N})_2\text{P}][\text{AlCl}_4]$.⁵ Furthermore, the triflate salt can be synthesised in good yield from bis(diisopropylamino)chlorophosphine and trimethylsilyltriflate with elimination of trimethylsilylchloride.^{6,7}

5.2. Reaction of 13c/13o with $[(i\text{-Pr}_2\text{N})_2\text{P}][\text{OTf}]$ to give 23

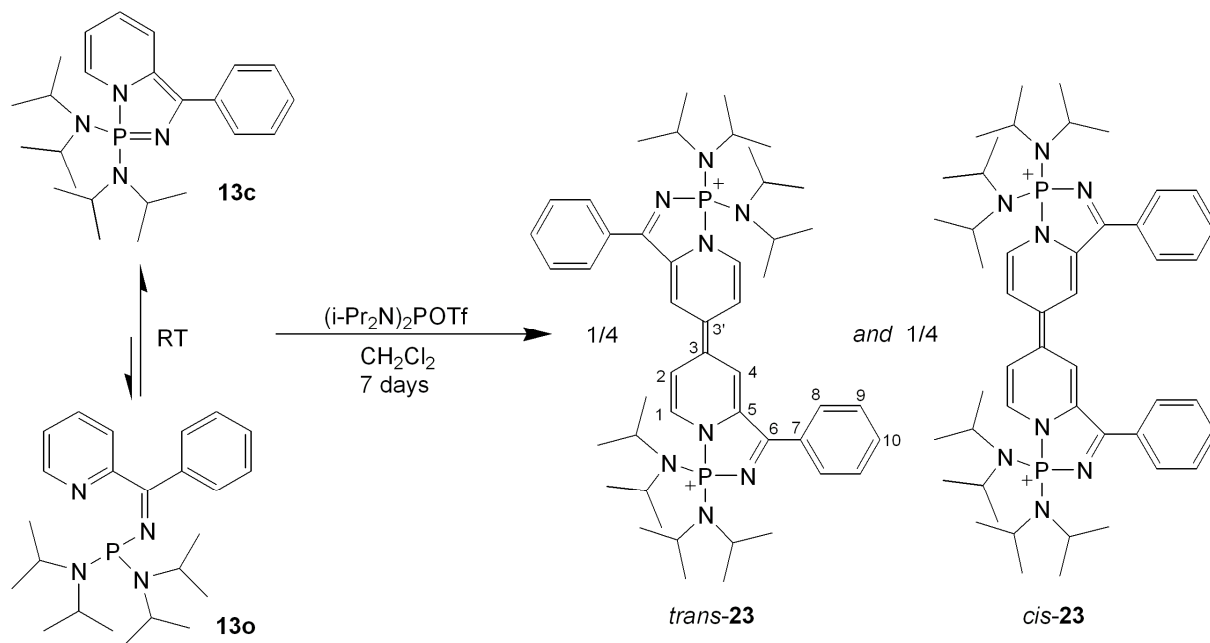
The reaction between **13c/13o** and $[(i\text{-Pr}_2\text{N})_2\text{P}][\text{OTf}]$ was carried out in dichloromethane because of the high solubility of the phosphonium salt in this solvent. Immediately following addition, the ^{31}P NMR spectrum of the resulting solution revealed two broad peaks at 52.0 and 62.6 ppm. The broadening observed in the NMR spectrum suggests a fluxional process and has been attributed to the presence of an adduct of the two reagents, $[(i\text{-Pr}_2\text{N})_2\text{P.13}][\text{OTf}]$ (Figure 3). This type of species is likely to form as a result of binding of the Lewis acidic phosphonium cation to **13c** through the iminophosphorane lone pair in a manner analogous to that seen with AlMe_3 (Chapter III). The coordination of phosphonium cations to amines and phosphines has been extensively explored, with displacement of the counter anion by one of these donor molecules often being observed.⁸⁻¹¹

Figure 3: Possible structures of $[(i\text{-Pr}_2\text{N})_2\text{P.13}]^+$



This reaction of **13c/13o** with $[(i\text{-Pr}_2\text{N})_2\text{P}][\text{OTf}]$ was repeated on a larger scale and allowed to stand for seven days, resulting in the formation of a dark solution above a green precipitate, **23**. Analytically pure **23** could be obtained by washing the green precipitate material with diethyl ether and then water. Recrystallisation of the green material gave a small quantity of single crystals suitable for an X-ray molecular diffraction study, from which the structure of the *trans* isomer of **23** was determined (see Scheme 2). It should be noted that these crystals were obtained alongside an amorphous green solid proposed to be the *cis* isomer of **23** (*vide infra*). For compound **23** these two isomers exist with the phenyl rings being either *cis* or *trans* to each other with respect to the C3C3' double bond (Scheme 2). The nature and formation of both *cis* and *trans* isomers of **23** will be returned to later.

Scheme 2: Synthesis of *trans*-**23** and *cis*-**23** from reaction of **13c/13o** with $[(i\text{-Pr}_2\text{N})_2\text{P}][\text{OTf}]$

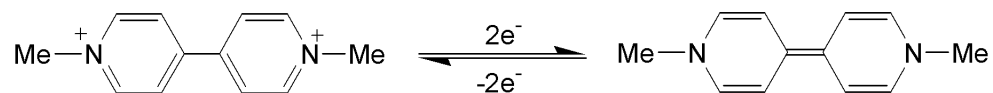


5.2.1. X-ray diffraction study of *trans*-**23**

The X-ray molecular structure of *trans*-**23** reveals that two molecules of **13c** have been “coupled together” at the 4-position of the pyridine ring to create a doubly-reduced ‘viologen’-containing central core, with each phosphorus atom bearing a single positive

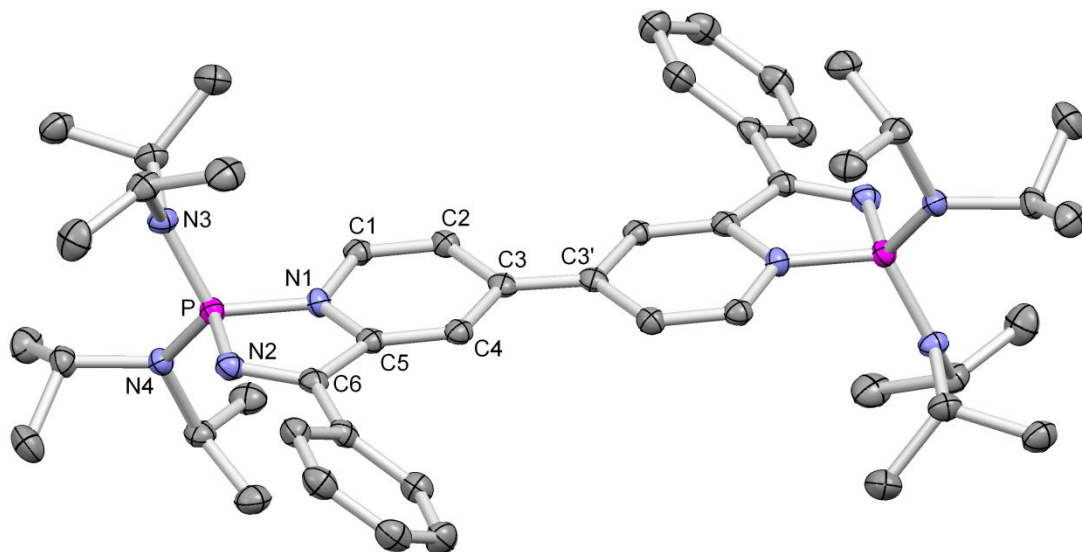
charge (Figure 4). The term 'viologen' denotes the class of compounds having the structure of bipyridine with quaternerised nitrogen atoms, whose simplest member is methyl viologen (Scheme 3).¹²

Scheme 3: The simplest viologen, methyl viologen, (left) and its doubly reduced form (right).



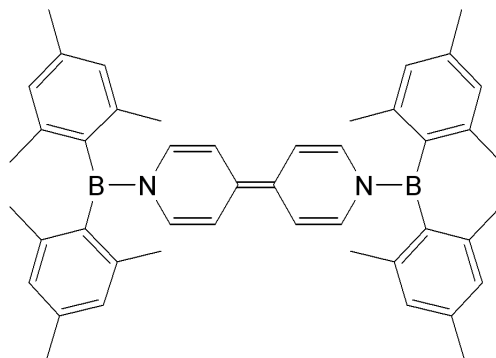
The overall structure of *trans*-**23** is dicationic in nature with two triflate counter anions. The central core of *trans*-**23** is essentially planar with the phosphorus atoms slightly above and below the plane of the doubly-reduced viologen by 0.23 Å, and the phenyl rings twisted relative to this plane with a dihedral angle of 38.7 °. Localised bonding exists throughout the diphosphonium cation with alternating single and double bonds. The central double bond C3=C3', 1.394(5) Å, is of the length expected from a similar doubly-reduced viologen reported by Kaim, namely 1,1'-bis(dimesitylboryl)-1,1',4,4'-tetrahydro-4,4'-bipyridylidene, having a central carbon-carbon bond distance of 1.391(4) Å (Figure 5).¹³ The geometry around phosphorus in *trans*-**23** is tetrahedral with the single bonds to the exocyclic nitrogen atoms being slightly shorter than those in **13c**, undoubtedly due to the greater positive charge on the of phosphorus atoms in **23**.

Figure 4: Molecular structure of *trans*-**23**, with selected bond lengths (Å) and angles (°) with triflate counter anions and hydrogen atoms excluded for clarity. (Thermal ellipsoids set at 50 % level)



P-N1	1.687(2)	C3-C4	1.433(4)
P-N2	1.657(2)	C4-C5	1.355(4)
P-N3	1.619(2)	C5-C6	1.468(4)
P-N4	1.612(2)	C5-N1	1.407(3)
N1-C1	1.402(2)	N2-C6	1.306(4)
C1-C2	1.343(4)	N1-P-N2	95.58(11)
C2-C3	1.457(4)	N3-P-N4	109.27(12)
C3-C3'	1.394(5)	P-N2-C6	110.72(19)

Figure 5: A doubly-reduced viologen derivative reported by Kaim¹³



5.2.2. Analysis of **23** by solution-state ^1H and ^{31}P NMR spectroscopies

The solution-state ^{31}P NMR spectrum of **23** gave two signals at 51.4 and 51.9 ppm. Since *trans*-**23** is symmetric about its centre, both phosphorus atoms must have the same chemical environment and ^{31}P NMR chemical shift. Hence, it is logical, therefore, to assume that one signal in the solution-state phosphorus NMR spectrum corresponds to the *trans* isomer and the other to a *cis* isomer. These two geometric isomers would be expected to exhibit similar chemical shifts in their NMR spectra. It should be noted that in the *cis* isomer the proximity of the phenyl rings is likely to result in a slight twisting of the central doubly-reduced viologen core, something that causes the observed chemical shift difference for *cis*-**23** relative to *trans*-**23**.

The formation of both *cis*- and *trans*-**23** indicates that the steric interaction between the phenyl rings of the *cis* isomer is small. It would be expected that *trans*-**23** is thermodynamically favoured over *cis*-**23** due to the absence of unfavourable phenyl-phenyl interactions in the former, which may cause slight distortions to the planarity of the doubly-reduced viologen core. Computational DFT investigations were conducted at the 6-31G*/B3LYP level of theory in an attempt to quantify the energy difference between the two isomers. Optimisation of the geometries of *cis*-**23** and *trans*-**23** gave results that for the *trans* isomer compared favourably with the X-ray molecular structure determined for *trans*-**23**. The calculated energies of the isomers showed *trans*-**23** to be only 1.8 kJ mol⁻¹ lower in energy than *cis*-**23**. This difference is very small and from the experimental observation of a near 1:1 ratio of isomers in isolated **23**, shows that in fact the phenyl-phenyl steric interaction has little influence on the formation of the *cis* isomer.

To exclude interconversion between the two isomers being the cause of the two resonances observed on solution, variable temperature NMR spectroscopy was employed. The ^{31}P NMR spectrum of a tetrachloroethane solution of **23** was recorded at 80 °C and was found to be identical to that determined at 25 °C. The same solution was then subject to a selective inversion NMR experiment, but no interconversion between isomers was observed

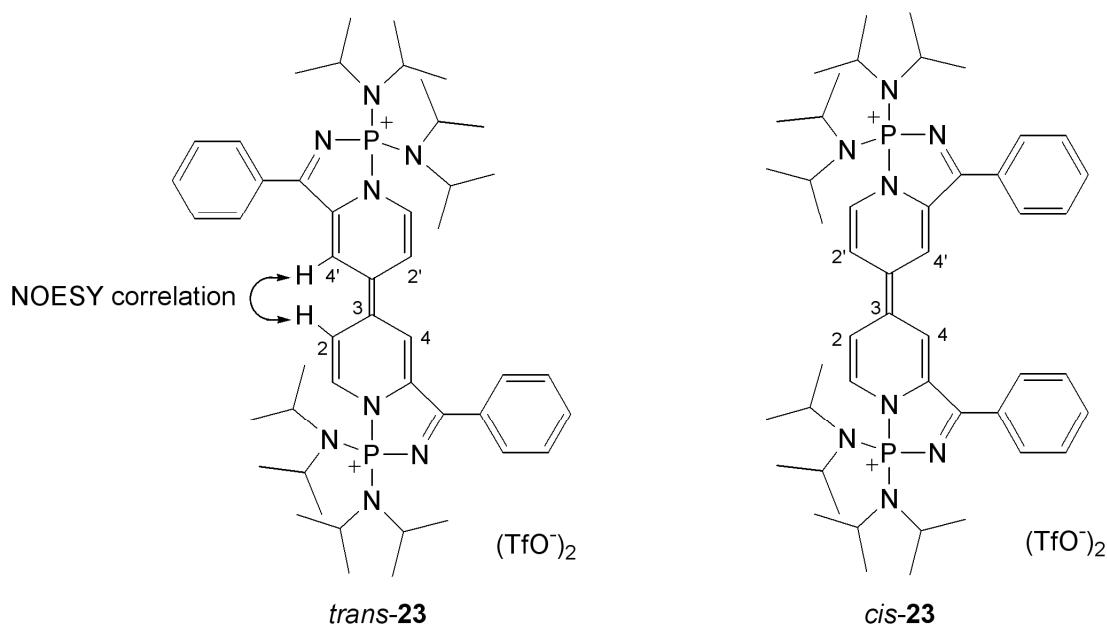
at 40 °C. This does not, however, exclude a rate of exchange slower than the NMR time scale, but without isolation of a single isomer a possible interconversion process is difficult to discount.

Dissolution of precipitated **23** was generally observed to give an approximately 1:1 ratio of the signals for *cis* and *trans* isomers by ^1H and ^{31}P NMR spectroscopy. It was noted, however, that a slightly greater proportion of *trans*-**23**, relative to *cis*-**23**, was sometimes obtained by recrystallisation of **23**. A possible explanation of this irregularity would be a lower solubility of *trans*-**23** in comparison to *cis*-**23**, thereby favouring crystallisation of the *trans* isomer. It must be stressed, however, that neither isomer was isolated pure from the other. Attempts to separate the isomers by chromatography were unsuccessful, something attributed to the similar chemical properties of the two isomers.

5.2.3. Analysis of **23** by 2D NMR spectroscopy

Analysis of the ^1H NMR spectrum of precipitated **23** reveals two sets of distinguishable peaks for the quinoidal protons of the *cis* and *trans* isomers of **23**, whereas the phenyl resonances are found to overlap due to the similarity of their environments. The chemical shifts of the core quinoidal protons lie in the range 6.5 – 7.4 ppm, the region expected for an extensively conjugated system.¹³ The *cis* and *trans* isomers can be distinguished in the ^1H NMR spectrum of the mixture by the use of a two dimensional NOESY experiment. Unlike HSQC and HMBC that provide through bond correlations between nuclei, NOESY gives information about ‘through-space’ distances between nuclei. It was proposed that *trans*-**23** would display a ‘through-space’ correlation between the protons C^2H and $\text{C}^{4'}\text{H}$ whereas *cis*-**23** would not (Figure 6). This was found to be the case and allowed the two isomers to be distinguished.

Figure 6: NOESY correlation detected between C^2H and $C^{4'}H$ of *trans*-**23**



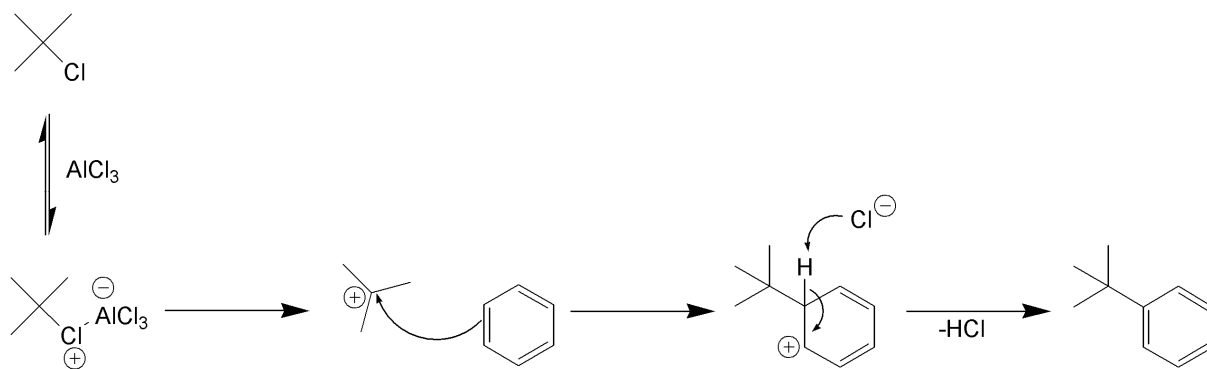
In the ^{31}P NMR spectrum of a mixture of *cis* and *trans*-**23** two signals are observed (51.4 and 51.9 ppm) and assignment of these resonances was possible upon analysis of a mixture where the ratio of the isomers was not exactly 1:1. Examination of the ^1H NMR spectrum revealed the major component to be *trans*-**23** and corresponded to the ^{31}P NMR spectroscopic signal at 51.4 ppm.

5.3. Possible mechanisms of formation of **23**

5.3.1. The loss of a hydrogen atom from **13c/13o**

The reaction of **13c/13o** with [(i-Pr₂N)₂P][OTf] has been demonstrated to give **23** in reasonable yields (61 %), however, the mechanism of formation of **23** is unclear. Clearly, the conversion of **13c/13o** to **23** involves the loss of a hydrogen atom at the position *para* to the pyridyl nitrogen with formation of a carbon-carbon bond. This process is somewhat reminiscent of Friedel-Crafts alkylation which concerns the electrophilic substitution of aromatic rings with alkyl groups (Scheme 4).¹⁴

Scheme 4: Example of Friedel-Crafts alkylation¹⁴



In Friedel-Crafts alkylation a hydrogen atom is lost in the form of a proton and it is logical to assume that the same occurs in the formation of **23** (Scheme 4).¹⁴ Although the hydrogen atom lost from **13c/13o** could be envisaged to leave as dihydrogen, the evolution of gas was not observed in any reaction that gave rise to **23**. In addition, the removal of a hydride from a carbon ring is unlikely given the polarisation of the C-H bond with Pauling electronegativity values (χ) for carbon and hydrogen of 2.55 and 2.20, respectively.¹⁵ Therefore, the following discussion assumes that a proton is lost from **13c/13o** in the reaction with $[(i\text{-Pr}_2\text{N})_2\text{P}][\text{OTf}]$.

5.3.2. Assessment of the formal oxidation state changes in the reaction of **13c/13o** with $[(i\text{-Pr}_2\text{N})_2\text{P}][\text{OTf}]$ to give **23**

Examination of the constituent atoms of **13c** and **23** shows that the formal oxidation states for both carbon-3 and carbon-6 increase and hence, the coupling of two molecules of **13c** to give **23** may be regarded as an oxidation (Figure 7 and Table 1). Therefore a reduction must also occur and this leads to the possibility of $[(i\text{-Pr}_2\text{N})_2\text{P}][\text{OTf}]$ being reduced in the reaction. However, in order to consider this overall redox process further, the fate of the phosphonium cation must be addressed.

Figure 7: Formal oxidation states of atoms that undergo redox processes in the conversion of **13c/13o** to compound **23**, with the isomer **13c** chosen for simplicity

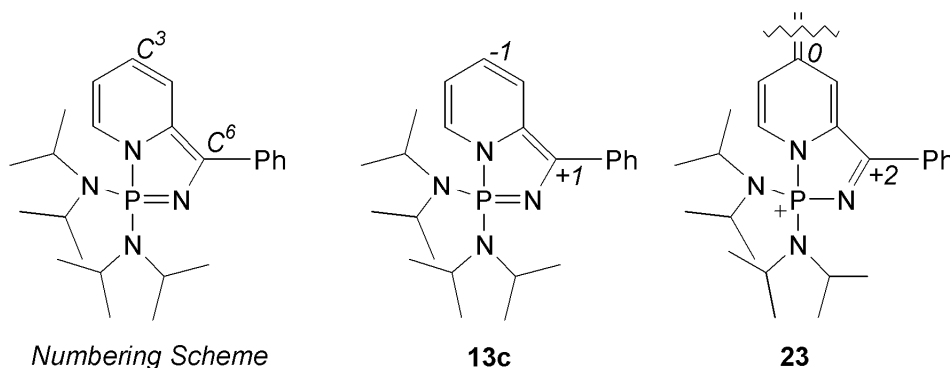
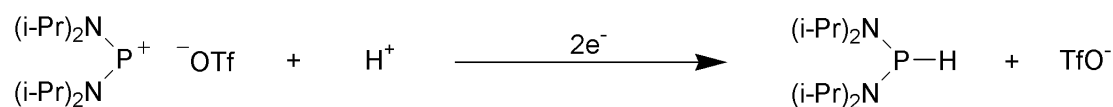


Table 1: Formal oxidation states of atoms that undergo redox processes

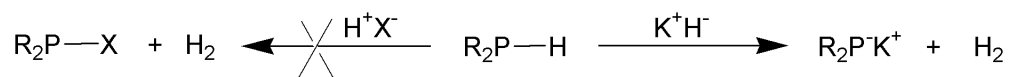
	13c	23
C^3	-1	0
C^6	+1	+2

To balance the loss of a proton and the gain of a triflate counter anion for each coupled molecule of **13c/13o** to produce **23**, the generation of the secondary phosphine from the phosphonium cation is necessary. The conversion of $[(i\text{-Pr}_2\text{N})_2\text{P}][\text{OTf}]$ to $(i\text{-Pr}_2\text{N})_2\text{PH}$ is a reduction and reflected by the formal oxidation states of phosphorus in these compounds, + 3 and + 1, respectively. For secondary phosphines, it should be noted that in general the P-H bond is considered to be a proton bonded to a phosphide (R_2P^-) although, owing to the low polarity of the bond (H: $\chi = 2.20$, P: $\chi = 2.19$), hydridic character has been observed in rare cases.^{16,17}

Scheme 5: Reduction of $[(i\text{-Pr}_2\text{N})_2\text{P}][\text{OTf}]$ to $(i\text{-Pr}_2\text{N})_2\text{PH}$



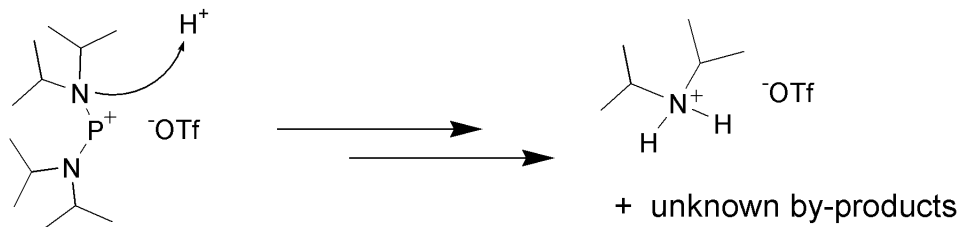
Scheme 6: Typical reactivity of phosphorus-hydrogen bonds, generally polarised $P^{\delta-}-H^{\delta+}$. Rare exceptions of hydridic reactivity are known, however, where R_2PH liberates H_2 from addition of an acid¹⁶



5.3.3. The fate of the phosphenium cation following its reaction with **13c/13o**

In the formation of **23**, the mode of reaction of the phosphenium cation with **13c/13o** is unclear. Exchange of a triflate for a proton is, hypothetically, a viable reaction with the generation of the secondary phosphine and the phosphorus centre reduced from +3 to +1, hence facilitating the oxidative coupling. However, the secondary phosphine was not detected by ³¹P NMR spectroscopy in sealed NMR tube experiments.^{18*} The only by-product observed was a colourless compound found to crystallise along side **23**, with subsequent X-ray diffraction studies revealing it to be bis(diisopropyl)ammonium triflate (Scheme 8). This ammonium salt is tentatively proposed to arise from protonation of an amido group of the phosphenium cation with subsequent decomposition. The remaining phosphorus-containing degradation products, however, could not be determined.

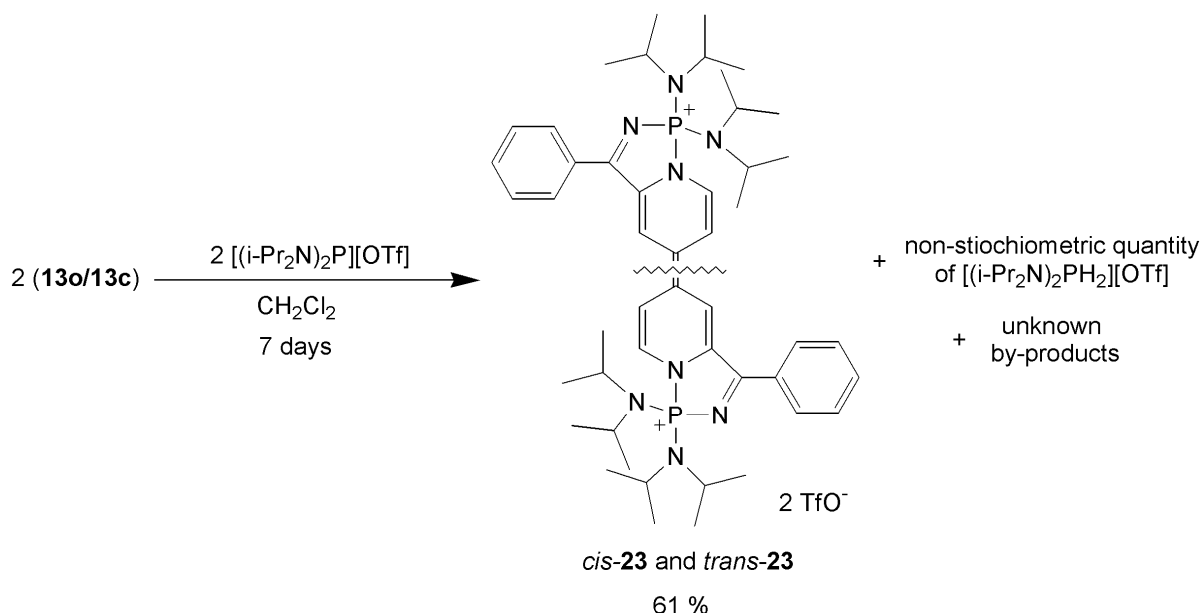
Scheme 7: Possible decomposition of $[(i\text{-Pr}_2\text{N})_2\text{P}][\text{OTf}]$ by protonation giving rise to $[i\text{-Pr}_2\text{NH}_2][\text{OTf}]$ and other unknown by-products



* $(i\text{-Pr}_2\text{N})_2\text{PH}$ ³¹P NMR δ : + 42.1 ppm¹⁸

Although $(i\text{-Pr}_2\text{N})_2\text{PH}$ is not observed spectroscopically in the synthesis of **23**, its formation and subsequent decomposition cannot be excluded. The secondary phosphine would be generated, in this reaction, as the phosphonium salt was consumed and these compounds are likely to form Lewis acid – Lewis base adducts^{1,9} for which the stabilities of these secondary phosphine-phosphenium adducts are not well known. The absence of any phosphorus-containing by-products according to ^{31}P NMR spectroscopy, for the formation of **23**, suggests a possible oligomerisation process. Oligomeric species could contain a large number of phosphorus environments, which could potentially be difficult to detect by NMR spectroscopy. Additionally, any oligomeric material could be insoluble in dichloromethane and therefore would not have been detected by solution-state NMR spectroscopy in the sealed NMR tube experiments conducted.

*Scheme 8: Reaction of **13c/13o** with $[(i\text{-Pr}_2\text{N})_2\text{P}][\text{OTf}]$ to give **23** and possibly the secondary phosphine, $(i\text{-Pr}_2\text{N})_2\text{PH}$*



The possibility of a radical-mediated process must also be addressed. Phosphenium cations are well established to exist in an electronic ground state where the electrons are paired, *i.e.* a singlet state.¹ Calculations by Harrison compute a large energy gap between the singlet and triplet states of 20 – 84 kcal mol^{-1} , with the magnitude of the difference

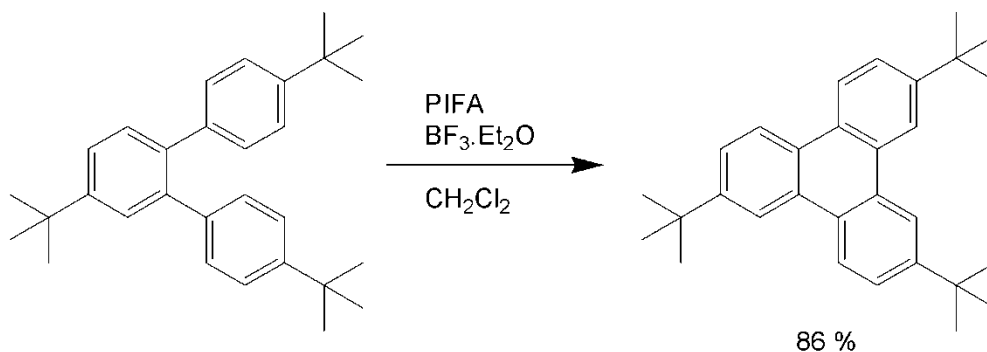
increasing with electronegativity of the substituents on phosphorus.¹⁹ However, this evidence would strongly disfavour radical involvement.

To summarise, the final fate of the phosphorus by-product in the formation of **23** is unclear, but the detection of bis(diisopropyl)ammonium triflate is suggestive of proton transfer to the substituents of the phosphonium cation with subsequent decomposition. In an attempt to gain an insight into the possible mechanism for the generation of compound **23**, more established coupling reagents were sought to replace [i-Pr₂N₂P][OTf].

5.4. The ‘Scholl coupling’ of aryl rings

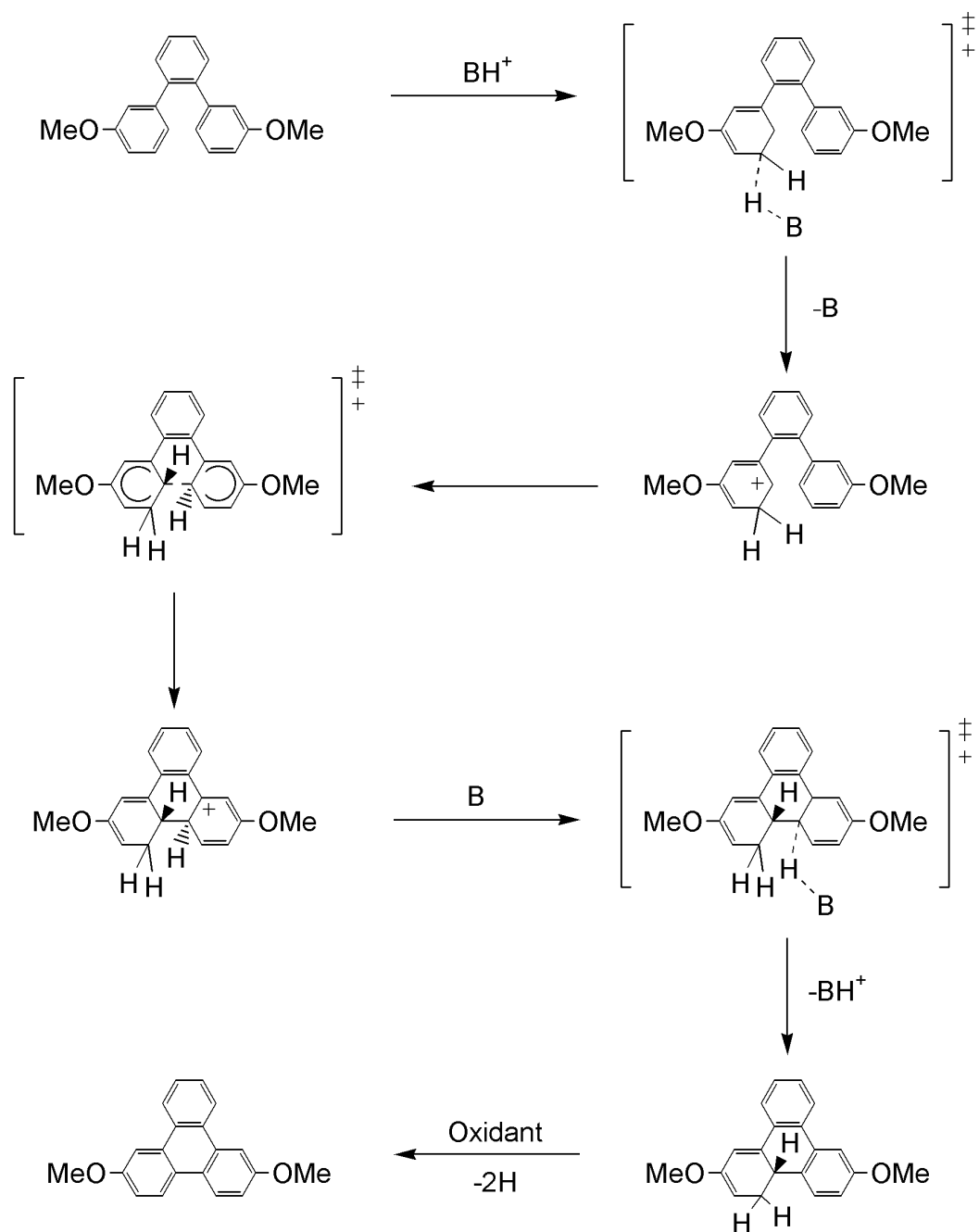
The formation of **23** is proposed to be an oxidative coupling of two molecules of **13**, and although somewhat reminiscent of Friedel-Crafts alkylation this reaction is better considered as a Friedel-Crafts arylation also known as a ‘Scholl reaction’ (see Scheme 9).^{20,21} The ‘Scholl-type’ methodology is generally applied to the coupling of aromatic carbon rings, and requires an oxidant and a Lewis acid, for example (CF₃COO)₂I^{III}C₆H₅ (PIFA) with BF₃·Et₂O.²¹ Dichloromethane is usually the solvent of choice for these transformations, with faster rates observed than reactions conducted in nitromethane or hexane.²¹ The synthetic potential of this reaction is, however, limited as the position of bond formation between rings is often hard to control. Efficient coupling is often only achieved by designing molecules that will undergo an intramolecular reaction.²² However, even for these systems sterically-demanding blocking groups are usually necessary to stop undesired oligomerisation of the substrate. An example is presented in Scheme 9, where the formation of a single bond between two conformationally-locked phenyl rings can be achieved in 86 % yield.²¹

Scheme 9: Example of a 'Scholl coupling' reported by King²¹

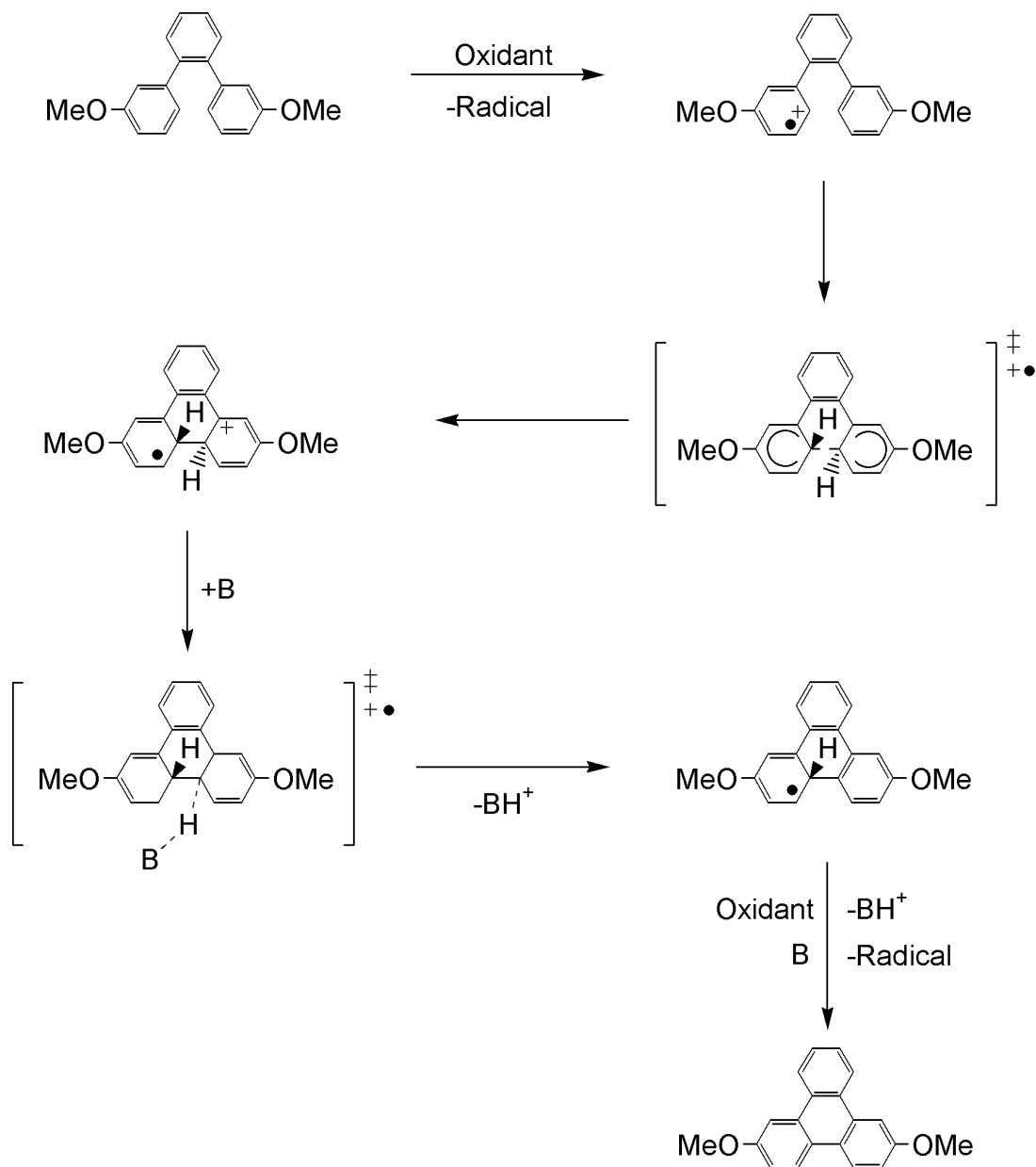


Mechanistically, two possible pathways have been proposed for the 'Scholl coupling': an arenium cation or a radical-mediated process (Scheme 10 and Scheme 11). These mechanisms are seemingly indistinguishable experimentally, however, calculations have been conducted by King in order to clarify the situation.²⁰ This *in silico* study revealed that the arenium cation pathway has lower transition state barriers. Hence it is proposed that this is the more likely mechanism for the 'Scholl coupling'.²⁰

Scheme 10: Mechanism of the suggested arenium cation pathway for 'Scholl coupling', $B = \text{Base}^{21}$



Scheme 11: Mechanism of the suggested radical cation pathway for 'Scholl coupling', $B = \text{Base}^{21}$



5.5. Formation of compound **23** using ferrocenium salts as the oxidant

5.5.1. Reaction of ferrocenium salts with **13c/13o**

The similarity between the ‘Scholl coupling’ and the conversion of **13c/13o** to **23** prompted the investigation of the reaction of **13c/13o** with oxidising agents. Ferrocenium hexafluorophosphate[†] was chosen as a simple one-electron oxidant. An equimolar combination of **13** and [Fc][PF₆] in dichloromethane gave a dark green solution within one hour, with ³¹P NMR spectroscopy subsequently revealing a broad peak at 52 ppm, a septet at – 134 ppm (PF₆[–]) and no remaining **13c/13o**. In addition a very small signal was observed at 33 ppm (20 %), which was noted to grow in intensity over a 24 h period (to 50 %). The resonance at 52 ppm (in conjunction with the resonance at – 134 ppm) was suspected to be the hexafluorophosphate analogue of the diphosphonium salt **23**. Indeed, following work-up of the reaction mixture a green residue was isolated. This was confirmed by ¹H, ³¹P NMR and UV/vis spectroscopies as the hexafluorophosphate salt of cation **23**.

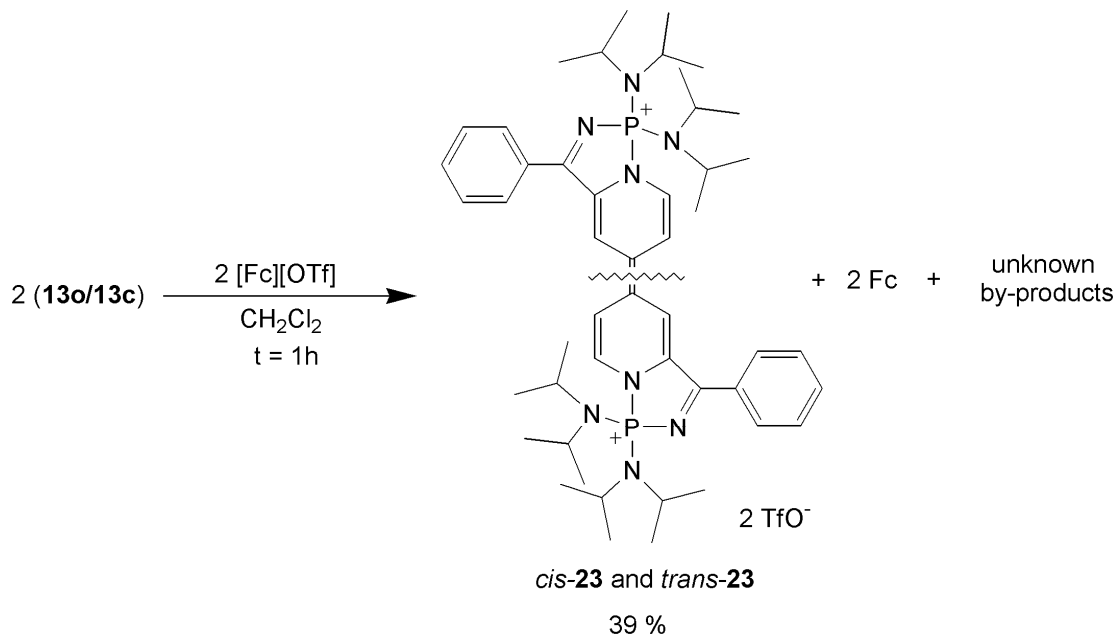
The use of ferrocenium triflate, allowed the oxidation of **13c/13o** to compound **23** to be achieved on a larger scale (~ 100 mg, Scheme 12). The switch from [Fc][PF₆] to [Fc][OTf] was found to be beneficial in the work-up of the reaction, with **23** proving easier to recrystallise as the triflate salt than the hexafluorophosphate salt.

The yield of **23**, by use of [Fc][OTf], is low (39 %), and perhaps due to the lack of sufficient oxidant relative to **13c/13o**. Examination of the stoichiometry shows that one equivalent of ferrocenium abstracts one electron per molecule of **13** sufficient for the generation of **13c/13o**⁺. However, the removal of the hydrogen atom *para* to the pyridyl nitrogen must also be considered, with either a molecule of dinitrogen or two protons being

[†] The notation [Fc][X] represents a ferrocenium salt, Fc⁺ corresponds to ferrocenium and Fc signifies ferrocene.

generated from the reaction with the latter requiring additional oxidant. Consequently, essentially two molecules of ferrocenium would be needed to generate **13c/13o**⁺ and H⁺. If protons were generated in the formation of compound **23** they could potentially react with the amino groups present in the substrate **13c/13o** and the product **23**, feasibly leading to decomposition and perhaps accounting for the low yield.

*Scheme 12: Reaction of [Fc][OTf] with **13o/13c** to give compound **23***



Since no evidence for the production of dihydrogen was noted (no evolution of gas was observed) the generation of protons was deemed to be likely. Hence, it was logical to attempt the formation of **23** using ferrocenium triflate with a greater quantity of oxidant (2 Fc⁺ : **13**) with the aim of increasing the yield. A base was also provided to try and sequester any protons generated in the reaction and attempt to stop any unwanted side reactions occurring. Initially the combination of two equivalents of [Fc][OTf] with **13c/13o** in the presence of 2,6-dimethylpyridine gave a dark green solution as before, but upon work-up only an oily black residue was obtained. The residue was silent by ³¹P NMR spectroscopy, possibly due to residual ferrocenium that could cause paramagnetic broadening of signals. Alternatively, the absence of resonances in the ³¹P NMR spectrum may arise from the

decomposition of **23** by protonation if 2,6-dimethylpyridine was unable to efficiently sequester the generated H^+ ions.

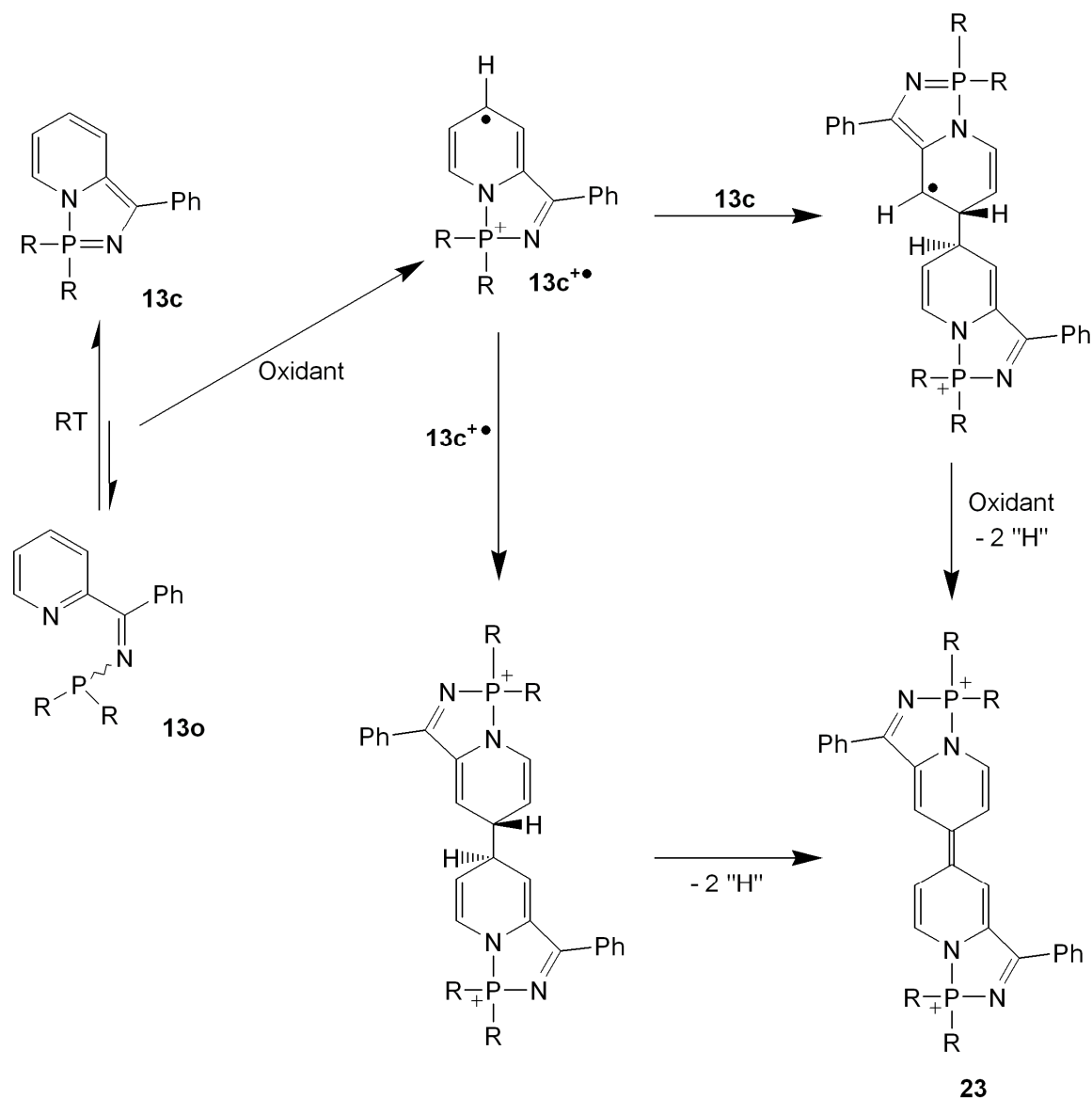
In summary, an overall ratio of 1:1 (Fc^+ : **13c/13o**) was found suitable for the synthesis of **23**, but in low yield, although the form in which the hydrogen atoms are lost is uncertain. Additionally, a 2:1 stoichiometry, was explored for the reaction of $[Fc][OTf]$ with **13**, but unfortunately a greater yield of **23** was not achieved.

5.5.2. Possible mechanisms for the formation of compound **23** from reaction of ferrocenium salts with **13c/13o**

Two mechanisms for the formation of **23** from reaction of **13c/13o** with a ferrocenium salt can be envisaged (Scheme 13). Firstly, oxidation of **13c/13o** will give a radical cation that could react with a neutral molecule of **13c/13o** giving a singly-charged adduct as an intermediate in the generation of **23**. Alternatively, coupling could occur between two radical cations. In both cases, atoms of H are still present upon coupling and whether these are lost as dihydrogen gas or as protons is unclear (*vide supra*).

Clearly, ferrocenium triflate is capable of inducing a coupling between two molecules of **13c/13o** to give **23**. However, the yield for this transformation was found to be lower than the route utilising $[(i-Pr_2N)_2P][OTf]$. The mechanism of the ferrocenium salt reaction is likely to be related to those proposed for the 'Scholl-coupling' (Scheme 10 and Scheme 11) and is not believed to be directly analogous to the generation of **23** from $[(i-Pr_2N)_2P][OTf]$.

*Scheme 13: Possible mechanisms for the formation of **23** from **13c/13o** using of $[Fc][X]$, $X = TfO^-$ or PF_6^- . Only the trans isomer is drawn for clarity. In the final step two hydrogen atoms are lost possibly as H_2 or H^+ . $R = i-Pr_2N$*

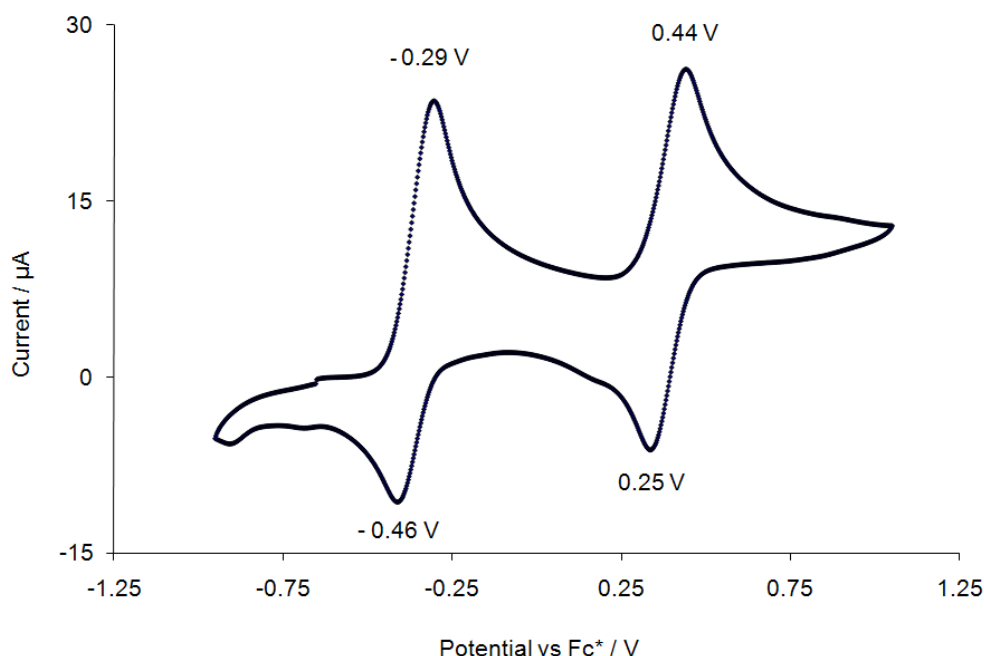


5.6. Electrochemical study of **13c/13o**

To further explore the nature of the oxidative coupling that gives rise to **23**, an electrochemical investigation of the inseparable equilibrium mixture of **13c/13o** was conducted. The cyclic voltammogram recorded for a dichloromethane solution of **13c/13o**

with decamethylferrocene as a reference shows both an oxidation and a reduction peak. The reduction and oxidation are both observed to be partially, but not fully reversible. The electrochemical oxidation of **13c/13o** is in agreement with the chemical oxidation by ferrocenium salts whose redox potential is of a greater magnitude, 0.45 V, than that of **13c/13o**, 0.44 V. Spectroelectrochemical investigations were not attempted as the lifetime of $[\mathbf{13c/13o}]^+$ is believed to be too short to be studied by this method.

Figure 8: Cyclic voltammogram of **13c/13o** referenced to decamethylferrocene

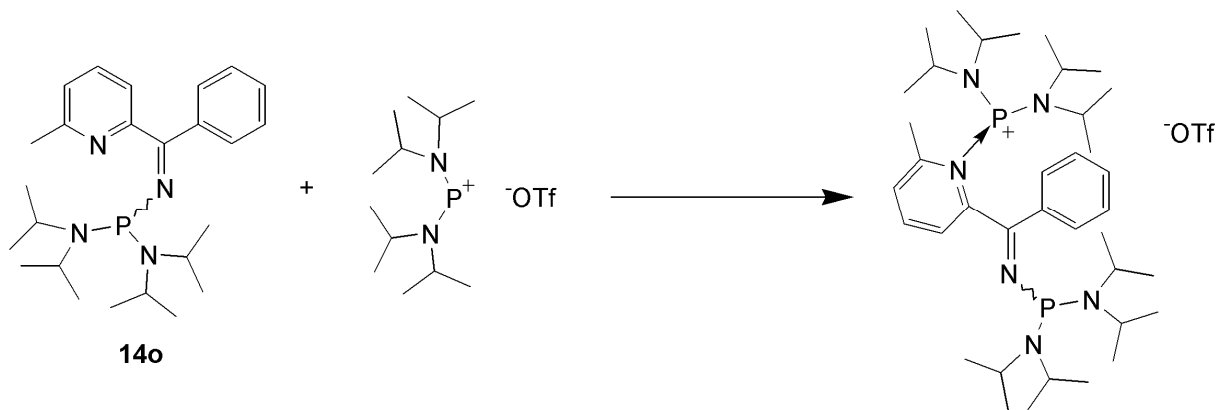


5.7. Reaction of **14o** with $[(i\text{-Pr}_2\text{N})_2\text{P}][\text{OTf}]$

In order to gain a greater insight into the reaction of **13c/13o** with $[(i\text{-Pr}_2\text{N})_2\text{P}][\text{OTf}]$, compound **14o** was investigated. The structure of **14o** is that of a *N*-phosphino-pyridyl imine and has no observed ‘closed’ valence tautomer due to steric constraints imposed by the additional methyl group on the pyridyl ring compared with **13o** (see Chapter III). The treatment of **14o** with $[(i\text{-Pr}_2\text{N})_2\text{P}][\text{OTf}]$ was therefore an important control reaction, with the

potential for highlighting the importance of the valence isomer **13c** in the ring coupling to form **23**.

Scheme 14: Reaction of **14o** with $[(i\text{-Pr}_2\text{N})_2\text{P}][\text{OTf}]$ to give $[(i\text{-Pr}_2\text{N})_2\text{P}.\mathbf{14o}][\text{OTf}]$

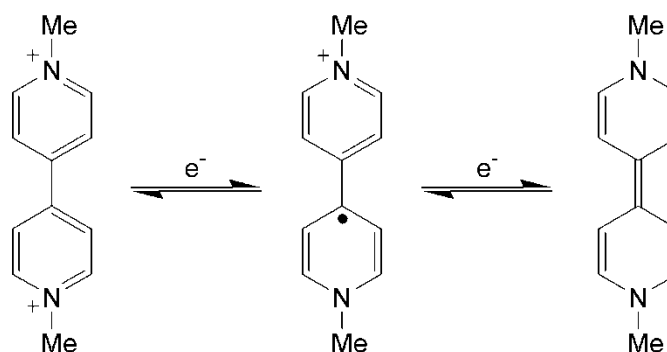


In a Young's NMR tube, a combination of **14o** (^{31}P NMR $\delta = 71$ ppm) and $[(i\text{-Pr}_2\text{N})_2\text{P}][\text{OTf}]$ (^{31}P NMR $\delta = 302$ ppm) instantly gave two singlet resonances at 140 and 61 ppm according to ^{31}P NMR spectroscopy, which did not evolve further over time. The binding of phosphonium cations to Lewis bases is well documented and these data are consistent with the formation of a Lewis acid – Lewis base adduct having occurred. Several possible binding sites are present in **14o**: the pyridyl N, imine N and the phosphine. No J_{PP} coupling is observed in the $^{31}\text{P}\{^1\text{H}\}$ NMR spectrum of the product, with both the peaks at 140 and 61 ppm found to be singlets. This is consistent with coordination of the phosphonium cation to the pyridyl nitrogen lone pair. Binding of the phosphonium cation to either the imine N or the phosphine would likely result in distinctive J_{PP} couplings. The sharp nature of the signals in the $^{31}\text{P}\{^1\text{H}\}$ NMR spectrum also favours a discrete structure, which is not undergoing exchange of phosphorus moieties, as is proposed to be the case for the adduct $[(i\text{-Pr}_2\text{N})_2\text{P}.\mathbf{13}][\text{OTf}]$. In conclusion, the *N*-phosphino-pyridyl imine **14o** does not undergo oxidative coupling in the presence of $[(i\text{-Pr}_2\text{N})_2\text{P}][\text{OTf}]$, something that is likely to result from the steric hindrance between the methyl *ortho* to the pyridyl nitrogen and the diisopropylamino substituents, which inhibits ring closure preventing the formation of a compound analogous to **23**.

5.8. Spectroscopic and electrochemical studies of **23**

Viologen-containing systems are being actively studied in the development of electrochemical display devices and photochemical sensitizers.²³ Interest in such compounds stems from the redox chemistry associated with the viologens which can exist in an oxidation state of 2+, 1+ or 0 (Figure 9), with the singly- and doubly-reduced forms often exhibiting strong absorption bands in their UV/vis spectra. Since compound **23** possesses a doubly-reduced viologen core, it was of interest to compare the properties of **23** to those of simple viologens, for example methylviologen.^{12†}

Figure 9: Methylviologen (left), with the singly-reduced radical (middle) and doubly-reduced forms (right)¹²



5.8.1. UV/visible spectrum of **23**

Dissolution of **23** in dichloromethane gives rise to an intensely green-coloured solution, which gave a strong band at 740 nm with a molar absorption coefficient of $20,200 \text{ dm}^3 \text{ mol}^{-1} \text{ cm}^{-1}$ by UV/vis spectroscopy. It was of interest to investigate the origin of this band further, because of its strong intensity and presence in the near infra-red region of the electromagnetic spectrum.

[†] All spectrochemical and electrochemical data recorded for **23** in this report were obtained from a 1:1 mixture of the two isomers *cis*-**23** and *trans*-**23**.

UV/vis spectroscopic studies of **23** in solution show the absorbance to be anion-independent, but solvatochromic for the solvents THF, dichloromethane and methanol. An increase in solvent dielectric constant brings about a hypsochromic shift, with a magnitude of 52 nm between spectra recorded in THF and methanol. The absence of spectroscopic data in water and less polar solvents is due to the insolubility of **23** in these media.

Figure 10: UV/vis spectra of **23** in the solvents THF, DCM and methanol plotted as wavelength in nanometres versus absorbance in terms of molar absorptivity. The ‘gap’ in the absorbance band at 850 nm is because of a lamp change.

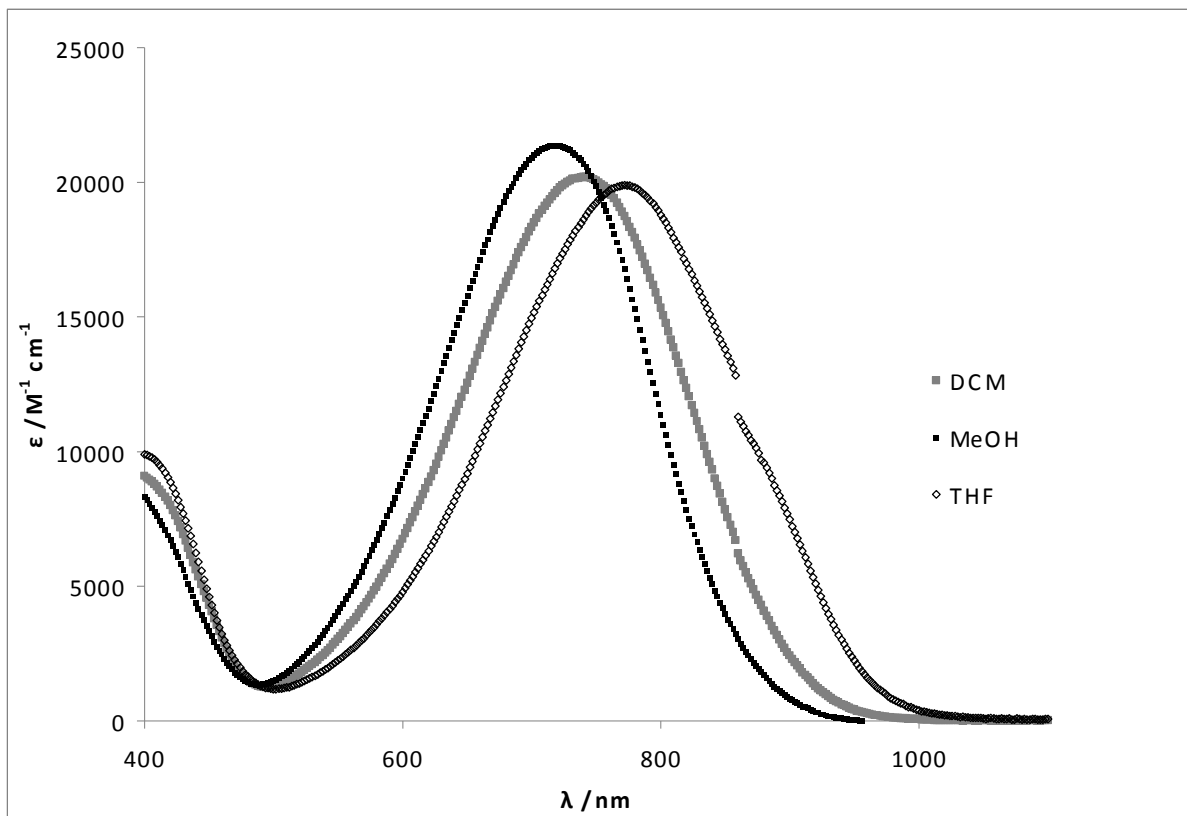


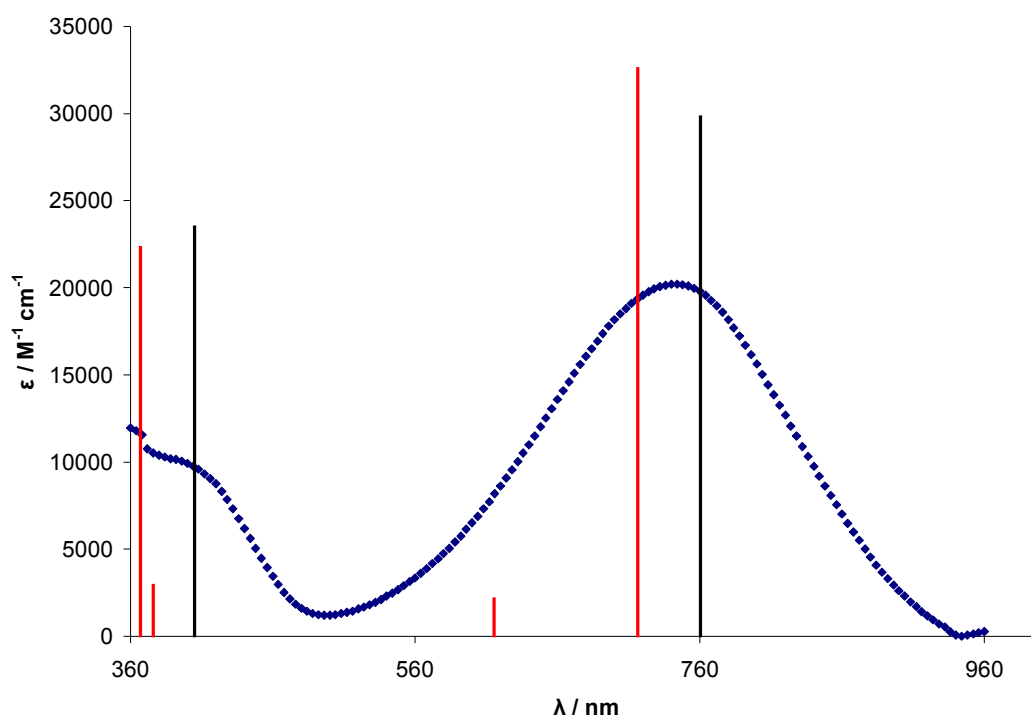
Table 2: UV/visible light absorbance data for **23**

Solvent	ϵ_r^{24}	λ_{\max} (nm)	ϵ (dm ³ mol ⁻¹ cm ⁻¹)	λ_{\max} (nm)	ϵ (dm ³ mol ⁻¹ cm ⁻¹)
THF	7.5	398	9,900	772	19,900
CH ₂ Cl ₂	9.1	392	9,187	740	20,200
MeOH	32.6	380 [§]	9,050	720	21,400

[§] Band partially obscured by higher frequency bands

It is important to note the UV/vis data above (Figure 10 and Table 2) refer to an equal mixture of the *cis* and *trans* isomers. Consequently a computational study was required to determine the contribution from each isomer to the experimentally determined spectra. TD-DFT calculations at the B3LYP/6-31G* level of theory predicted bands at 717, 387 and 381 nm for the *cis* isomer and at 761 and 400 nm for the *trans* (Figure 11). These data correspond very favourably with the experimentally observed range for the mixture of *cis*-**23** and *trans*-**23**, i.e. 720 - 772 nm for the different solvents employed (Figure 10).

Figure 11: Observed UV/vis spectrum for a equal mixture of *cis*-**23** and *trans*-**23** (blue) and TD-DFT calculated (stick) spectra for *trans*-**23** (black) and *cis*-**23** (red)



5.8.2. Comparison of the calculated MOs of *trans*-**23** and doubly-reduced methylviologen

The presence of the strong absorption in the low energy visible light region of the electromagnetic spectrum is due to the extended π -conjugated system of compound **23**,

however, the nature of the transition was unclear. To explore the origin and composition of this band further, the frontier molecular orbitals were computed for *trans*-**23** (Figure 12). Both the HOMO and LUMO are delocalised across the central core of the molecule with virtually no electron density residing on the diamino substituents and only a small proportion present on the phenyls for the LUMO. A comparison between the HOMO of **23** and the HOMO of the doubly-reduced form of methylviologen reveals a marked similarity, with electron density localised in the central planar core. There is also a weak resemblance upon evaluation of the LUMOs of *trans*-**23** and doubly-reduced form of methylviologen, with correlation between the C5-C4-C3-C3' fragments (Figure 12). The asymmetry of **23** distinguishes its LUMO from that of doubly-reduced methylviologen with a visibly lower orbital density over C1-C2 for the former. The HOMO–LUMO gap of 1.7 eV for **23** is considerably smaller than those reported for other *N,N'*-R₂-doubly-reduced viologens (*e.g.* R = Me, 3.0 eV;²⁵ R = Ph, 2.7 eV; ²⁶ R = B(mes)₂, 2.6 eV¹³), consistent with the π -conjugation extending across the two imino groups as well as the quinoidal moiety.

Figure 12: The LUMO+2 (upper), LUMO (middle) and HOMO (lower) of *trans*-**23**

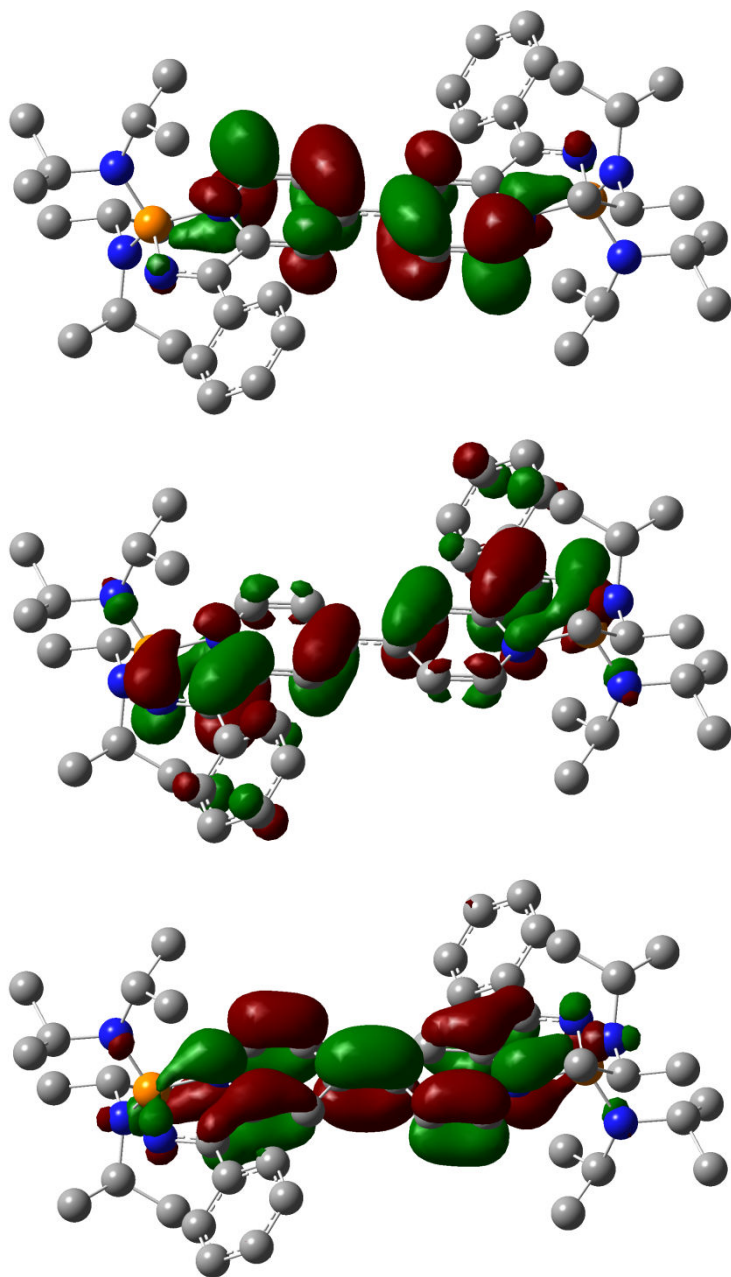
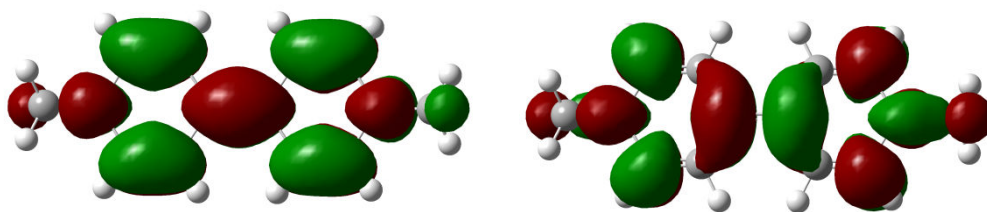


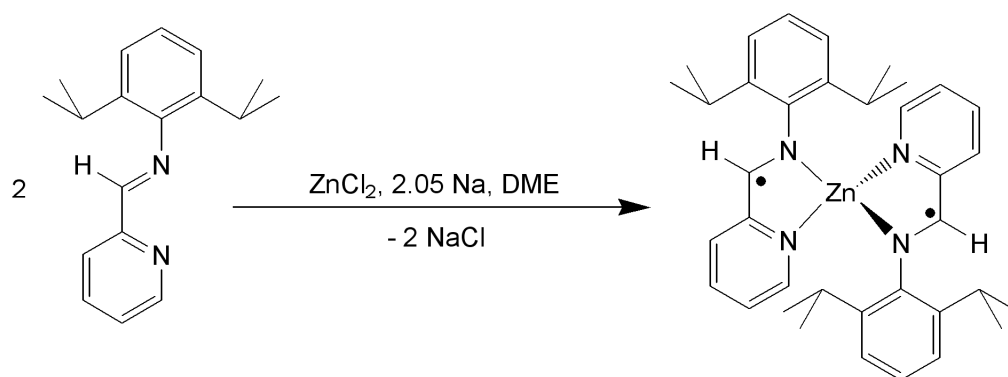
Figure 13: HOMO (left) and LUMO (right) of doubly-reduced methylviologen



5.8.3. Assessment of the composition of the electronic transitions of compound 23

The composition of the electronic transitions of *trans*-**23** can be predicted by computational studies. Assessment of the electronic transition at 761 nm for *trans*-**23** reveals that it is primarily HOMO→LUMO in character (65 %). Examination of the regions of molecular orbital density in both the HOMO and LUMO (*Figure 12*) give an indication of where the electron involved in the transition is moving from and to. Therefore *trans*-**23** was subdivided into fragments and the percentage electron density calculated for each fragmented region (*Table 3*). For the 761 nm transition it is calculated that the electron density shifts from the central quinoidal core (P-N1-C1-C2-C3) to the imine moiety (C6-N2), consistent with the reducible nature of iminopyridines.²⁷ It has been established by Wieghardt that the iminopyridine 2,6-(*i*-Pr)₂PhN=C(H)(C₅H₄N) can be singly-reduced in the presence of suitable reductants, often low oxidation state metal complexes, to give a radical species (*Scheme 15*).²⁸ X-ray diffraction studies of these species has shown that the unpaired electron is predominantly localised over the imine fragment of [2,6-(*i*-Pr)₂PhN=C(H)(C₅H₄N)]^{•−} and is supportive of the shift of electron density to the imine calculated for the 761 nm transition of *trans*-**23**.

Scheme 15: Reduction of 2,6-(i-Pr)₂PhN=C(H)(C₅H₄N) with ZnCl₂ reported by Weighardt²⁸



It should be noted that the predicted contribution to the 761 nm electronic transition from the phenyl groups is small and almost negligible for the amino groups, with changes in

the molecular orbital density being low. It is therefore likely that modification of compound **23** with replacement of the phenyl rings for different aryl groups would affect the nature of the electronic transition, however, the size of any change would probably be small. Additionally the chromophore is unlikely to be influenced by alteration of the isopropyl groups, unless significant geometric changes are caused at phosphorus. It can be envisaged that with variation of the substituent on the amino groups, the hybridisation of phosphorus could be altered. This in turn would affect the interaction between phosphorus and the conjugated π -system.

Figure 14: Atom numbering scheme for *trans*-**23**

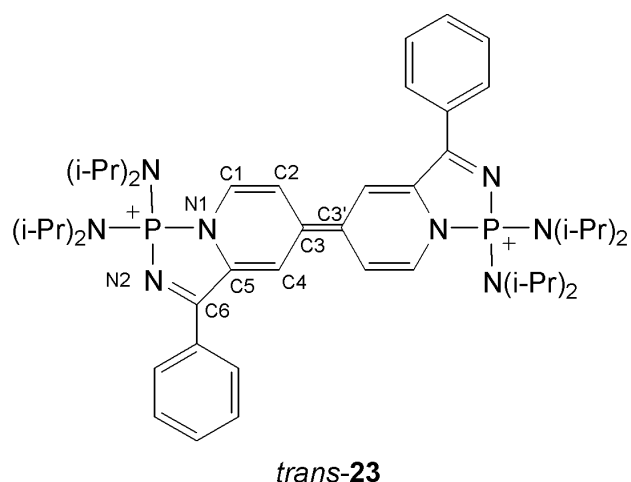


Table 3: Percentage composition of selected molecular orbitals of *trans*-**23**

MO		eV	Ph	N(i-Pr) ₂	C6=N2	C1=C2	C3=C3'	C4=C5	P–N1
225	LUMO+2	– 5.53	1	3	2	61	14	13	6
224	LUMO+1	– 6.45	17	2	40	5	7	25	3
223	LUMO	– 7.41	12	4	37	4	8	24	9
222	HOMO	– 9.17	4	5	7	25	21	15	22
221	HOMO–1	– 11.07	83	6	8	0	0	0	2

Table 4: Details of the electronic transition at 761 nm of *trans*-**23**

Energy (cm ⁻¹)	Wavelength (nm)	Osc. Strength	Major contribution
13147	761	0.595	HOMO→LUMO (65 %)

Table 5: Percentage change in terms of molecular orbital density between the ground state and excited state for the electronic transition at 761 nm of *trans*-**23**

Ph	N(i-Pr) ₂	C6=N2	C1=C2	C3=C3'	C4=C5	P-N1
4→11	5→4	7→34	25→10	21→9	15→23	22→9
(7)	(- 1)	(27)	(- 15)	(- 12)	(8)	(- 13)

The MOs were also calculated for *cis*-**23** and analysis conducted upon the composition of the electronic transitions. However, similar results were obtained to those found for *trans*-**23** and therefore will not be discussed here.^{**}

5.8.4. Electrochemistry of **23**

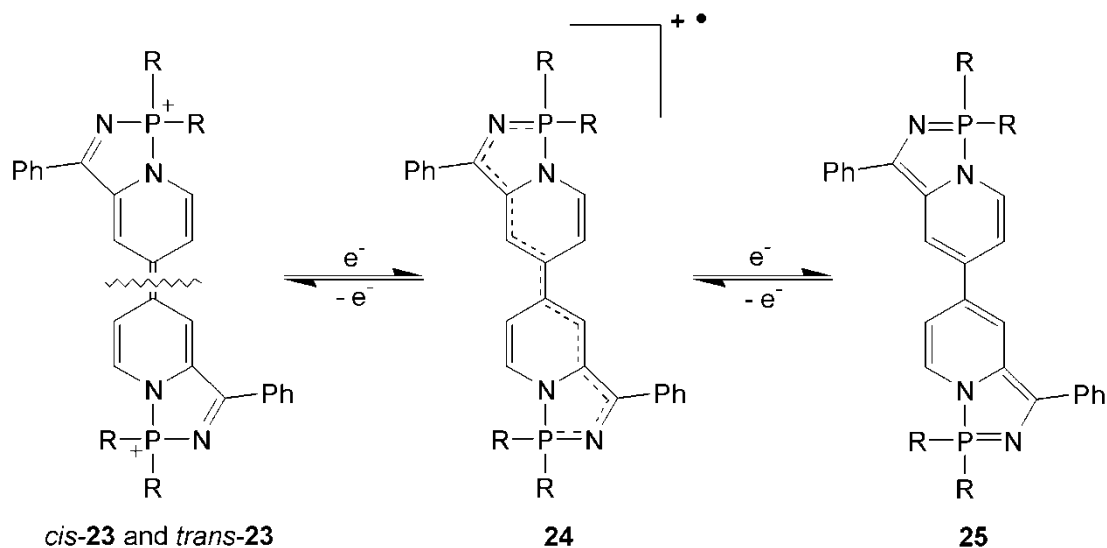
The central core of **23** is essentially that of a doubly-reduced viologen and the presence of two imines in the same plane of core gives rise to a longer extended π -conjugated system. The redox chemistry associated with viologens is well established (Figure 9) and it was of interest to explore whether **23** would display similar properties.²³

Consequently, the cyclic voltammogram of **23** was recorded in dichloromethane under anaerobic conditions. Upon the application of negative voltage, two reduction steps (-0.46 and -0.55 V) are observed and found to be fully reversible on reoxidation. The first reoxidation step is visible as a shoulder upon the more clearly defined second reoxidation

^{**} For a summary of the computational analyses regarding the composition of the electronic transitions for *cis*-**23** and the ~400 nm band for *trans*-**23** please see the appendix.

(Figure 15). It is assumed that the overall reduction is two-electron in nature and that the individual steps involve single-electron transfer; this assumption is confirmed in section 5.8.5. A four-electron reduction of **23** would give rise to a doubly negatively charged species, for which a sensible structure is hard to propose. Instead, a neutral species, **25**, is expected to be the ultimate product of reduction with a radical monocation **24** as the intermediate (Scheme 16).

*Scheme 16: Electrochemical reduction of **23** to **24** and **25***



Oxidation of **23** was also explored in the cyclic voltammetric study with an irreversible event being found to occur at + 0.79 V (Figure 15). The irreversibility of this oxidation is presumed to arise from the formation of an unstable 3+ or 4+ species, which undergoes rapid decomposition.

The cyclic voltammetry was also conducted at low temperature (-78 °C) and at a slower scan rate (50 mV s⁻¹) in order to see if any further information could be gained (Figure 16). No improvement in the reversibility of the oxidation was observed, indicating that the cooler temperature does not help to stabilise the oxidised version of **23**. However, for the reduction process, the first reoxidation step is now far more obvious at the lower temperature and slower scan rate. This is likely to result from the increased length of time between the one-electron oxidation steps.

Figure 15: Cyclic voltammogram of **23** (10^{-4} M in $\text{CH}_2\text{Cl}_2/10^{-1}$ M Bu_4NBF_4) at $\mu = 100 \text{ mV s}^{-1}$ with Fc as reference

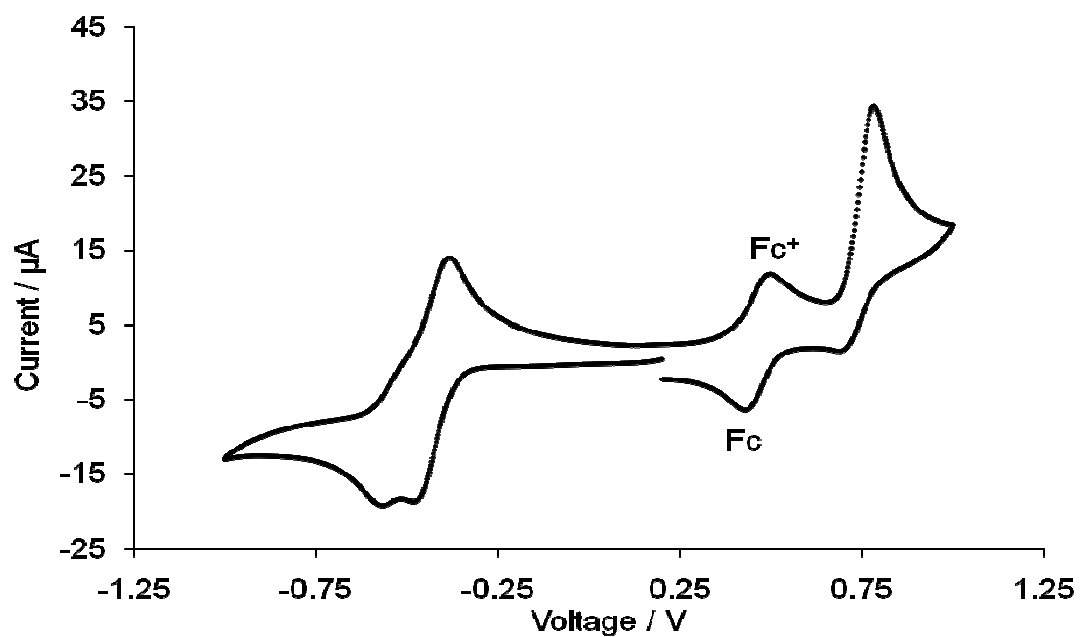
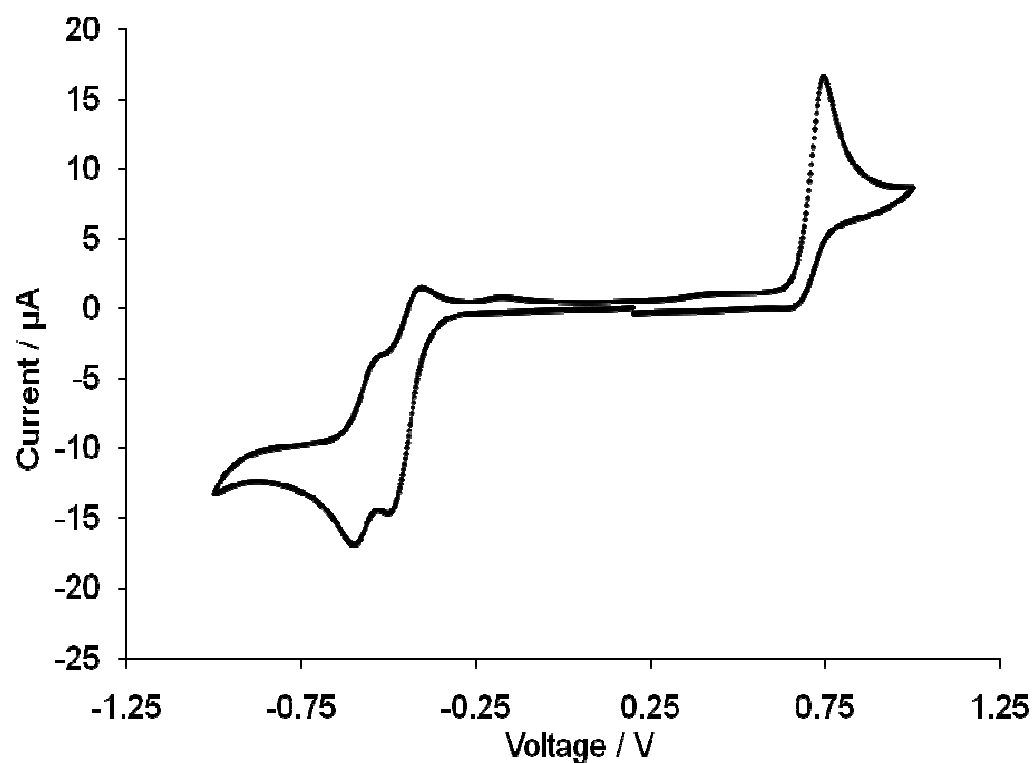


Figure 16: Cyclic voltammogram of **23** (10^{-4} M in $\text{CH}_2\text{Cl}_2/10^{-1}$ M Bu_4NBF_4) at $\mu = 50 \text{ mV s}^{-1}$ at -78 °C



5.8.5. Spectroelectrochemistry of **23**

The cyclic voltammogram of **23** shows that two one-electron reduction steps take place giving rise to two species, proposed as **24** and **25** (Scheme 16). To further explore the nature of these compounds spectroelectrochemistry was used. This technique allows the UV/visible or IR absorbance of a compound to be measured in solution as an electropotential is applied.^{29,30} Thus, a UV/vis spectroscopic study was undertaken in dichloromethane and the data obtained presented in Figure 17. Unfortunately the low solubility of compound **23** prevented an analogous study by IR spectroscopy with varying voltage.

Figure 17: UV/vis spectroelectrochemical data for compound **23**

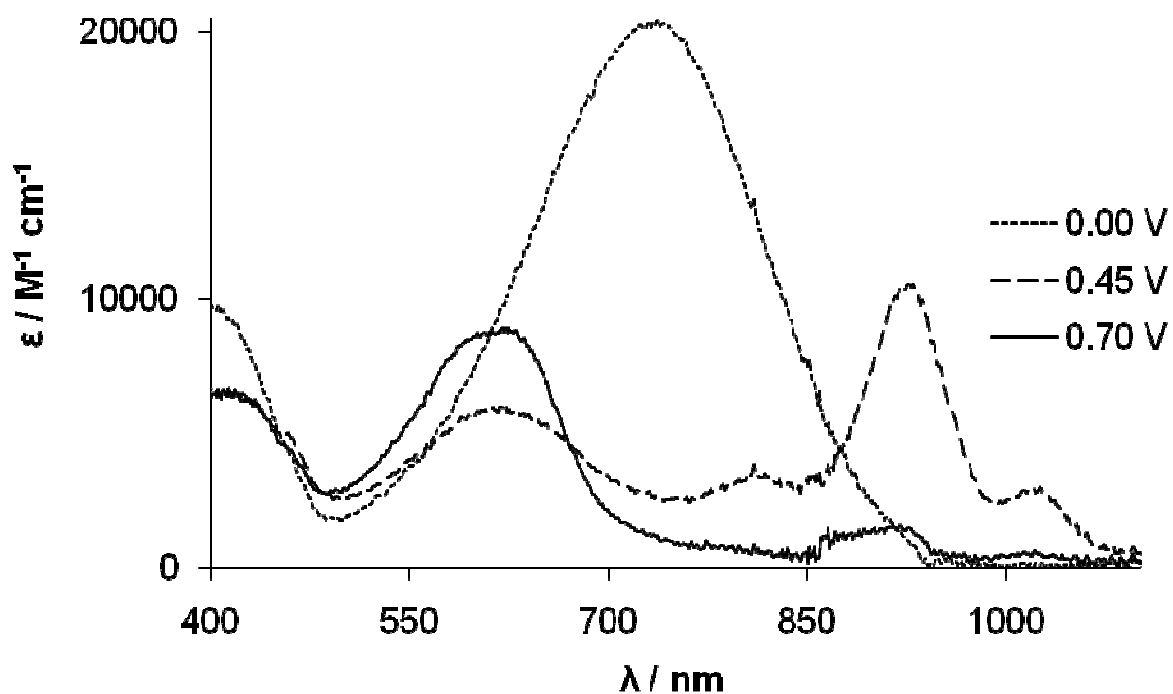


Figure 17 displays the absorbance at different electropotentials obtained upon reduction of **23**, with similar spectra being recorded upon reoxidation.^{††} The UV/visible spectrum recorded at 0.00 V is that of **23**, clearly showing the characteristic absorbance band at 740 nm. A reducing potential was applied to **23** and spectra were then subsequently recorded at increments of 0.05 V. This slow increase in voltage is necessary to allow charge diffusion to occur across the width of the spectrochemical cell (0.02 cm). If time is not allowed for charge diffusion then the potential at the centre of the cell (*i.e.* where the spectra are observed) will lag behind the potential applied to the cell edges. Of the recorded spectra, those at 0.45 V and 0.70 V are chosen to be the most representative of the singly-reduced (**24**) and doubly-reduced (**25**) species, of which the latter is addressed first.

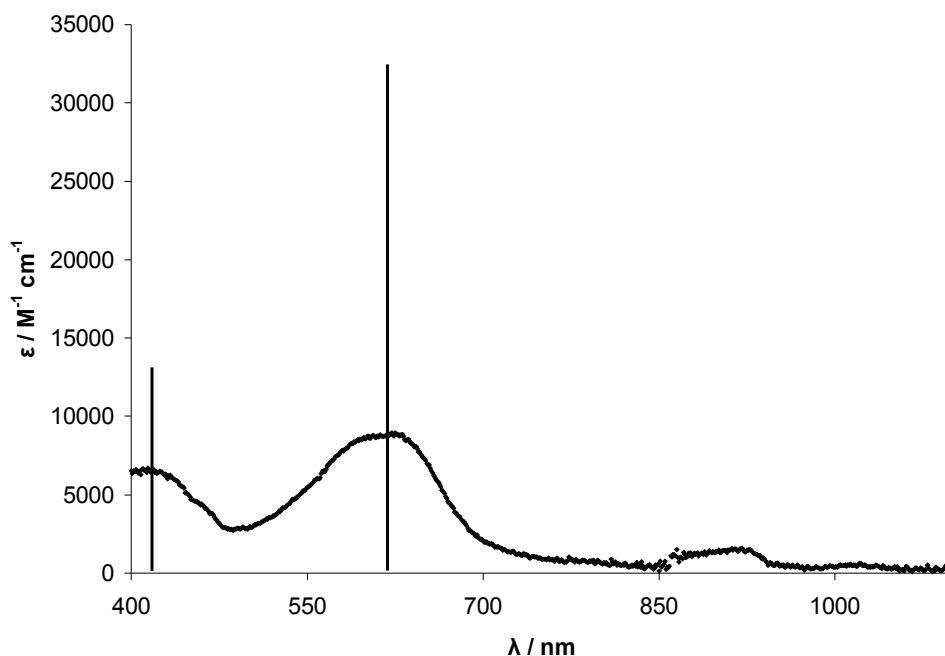
5.8.5.1. Spectroelectrochemical observation of **25**

Application of an electropotential of 0.70 V produces a spectrum with intense bands at 622 nm and lower wavelength bands below 450 nm. It is known from the cyclic voltammogram of **23** (Section 5.8.4) that the two one-electron reduction steps occur at - 0.46 and - 0.55 V, relative to Fc/Fc⁺, and therefore it is logical to assume that the spectrum at 0.70 V (Figure 18) is that of the doubly-reduced species, **25** (Scheme 16). Compound **25** is envisaged to consist of two 1 λ^5 -[1,3,2]diazaphospholo[1,5-a]pyridine moieties joined at the *para* position of the dearomatised pyridyl ring. Modelling of **25** computationally by TD-DFT gives rise to a predicted band at 617 nm which is in excellent agreement with that observed experimentally (622 nm), confirming the proposed structure (Scheme 16). Although the calculated absorbance intensity is notably higher than that observed (Figure 18), this could, in part, be explained by the increased sensitivity of **25** to oxygen and moisture, relative to **23**, with completely anaerobic reaction conditions being difficult to achieve experimentally.

^{††} The voltage readings for the spectroelectrochemistry are not calibrated, however, since the values recorded correlate with those noted in the cyclic voltammogram they are taken as being a fair representation.

Therefore, it cannot be excluded that some decomposition of **25** may have occurred in the spectroelectrochemistry, giving rise to a lower molar extinction coefficient.

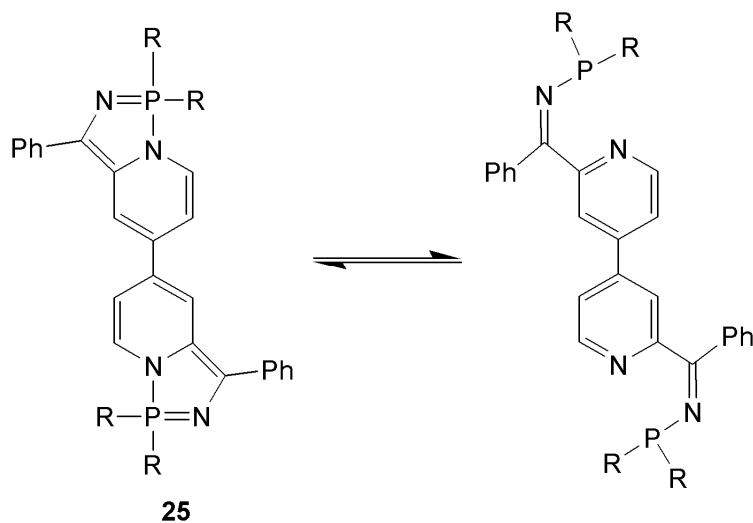
Figure 18: Experimentally observed and TD-DFT calculated (stick) UV/vis spectra for **25**. The band centred at 912 nm is tentatively assigned as a residual trace of **24** (see Figure 19)



It should also be mentioned that a weak intensity band at ~ 900 nm is observed in the spectrum recorded at 0.70 V (Figure 18). Since no transitions of appropriate energy are predicted in the calculated UV/vis spectrum of **25** and a band at a similar wavelength (926 nm) is recorded in the spectrum at 0.45 V (Figure 17), this weak intensity band is attributed to trace quantities of an intermediate, most likely the singly-reduced species **24**.

The structure of **25** is directly comparable to that of **13c**, being comprised of two molecules of the latter coupled at the 4-position of the dearomatised pyridine. Since the ‘closed’ diazaphosphole **13c** exists in equilibrium with its ‘open’ isomer **13o** at RT (Scheme 1), then the same equilibrium is feasible for **25**. As reported earlier, the band at 620 nm is predicted computationally to belong to the ‘closed’ diazaphosphole **25** and, although additional bands at lower wavelengths are observed in the UV/vis spectrum recorded at 0.7 V, these are not diagnostic of the presence or absence of an ‘open’ isomer of **25**.

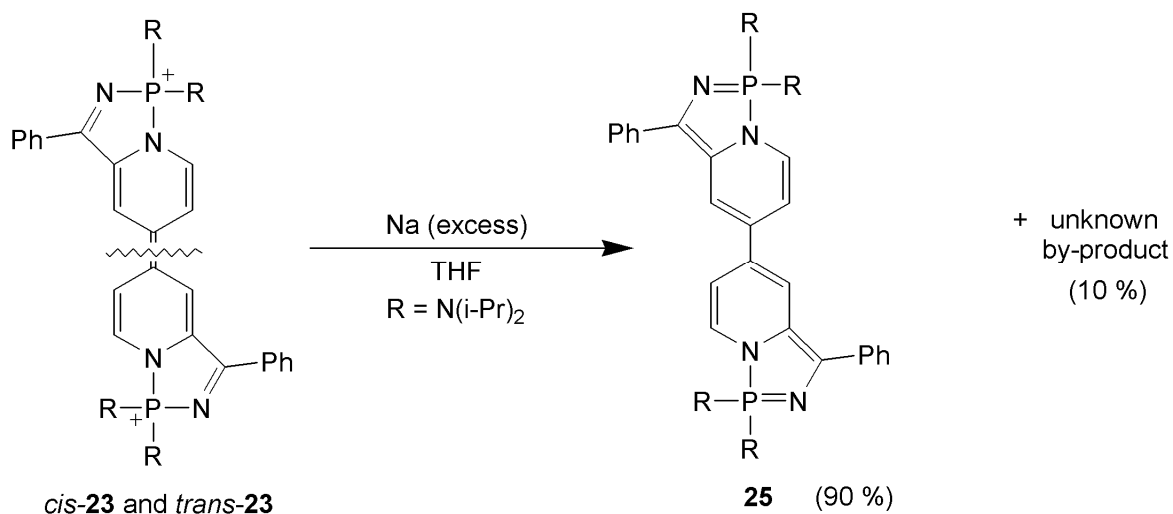
Scheme 17: Compound **25** (left) and its possible 'open' isomer (right)



5.8.5.2. Chemical generation of **25**

The chemical generation of **25** from **23** was attempted in a Young's NMR tube by the addition of an excess of finely cut sodium to a deuterated THF solution of **23** (Scheme 18). After two days standing the mixture was found to have changed from green to blue with ^{31}P NMR spectroscopy revealing the presence of two new species with resonances at 39.1 and 39.9 ppm in a ratio of 90 : 10. The former species is assigned to **25** with the aid of the ^1H NMR spectrum of the mixture, revealing the expected resonances from the dearomatised pyridyl rings. However, the minor component of the mixture could not be identified. The ^{31}P NMR chemical shift of **25** (^{31}P δ : 39.1) is in good agreement with that of **13c** in deuterated THF (^{31}P δ : 40.4). Unfortunately, in the presence of sodium, compound **25** was noted to be unstable and decomposition to unknown species was observed over a period of over several days.

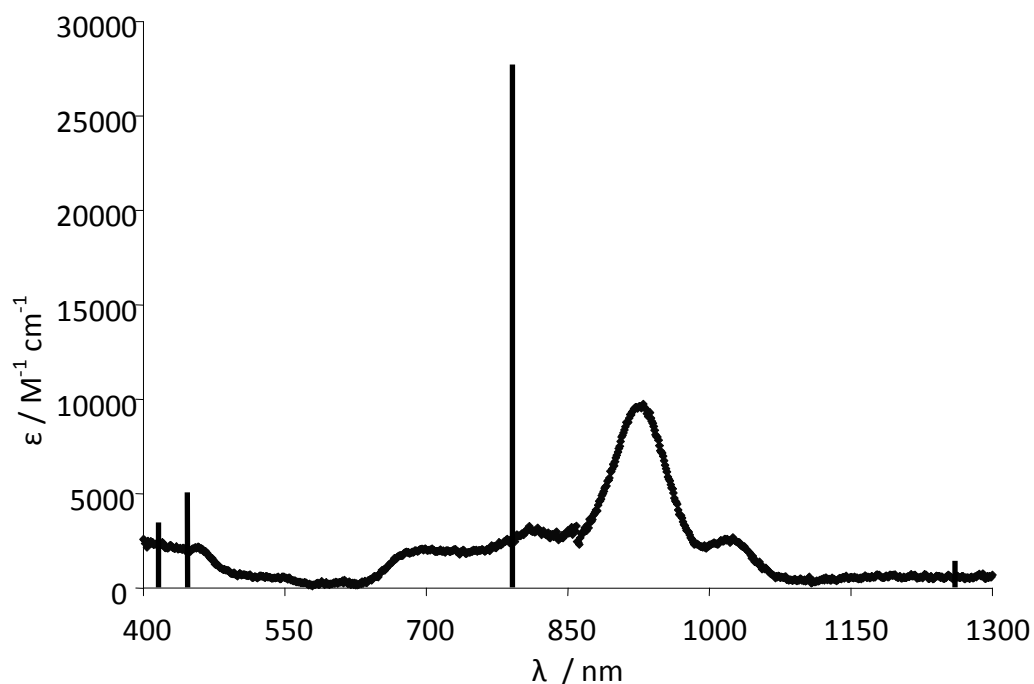
Scheme 18: Reduction of **23** by metallic sodium.



5.8.5.3. Spectroelectrochemical observation of **24**

Returning to the spectroelectrochemical study of **23**, the spectrum observed at 0.45 V contains a band at 621 nm, which now evidently belongs to the neutral compound **25**. The remaining bands at 926 and 1025 nm, however, are assigned to the monocationic species **24** (Scheme 16 and Figure 19). At no point during the spectroelectrochemical study could a spectrum of solely **24** be obtained. This is undoubtedly because of the very close reduction potentials for **23**→**24** and **24**→**25** of -0.46 and -0.55 V, respectively. A computational study of **24** was conducted and, despite calculations for open-shell compounds often being difficult, the computations for **24** were moderately successful, predicting two bands above 700 nm (Figure 19), although these are somewhat distant from the bands at 926 and 1025 nm. In addition, the structure for **24** was optimised and shows an extensively delocalised radical, over the central quinodal framework and onto the imine fragments. In conclusion, spectroelectrochemistry has provided a greater understanding of the data obtained from cyclic voltammetry and, when coupled with calculations, predicts reasonable structures for both species **24** and **25**.

Figure 19: Calibrated UV/vis spectrum for **24** with the TD-DFT calculated (stick) spectrum

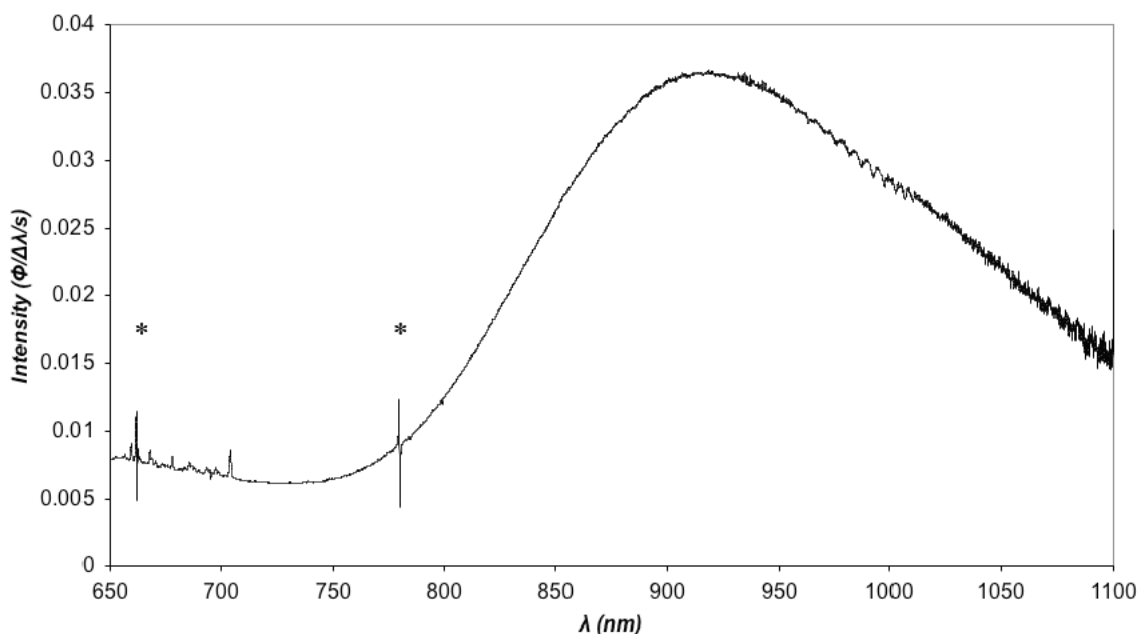


5.8.6. Near-IR emission

The main absorption band of **23** was noted to be at the edge of the visible light region (740 nm in CH₂Cl₂) of the electromagnetic spectrum and it was proposed that if this band was irradiated then any emission would be in the near-IR. A sample of **23** in dichloromethane was subject to excitation at 633 nm and near-IR emission detected at 920 nm.^{††} Unfortunately, quantification of the magnitude of emission (quantum yield) in this region of the electromagnetic spectrum is challenging with the available instrumentation and hence, a quantum yield was not obtained. Qualitatively, however, the magnitude of the emission intensity is rather low.

^{††} Experiments and analysis regarding the detection of near-IR emission were carried out by Dr. A. Beeby (Durham University).

Figure 20: Normalised emission spectrum of **23** in CH₂Cl₂. (* solvent/Raman lines).



Interest in near-IR-absorbing and -emitting materials has grown in recent years.³¹ Among their current and potential applications are those in the fields of biochemistry and medicine, primarily because a significant portion of biological tissue is found to be transparent to near-IR wavelength light. Therefore, a range of uses can be envisaged for compounds capable of near-IR absorption and emission, for example as *in vivo* sensors and as drug components that can be activated at a chosen biological location.³² For **23**, the herbicidal nature of the parent compound methylviologen and its proven toxicity towards humans likely excludes **23** from application in this area at the present time.³³

5.9. Summary

It has been demonstrated the addition of [(i-Pr₂N)₂P][OTf] to the equilibrium mixture **13c/13o** gives rise to the doubly-reduced viologen-containing species **23** in reasonable yields (61 %). This oxidative coupling of two aryl rings by a phosphonium cation is unprecedented; however, to date the mechanism is unclear, in part, due to the unknown by-products of the reaction. To investigate whether more traditional oxidants were capable of transforming

13c/13o to **23**, ferrocenium triflate was used, and also found to give **23**, although in lower yields (39 %) than those observed for the reaction of [(i-Pr₂N)₂P][OTf] with **13c/13o**. It is envisaged in future studies, however, that the use of ferrocenium triflate, in preference to [(i-Pr₂N)₂P][OTf], will facilitate the synthesis of variants of **23**.

In addition, an investigation of the electrochemical properties of **23** reveals a versatile redox chemistry with two reversible reductions recorded by cyclic voltammetry. These reductions give rise to singly- and doubly-reduced viologen-containing species, **24** and **25** respectively, and have been assigned by a combination of spectroelectrochemical and computational studies. Attempts to oxidise **23** resulted in an irreversible oxidation, presumably due to decomposition of a tricationic or tetracationic analogue of **23**. These interesting electrochemical properties along with the novel oxidative coupling of **13c/13o** by a phosphonium cation invite further study.

¹ A. H. Cowley, R. A. Kemp, *Chem. Rev.*, 1985, **85**, 367.

² Y. G. Gololobov, L. F. Kasukhin, *Tetrahedron*, 1992, **48**, 1353.

³ S. A. Weissman, S. G. Baxter, A. M. Arif, A. H. Cowley, *Chem. Commun.*, 1986, 1081.

⁴ S. A. Weissmann, S. G. Baxter, A. M. Arif, A. H. Cowley, *J. Am. Chem. Soc.*, 1986, **108**, 529.

⁵ D. Gudat, *Coord. Chem. Rev.*, 1997, **163**, 71.

⁶ A. H. Cowley, M. C. Cushner, J. S. Szobota, *J. Am. Chem. Soc.*, 1978, **100**, 7784.

⁷ M. R. Mazieres, C. Roques, H. Sanchez, J.P. Majoral, R. Wolf, *Tetrahedron*, 1987, **43**, 2109.

⁸ N. Burford, P. J. Ragogna, R. McDonald, M. J. Ferguson, *J. Am. Chem. Soc.*, 2003, **125**, 14404.

⁹ C. W. Schultz, R. W. Parry, *Inorg. Chem.*, 1976, **15**, 3046.

¹⁰ N. Burford, P. Losier, A. D. Phillips, P. J. Ragogna, T. S. Cameron, *Inorg. Chem.*, 2003, **42**, 1087.

¹¹ Y. Carpenter, C. A. Dyker, N. Burford, M. D. Lumsden, A. Decken, *J. Am. Chem. Soc.*, 2008, **130**, 15732.

¹² E. L. Clennan, *Coord. Chem. Rev.*, 2004, **248**, 477.

¹³ A. Lichtblau, H. D. Hausen, W. Schwarz, W. Kaim, *Inorg. Chem.*, 1993, **32**, 73.

¹⁴ J. Clayden, N. Greeves, S. Warren, P. Wothers, *'Organic Chemistry'*, Oxford University Press, Oxford, 2001, p. 553.

-
- ¹⁵ A. L. Allred, *J. Inorg. Nucl. Chem.*, 1961, **17**, 215.
- ¹⁶ F. Carré, C. Chuit, R. J. P. Corriu, A. Mehdi, C. Reyé, *J. Organomet. Chem.*, 1997, **529**, 59.
- ¹⁷ D. Gudat, A. Haghverdi, M. Nieger, *Angew. Chem. Int. Ed.*, 2000, **39**, 3084.
- ¹⁸ R. B. King, P. M. Sundaram, *J. Org. Chem.*, 1984, **49**, 1784.
- ¹⁹ J. F. Harrison, *J. Am. Chem. Soc.*, 1981, **103**, 7406.
- ²⁰ P. Rempala, J. Kroulík, B. T. King, *J. Org. Chem.*, 2006, **71**, 5067.
- ²¹ B. T. King, J. Kroulík, C. R. Robertson, P. Rempala, C. L. Hilton, J. D. Korinek, L. M. Gortari, *J. Org. Chem.*, 2007, **72**, 2279.
- ²² M. D. Watson, A. Fechtenkötter, K. Müllen, *Chem. Rev.*, 2001, **101**, 1267.
- ²³ P. M. S. Monk, *"The Viologens. Physicochemical Properties, Synthesis and Applications of the Salts of 4,4'-Bipyridine"*, John Wiley & Sons, Chichester, 1998.
- ²⁴ I. M. Smallwood, *'Handbook of Organic Solvent Properties'*, Arnold, London, **1996**.
- ²⁵ A. di Matteo, *Chem. Phys. Letts.*, **2007**, 439, 190.
- ²⁶ W. W. Porter, T. P. Vaid, *J. Org. Chem.*, **2005**, 70, 5028.
- ²⁷ S. C. Bart, K. Chłopek, E. Bill, M. W. Bouwkamp, E. Lobkovsky, F. Neese, K. Wieghardt, P. J. Chirik, *J. Am. Chem. Soc.*, 2006, **128**, 13901.
- ²⁸ C. C. Lu, E. Bill, T. Weyhermüller, E. Bothe, K. Wieghardt, *J. Am. Chem. Soc.*, 2008, **130**, 3181.
- ²⁹ M. Krejčík, M. Daněk, F. Hartl, *J. Electroanal. Chem.*, 1991, **317**, 179.
- ³⁰ M. A. Fox, R. L. Roberts, W. M. Khairul, F. Hartl, P. J. Low, *J. Organomet. Chem.*, 2007, **692**, 3277.
- ³¹ P. Carol, S. Sreejith, A. Ajayaghosh, *Chem. Asian J.*, 2007, **2**, 338.
- ³² X. Shu, A. Royant, M. Z. Lin, T. A. Aguilera, V. Lev-Ram, P. A. Steinbach, R. Y. Tsien, *Science*, 2009, **325**, 804.
- ³³ *'WHO Recommended Classification of Pesticides by Hazard and Guidelines to Classification 1996-97'*, WHO/PCS/96.3, WHO, Geneva, 1996.

Chapter VI

6. Investigations into *N*-phosphino-pyridyl imines in the coordination sphere of palladium(0)

6.1. Introduction

Palladium complexes are widely known to be able to catalyse a vast number of organic transformations using a range of substrates.¹⁻³ The active species in these processes are frequently thought to be based around palladium(0) fragments, often ligated by one or two phosphines (or other neutral ligands), and which are commonly generated from palladium(II) precursors *in situ*.¹ To this end, investigations into the use of palladium dimethyl complexes as precursors to well defined palladium(0) species by reductive elimination of ethane have been conducted, with the compound [PdMe₂(TMEDA)] being the most extensively studied, as first reported by Boersma and coworkers.⁴⁻⁷ This methodology is particularly attractive due to the ease of preparation of the necessary Pd(II) species and the facile exchange of TMEDA with many different chelating ligands.

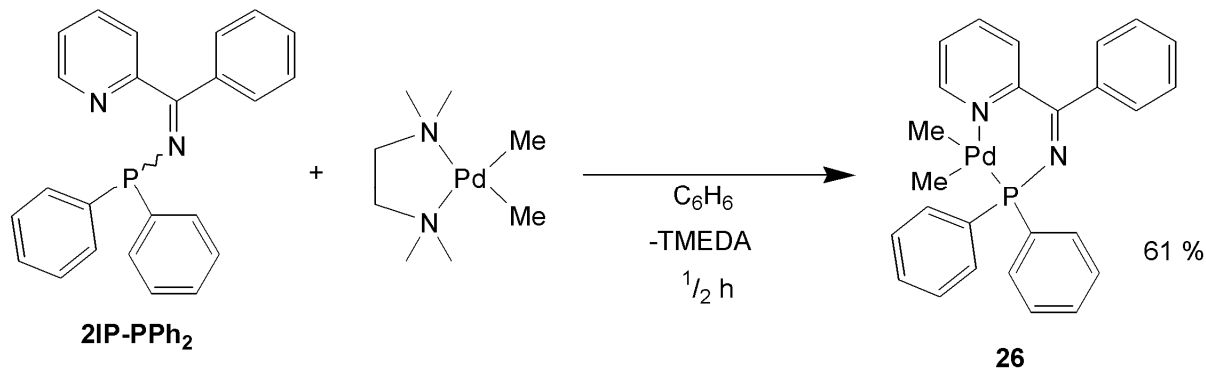
Since, a wide range of bidentate P^N ligands have been demonstrated to be efficient for palladium(0)-mediated cross-coupling,⁸ it was therefore of interest to attempt the introduction of the bidentate P^N ligands *N*-phosphino-pyridyl imines into the coordination sphere of palladium(0). The synthesis of these *N*-phosphino-pyridyl imines and their subsequent facile coordination to palladium dichloride is described in Chapter II. It was hoped that by use of the precursor [PdMe₂(TMEDA)] that P^N ligated-palladium dimethyl complexes could be generated that would give rise to well-defined palladium(0) species. Subsequent application of these species in catalytic processes was envisaged, exploiting the steric protection imparted by such *N*-phosphino-pyridyl imine scaffolds by the close proximity of the substituents at phosphorus and the pyridyl moiety (Chapter II).

6.2. Investigation into the synthesis and thermolysis of $[\text{PdMe}_2(\kappa^2\text{-}N,P\text{-}2\text{IP-PPh}_2)]$, **26**

6.2.1. Synthesis and characterisation of complex **26**

With the objective of obtaining a well-defined palladium(0) species in mind, complex **26** was synthesised as a precursor to the proposed complex $[\text{Pd}^0(\kappa^2\text{-}N,P\text{-}2\text{IP-PPh}_2)]$. The combination of equimolar quantities of **2IP-PPh₂** and $[\text{PdMe}_2(\text{TMEDA})]$ in toluene resulted in the precipitation of an orange solid, **26**, within minutes.

Scheme 1: Synthesis of complex **26** from **2IP-PPh₂** and $[\text{PdMe}_2(\text{TMEDA})]$



Characterisation of complex **26** by multinuclear NMR spectroscopy revealed the structure to be $[\text{PdMe}_2(\kappa^2\text{-}N,P\text{-}2\text{IP-PPh}_2)]$ with a ^{31}P NMR spectroscopic shift of 63.4 ppm. The $^{13}\text{C}\{^1\text{H}\}$ NMR spectrum of **26** shows that the two methyl groups are inequivalent, as expected due to the asymmetric square planar geometry and the differing *trans* influence of phosphorus and nitrogen donors, giving rise to doublets at - 8.9 and + 7.2 ppm.⁹ The latter resonance is assigned to the methyl group *trans* to phosphorus due to the large $^2J_{\text{PC}}$ coupling constant of 115 Hz, in contrast to the $^2J_{\text{PC}}$ coupling constant of 6 Hz recorded for the resonance at - 8.9 ppm.¹⁰

The molecular structure of complex **26** has been determined by X-ray crystallographic techniques (Figure 1) and exhibits differing Pd-CH₃ bond lengths of 2.035(2) Å and 2.1017(19) Å for the *cis* and *trans* methyl groups with respect to phosphorus, as anticipated.⁹ The only previously crystallographically-characterised P[^]N ligand-supported palladium dimethyl

complex is **GM** (Figure 2), synthesised by Green *et al.*¹¹ Comparison of the X-ray molecular structures of **26** and **GM** reveals the PdMe₂ fragments to have identical bond distances within error (Figure 2). In addition, the Pd-N and Pd-P bond distances of each complex are also very similar.

Figure 1: Molecular structure of **26**.C₆H₅CH₃ (hydrogen atoms and solvent molecules are omitted for clarity) with selected bond lengths (Å) and angles (°). (Thermal ellipsoids set at 50 % level).

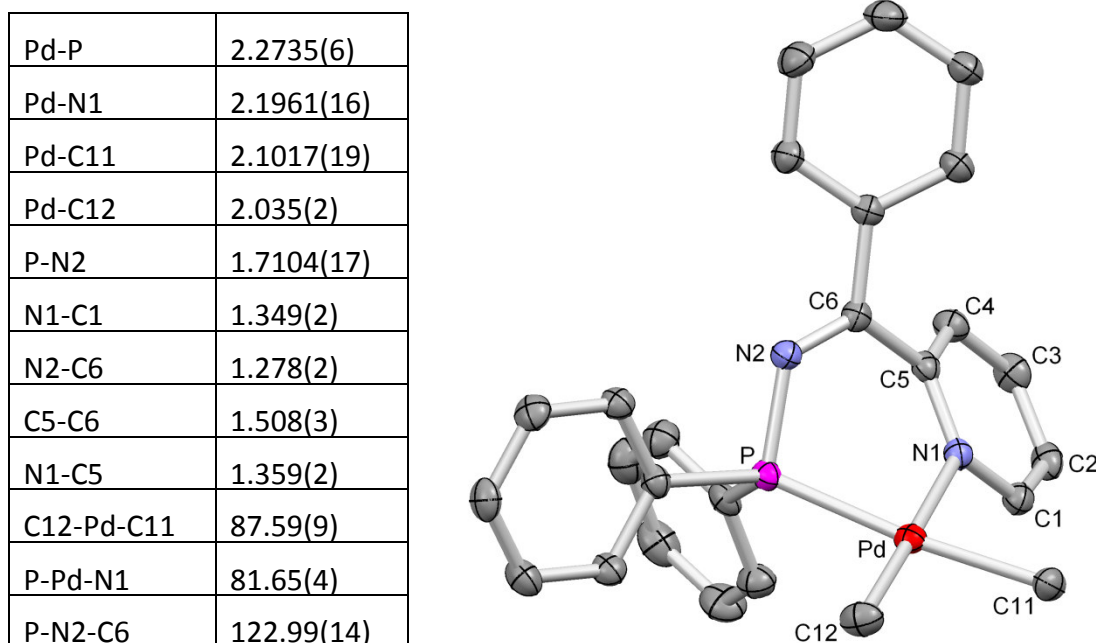
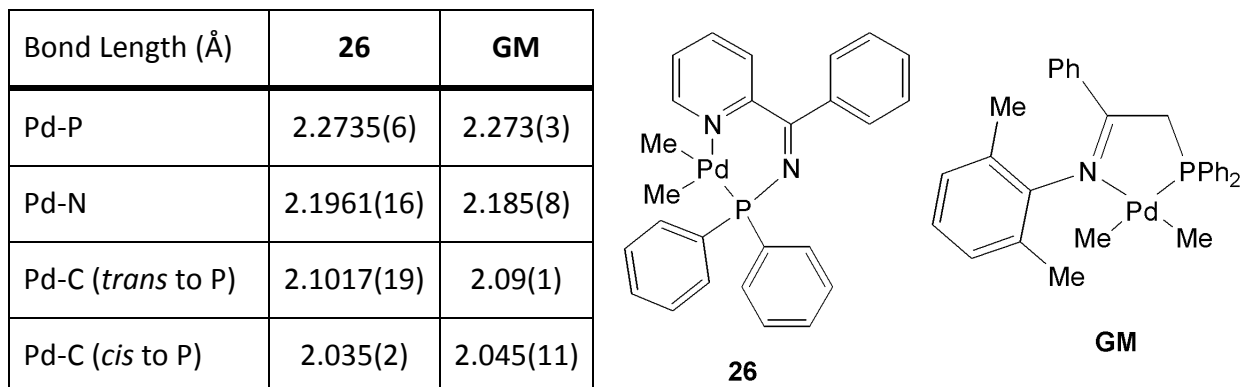


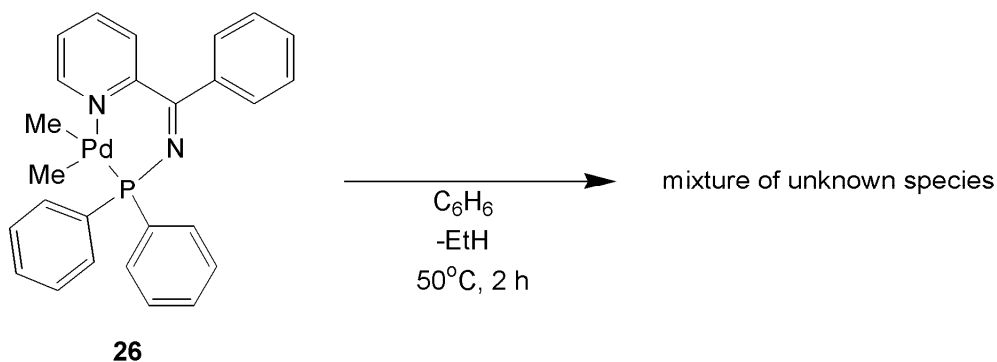
Figure 2: Comparison of selected bond lengths of [PdMe₂{κ²-P,N-(Ph₂PCH₂C(Ph)=N(2,6-Me₂C₆H₃))}], **GM**, reported by Green¹¹ and complex **26**



6.2.2. Thermolysis of $[\text{PdMe}_2(\kappa^2\text{-}N,P\text{-}2\text{IP-PPh}_2)]$, **26**

On warming a deuterated benzene solution of **26** to 50 °C the complex undergoes reductive elimination affording ethane (characterised by a singlet resonance observed at 0.7 ppm by ^1H NMR spectroscopy) in a matter of hours, a process that has been discussed in detail by other researchers.¹²⁻¹⁴ Unfortunately, thermolysis of complex **26** gave rise to multiple species as indicated by inspection of the ^1H NMR spectrum, which could not be separated or isolated before the onset of decomposition. These species are possibly monomeric or dimeric **2IP-PPh₂** ligated palladium(0) complexes. Hence, it was of interest the use of consider other *N*-phosphino-pyridyl imine ligands, of which several have been synthesised and characterised (**10-60**, Chapter II).

Scheme 2: Thermolysis of complex **26**



6.3. Synthesis and characterisation of the dimeric complex **27**

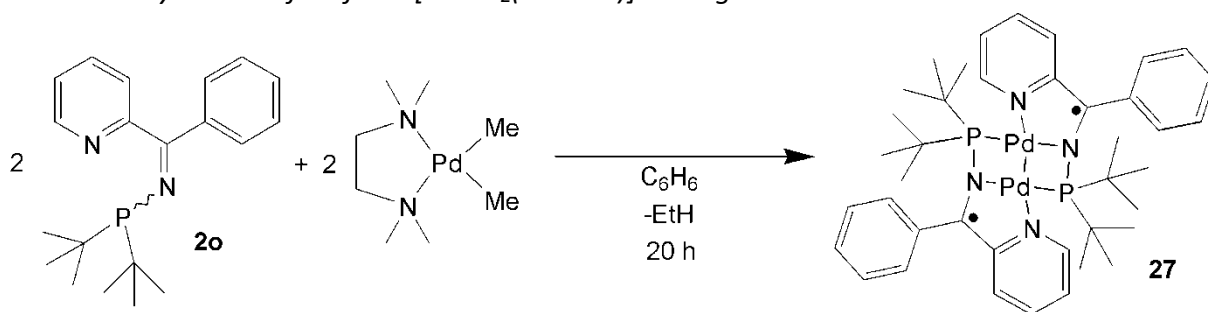
6.3.1. Reaction of $[\text{PdMe}_2(\text{TMEDA})]$ with ligand **2o**

Since, only unstable, unidentifiable products were obtained upon themolysis of complex **26**, it was hoped that the investigation of a different ligand, **2o**, in the coordination sphere of palladium(0) would give different results. The *N*-phosphino-pyridyl imine **2o**, is a variation of the **2IP-PPh₂** ligand where the phenyl substituents on phosphorus have been replaced by t-

butyl groups.* This was an attractive choice of ligand since it is both electron rich and bears bulky phosphorus-substituents mirroring the strongly electron donating bulky phosphines PCy_3 and $\text{P}(\text{t-Bu})_3$, which are highly active for the palladium(0)-mediated cross-coupling of aryl halides.¹⁵ Hence, with a view to catalytic applications, an exploration of the chemistry of **2o** in the presence of palladium(0) was warranted.

The reaction between the ligand **2o** and $[\text{PdMe}_2(\text{TMEDA})]$ in an NMR spectroscopy tube allowed the formation of ethane to be detected by ^1H NMR spectroscopy forming slowly over a period of 20 h. Despite the observation of ethane formation arising from reductive elimination the resulting products were silent by ^{31}P NMR spectroscopy. Repetition of the reaction on a larger scale allowed the isolation of complex **27**, as a dark crystalline solid, in 73 % yield. Suitable single crystals for were grown for an X-ray structure determination from benzene and complex **27** was found to be dimeric in the solid state (Scheme 3).

*Scheme 3: Synthesis of **27** from $[\text{PdMe}_2(\text{TMEDA})]$ and ligand **2o***



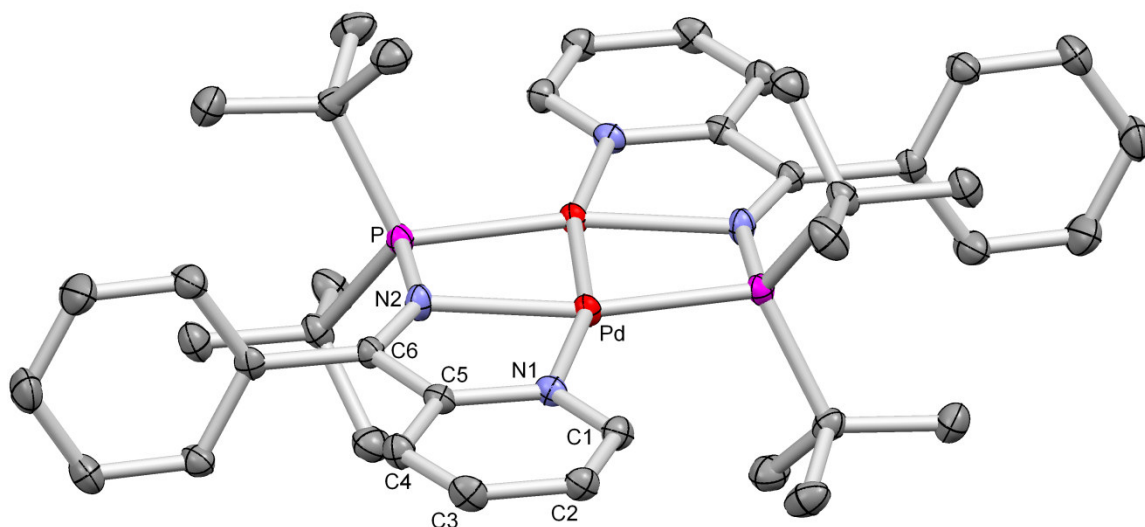
6.3.2. X-ray molecular structure of complex **27**

In the X-ray molecular structure of **27** a dimeric structure consisting of a palladium(I)-palladium(I) core supported by two singly-reduced **2o** ligands is found (Scheme 3 and Figure 3). Each palladium centre is supported by the pyridyl nitrogen lone pair and an amido moiety (resulting from reduction of the imine) of one ligand and the phosphorus lone pair of the second ligand. This $\kappa^2\text{-N,N-}\kappa^1\text{-P-}$ binding mode is markedly different from that determined for previously synthesised compounds with this type of $((\text{C}_5\text{H}_5\text{N})\text{-C}(\text{Ph})=\text{NPR}'_2)$ ligand backbone,

* See Chapter II for the synthesis of **2o** and its complexation to palladium dichloride

which, in palladium(II) and platinum(II) dichloride complexes, bind in a κ^2 -*P,N*-fashion through the phosphine and pyridine donor moieties.¹⁶

Figure 3: Molecular structure of 27.2C₆D₆ (hydrogen atoms and solvent molecules are omitted for clarity) with selected bond lengths (Å) and angles (°). (Thermal ellipsoids set at 50 % level).



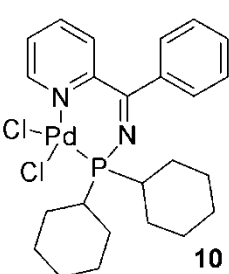
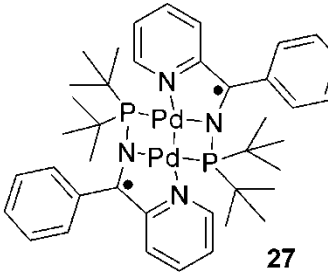
Pd-N1	2.1376(15)	Pd-Pd'-P	74.571(14)
Pd-N2	2.0614(16)	Pd-N2-P	99.11(8)
Pd-Pd'	2.4565(3)	Pd'-Pd-N1	164.12(4)
Pd'-P	2.2533(5)	Pd'-Pd-N2	84.94(4)
P-N2	1.6795(16)	N1-Pd-N2	79.26(6)
N2-C6	1.348(2)	P-N2-C6	145.44(12)
C5-C6	1.433(2)	N2-P-Pd'	101.38(6)
N1-C5	1.383(2)	N2-Pd-P	159.51(5)
N1-C1	1.345(2)	C6-N2-Pd	115.20(12)

6.3.2.1. Comparison of the *N*-phosphino-pyridyl imine framework in complex **27** to known coordinated pyridyl imine scaffolds

As exemplified by X-ray diffraction, the dimer **27** exists as a palladium(I)-palladium(I) core supported by two singly-reduced **2o** ligands, which is apparent upon comparison of the bond lengths and angles of complex **27** relative to those found in the molecular structures of metal-coordinated neutral *N*-phosphino-pyridyl imine ligands. The most significant differences are highlighted in Figure 4 against a representative palladium(II) compound [PdCl₂(κ²-*P,N*-**4o**)], **10**, that was synthesised and characterised in Chapter II. The bond length N2-C6 in complex **10** is 1.27 Å, typical of a C=N double bond, whereas in the palladium dimer **27** this length is markedly different, 1.35 Å. In contrast, the bond C5-C6 is noticeably shorter in complex **27** than in the comparable complex **10**. The rest of the **2o** framework is unchanged in complex **27**, relative to *N*-phosphino-pyridyl imines bound κ²-*P,N* in palladium(II) complexes, apart from a slight lengthening observed for the bond N1-C5.

Figure 4: Selected bond distances for the X-ray molecular structures of complexes **10** and **27** (left) with bonding descriptions (right)

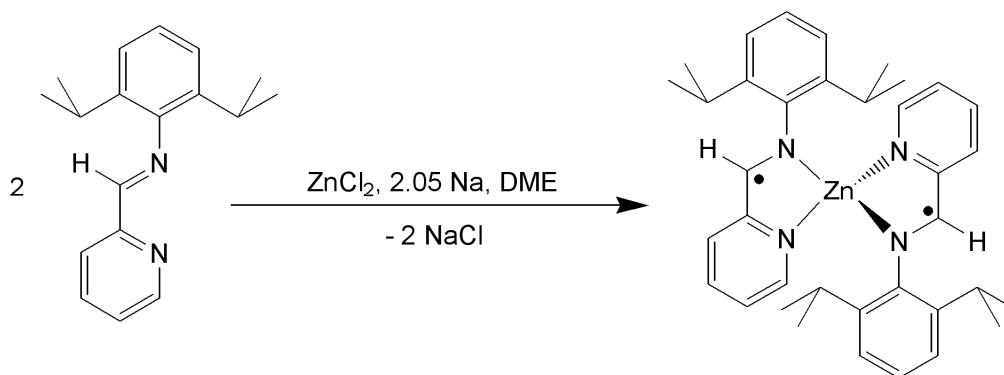
	Bond Lengths (Å)		
	N2-C6	C5-C6	N1-C5
10	1.272(3)	1.500(3)	1.352(3)
27	1.348(2)	1.433(2)	1.383(2)

The observed contraction and expansion of the bond distances C5-C6 and N2-C6, respectively, in the iminopyridyl fragment of complex **27** has precedent.^{17,18} Wieghardt has established that the pyridyl imine 2,6-(*i*-Pr)₂PhN=C(H)(C₅H₄N) can be singly-reduced by suitable reductants, often low oxidation state metal species, to give a ligand-based radical-containing complex (Scheme 4).¹⁹ X-ray diffraction studies of these [M{κ²-*N,N*-(2,6-(*i*-

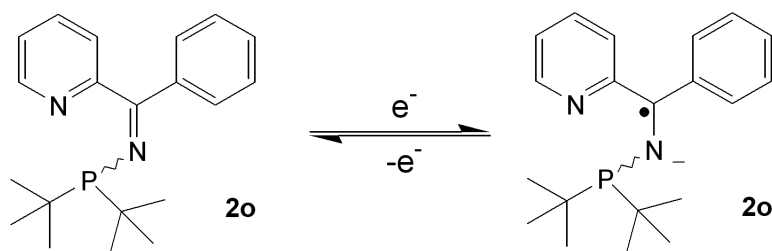
$\text{Pr}_2\text{PhN}=\text{C}(\text{H})(\text{C}_5\text{H}_4\text{N}_2)]\}$ complexes has shown that the unpaired electron is predominantly localised over the reduced imine and the exocyclic C-C bond of the pyridyl ring.

Scheme 4: Reduction of 2,6-(i-Pr)₂PhN=C(H)(C₅H₄N) with ZnCl₂ reported by Weighardt¹⁹



The observed changes in the N2-C6 and C5-C6 bonds in complex **27**, compared with complex **10**, are consistent with a singly-reduced pyridyl imine with a ligand-centred radical delocalised predominately over the atoms N2, C6 and C5 (Scheme 5). The reduction of the **2o** ligand is accompanied by with the oxidation of palladium(0) to give the bimetallic palladium(I) complex **27** possessing a metal-metal bond.

*Scheme 5: Two possible redox states of **2o**, where the neutral form is found for free and κ^2 -P,N metal-coordinated **2o** and the reduced form found for κ^2 -N,N- κ^1 -P-metal-coordinated **2o***



6.3.2.2. Examination of palladium(I)-palladium(I) bond distance of complex **27**

Inspection of the X-ray molecular structure of **27** (Figure 4) reveals the metal-metal distance to be 2.4565(3) Å, which is unusually short for a palladium-palladium bond. Typical palladium(I)-palladium(I) bond distances are in the range 2.35 - 2.70 Å, with only four crystallographically-characterised palladium-palladium distances of any sort being found to be shorter than 2.45 Å.²⁰⁻²⁴ Of these latter four structures, the majority are palladium(I) dimers,²¹⁻²³ however, in one of the systems the palladium centres exist in the + 3 oxidation state (Figure 5).²⁴ In contrast, dimeric forms of palladium(0), of which a number have been subject to X-ray molecular structure determinations, exhibit far longer palladium-palladium distances between 2.71 and 2.86 Å (Figure 6).^{6,7,25,26} Thus, the palladium-palladium bond distance of complex **27** is at the short end of the range expected for palladium(I) dimers, but clearly consistent with the proposed structure of **27** (Figure 4).

Figure 5: Two examples of short palladium-palladium bonds. A palladium(I)-palladium(I) dimer²² (left) and a palladium(III)-palladium(III) complex²⁴ (right) with Pd-Pd distances of 2.429(4) Å and 2.391(2) Å, respectively.

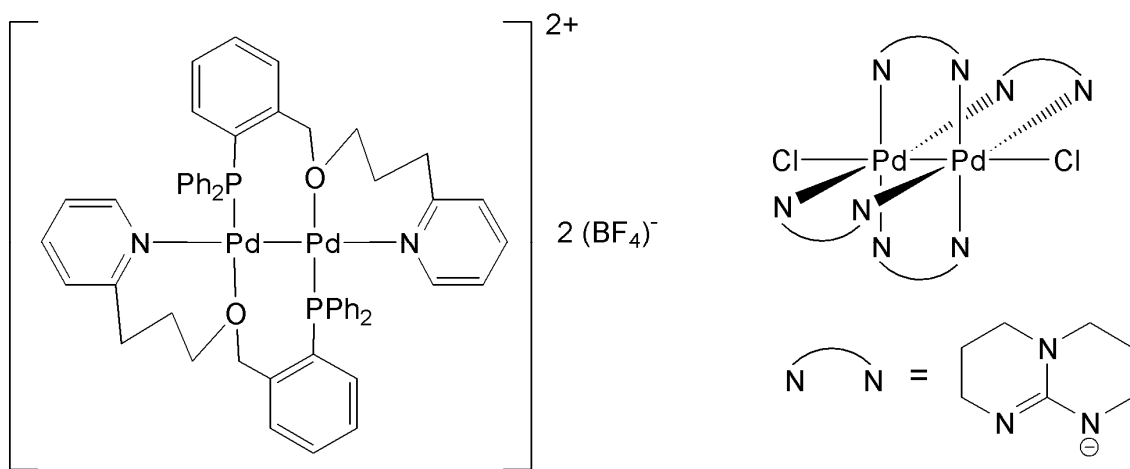
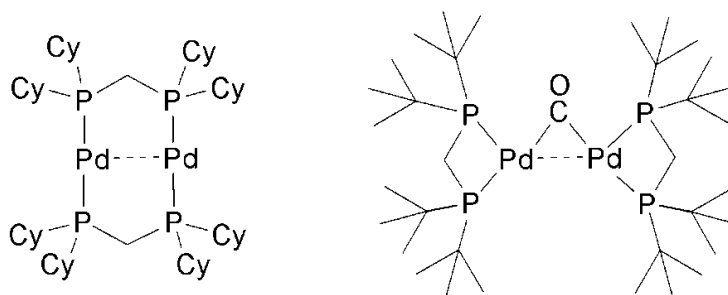


Figure 6: Two examples of dimeric palladium(0) species synthesised by Fink⁶ (left) and Porschke²⁶ (right) with Pd-Pd distances of 2.8582(6) Å and 2.714(1) Å, respectively.



6.3.2.3. Summary of the crystallographic data of complex **27**

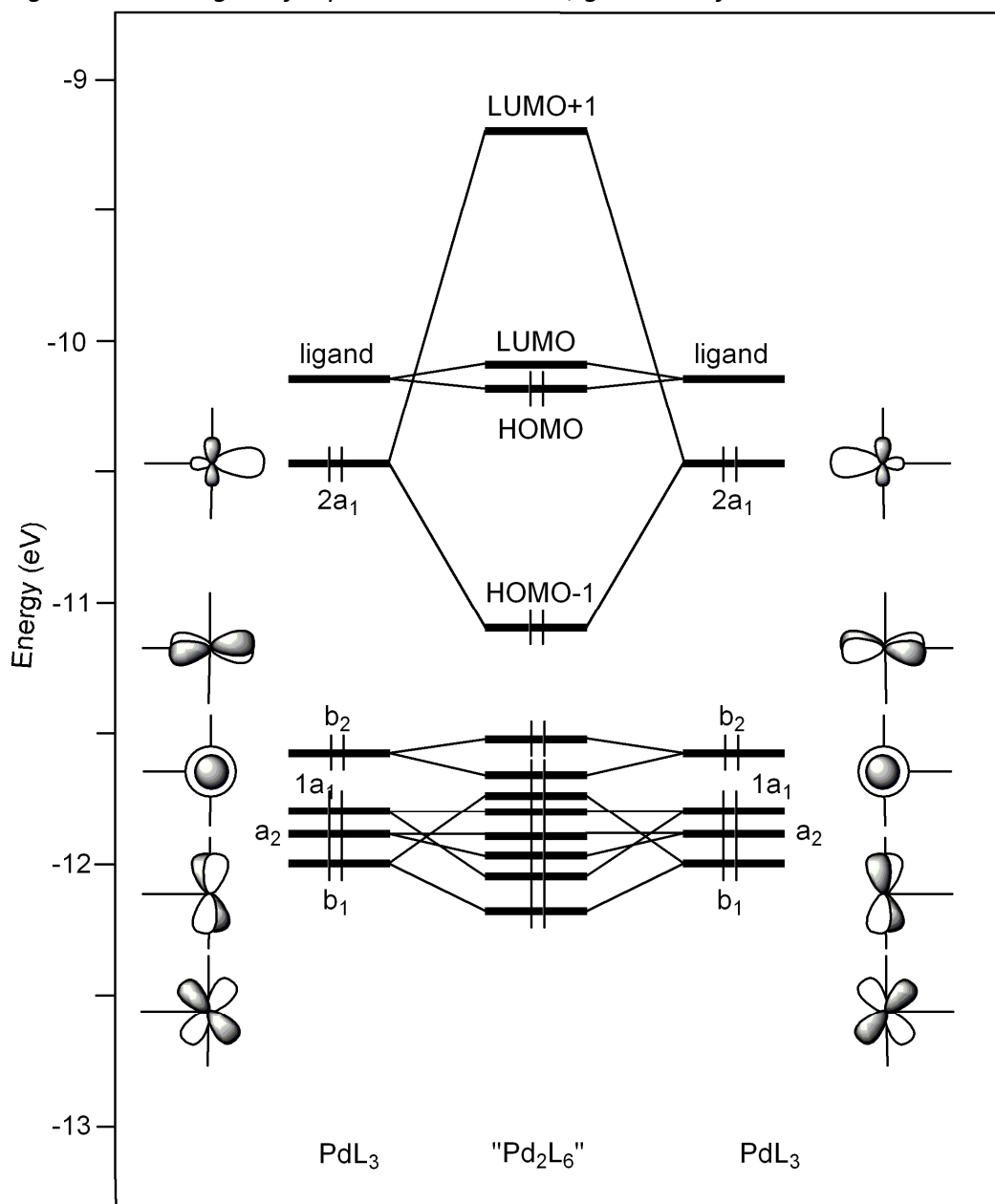
The X-ray diffraction study of complex **27** clearly shows a bimetallic palladium(I) dimer with two singly-reduced *N*-phosphino-pyridyl imine ligands. The $\kappa^2\text{-}N,N\text{-}\kappa^1\text{-P}$ -binding motif is thought to be crucial to the reduction of the **2o** ligand with the imine nitrogen binding direct to palladium and is analogous to similar coordinated pyridyl imine systems reported by Wieghardt.¹⁸ One of the driving forces for adopting the unusual structure of complex **27** is likely to be the favourable redox chemistry, between palladium(0) and **2o**. In addition, the dimeric $\kappa^2\text{-}N,N\text{-}\kappa^1\text{-P}$ binding scenario adopted (**27**) avoids an exposed palladium centre that would undoubtedly exist in a $\kappa^2\text{-P},N$ bound monomeric species. The unusual structure of complex **27** prompted a further investigation into the bonding of this system and so a computational study was conducted.

6.3.3. Computational investigations into the structure of complex **27**

Calculations have been carried out in order to probe the unusual structure and bonding of complex **27** in greater depth by J.-F. Halet and K. Costuas.[†] A partial MO diagram for the dimer can be constructed using Extended Huckel Theory starting from two PdL_3 fragments in which palladium has a d^{10} valence electron count (Figure 7).²⁷

[†] Drs J.-F. Halet and K. Costuas are based at the Université de Rennes 1

Figure 7: MO diagram for palladium dimer **27**, generated from Extended Huckel Theory



Each fragment possesses five metallic d-type frontier orbitals (FOs), above which lies an empty orbital strongly ligand in character. If these two sets of fragment FOs are allowed to interact then ten metallic and two ligand MOs are produced (Figure 7). If, as originally expected, all of the metallic MOs were of lower energy and subsequently filled by electrons this would lead to no bonding interaction between the two fragments. This is not the case however, because it is found that one of the metallic MOs is strongly antibonding and remains unoccupied after interaction of the two PdL_3 fragments. Therefore palladium-palladium bonding occurs with a σ -type bonding MO (HOMO-1) and a σ^* -type antibonding

MO (LUMO+1). The two electrons lost from the metallic MO now lie in the lowest energy ligand-type MO (HOMO). To summarise, this consideration of complex **27** by Extended Huckel Theory results in a bonding description consisting of two fifteen-electron [PdL₃] fragments with a σ bond between the metals to give a valence electron count of 16 electrons per palladium. Halet and Costuas have also run DFT calculations[‡] on complex **27**, with the resulting optimised geometry comparing favourably with that determined by X-ray diffraction. There is, however, a slight lengthening of the bond distances to palladium in the computationally-optimised structure relative to those determined in the X-ray molecular structure (Table 1). The computed frontier/near-frontier molecular orbitals for complex **27** are shown in Figure 8. The LUMO-1 corresponds to the empty palladium-palladium σ^* -antibonding combination with the σ -bonding filled combination being “diluted” across the occupied bonding MOs; HOMO-3, HOMO-4, HOMO-8 and HOMO-9.

*Table 1: Comparison of the bond distances of complex **27** obtained by an X-ray diffraction study and by calculations undertaken by the group of J.-F. Halet*

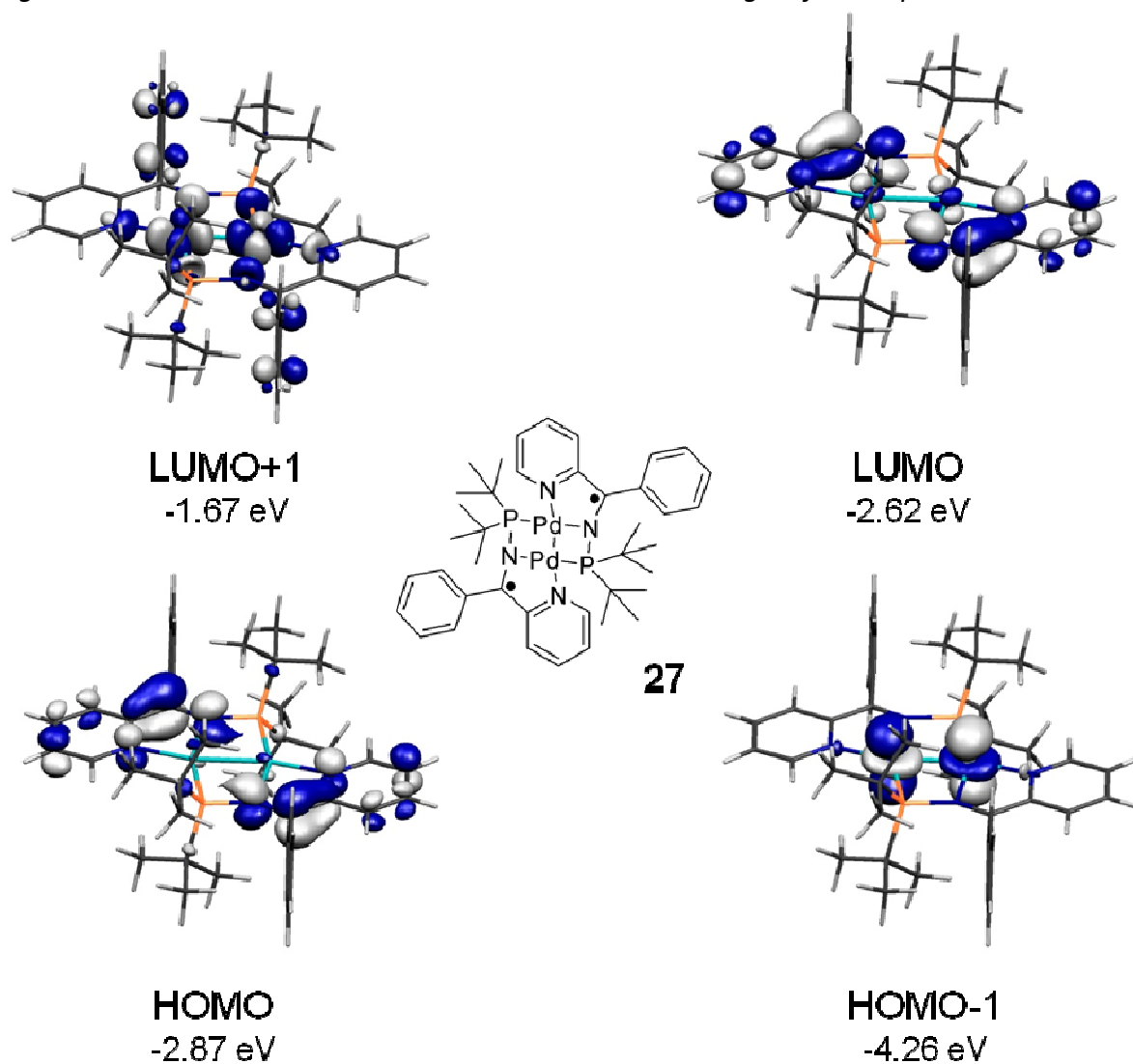
Bond length (Å)	Pd-Pd	Pd-P	Pd'-P	Pd-N1	Pd-N2
X-ray molecular structure	2.4565(3)	2.2533(5)	2.8577(5)	2.1376(15)	2.0614(16)
DFT calculations [‡]	2.511	2.300	2.922	2.162	2.100

The calculations on the palladium dimer **27** suggest a small HOMO-LUMO gap, which potentially affords the complex the option of being in a high or a low spin state depending on whether an electron can be excited from the HOMO to the LUMO. The geometry has been optimised for both the high and low spin configurations, giving similar energies (0.02 eV in favour of the high spin state at 0 K). Investigation of the bond lengths yields no clues as to which spin configuration is adopted by **27**, as both the HOMO and LUMO are the in-phase and out-of-phase combination of the same frontier orbital with comparable distances being

[‡] DFT calculations were carried out at the scalar ZORA BP86/TZP (frozen-core) level of theory for optimization and at the scalar ZORA B3LYP/TZP (all electrons) level for the single point energy evaluation, using the ADF package (www.scm.com)

found for both high and low spin. To further explore whether **27** adopts a high or low spin configuration, cyclic voltammetry was attempted under an inert atmosphere; due to the sensitivity of complex **27** towards chlorinated solvents (*vide infra*) acetonitrile was chosen.[§] Unfortunately neither oxidation nor reduction could be detected for complex **27** within the window allowed by the acetonitrile solvent.

Figure 8: Selected molecular orbitals in the LUMO-HOMO region for complex **27**

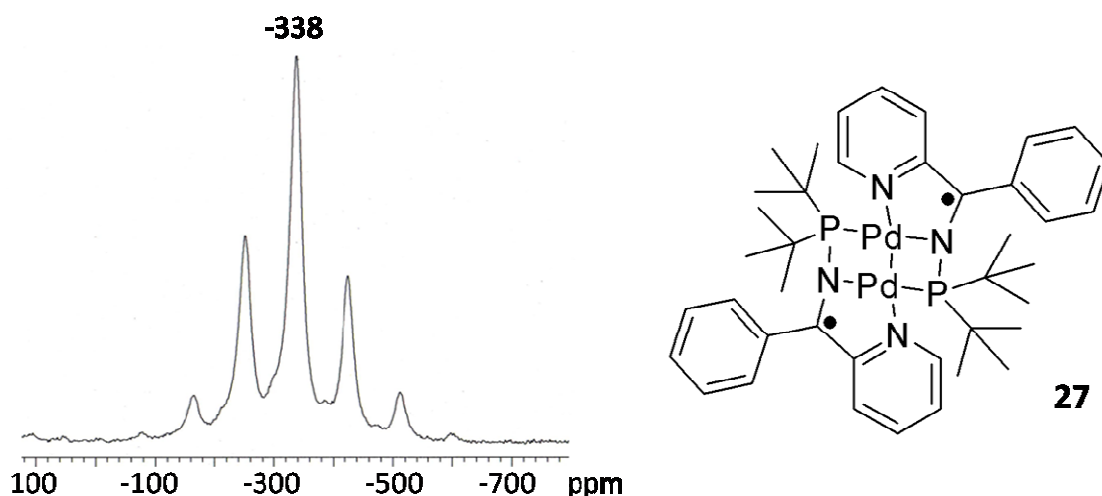


[§] Cyclic voltammetry was conducted by Dr P. J. Low

6.3.4. Solid-state NMR spectroscopic studies of complex **27**

As previously mentioned, complex **27** was found to be silent by solution-state NMR spectroscopy, something that has been attributed in part to the compound's low solubility and paramagnetic line broadening. Consequently, in order to obtain information about the bulk sample of complex **27**, solid-state ^{31}P NMR spectroscopy was conducted. Only one resonance was detected for **27** at -338.2 ($\nu_{1/2} = 3880$ Hz) ppm with associated spinning sidebands, and was confirmed by spectral acquisition at varying spin rates. The phosphorus NMR chemical shift is beyond the normal range expected due to the proximity of phosphorus to the radical, causing a paramagnetic shift. This ^{31}P NMR chemical shift is supportive of the symmetrical, paramagnetic dimeric structure proposed for complex **27** (Figure 9).

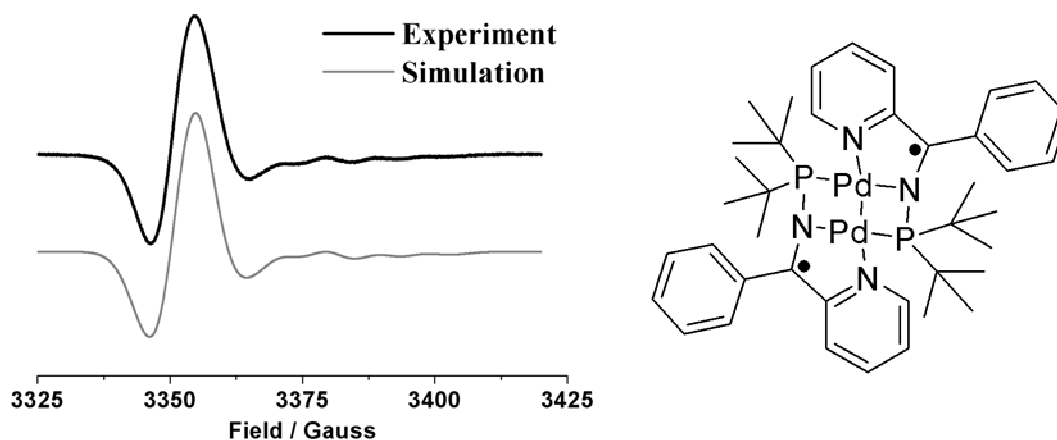
Figure 9: Solid state ^{31}P Direct Polarisation MAS NMR spectrum (frequency = 162 MHz, acquisition time = 5.0 ms, recycle 0.5 sec, spin rate 13997 Hz) (left) and structure (right) of complex **27**



6.3.5. Electron paramagnetic resonance (EPR) and solid state magnetic studies of complex **27**

To further confirm the nature of the complex, as a bimetallic palladium(I) system with two singly-reduced ligands, EPR experiments were conducted.^{**} A study of a solid sample of **27** at ambient temperature gave the spectrum reported in Figure 10, indicating the presence of a paramagnetic species. This spectrum, shows a five line 1:2:3:2:1 splitting pattern due to coupling of the unpaired electron to two ^{14}N atoms (splitting 8.80 G), as would be expected for coupling to nuclei of spin $I = 1$. The g_{axial} values ($g_{(\text{xy})}=2.0062$; $g_{(\text{z})}=1.9894$) are representative of a free electron located on a carbon atom.²⁸ Any phosphorus contribution to the EPR pattern is assumed to be lost due to the large linewidths encountered. Together, these data suggest that there is a radical on the organic framework of complex **27** and likely to lie between the two nitrogen atoms (Figure 10). This is consistent with the X-ray crystallographic data, where an unpaired electron is inferred to be delocalised over the N2-C6 and C6-C5 bonds of the *N*-phosphino-pyridyl imine ligand.

Figure 10: X-Band second derivative EPR spectrum (9.4 GHz, power = 0.02 mW, 293 K) (left) and bonding description of complex **27** (right)

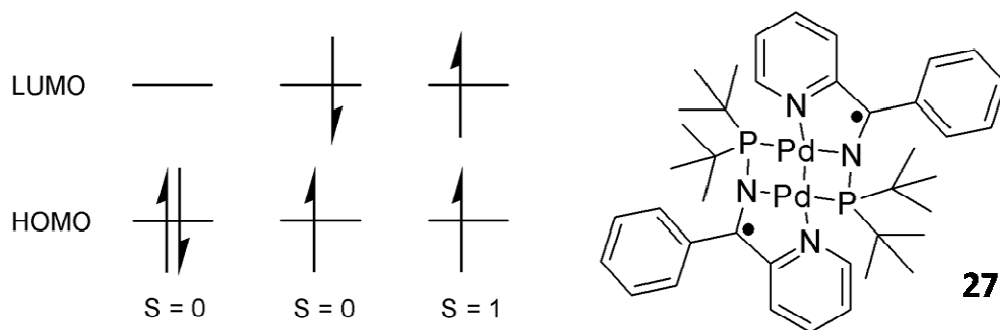


^{**} These experiments, and help with interpretations, were kindly conducted by Dr R. Edge and Prof. D. Collison of the EPSRC EPR National Service at the University of Manchester

The observed EPR signal exhibits no coupling between the two radicals, as a result no half-field signal is observed due to weak electron-electron coupling. This lack of coupling is to be expected due to the large distance between the two unpaired electrons. Given that, the palladium(I) centres are spin-coupled, they do not give rise to an EPR signal.

Since, EPR spectroscopy revealed a paramagnetic species present in samples of complex **27** it was of interest to explore the overall magnetic character of the sample. Whereas EPR spectroscopy is able to provide information about the environment of a radical within a species, a measurement of the magnetic moment allows for a quantification of the sample homogeneity. As predicted by the DFT calculations (Section 6.3.3), complex **27** can exist in either a high ($S = 1$) or low spin ($S = 0$) state due to the small energy gap between the HOMO and the LUMO (Figure 11).

Figure 11: Possible high and low spin states (left) and structure of complex **27** (right)



To determine μ_{eff} a finely ground sample of complex **27** was subject to a magnetic susceptibility measurement using a Johnson-Matthey-Evans Magnetic susceptibility balance.^{††} A value of $\mu_{\text{eff}} = 1.80 \mu_{\text{B}}$ was obtained and corresponds to approximately one unpaired electron per molecule of complex **27**, suggesting that the complex exists in a mixture of high spin and low spin states with no ferromagnetic or antiferromagnetic coupling.

^{††} For magnetic susceptibility data recorded for complex **27** and subsequent analysis see appendix

6.4. Reactivity of palladium dimer **27**

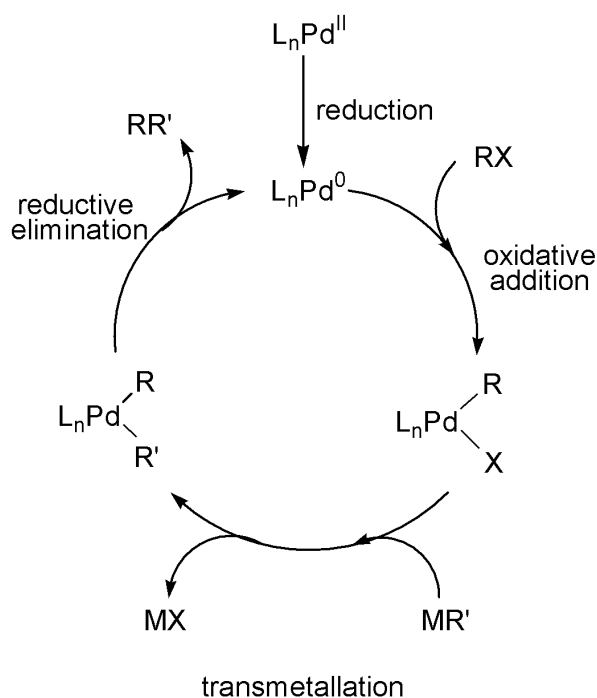
6.4.1. Reactivity of complex **27** towards aryl halides

6.4.1.1. Introduction to oxidative addition of aryl halides in palladium(0)-mediated catalytic cross-coupling

The catalytic versatility of palladium(0) systems towards a wide range of substrates including alkenes, alkynes, aryl halides and aryl boronic acids has long been known.^{1,29} Of these, aryl halides are amongst the most common precursors in catalytic cross-coupling with their reactivity generally following the order $\text{ArI} > \text{ArBr} > \text{ArCl}$.³⁰ The aryl iodides and bromides are generally more widely used in preference to the harder to activate aryl chlorides. In recent years, however, there has been a greater drive to utilise aryl chlorides for cross-coupling. This is both an academic challenge due to their less reactive C-X bond and a commercial objective with aryl chlorides cheaper being and more readily available than aryl bromides and iodides.

The oxidative addition of aryl halides is often the first step in a palladium-mediated cross-coupling cycle starting from a palladium(0) species (see Figure 12). To oxidatively add the less reactive Ar-Cl bond, relative to the Ar-Br bond, a far more nucleophilic palladium centre is required, often achieved by the ligation of electron-donating phosphine donors, with commonly used phosphines including $\text{P}(\text{t-Bu})_3$ and PCy_3 .¹⁵ Additionally, use of these sterically demanding phosphorus donors favours mono- and bi-ligated palladium species that are thought to be the active species in palladium(0)-mediated cross-coupling. Therefore, given the electron rich phosphine moiety of **20** it was of interest to explore the reactivity of its palladium complex, **27**, with aryl chlorides.

Figure 12: Generic palladium(0)-mediated catalytic cross-coupling cycle¹



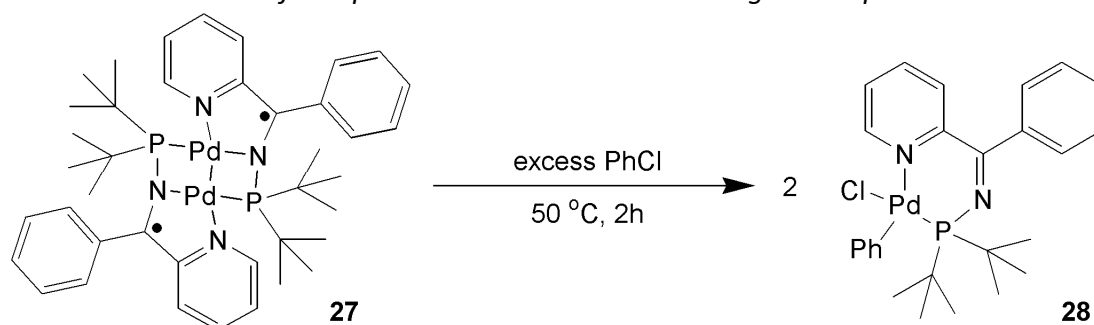
6.4.1.2. Reactivity of complex **27** towards chlorobenzene

Complex **27** consists of two singly-reduced *N*-phosphino-pyridyl imines which produce a formal oxidation state of + 1 at each metal centre and this unusual structure undoubtedly results from a redox reaction of the palladium(0) and neutral ligand precursors. It was of interest to explore if this redox event was reversible. Therefore, the addition of simple molecules to complex **27** was conducted with the aim of disrupting the κ^2 -*N,N*- κ^1 -P-binding motif, proposed to be crucial to maintaining the structure of the bimetallic palladium(I) system, in order to generate a palladium(0) or palladium(II) species.

A logical choice of reactant to perturb the binding of complex **27** was an aryl halide as oxidative addition at low-oxidation state metal centres is often found to be irreversible and hopefully result in a well-defined product. In addition, the oxidative addition of aryl halides is a key reaction in many palladium-mediated cross-coupling cycles.¹⁵

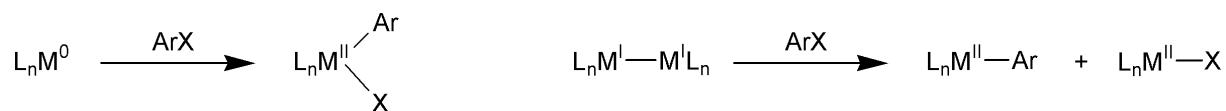
Therefore, the aryl halide chlorobenzene was added to a solid sample of complex **27** and the resulting suspension warmed to 50 °C. Within two hours complete consumption of solid was apparent, accompanied by the generation of a clear, homogeneous yellow solution. Analysis of this solution by ^1H , $^{13}\text{C}\{^1\text{H}\}$, and ^{31}P NMR spectroscopies confirmed the formation of $[\text{PdCl}(\text{Ph})(\kappa^2\text{-P,N-2o})]$, **28**, as the sole product, and this palladium(II) complex was found to be diamagnetic with a neutral coordinated *N*-phosphino-pyridyl imine, hence demonstrating that the ligand is capable of re-oxidation. This ligand redox change, from complex **27** to **28**, is attributed primarily to the disruption of the $\kappa^2\text{-N,N-}\kappa^1\text{-P}$ -binding motif.

*Scheme 6: Reaction of complex **27** with chlorobenzene to give complex **28***



In order to account for the formation of complex **28** from addition of PhCl to the palladium dimer **27** two likely mechanisms can be envisaged. Firstly, the addition of the substrate across the metal-metal bond is possible, termed “binuclear oxidative addition” and would result in the initial formation of M-Ph and M-Cl species (M = metal),³¹ with subsequent reactions leading to complex **28**. An alternative mechanism is the oxidative addition of the aryl halide *via* a palladium(0) intermediate. The generation of such an intermediate can be envisaged by the concomitant dissociation of the dimer **27** accompanied by reduction and oxidation of the metal centre and ligand, respectively, to give a palladium(0) fragment ligated by a neutral *N*-phosphino-pyridyl imine. Although this latter process is feasible no NMR spectroscopic evidence of a monomeric species was found in solutions of **27**, although it is possible that the monomer may exist in trace amounts or is paramagnetically line-broadened by **27**, which would prevent detection.

Scheme 7: Oxidative addition of an aryl halide, ArX, at a monomeric metal complex (left) and “binuclear oxidative addition” of an aryl halide by a dimeric metal species (right)³¹



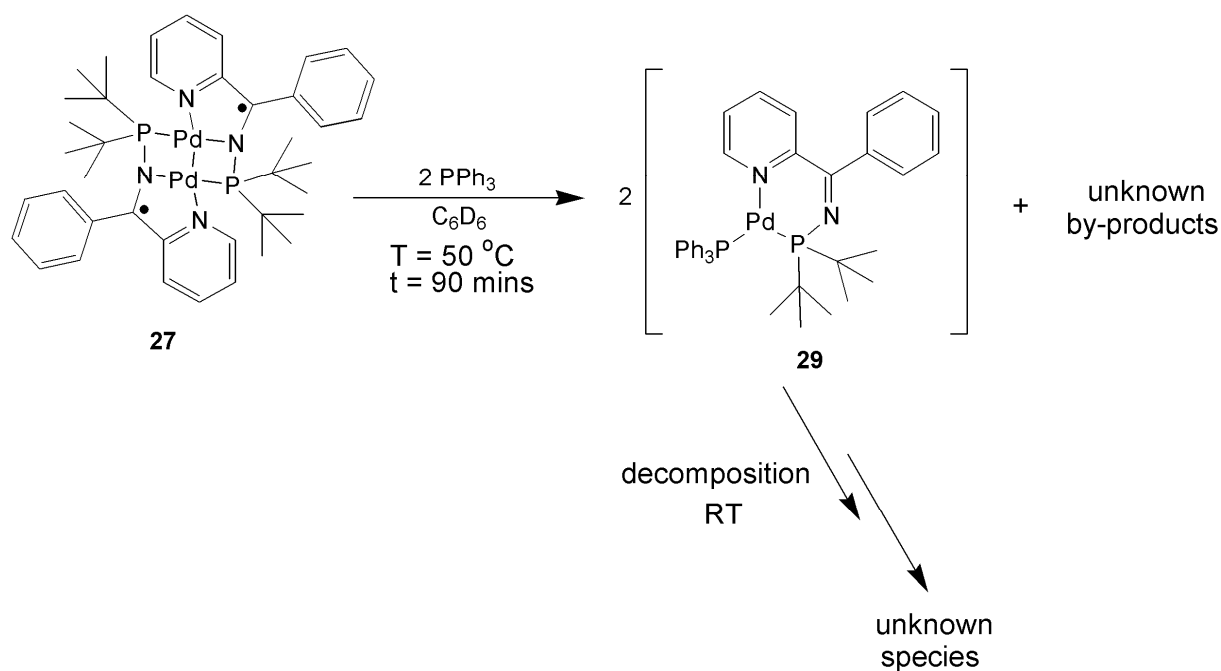
Although the mode of oxidative addition of PhCl to complex **27** is not readily apparent, the reactivity of **27** can be considered to be that of a ‘masked’ source of palladium(0) as the resultant palladium(II) aryl chloride is formed. This ‘palladium(0)-like’ reactivity in conjunction with versatile redox properties exhibited by ligand **2o** suggests further studies of complex **27** may reveal it to be a promising initiator for palladium(0)-mediated cross-coupling reactions.^{1,29}

6.4.2. Reactivity of complex **27** towards donor molecules

To further probe the reactivity of dimeric complex **27**, the addition of potential donor ligands was considered. It was proposed that the addition of a donor to complex **27** may disrupt the $\kappa^2\text{-N,N-}\kappa^1\text{-P}$ coordination of ligand **2o** and potentially reverse the redox process to give neutral bound **2o** and a palladium(0) centre. Triphenylphosphine was chosen as the donor, with the ‘soft’ nature of the phosphine often preferentially coordinating to ‘soft’ late transition metals such as palladium, relative to ‘hard’ amine donors in accordance with Pearson’s HSAB rules.³²

The reaction between complex **27** and two equivalents of PPh_3 was conducted in a Young’s NMR tube and followed by ^{31}P NMR spectroscopy. After 90 minutes of heating at 50 °C the appearance of two doublets was observed at 106.6 and 26.7 ppm each with a J_{PP} coupling of 139 Hz corresponding to a new compound, **29**. In addition, two singlet resonances at 97.4 and 23.8 ppm were observed existing as 7 % and 13 % of the total mixture which could not be conclusively identified. Unfortunately species **29** could not be isolated, however, in spite of this, the large J_{PP} coupling constant observed is strong evidence for the binding of both PPh_3 and **2o** to a single palladium centre, and therefore the structure $[\text{Pd}(\text{PPh}_3)(\kappa^2\text{-P,N-2o})]$ is proposed for complex **29**.

Scheme 8: Reactivity of complex **27** with triphenylphosphine to give the unstable species **29**



The magnitude of the $^2J_{\text{PP}}$ coupling (139 Hz) observed for complex **29** is in agreement with that expected for a trigonal planar structure.³³ Since the magnitude of a coupling between two nuclei observed in NMR spectroscopy is dependent upon the angle between them, commonly known as the Karplus relationship,¹⁰ the $^2J_{\text{PP}}$ coupling of **29** is a useful indicator of the structure of a complex.³⁴ By virtue of the Karplus relationship it is well established that a $^2J_{\text{PP}}$ coupling arising from a *cis* geometry will be smaller than from a *trans* geometry and therefore an intermediate angle, between 90 and 180 would be expected to give rise to an intermediate magnitude for the $^2J_{\text{PP}}$ coupling. The proposed structure of complex **29** is that of a trigonal planar palladium centre³⁵ where the P^N bite angle of $\kappa^2\text{-P,N-2o}$ is assumed to be 90° ,^{††} then the remaining angles between the donor atoms at the phosphorus centre will be 135° , so that the sum of the angles is 360° . This proposed P-Pd-P angle of 135° in complex **29** is similar in size to that reported in a trigonal planar species studied by Bunel, $[\text{Pd}(\text{PCy}_3)\{(\text{i-Pr})_2\text{P}(\text{CH}_2)_3\text{P}(\text{i-Pr})_2\}]$, with a P-Pd-P angle of 127° .³³ The $^{31}\text{P}\{^1\text{H}\}$ NMR spectrum of $[\text{Pd}(\text{PCy}_3)\{(\text{i-Pr})_2\text{P}(\text{CH}_2)_3\text{P}(\text{i-Pr})_2\}]$ displays an AX_2 coupling system with a $^2J_{\text{PP}}$ coupling constant of 81 Hz. In theory the magnitude of the $^2J_{\text{PP}}$ coupling constant for this

^{††} Based on X-ray molecular structures of complex $[\text{PdCl}_2(\kappa^2\text{-P,N-4o})]$, **10**, and related *N*-phosphino-pyridyl imine ligands bound $\kappa^2\text{-P,N}$ to palladium (see Chapter II)

latter complex would be expected to be lower than that of complex **29** due to the slightly smaller P-Pd-P angle in the former, which is closer to the *cis* geometry, for which the minimum coupling would be recorded.¹⁰ Since overall the magnitude of the $^2J_{PP}$ coupling constants in both complexes **29** and $[Pd(PCy_3)\{(i\text{-}Pr)_2P(CH_2)_3P(i\text{-}Pr)_2\}]$ is comparable, this supports the proposed structure of $[Pd(PPh_3)(\kappa^2\text{-}P,N\text{-}\mathbf{2o})]$ for **29**. Despite a number of attempts, complex **29**, proposed to be $[Pd(PPh_3)(\kappa^2\text{-}P,N\text{-}\mathbf{2o})]$, could not be isolated something attributed, in part, to the low stability of trigonal planar palladium(0) complexes, which are coordinatively unsaturated.³⁶

6.5. Summary

In conclusion two *N*-phosphino-pyridyl imines, **2IP-PPh₂** and **2o**, have been investigated as ligands for palladium dimethyl and palladium(0) fragments. The dimeric complex **27** has been isolated and characterised by solid-state NMR spectroscopy, a single crystal X-ray diffraction study and EPR spectroscopy. These experiments reveal the compound to exist as a palladium(I) dimer with two singly-reduced ligands. Reactions of complex **27** show that it behaves as a ‘masked’ form of palladium(0) with the *N*-phosphino-pyridyl imine ligand returning to its neutral state. This reversible redox property of ligand **2o** encourages the investigation of complex **27** as an initiator in palladium(0)-mediated cross-coupling.^{1,29}

¹ R. Chincilla, C. Nájera, *Chem. Rev.*, 2007, **107**, 874.

² J. Liebscher, *Chem. Rev.*, 2007, **107**, 133.

³ D. Alberico, M. E. Scott, M. Lautens, *Chem. Rev.*, 2007, **107**, 174.

⁴ W. de Graaf, J. Boersma, W. J. J. Smeets, A. L. Speck, G. van Koten, *Organometallics*, 1989, **8**, 2907.

⁵ S. M. Reid, R. C. Boyle, J. T. Mague, M. J. Fink, *J. Am. Chem. Soc.*, 2003, **125**, 7816.

⁶ S. M. Reid, J. T. Mague, J. Fink, *J. Am. Chem. Soc.*, 2001, **123**, 4081.

⁷ Y. Pan, J. T. Mague, J. Fink, *J. Am. Chem. Soc.*, 1993, **115**, 3842.

⁸ P. J. Guiry, C. P. Saunders, *Adv. Synth. Catal.*, 2004, **346**, 497.

⁹ T. G. Appleton, H. C. Clark, L. E. Manzer, *Coord. Chem. Rev.*, 1973, **10**, 335.

¹⁰ M. Karplus, *J. Phys. Chem.*, 1959, **64**, 1793.

-
- ¹¹ K. S. Coleman, M. L. H. Green, S. I. Pascu, N. H. Rees, A. R. Cowley, L. H. Rees, *Dalton Trans.*, 2001, 3384.
- ¹² A. Gillie, J. K. Stille, *J. Am. Chem. Soc.*, 1980, **102**, 4933.
- ¹³ J. M. Brown, N. A. Cooley, *Chem. Rev.*, 1988, **88**, 1031.
- ¹⁴ J. F. Hartwig, *Inorg. Chem.*, 2007, **46**, 1936.
- ¹⁵ A. F. Littke, C. Dai, G. C. Fu, *J. Am. Chem. Soc.*, 2000, **122**, 4020.
- ¹⁶ P. W. Dyer, J. Fawcett, M. J. Hanton, *J. Organomet. Chem.*, 2005, **690**, 5264.
- ¹⁷ D. Enwright, S. Gambarotta, G. P. A. Yap, P. H. M. Budzelaar, *Angew. Chem. Int. Ed.*, 2002, **41**, 3873.
- ¹⁸ S. C. Bart, K. Chłopek, E. Bill, M. W. Bouwkamp, E. Lobkovsky, F. Neese, K. Wieghardt, P. J. Chirik, *J. Am. Chem. Soc.*, 2006, **128**, 13901.
- ¹⁹ C. C. Lu, E. Bill, T. Weyhermüller, E. Bothe, K. Wieghardt, *J. Am. Chem. Soc.*, 2008, **130**, 3181.
- ²⁰ F. H. Allen, *Acta Cryst.*, 2002, **B58**, 380. Date: October 2009.
- ²¹ E. G. Mednikov, N. K. Eremenko, Y. L. Slovokhotov, Y. T. Struchkov, *Chem. Commun.*, 1987, 218.
- ²² K. Tani, S. Nakamura, T. Yamagata, Y. Kataoka, *Inorg. Chem.*, 1993, **32**, 5398.
- ²³ P. Lord, M. M. Olmstead, A. L. Balch, *Angew. Chem. Int. Ed.*, 1999, **38**, 18.
- ²⁴ F. A. Cotton, J. Gu, C. A. Murillo, D. J. Timmons, *J. Am. Chem. Soc.*, 1998, **120**, 13280.
- ²⁵ M. T. Reetz, E. Bohras, R. Goddard, M. C. Holthausen, W. Thiel, *Chem. Eur. J.*, 1999, **5**, 2101.
- ²⁶ R. Trebbe, R. Goddard, A. Ruffin, K. Seevogel, K.-R. Pörschke, *Organometallics*, 1999, **18**, 2466.
- ²⁷ EHT calculations were performed using the CACAO programme: C. Mealli, D. H. Proserpio, *J. Chem. Educ.*, 1990, **67**, 399.
- ²⁸ E. A. V. Ebsworth, D. W. H. Rankin, S. Craddock, "Structural Methods in Inorganic Chemistry", Blackwell Scientific Publications, Oxford, 1987, p. 105 - 124.
- ²⁹ I. P. Beletskaya, A. V. Cheprakov, *Chem Rev.*, 2000, **100**, 3012.
- ³⁰ F. Barrios-Landeros, J. F. Hartwig, *J. Am. Chem. Soc.*, 2005, **127**, 6944.
- ³¹ R. H. Crabtree, "The Organometallic Chemistry of the Transition Metals", 4th ed., Wiley-Interscience, New York, 2005, p 160 - 161.
- ³² D. F. Shriver, P. W. Atkins, 'Inorganic Chemistry', 3rd ed., Oxford University Press, Oxford, 1999, p. 167.
- ³³ P. J. Perez, J. C. Calabrese, E. E. Bunel, *Organometallics*, 2001, **20**, 337.
- ³⁴ A. W. Verstuyft, D. A. Redfield, L. W. Cary, J. H. Nelson, *Inorg. Chem.*, 1976, **15**, 1128.
- ³⁵ J. P. Stambuli, M. Bühl, J. F. Hartwig, *J. Am. Chem. Soc.*, 2002, **124**, 9346.
- ³⁶ U. Christmann, R. Vilar, *Angew. Chem. Int. Ed.*, 2005, **44**, 366.

Chapter VII

7. Experimental procedures and preparations

7.1. General Considerations

All operations were conducted under an atmosphere of dry nitrogen using standard Schlenk and cannula techniques, or in a nitrogen-filled glove box (Saffron Scientific), unless stated otherwise. All NMR-scale reactions were conducted using NMR tubes fitted with Young's tap valves. Bulk solvents were purified using an Innovative Technologies SPS facility and degassed prior to use. NMR solvents (CDCl_3 , C_6D_6 , CD_2Cl_2 , $\text{C}_6\text{D}_5\text{CD}_3$, $\text{C}_2\text{D}_2\text{Cl}_4$, THF-d_8) were dried over P_2O_5 or CaH_2 , distilled and degassed prior to use. 1,2-Dimethoxyethane (DME) and 1,4-dioxane were distilled from sodium/benzophenone under nitrogen. The following compounds were prepared according to literature procedures; (anthracenyl) PPh_2 ,¹ $[\text{VCl}_2(\text{py})_4]$,² $[\text{Rh}(\text{CO})_2\text{Cl}]$,³ $[\text{PdCl}_2(\text{MeCN})_2]$,⁴ $[\text{PdCl}_2(\text{TMEDA})]$,⁵ $[\text{PdMe}_2(\text{TMEDA})]$,⁵ $[\text{Ni}(\text{acac})_2(\text{TMEDA})]$,⁶ $[\text{MgMe}_2(\text{TMEDA})]$,⁷ diphenylphosphino(phenyl pyridin-2-yl methylene)amine abbreviated to **2IP-PPh₂**,⁸ $[(^i\text{Pr}_2\text{N})_2\text{P}][\text{OTf}]$,⁹ 2,6-bis[1-(2,6-diisopropylphenylimino)ethyl]pyridine,¹⁰ $(\text{MeNC}_2\text{H}_4\text{NMe})\text{PCl}$,¹¹ bis(*N*-*p*-methoxyphenyl)ethane-1,2-diimine,¹² anthracenyl lithium,¹ 2-pyridyl lithium,¹³ $[(\text{CH}_2\text{CH}_2\text{C}(\text{O})\text{O})\text{Ni}(\text{TMEDA})]$,¹⁴ $[(\text{CH}_2\text{CH}_2\text{C}(\text{O})\text{O})\text{Ni}(\text{py})_2]$,¹⁵ $[(\text{MeCN})_4\text{Pd}(\text{BF}_4)_2]$,¹⁶ picolyl lithium,¹⁷ 2,6-bis[(di-*t*-butylphosphino)methyl]pyridine,¹⁸ $(i\text{-Pr}_2\text{N})_2\text{PH}$,¹⁹ ferrocenium triflate²⁰ and $(i\text{-Pr}_2\text{N})_2\text{PCl}$.²¹

Routine solution phase NMR spectra were collected on a Varian Mercury 400 or 200, a Varian Inova 500, a Varian VNMRs-700 and a Bruker Avance 400 at ambient probe temperatures (~290 K) unless stated otherwise. Chemical shifts were referenced to residual protio impurities in the deuterated solvent (^1H), ^{13}C shift of the solvent (^{13}C), or to external aqueous 85% H_3PO_4 (^{31}P). Solvent proton shifts (ppm): CDCl_3 , 7.26 (s); C_6D_6 , 7.15 (s), CD_2Cl_2 5.32 (t), $\text{C}_6\text{D}_5\text{CD}_3$, 2.09 (quin) 6.98 (quin) 7.00 (s) 7.09 (m), THF-d_8 1.73 (s) 3.58 (s). Solvent carbon shifts (ppm): CDCl_3 , 77.36 (t); C_6D_6 , 128.62 (t); CD_2Cl_2 ,

54.00 (quin), C₆D₅CD₃ 20.4 (sept) 125.5 (t) 128.3 (t) 129.2 (t) 137.9 (s), THF-d₈ 25.5 (quin) 67.7 (quin).²² ¹H NMR and ¹³C NMR spectra were assigned with the aid of COSY, NOESY, DEPT 135, HMBC and HMQC. Solid-state NMR spectra were collected by the EPSRC National Solid-state NMR Research Service on a Varian 400 VNMRS; chemical shifts were referenced to H₃PO₄ (³¹P). Chemical shifts are reported in ppm and coupling constants in Hz.

Mass spectra were recorded by the EPSRC National Mass Spectrometry Service at the University of Wales, Swansea, (EI: Finnigan MAT 95XP, ESI: Waters ZQ-4000, nano-ESI: Waters ZQ-4000, LTQ Orbitrap XL, FAB: Finnigan MAT 95XP) and are reported in (*m/z*). The isotope distributions for all parent ion peaks were verified *via* comparison with the theoretical isotope pattern. Elemental analyses were performed by The Analytical Services Department of the Chemistry Department, Durham University. Infra-Red spectra were recorded on a Perkin Elmer Spectrum 100 FTIR and UV/vis on an ATI Unicam 2 instrument.

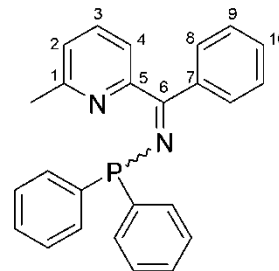
EPR spectra were obtained by the EPSRC National EPR Service at the University of Manchester, Manchester: X-band EPR spectra were acquired on a Bruker EMX-Micro equipped with a rectangular resonator (Bruker EMX High Sensitivity Probehead) operating at a frequency of approximately 9.4 GHz. A nitrogen gas flow quartz insert allowed variable temperature studies (93 K - 373 K). S-band (~3.4 GHz), K-band (24 GHz) and Q-band (34 GHz) EPR spectra were recorded on a Bruker Eleksys E500 spectrometer with the appropriate Bruker microwave bridges and dielectric resonators ER-4118-SPT-NI, ER-6706-KT and ER-5106-QT, respectively. All EPR spectra were found to be independent of temperature. Simulations were carried out using WinEPR SimFonia, with all *g*-values being corrected to strong pitch.

Cyclic voltammograms were recorded from solutions of approximately 10⁻⁴ M in analyte in dichloromethane containing 10⁻¹ M [NBu₄][BF₄] (recrystallized twice from absolute ethanol and dried overnight under vacuum at 80 °C before use) at μ = 100 mV s⁻¹ in a gas-tight single-compartment three-electrode cell equipped with glassy carbon disk working (apparent surface area of 0.42 mm²), coiled platinum wire auxiliary, and

platinum wire pseudo-reference electrodes. All redox potentials are reported against the SCE scale, with either the decamethylferrocene/decamethylferrocenium ($\text{Fc}^*/\text{Fc}^{*+}$; -0.08 V vs SCE) or ferrocene/ferrocenium (Fc/Fc^+ ; $+0.45$ V vs SCE) redox couples used as the internal reference systems.^{23,24} Data were collected using a computer-interfaced EcoChemie PGSTAT-30 potentiostat. Spectroelectrochemical experiments at room temperature were performed with an airtight optically transparent thin-layer electrochemical (OTTLE) cell equipped with a Pt mini-grid working electrode (32 wires cm^{-1}) and CaF_2 windows.^{25,26} The cell was positioned in the sample compartment of a ATI Unicam 2 spectrophotometer. The controlled-potential electrolyses were carried out with a potentiostat constructed in-house.

7.2. N-phosphino-pyridyl imines

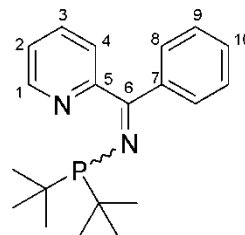
Diphenylphosphino(phenyl *ortho*-methylpyridin-2-yl methylene)amine: **1o**



To a stirred, cooled (-78 °C) solution of dried 2-cyano-6-methylpyridine (451 mg, 3.81 mmol) in diethyl ether (30 mL) was added dropwise phenyllithium (1.8 M in dibutylether, 2.12 mL, 3.81 mmol). The solution stirred for 1 h and allowed to warm to room temperature giving a red solution above a brick red precipitate. The solution was cooled (-78 °C) and dropwise addition of an ethereal solution (10 mL) of Ph₂PCl (0.68 mL, 3.81 mmol) gave a bright orange solution. The mixture stirred for 1 h before warming to room temperature and subsequently stirred for 14 h resulting in a brown solution above a white precipitate. The solution was isolated by filtration and reduced to solid *in vacuo*, before a solution of hexane/ether (33 %: 67 %) added to dissolve the desired product. The hexane/ether soluble fraction was isolated by filtration, reduced *in vacuo* and left to dry for 24 h *in vacuo* to remove traces off dibutylether. An orange oily residue was obtained (609 mg, 42 %).

¹H NMR (499.77 MHz, CDCl₃) δ: 2.44 (3H, s, CH₃), 7.01 (1H, d, ³J_{HH} = 8, C²H), 7.17 (1H, d, ³J_{HH} = 7.5, C⁴H), 7.22 - 7.30 (5H, m, aromatic protons), 7.40 - 7.58 (9H, m, aromatic protons and C³H), 7.77 (2H, d, ³J_{HH} = 7.5, C⁸H). ¹³C {¹H} NMR (125.67 MHz, CDCl₃) δ: 24.6 (s, CH₃), 120.6 (d, ⁴J_{PC} = 1.9, C⁴), 123.2 (s, C²), 128.3 (s, C⁹), 128.4 (d, ²J_{PC} = 8.2, {*o*-C₆H₅})₂P), 128.6 (s, {*p*-C₆H₅})₂P), 129.2 (d, ⁴J_{PC} = 1.9, C⁸), 130.7 (s, C¹⁰), 132.2 (d, ³J_{PC} = 2.0, {*m*-C₆H₅})₂P), 136.6 (s, C³), 139.7 (d, ¹J_{PC} = 5.8, {*i*-C₆H₅})₂P), 142.3 (d, ³J_{PC} = 5.6, C⁷), 156.5 (d, ³J_{PC} = 5.3, C⁵), 158.3 (s, C¹), 171.4 (d, ²J_{PC} = 5.8, C⁶). ³¹P {¹H} NMR (161.91 MHz, CDCl₃) δ: + 38.4 (s). MS (ESI+) m/z: 381.3 (M-H)⁺.

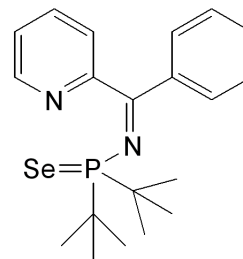
Ditertiarybutylphosphino(phenyl pyridin-2-yl methylene)amine: 2o



To a stirred, cooled (-78 °C) solution of dried 2-cyanopyridine (500 mg, 4.8 mmol) in dimethoxyethane (40 mL) was added dropwise phenyllithium (1.8 M in dibutylether, 2.66 mL, 4.8 mmol) and stirred for 1 h, giving a dark red solution. A solution of t-Bu₂PtCl (870 mg, 4.8 mmol) in dimethoxyethane (10 mL) was added slowly by cannula. The mixture was allowed to warm to room temperature and stirred for 22 h. Volatile components were removed under reduced pressure, hexane (200 mL) added and the resulting solution filtered. The filtrate was evaporated under reduced pressure to leave an orange solid, which was dried *in vacuo* (920 mg, 70 %).

¹H NMR (499.77 MHz, C₆D₆) δ: 1.24 (18H, d, ³J_{PH} = 11.0, CH₃), 6.64 (1H, dd, ³J_{HH} = 7.6 ³J_{HH} = 4.8, C²H), 7.10 - 7.20 (4H, m, C⁹H, C¹⁰H and C³H), 7.41 (1H, d, J_{HH} = 7.8, C⁴H), 7.84 (2H, d, ³J_{HH} = 6.5, C⁸H), 8.47 (1H, d, J_{HH} = 4.8, C¹H). ¹³C {¹H} NMR (125.67 MHz, C₆D₆) δ: 29.2 (d, ²J_{PC} = 14.8, CH₃), 35.2 (d, ¹J_{PC} = 23.0, CCH₃), 123.7 (s, C²), 124.3 (d, ⁴J_{PC} = 2.8, C⁴), 128.7 (s, C⁹), 130.1 (s, C⁸), 130.7 (s, C¹⁰), 135.9 (s, C³), 140.6 (d, ³J_{PC} = 6.3, C⁷), 149.7 (s, C¹), 159.2 (d, ³J_{PC} = 7.2, C⁵), 177.4 (d, ²J_{PC} = 17.6, C⁶). ³¹P {¹H} NMR (161.91 MHz, C₆D₆) δ: + 81.2 (s). MS (FAB⁺) m/z: 327.3 (M-H)⁺. *Anal.* Found: C, 73.51 H, 8.24; N 8.44 %, Calc. C, 73.59; H, 8.34; N, 8.58 %.

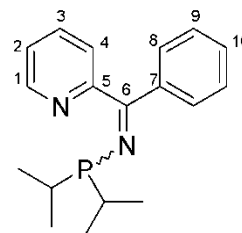
Ditertiarybutylphosphino selenide (phenyl pyridin-2-yl methylene)amine: **2o.Se**



A Young's tap NMR tube was charged with selenium (19 mg, 0.236 mmol) under an inert atmosphere and the tube sealed and transferred to a Schlenk line. A solution of **2o** (50 mg, 0.1534 mmol) in 1 mL of CDCl₃ was added and the tube was allowed to stand for 1 h.

³¹P {¹H} NMR (161.91 MHz, CDCl₃) δ : + 91.5 (s + satellites, ¹J_{SeP} = 746).

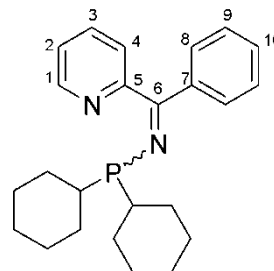
Diisopropylphosphino(phenyl pyridin-2-yl methylene)amine: **3o**



To a stirred, cooled (-78 °C) solution of 2-cyanopyridine (0.417 mg, 4.00 mmol) in diethyl ether (30 mL) was added dropwise phenyllithium (1.8 M in dibutylether, 2.22 mL, 4.00 mmol) and the mixture stirred for 4 h, to give a red solution. An ethereal solution (15 mL) of i-Pr₂PCl (0.64 mL, 4.00 mmol) was added dropwise and allowed to stir for 1 h before warming to room temperature. The solution was removed by filtration, reduced to dryness *in vacuo* and hexane added (50 mL). The resultant solution was filtered and volatile components removed under reduced pressure to give an oily orange-red residue (385 mg, 32 %).

^1H NMR (499.80 MHz, CDCl_3) δ : 1.01 (6H, dd, $^3J_{\text{HH}} = 7.5$ $^3J_{\text{PH}} = 14.5$, CH_3), 1.11 (6H, dd, $^3J_{\text{HH}} = 7.2$ $^3J_{\text{PH}} = 11.3$, CH_3'), 1.92 (2H, septet, $^3J_{\text{HH}} = 7.0$, CH), 7.29 (1H, ddd, $^3J_{\text{HH}} = 7.5$ $^3J_{\text{HH}} = 5.0$ $^4J_{\text{HH}} = 1.0$, C^2H), 7.35 - 7.40 (3H, m, $\text{C}^9\text{H} + \text{C}^{10}\text{H}$), 7.55 (2H, dd, $^3J_{\text{HH}} = 8.0$ $^4J_{\text{HH}} = 1.5$, C^8H), 7.64 (1H, d, $^3J_{\text{HH}} = 8.0$, C^4H), 7.75 (1H, td, $^3J_{\text{HH}} = 7.5$, $^4J_{\text{HH}} = 2.0$, C^3H), 8.65 (1H, d, $^3J_{\text{HH}} = 4.5$, C^1H). ^1H $\{^{31}\text{P}\}$ NMR (499.77 MHz, CDCl_3) δ : 1.01 (6H, d, $^3J_{\text{HH}} = 7.0$, CH_3), 1.11 (6H, d, $^3J_{\text{HH}} = 7.5$, CH_3'), 1.92 (2H, septet, $^3J_{\text{HH}} = 7.0$, CH), 7.29 (1H, ddd, $^3J_{\text{HH}} = 7.5$ $^3J_{\text{HH}} = 5.0$ $^4J_{\text{HH}} = 1.0$, C^2H), 7.35 - 7.40 (3H, m, $\text{C}^9\text{H} + \text{C}^{10}\text{H}$), 7.55 (2H, dd, $^3J_{\text{HH}} = 8.0$ $^4J_{\text{HH}} = 1.5$, C^8H), 7.64 (1H, d, $^3J_{\text{HH}} = 8.0$, C^4H), 7.75 (1H, td, $^3J_{\text{HH}} = 7.5$, $^4J_{\text{HH}} = 2.0$, C^3H), 8.65 (1H, d, $^3J_{\text{HH}} = 4.5$, C^1H). ^{13}C $\{^1\text{H}\}$ NMR (125.67 MHz, CDCl_3) δ : 18.6 (d, $^2J_{\text{PC}} = 9.0$, CH_3), 18.9 (d, $^2J_{\text{PC}} = 17.7$, CH_3'), 27.4 (d, $^1J_{\text{PC}} = 12.4$, CH), 123.7 (d, $^4J_{\text{PC}} = 2.5$, C^4), 123.9 (s, C^2), 128.3 (s, C^9), 128.9 (d, $^4J_{\text{PC}} = 1.5$, C^8), 130.2 (s, C^{10}), 136.3 (s, C^3), 139.7 (d, $^3J_{\text{PC}} = 6.2$, C^7), 149.3 (s, C^1), 158.0 (d, $^3J_{\text{PC}} = 6.7$, C^5), 175.1 (d, $^2J_{\text{PC}} = 12.0$, C^6). ^{31}P $\{^1\text{H}\}$ NMR (80.96 MHz, CDCl_3) δ : + 68.9 (s). MS (ESI+) m/z : 317.3 $\{\text{M}-(\text{OH}_2)\text{H}\}^+$.

Dicyclohexylphosphino(phenyl pyridin-2-yl methylene)amine: 4o

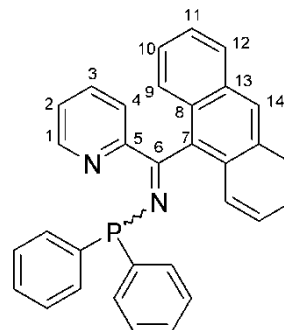


To a stirred, cooled ($-78\text{ }^\circ\text{C}$) solution of 2-cyanopyridine (0.417 mg, 4.00 mmol) in diethyl ether (30 mL) was added dropwise phenyllithium (1.8 M in dibutylether, 1.33 mL, 2.39 mmol) and the mixture stirred for 4 h to give a red solution. An ethereal solution (15 mL) of Cy_2PCI (556 mg, 2.25 mmol) was added slowly, stirred for 16 h, warmed to room temperature and filtered. The resultant solution was evaporated under reduced pressure and the desired product dissolved in hexane (50 mL). This solution was filtered, the volatile components removed under reduced pressure and oily-red residue dried *in vacuo*, (355 mg, 39 %). This residue was found to be only approximately 90 % pure.

Attempts to purify further were unsuccessful and therefore the impure material was used in further syntheses.

^{31}P { ^1H } NMR (161.91 MHz, CDCl_3) δ : + 63.4 (s).

Diphenylphosphino (anthracenyl pyridin-2-yl methylene)amine: 5o

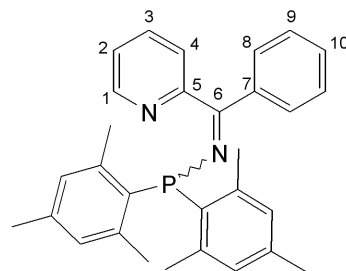


9-Bromoanthracene (1.60 g, 94% purity, 5.84 mmol) was dissolved in ether (40 mL) and slowly added to *n*-BuLi (1.6 M in hexanes, 3.65 mL, 5.84 mmol) at $-30\text{ }^{\circ}\text{C}$ producing an ethereal suspension of anthracenyllithium.¹ The suspension was subsequently added by cannula to a stirred, cooled ($-78\text{ }^{\circ}\text{C}$) solution of 2-cyanopyridine (607 mg, 5.84 mmol) in diethyl ether (80 mL) and allowed to stir for 1 h before warming to room temperature. The solution was cooled ($-78\text{ }^{\circ}\text{C}$) and Ph_2PCL (1.05 mL, 5.84 mmol) in ether (30 mL) added dropwise with vigorous stirring. The mixture was allowed to warm to room temperature, stirred for 4 d, filtered and the resultant solution evaporated under reduced pressure. The desired product was extracted by addition of CH_2Cl_2 to give a solution that was isolated by filtration. The addition of hexane and cooling ($-30\text{ }^{\circ}\text{C}$) gave a bright yellow solid (1.10 g, 41 %).

^1H NMR (499.77 MHz, CDCl_3) δ : 6.94 - 6.99 (Ph-*H*), 7.00 - 7.05 (Ph-*H*), 7.06 - 7.11 (Ph-*H*), 7.26 - 7.31 (3H, m, $\text{C}^2\text{H} + \text{C}^{10}\text{H}$), 7.38 - 7.43 (2H, t, $J_{\text{HH}} = 1.7$, C^{11}H), 7.60 (2H, d, $J_{\text{HH}} = 8.9$, C^9H), 7.87 (1H, td, $J_{\text{HH}} = 7.9$, $J_{\text{HH}} = 1.7$, C^3H), 7.94 (2H, d, $J_{\text{HH}} = 8.9$, C^{12}H), 8.33 (1H, s, C^{14}H), 8.48 (1H, d, $J_{\text{HH}} = 5.0$, C^1H), 8.52 (1H, d, $J_{\text{HH}} = 8.3$, C^4H). ^{13}C { ^1H } NMR (125.67 MHz, CDCl_3) δ : 122.4 (s, aromatic carbon), 124.8 (s, aromatic carbon), 125.3 (s, aromatic carbon), 126.1 (s, aromatic carbon), 126.2 (s, aromatic carbon), 127.9 (d, $^3J_{\text{PC}} = 7.3$, {m-

$C_6H_5\}_2P)$, 127.9 (s, aromatic carbon), 128.2 (d, $^4J_{PC} = 2.1$, C^8), 128.4 (s, aromatic carbon), 128.8 (s, aromatic carbon), 131.3 (s, C^{13}), 132.3 (d, $^2J_{PC} = 20.9$, $\{o-C_6H_5\}_2P)$, 134.9 (d, $^3J_{PC} = 6.2$, C^7), 136.8 (s, C^3), 139.2 (d, $^1J_{PC} = 10.2$, $\{i-C_6H_5\}_2P)$, 149.8 (s, C^1), 158.0 (d, $^3J_{PC} = 8.6$, C^5), 172.0 (d, $^2J_{PC} = 6.4$, C^6). $^{31}P \{^1H\}$ NMR (161.91 MHz, $CDCl_3$) δ : + 39.8 (s).

Dimesitylphosphino(phenyl pyridin-2-yl methylene)amine: 6o

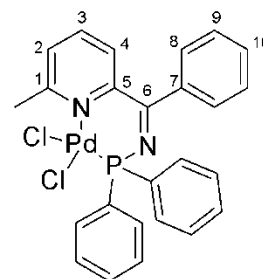


To a stirred, cooled ($-78\text{ }^{\circ}C$) solution of dried 2-cyanopyridine (0.500 mg, 4.80 mmol) in diethyl ether (30 mL) was added dropwise phenyllithium (1.8 M, dibutylether, 2.67 mL, 4.80 mmol) and the mixture stirred for 4 h. An ethereal solution (15 mL) of Mes_2PCl (1625 mg, 90 % purity, 4.80 mmol) was added dropwise, stirred for 1 h, warmed to room temperature and the volatile components removed under reduced pressure. Extraction of the residue with hexane (30 mL) by filtration and subsequent washings (2 x 15 mL) gave an orange solution. Concentration and cooling of the solution gave a yellow precipitate, which was isolated by filtration and dried *in vacuo*. (1.256 mg, 58 %).

1H NMR (400.13 MHz, $CDCl_3$) δ : 2.19 (6H, s, $C^{12}CH_3$), 2.20 (12H, s, $C^{14}CH_3$), 6.66 (4H, d, $^3J_{PH} = 3.1$, $C^{13}H$), 7.10 (1H, ddd, $^3J_{HH} = 7.5$, $J = 4.7$, $^4J_{HH} = 1.1$, C^2H), 7.21 - 7.38 (6H, m, $C^4H + C^8H + C^9H + C^{10}H$), 7.52 (1H, td, $^3J_{HH} = 7.6$, $^4J_{HH} = 1.8$, C^3H), 8.44 (1H, ddd, $J = 4.9$, $^4J_{HH} = 1.8$, $^4J_{HH} = 1.0$, C^1H). $^{13}C \{^1H\}$ NMR (125.67 MHz, $CDCl_3$) δ : 21.2 (s, $C^{14}CH_3$), 23.4 (d, $^3J_{PC} = 13.2$, $C^{12}CH_3$), 122.5 (d, $J = 2.7$, C^4), 123.2 (s, C^2), 128.1 (d, $J = 2.9$, C^{13}), 128.2 (s, C^9 or C^{10}), 129.4 (s, C^9 or C^{10}), 129.9 (d, $^4J_{PC} = 2.9$, C^8), 134.5 (d, $^1J_{PC} = 18.5$, C^{11}), 135.9 (s, C^3), 138.2 (s, C^{14}), 139.7 (d, $^3J_{PC} = 6.6$, C^7), 142.1 (d, $^2J_{PC} = 15.2$, C^{12}), 149.4 (s, C^1), 157.7 (d, $^3J_{PC} = 6.8$, C^5), 167.1 (d, $^2J_{PC} = 11.6$, C^6). $^{31}P \{^1H\}$ NMR (161.91 MHz, $CDCl_3$) δ : + 33.3.

7.3. Palladium dichloride complexes of *N*-phosphino-pyridyl imines

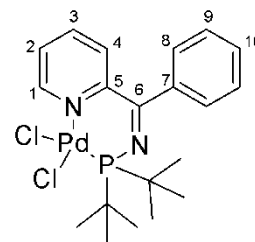
Diphenylphosphino(phenyl *ortho*-methylpyridin-2-yl methylene)amine palladium dichloride: **7**



To a stirred solution of $[\text{PdCl}_2(\text{MeCN})_2]$ (138 mg, 0.530 mmol) in CH_2Cl_2 (10 mL) was added **1o** (201 mg, 0.530 mmol) in CH_2Cl_2 (10 mL) dropwise via cannula. The resultant solution was left to stir for one hour and the solvent subsequently removed under reduced pressure. The solid was washed with hexane (2 x 10 mL) and diethyl ether (1 x 5 mL) and dried *in vacuo* to leave a bright-yellow solid (204 mg, 69 %). Yellow crystals suitable for an X-ray structure determination were grown by cooling (-30°C) a saturated deuterio-chloroform solution for 3 d.

^1H NMR (699.74 MHz, CDCl_3) δ : 3.63 (3H, s, CH_3), 7.28-7.33 (3H, m, aromatic protons), 7.37 - 7.46 (4H, m, aromatic protons), 7.48 - 7.53 (1H, m, aromatic proton), 7.57 (2H, t, $^3J_{\text{HH}} = 7.7$, C^9H), 7.60 - 7.67 (3H, m, aromatic protons), 7.71 (1H, t, $^3J_{\text{HH}} = 7.7$, C^{10}H), 7.75 (2H, dd, $J = 7.7$ $J = 13.3$, aromatic protons), 7.95 (2H, d, $^3J_{\text{HH}} = 7.0$, C^8H). ^{13}C $\{^1\text{H}\}$ NMR (175.95 MHz, CDCl_3) δ : 30.4 (s, CH_3), 125.8 (s, C^4), 128.6 (d, $J = 13.1$, aromatic carbon), 129.3 (s, C^9), 129.4 (s, aromatic carbon), 130.7 (s, C^8), 130.8 (s, C^2), 131.5 (d, $J = 12.0$, aromatic carbon), 132.2 (s, aromatic carbon), 132.9 (s, aromatic carbon), 132.9 (d, $J = 11.0$, aromatic carbon), 134.1 (s, C^{10}), 137.5 (d, $^3J_{\text{PC}} = 19.2$, C^7), 139.4 (s, C^3), 148.2 (d, $^3J_{\text{PC}} = 19.4$, C^5), 166.1 (s, C^1), 181.9 (d, $^2J_{\text{PC}} = 21.7$, C^6). ^{31}P $\{^1\text{H}\}$ NMR (161.91 MHz, CDCl_3) δ : + 67.0 (s). *Anal.* Found: C, 53.89; H, 3.83; N, 4.98 %. Calc. C, 53.84; H, 3.80; N, 5.02 %.

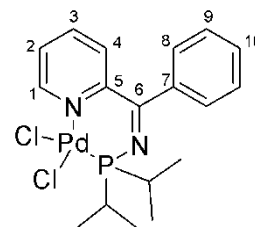
Ditertiarybutylphosphino(phenyl pyridin-2-yl methylene)amine palladium dichloride: 8



To a stirred solution of $[\text{PdCl}_2(\text{MeCN})_2]$ (159 mg, 0.613 mmol) in CH_2Cl_2 (10 mL) was added **2o** (200 mg, 0.613 mmol) in CH_2Cl_2 (10 mL) dropwise via cannula. The resultant solution was left to stir for 1 h and the solvent subsequently removed under reduced pressure. The solid was washed with hexane (2 x 10 mL) and diethyl ether (1 x 5 mL) and dried *in vacuo* to leave a grey-yellow solid (190 mg, 62 %).

^1H NMR (399.96 MHz, CDCl_3) δ : 1.45 (18H, d, $^3J_{\text{PH}} = 7.8$, CH_3), 7.55 (2H, t, $^3J_{\text{HH}} = 7.6$, C^9H), 6.63 - 7.73 (5H, m, C^2H , C^4H , C^8H and C^{10}H), 8.00 (1H, td, $^3J_{\text{HH}} = 6.8$ $^4J_{\text{HH}} = 1.6$, C^3H), 10.48 (1H, d, $^3J_{\text{HH}} = 3.2$, C^1H). ^{13}C $\{^1\text{H}\}$ NMR (125.67 MHz, CDCl_3) δ : 29.6 (d, $^2J_{\text{PC}} = 2.9$, CH_3), 43.2 (d, $^1J_{\text{PC}} = 25.0$, CCH_3), 128.6 (s, C^2 , C^4 , C^8 or C^{10}), 128.8 (s, C^2 , C^4 , C^8 or C^{10}), 129.3 (s, C^9), 130.2 (s, C^2 , C^4 , C^8 or C^{10}), 133.2 (s, C^2 , C^4 , C^8 or C^{10}), 138.1 (d, $^3J_{\text{PC}} = 14.8$, C^7), 140.1 (s, C^3), 141.5 (d, $^3J_{\text{PC}} = 14.5$, C^5), 158.9 (s, C^1), 179.4 (d, $^2J_{\text{PC}} = 9.2$, C^6). ^{31}P $\{^1\text{H}\}$ NMR (161.91 MHz, CDCl_3) δ : + 109.6 (s). *Anal.* Found: C, 47.88; H, 5.48; N, 5.51 %. Calc. C, 47.69; H, 5.40; N, 5.56 %.

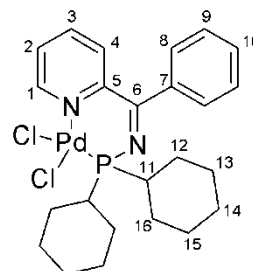
Diisopropylphosphino(phenyl pyridin-2-yl methylene)amine palladium dichloride: 9



To a stirred solution of $[\text{PdCl}_2(\text{MeCN})_2]$ (244 mg, 0.940 mmol) in CH_2Cl_2 (10 mL) was added **3o** (280 mg, 0.940 mmol) in CH_2Cl_2 (10 mL) dropwise via cannula. The resultant orange solution was left to stir for 1 h and the solvent subsequently evaporated to 4 mL under reduced pressure. Hexane (10 mL) was added and the resultant solid isolated by filtration. The solid was washed with hexane (1 x 10 mL) and diethyl ether (2 x 10 mL) and dried *in vacuo* to leave a yellow solid (350 mg, 78 %).

^1H NMR (499.80 MHz, CDCl_3) δ : 0.92 (6H, dd, $^3J_{\text{HH}} = 7.0$ $^3J_{\text{PH}} = 16.5$, CH_3), 1.37 (6H, dd, $^3J_{\text{HH}} = 7.0$ $^3J_{\text{PH}} = 19.0$, CH_3'), 2.70 (2H, m, CH), 7.51 (2H, t, $^3J_{\text{HH}} = 8.0$, C^9H), 7.63 (1H, t, $^3J_{\text{HH}} = 7.5$, C^{10}H), 7.67-7.73 (4H, m, C^2H C^4H and C^8H), 8.08 (1H, td, $^3J_{\text{HH}} = 8.0$ $^4J_{\text{HH}} = 1.5$, C^3H), 10.32 (1H, d, $^3J_{\text{HH}} = 6.0$, C^1H). ^1H $\{^{31}\text{P}\}$ NMR (499.77 MHz, CDCl_3) δ : 0.92 (6H, d, $^3J_{\text{HH}} = 7.0$, CH_3), 1.37 (6H, d, $^3J_{\text{HH}} = 7.0$, CH_3'), 2.70 (2H, septet, $^3J_{\text{HH}} = 7.0$, CH), 7.51 (2H, t, $^3J_{\text{HH}} = 8.0$, C^9H), 7.63 (1H, t, $^3J_{\text{HH}} = 7.5$, C^{10}H), 7.67-7.73 (4H, m, C^2H C^4H and C^8H), 8.08 (1H, t, $^3J_{\text{HH}} = 8.0$, C^3H), 10.32 (1H, d, $^3J_{\text{HH}} = 6.0$, C^1H). ^{13}C $\{^1\text{H}\}$ NMR (125.67 MHz, CDCl_3) δ : 16.7 (d, $^2J_{\text{PC}} = 3.3$, CH_3), 17.7 (d, $^2J_{\text{PC}} = 1.1$, CH_3'), 27.4 (d, $^1J_{\text{PC}} = 36.4$, CH) 128.8 (s, C^2 , C^4 or C^9), 128.9 (s, C^2 , C^4 or C^9), 129.1 (s, C^2 , C^4 or C^9), 130.2 (s, C^8), 133.3 (s, C^{10}), 137.5 (d, $^3J_{\text{PC}} = 16.2$, C^7), 140.4 (s, C^3), 142.8 (d, $^3J_{\text{PC}} = 16.7$, C^5), 158.3 (s, C^1), 180.8 (d, $^2J_{\text{PC}} = 8.0$, C^6). ^{31}P $\{^1\text{H}\}$ NMR (161.91 MHz, CDCl_3) δ : + 105.4 (s). *Anal.* Found: C, 45.61; H, 4.95; N, 5.79 %. Calc. C, 45.45; H, 4.87; N, 5.89 %.

Dicyclohexylphosphino(phenyl pyridin-2-yl methylene)amine palladium dichloride: 10

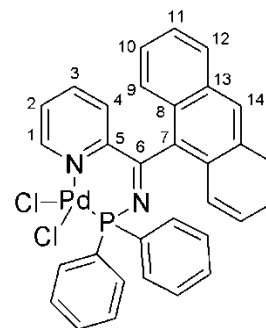


To a stirred solution of $[\text{PdCl}_2(\text{MeCN})_2]$ (124 mg, 0.476 mmol) in CH_2Cl_2 (10 mL) was added **4o** (200 mg, 0.476 mmol, ~90 % pure) in CH_2Cl_2 (10 mL) dropwise via cannula. The resultant solution was left to stir for 1 h and the solvent subsequently removed under reduced pressure. The solid was recrystallised from CH_2Cl_2 and hexane to give a light yellow crystalline solid (105 mg, 40 %). Crystals suitable for an X-ray structure determination were grown over a period of 3 d by layering a CH_2Cl_2 solution with hexane.

^1H NMR (499.77 MHz, CDCl_3) δ : 1.10-1.41 (10H, m, Cy-*H*), 1.49-1.69 (6H, m, Cy-*H*), 1.73-1.84 (2H, m, Cy-*H*), 2.22-2.31 (2H, m, Cy-*H*), 2.48-2.57 (2H, m, PCH), 7.54 (2H, t, $^3J_{\text{HH}} = 8.0$, C^9H), 6.63-7.72 (5H, m, aromatic protons), 8.00 (1H, td, $^3J_{\text{HH}} = 7.5$ $^4J_{\text{HH}} = 1.5$, C^3H), 10.40 (1H, dd, $^3J_{\text{HH}} = 6.0$ $^4J_{\text{HH}} = 1.0$, C^1H). ^{13}C $\{^1\text{H}\}$ NMR (125.67 MHz, CDCl_3) δ : 25.9 (d, $J_{\text{PC}} = 1.5$, Cy-C) 26.6 (d, $J_{\text{PC}} = 14.8$, Cy-C), 26.7 (d, $J_{\text{PC}} = 12.1$, Cy-C), 26.8 (d, $J_{\text{PC}} = 3.8$, Cy-C), 27.3 (s, C^{14}), 36.3 (d, $^1J_{\text{PC}} = 35.5$, C^{11}) 128.7 (s, C^2 , C^4 , C^8 or C^{10}), 128.7 (s, C^2 , C^4 , C^8 or C^{10}), 129.1 (s, C^9), 130.3 (s, C^8 or C^{10}), 133.2 (s, C^4 , C^8 or C^{10}), 37.7 (d, $^3J_{\text{PC}} = 16.3$, C^7), 140.0 (s, C^3), 142.7 (d, $^3J_{\text{PC}} = 17.0$, C^5), 158.6 (s, C^1), 180.2 (d, $^2J_{\text{PC}} = 8.4$, C^6). * ^{31}P $\{^1\text{H}\}$ NMR (161.91 MHz, CDCl_3) δ : + 98.3 (s). *Anal.* Found: C, 52.02; H, 5.64; N, 4.98 %. Calc. C, 51.86; H, 5.62; N, 5.04 %.

* Six carbon-13 signals are observed for the cyclohexyl groups which is proposed to be because of side-side inequivalence of the rings.

Diphenylphosphino (anthracenyl pyridin-2-yl methylene)amine palladium dichloride: 11

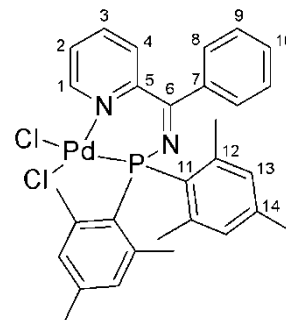


To a stirred solution of $[\text{PdCl}_2(\text{MeCN})_2]$ (223 mg, 0.86 mmol) in CH_2Cl_2 (10 mL) was added **5o** (400 mg, 0.86 mmol) in CH_2Cl_2 (10 mL) dropwise via cannula. An immediate colour change to dark red occurred and a bright orange solid precipitated as the solution stirred for 1 h. The solid was isolated by filtration, washed with CH_2Cl_2 and dried *in vacuo* to leave an orange solid (360 mg, 65 %). Orange crystals suitable for an X-ray structure determination were grown by cooling (- 30 °C) a saturated deuterio-chloroform solution.

^1H NMR (399.96 MHz, CDCl_3) δ : 7.22 (1H, d, $^3J_{\text{HH}} = 7.5$, C^4H), 7.39 - 7.48 (6H, m, aromatic protons), 7.49 - 7.56 (6H, m, aromatic protons), 7.59 - 7.69 (2H, m, aromatic protons), 7.84 - 7.92 (4H, m, aromatic protons), 8.11 (2H, d, $^3J_{\text{HH}} = 8.2$, An-H), 8.66 (1H, s, C^{13}H), 10.54 (1H, d, $^3J_{\text{HH}} = 8.2$, C^1H).[†] ^{31}P { ^1H } NMR (161.91 MHz, CDCl_3) δ : + 69.5 (s). *Anal.* Found: C, 59.89; H, 3.64; N, 4.40 %. Calc. C, 59.70; H, 3.60; N, 4.35 %.

[†] The compound was found to be insufficiently soluble for analysis by ^{13}C { ^1H } NMR spectroscopy

Dimesitylphosphino (phenyl pyridin-2-yl methylene)amine palladium dichloride: 12



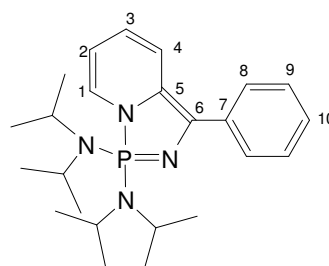
To a stirred solution of $[\text{PdCl}_2(\text{MeCN})_2]$ (232 mg, 0.895 mmol) in CH_2Cl_2 (20 mL) was added **6o** (403 mg, 0.895 mmol) in CH_2Cl_2 (10 mL) dropwise *via* cannula. The resultant brown solution was left to stir for 1 h and the solvent subsequently reduced (to approximately 5 mL) under reduced pressure. The solution was layered with hexane (5 mL) and the biphasic solution left to stand for two weeks. Yellow crystals formed and were isolated by filtration, washed twice with hexane and dried *in vacuo* to leave a yellow solid (390 mg, 62 %). Single crystals suitable for an X-ray diffraction study were grown over a period of 7 d from a CH_2Cl_2 solution of layered with hexane.

^1H NMR (400.13 MHz, CDCl_3) δ : 2.18 (6H, s, C^{14}CH_3), 2.59 (12H, broad signal, C^{12}CH_3), 6.73 (4H, s, C^{13}H), 7.23 (1H, dd, $^3J_{\text{HH}} = 7.7$, $^4J_{\text{HH}} = 0.9$, C^4H), 7.48 (2H, t, $^3J_{\text{HH}} = 7.3$, C^9H), 7.59 - 7.70 (4H, m, $\text{C}^8\text{H} + \text{C}^2\text{H} + \text{C}^{10}\text{H}$), 7.83 (1H, td, $^3J_{\text{HH}} = 7.8$, $^4J_{\text{HH}} = 4.5$, C^3H), 10.04 (1H, dd, $J_{\text{HH}} = 5.8$, $^4J_{\text{HH}} = 1.4$, C^1H). ^1H NMR (499.77 MHz, CDCl_3 , -60°C) δ : 1.70 (3H, s, methyl resonance), 2.08 (3H, s, methyl resonance), 2.18 (3H, s, methyl resonance), 2.24 (3H, s, methyl resonance), 2.80 (3H, s, methyl resonance), 3.50 (3H, s, methyl resonance), 6.61 (2H, s, C^{13}H and $\text{C}^{13}\text{H}'$), 6.71 (1H, s, $\text{C}^{13}\text{H}''$), 6.99 (1H, s, $\text{C}^{13}\text{H}'''$), 7.31 (1H, dd, $^3J_{\text{HH}} = 7.7$, $^4J_{\text{HH}} = 0.9$, C^4H), 7.49 (2H, t, $^3J_{\text{HH}} = 7.3$, C^9H), 7.59 - 7.70 (4H, m, $\text{C}^8\text{H} + \text{C}^2\text{H} + \text{C}^{10}\text{H}$), 7.90 (1H, td, $^3J_{\text{HH}} = 7.8$, $^4J_{\text{HH}} = 4.5$, C^3H), 9.96 (1H, dd, $J_{\text{HH}} = 5.8$, $^4J_{\text{HH}} = 1.4$, C^1H). ^{13}C $\{^1\text{H}\}$ NMR (125.67 MHz, CDCl_3) δ : 21.3 (s, C^{14}CH_3), 24.9 (s, C^{12}CH_3), 126.5 (s, C^4), 128.6 (s, C^2), 129.2 (s, C^9), 130.5 (s, aromatic carbon), 130.8 (broad, aromatic carbon), 133.4 (s, aromatic carbon), 137.0 (d, $^3J_{\text{PC}} = 18.6$, C^7), 140.0 (s, C^3), 142.2 (broad, aromatic carbon), 145.0 (d,

$^3J_{PC} = 20.2$, C^5), 156.7 (s, C^1), 174.5 (d, $^2J_{PC} = 4.9$, C^6).[‡] ^{31}P NMR (161.91 MHz, $CDCl_3$) δ : +58.9. *Anal.* Found: C, 57.51; H, 5.02; N, 4.28 %. Calc. C, 57.39; H, 4.98; N, 4.46 %.

7.4. Diazaphosphole synthesis and reactivity

1,1-Bis(diisopropylamino)-3-phenyl-1 λ^5 -[1,3,2]diazaphospholo[1,5- α]pyridine: 13c



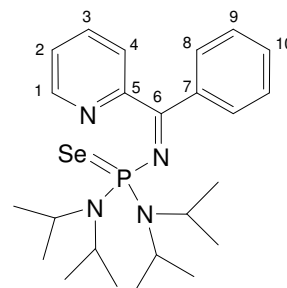
To a stirred, cooled (-78 °C) solution of dried 2-cyano-pyridine (1.00 g, 9.6 mmol) in dimethoxyethane (50 mL) was added dropwise phenyllithium (1.8 M in dibutylether, 5.34 mL, 9.6 mmol) and the mixture stirred for an hour, giving a dark red solution. A slurry of (i-Pr₂N)₂PCl (2.56 g, 9.6 mmol) in dimethoxyethane (70 mL) was added slowly by cannula. The mixture was allowed to warm to room temperature and stirred for 22 h. Volatile components were removed under reduced pressure, hexane (400 mL) added and the resulting solution filtered. On cooling the solution (-30 °C) red cuboidal crystals formed, which were isolated by filtration and dried *in vacuo*. Concentration of the filtrate to half its volume and further cooling (-30 °C) yielded an additional crop of crystals (2.33 g, 59 %). These crystals were found to be suitable for an X-ray structure determination.

1H NMR (699.74 MHz, C_6D_6) δ : 0.97 (12H, d, $^3J_{HH} = 6.4$, CH_3), 1.20 (12H, d, $^3J_{HH} = 6.4$, CH_3'), 3.30-3.45 (4H, m, $CHCH_3$), 5.22 (1H, t, $^3J_{HH} = 6.3$, C^2H), 5.32 (1H, dd, $^3J_{HH} = 10.5$ $^3J_{HH}$

[‡] Two carbons are not observed in the $^{13}C\{^1H\}$ NMR spectrum for this compound. This is assumed to be because the signals are highly broadened.

= 5.0, C^3H), 6.06 (1H, dd, $^3J_{HH} = 7.5$ $^3J_{PH} = 5.6$, C^1H), 7.05 (1H, t, $^3J_{HH} = 7.0$, $C^{10}H$), 7.14 (1H, d, $^3J_{HH} = 9.8$, C^4H), 7.29 (2H, t, $^3J_{HH} = 7.6$, C^9H), 8.01 (2H, d, $^3J_{HH} = 7.6$, C^8H). 1H $\{^{31}P\}$ NMR (499.77 MHz, C_6D_6) δ : 0.97 (12H, d, $^3J_{HH} = 6.4$, CH_3), 1.20 (12H, d, $^3J_{HH} = 6.4$, CH_3'), 3.38 (4H, septet, $^3J_{HH} = 6.5$, $CHCH_3$), 5.22 (1H, t, $^3J_{HH} = 6.3$, C^2H), 5.32 (1H, dd, $^3J_{HH} = 10.5$ $^3J_{HH} = 5.0$, C^3H), 6.06 (1H, d, $^3J_{HH} = 7.5$, C^1H), 7.05 (1H, t, $^3J_{HH} = 7.0$, $C^{10}H$), 7.14 (1H, d, $^3J_{HH} = 9.8$, C^4H), 7.29 (2H, t, $^3J_{HH} = 7.6$, C^9H), 8.01 (2H, d, $^3J_{HH} = 7.6$, C^8H). ^{13}C $\{^1H\}$ NMR (125.67 MHz, C_6D_6) δ : 22.9 (d, $^3J_{PC} = 1.3$, CH_3), 23.4 (d, $^3J_{PC} = 2.4$, CH_3'), 48.2 (d, $^2J_{PC} = 3.8$, $CHCH_3$), 107.3 (d, $^3J_{PC} = 5.8$, C^2), 112.9 (d, $^4J_{PC} = 1.3$, C^3), 123.1 (d, $^3J_{PC} = 34.1$, C^5), 123.2 (d, $^3J_{PC} = 9.2$, C^4), 125.2 (s, C^{10}), 126.5 (d, $^2J_{PC} = 1.5$, C^1), 127.2 (s, C^8), 128.8 (s, C^9), 140.5 (d, $^3J_{PC} = 24.9$, C^7) 158.5 (d, $^2J_{PC} = 7.7$, C^6). ^{31}P $\{^1H\}$ NMR (161.91 MHz, C_6D_6) δ : + 42.3 (s). MS (FAB $^+$) m/z : 412 (M^+). *Anal.* Found: C, 69.82; H, 9.10; N, 13.38 %. Calc. C, 69.87; H, 9.04; N, 13.58 %. ^{31}P CPMAS NMR (161.98 MHz) δ : 42.1. $\lambda_{max}(\text{hexane})/\text{nm}$ 390 ($\epsilon/\text{dm}^3 \text{mol}^{-1} \text{cm}^{-1}$ 10,500), 489 (3,650).

Bis(diisopropylamino)phosphino selenide (phenyl pyridin-2-yl methylene)amine: 13o.Se

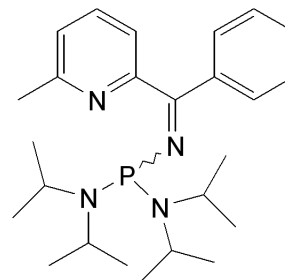


A Youngs NMR tube was partially filled with selenium to a depth of 4 mm and a solution of **13o/13c** (30 mg, 0.073 mmol) in C_6D_6 (1 mL) added to give a red solution above a black solid. After heating at 50 °C for 80 h complete conversion to the selenide was observed by ^{31}P NMR spectroscopy.

1H NMR (400.13 MHz, C_6D_6) δ : 1.34 (12H, d, $^3J_{HH} = 6.9$, CH_3), 1.45 (12H, d, $^3J_{HH} = 6.9$, CH_3'), 4.01 - 4.17 (4H, m, $CHCH_3$), 6.75 (1H, ddd, $^3J_{HH} = 7.5$ $J_{HH} = 5.0$ $^4J_{HH} = 1.2$, C^2H), 7.06-7.13 (4H, m, C^3H , C^9H and $C^{10}H$), 7.26 (1H, d, $^3J_{HH} = 7.7$, C^4H), 7.82 - 7.86 (2H, m, C^8H),

8.54 (1H, d, $^3J_{\text{HH}} = 4.9$, C^1H). ^1H $\{^{31}\text{P}\}$ NMR (499.77 MHz, C_6D_6) δ : 1.34 (12H, d, $^3J_{\text{HH}} = 6.9$, CH_3), 1.45 (12H, d, $^3J_{\text{HH}} = 6.9$, CH_3'), 4.07 (4H, septet, $^3J_{\text{HH}} = 6.9$, CHCH_3), 6.75 (1H, ddd, $^3J_{\text{HH}} = 7.5$, $^3J_{\text{HH}} = 5.0$, $^4J_{\text{HH}} = 1.2$, C^2H), 7.06 - 7.13 (4H, m, C^3H , C^9H and C^{10}H), 7.26 (1H, d, $^3J_{\text{HH}} = 7.7$, C^4H), 7.82 - 7.86 (2H, m, C^8H), 8.54 (1H, d, $^3J_{\text{HH}} = 4.9$, C^1H). ^{13}C $\{^1\text{H}\}$ NMR (125.67 MHz, C_6D_6) δ : 22.8 (d, $^3J_{\text{PC}} = 2.4$, CH_3), 24.6 (d, $^3J_{\text{PC}} = 2.0$, CH_3'), 47.2 (d, $^3J_{\text{PC}} = 6.7$, CHCH_3), 123.9 (s, C^2), 124.9 (s, C^4), 128.8 (s, C^9 or C^{10}), 130.6 (s, C^8), 132.3 (s, C^9 or C^{10}), 134.9 (s, C^3), 140.1 (d, $^3J_{\text{PC}} = 23.0$, C^7), 149.3 (s, C^1), 155.9 (d, $^3J_{\text{PC}} = 13.7$, C^5), 173.0 (d, $^2J_{\text{PC}} = 2.4$, C^6). ^{31}P $\{^1\text{H}\}$ NMR (80.96 MHz, C_6D_6) δ : + 55.5 (s + satellites, $^1J_{\text{SeP}} = 821$).

Bis(diisopropylamino)phosphino(phenyl *ortho*-methylpyridin-2-yl methylene)amine: 14o

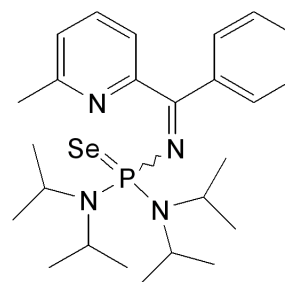


To a stirred, cooled ($-78\text{ }^\circ\text{C}$) solution of dried 2-cyano-6-methyl-pyridine (0.50 g, 4.23 mmol) in dimethoxyethane (50 mL) was added dropwise phenyllithium (1.8 M in dibutylether, 2.36 mL, 4.23 mmol) and the mixture stirred for an hour, giving a dark red solution. A slurry of $(i\text{-Pr}_2\text{N})_2\text{PCl}$ (1.13 g, 4.23 mmol) in dimethoxyethane (40 mL) was added slowly by cannula. The mixture was allowed to warm to room temperature and stirred for 72 h. The volatile components were removed under reduced pressure, hexane (100 mL) added, the resulting solution isolated by filtration and evaporated under reduced pressure to leave a brown solid, which was dried *in vacuo* (830 mg, 46 %).

^1H NMR (400.13 MHz, C_6D_6) δ : 1.19 (12H, d, $^3J_{\text{HH}} = 6.7$, NCHCH_3), 1.27 (12H, d, $^3J_{\text{HH}} = 6.7$, NCHCH_3'), 2.36 (3H, s, C^1CH_3), 3.84-3.96 (4H, m, CHCH_3), 6.65 (1H, d, $^3J_{\text{HH}} = 6.7$, C^4H), 7.10-7.23 (5H, m, aromatic protons), 7.87 (2H, d, $^3J_{\text{HH}} = 7.3$, C^8H). ^{13}C $\{^1\text{H}\}$ NMR (100.61

MHz, C₆D₆) δ : 24.7 (s, C¹CH₃), 24.7 (d, ³J_{PC} = 9.0, CHCH₃), 24.7 (d, ³J_{PC} = 7.0, NCHCH₃'), 45.9 (d, ²J_{PC} = 12.5, CHCH₃), 120.2 (d, ⁴J_{PC} = 3.7, C⁴), 122.7 (s, C²), 128.4 (s, C⁹ or C¹⁰), 129.5 (d, ⁴J_{PC} = 2.1, C⁸), 130.0 (s, C⁹ or C¹⁰), 136.0 (s, C³), 140.8 (d, ³J_{PC} = 7.3, C⁵ or C⁷), 158.2 (s, C¹), 158.7 (d, ³J_{PC} = 8.1, C⁵ or C⁷), 165.8 (d, ²J_{PC} = 29.6, C⁶). ³¹P {¹H} NMR (80.96 MHz, C₆D₆) δ : + 71.3. MS (EI⁺) *m/z*: 426 (M⁺). *Anal.* Found: C, 70.55; H, 9.24; N, 13.15 %. Calc. C, 70.39; H, 9.22; N, 13.13 %.

Bis(diisopropylamino)phosphino selenide (phenyl *ortho*-methylpyridin-2-yl methylene)amine: **14o.Se**



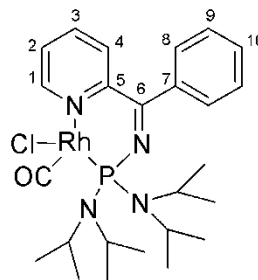
A Young's NMR tube was partially filled with selenium to a depth of 4 mm and a solution of **14o** (30 mg, 0.073 mmol) in C₆D₆ (1 mL) added to give a red solution above a black solid. After heating at 50 °C for 15 h complete conversion to the selenide was observed by ³¹P NMR spectroscopy.

¹H NMR (400.13 MHz, C₆D₆) δ : 1.35 (12H, d, ³J_{HH} = 6.8, CH₃), 1.46 (12H, d, ³J_{HH} = 6.8, CH₃'), 2.43 (3H, s, C¹CH₃), 4.00 - 4.17 (4H, m, CHCH₃), 6.76 (1H, t, J_{HH} = 4.0, C²H), 7.09 - 7.18 (5H, m, C³H, C⁴H, C⁹H and C¹⁰H), 7.86 - 7.91 (2H, m, C⁸H). ¹³C {¹H} NMR (100.61 MHz, C₆D₆) δ : 23.2 (d, ³J_{PC} = 2.1, CHCH₃), 24.9 (d, ³J_{PC} = 2.2, CHCH₃'), 24.9 (s, C¹CH₃), 47.5 (d, ³J_{PC} = 6.5, CHCH₃), 122.1 (s, C²), 123.5 (s, C⁴), 129.0 (s, C⁹ or C¹⁰), 130.9 (s, C⁸), 132.5 (s, C⁹ or C¹⁰), 135.5 (s, C³), 140.4 (d, ³J_{PC} = 23.0, C⁷), 155.2 (d, ³J_{PC} = 14.0, C⁵), 158.3 (s, C¹), 173.2 (d, ²J_{PC} = 2.2, C⁶). ³¹P {¹H} (80.96 MHz, C₆D₆) δ : + 54.3 (s + satellites, ¹J_{SeP} = 824).

Thermal stability of bis(diisopropylamino)phosphino(phenyl *ortho*-methylpyridin-2-yl methylene)amine

To a Young's tap NMR tube were added **4o** (25 mg, 0.059 mmol) and deuterated benzene (0.8 mL) and the resultant solution heated for 70 h at 70 °C. ^1H and ^{31}P NMR spectroscopies revealed no change and the reaction was discontinued.

Bis(diisopropylamino)phosphino(phenyl pyridin-2-yl methylene)amine rhodium carbonyl chloride: **15**



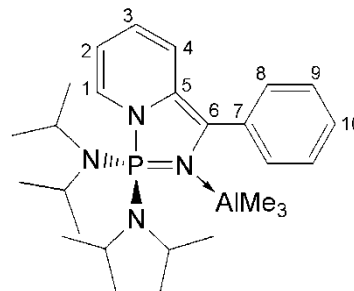
The compound $[\text{RhCl}(\text{CO})_2]_2$ (92 mg, 0.24 mmol) was dissolved in toluene (10 mL) and added to **13o/13c** (198 mg, 0.48 mmol) also dissolved in toluene (10 mL). The mixture was degassed and allowed to stir for 24 h, after which time the reaction was observed to be complete by ^{31}P NMR spectroscopy. Removal of the volatile components under reduced pressure gave a red brown solid (252 mg, 91 %). Single crystals suitable for an X-ray structure determination were grown by slow evaporation from a saturated solution of benzene over a period of 2 d.

^1H NMR (499.80 MHz, CDCl_3) δ : 1.12 (12H, d, $^3J_{\text{HH}} = 7.0$, CH_3), 1.16 (12H, d, $^3J_{\text{HH}} = 6.5$, CH_3'), 4.06 - 4.17 (4H, m, CHCH_3), 7.38 (1H, d, $^3J_{\text{HH}} = 7.5$, C^4H), 7.42 (2H, t, $^3J_{\text{HH}} = 7.5$, C^9H), 7.48 - 7.60 (4H, m, C^8H , C^2H and C^{10}H), 7.89 (1H, td, $^3J_{\text{HH}} = 7.5$ $^4J_{\text{HH}} = 1.5$, C^3H), 9.68 (1H, d, $^3J_{\text{HH}} = 5.5$, C^1H). ^{13}C $\{^1\text{H}\}$ NMR (125.67 MHz, CDCl_3) δ : 23.7 (d, $^3J_{\text{PC}} = 2.9$, CH_3), 25.1 (d, $^3J_{\text{PC}} = 1.5$, CH_3'), 48.0 (d, $^3J_{\text{PC}} = 10.1$, CHCH_3), 126.8 (s, C^2 or C^4), 126.9 (s, C^2 or C^4), 128.7 (s, C^9), 130.0 (s, C^8 or C^{10}), 131.8 (s, C^8 or C^{10}), 138.8 (s, C^3), 139.4 (d, $^3J_{\text{PC}} = 15.9$, C^7), 147.0 (d, $^3J_{\text{PC}} = 17.2$, C^5), 155.3 (s, C^1), 171.1 (s, C^6). ^{31}P $\{^1\text{H}\}$ NMR (161.91 MHz, CDCl_3) δ :

[§] In spite of increased relaxation times and increasing the number of scans the carbonyl carbon could not be found by carbon-13 NMR spectroscopy.

+ 117.8 (d, $^1J_{\text{PRh}} = 209$). MS (FAB⁺) m/z : 550 (M-CO⁺), 543 (M-Cl⁺). IR (KBr, 25% CDCl₃/CHCl₃ solution): $\nu(\text{CO}) = 1997\text{cm}^{-1}$. Anal. Found: C, 51.92; H, 6.45; N, 9.65 %. Calc. C, 51.87; H, 6.44; N, 9.68 %.

1,1-Bis(diisopropylamino)-3-phenyl-1 λ^5 -[1,3,2]diazaphospholo[1,5- α]pyridine.trimethyl aluminium: 16

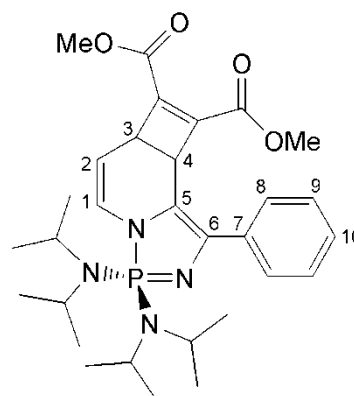


A solution of trimethylaluminium (25 mg, 0.35 mmol) in hexane (10 mL) was added slowly to a solution of **13o/13c** (157 mg, 0.38 mmol, 1.1 equivalents) in hexane (30 mL). The immediate precipitation of an orange solid was observed and the solution was allowed to stir for 1 h. The precipitate was isolated by filtration, washed with hexane (3 x 4 mL) and dried *in vacuo* (116 mg, 69 %). Single crystals suitable for an X-ray structure determination were grown by cooling (- 30 °C) of a saturated solution of CH₂Cl₂.

^1H NMR (699.73 MHz, CD₂Cl₂) δ : - 1.18 (9H, s, AlCH₃), 1.34 (12H, d, $^3J_{\text{HH}} = 6.8$, CHCH₃), 1.36 (12H, d, $^3J_{\text{HH}} = 7.0$, CHCH₃'), 3.97 (4H, m, CHCH₃ and CHCH₃'), 5.36 - 5.40 (1H, m, C²H), 5.49 (1H, dd, $^3J_{\text{HH}} = 9.8$ J = 5.6 C³H), 5.93 (1H, d, $^3J_{\text{HH}} = 9.7$, C⁴H), 6.23 (1H, dd, $^3J_{\text{PH}} = 6.4$, $^3J_{\text{HH}} = 6.4$, C¹H), 7.24 - 7.31 (5H, m, C⁸H, C⁹H and C¹⁰H). ^1H { ^{31}P } NMR (699.73 MHz, CD₂Cl₂) δ : - 1.18 (9H, s, AlCH₃), 1.34 (12H, d, $^3J_{\text{HH}} = 6.8$, CHCH₃), 1.36 (12H, d, $^3J_{\text{HH}} = 7.0$, CHCH₃'), 3.97 (4H, m, CHCH₃ and CHCH₃'), 5.37 (1H, dd, J = 7.0, C²H), 5.49 (1H, dd, $^3J_{\text{HH}} = 9.8$ J = 5.6, C³H), 5.93 (1H, d, $^3J_{\text{HH}} = 9.7$, C⁴H), 6.23 (1H, d, $^3J_{\text{HH}} = 6.4$, C¹H), 7.24 - 7.31 (5H, m, C⁸H, C⁹H and C¹⁰H). ^{13}C { ^1H } NMR (125.68 MHz, CD₂Cl₂) δ : - 4.5 (b, AlCH₃), 23.9 (d, $^3J_{\text{PC}} = 3.8$, CHCH₃), 24.1 (d, $^3J_{\text{PC}} = 5.0$, CHCH₃'), 49.8 (d, $^2J_{\text{PC}} = 3.8$, CHCH₃), 107.0 (d, $^3J_{\text{PC}} = 7.5$, C²), 116.8 (d, $^4J_{\text{PC}} = 2.5$, C³), 120.3 (d, $^3J_{\text{PC}} = 6.3$, C⁴), 122.3 (d, $^3J_{\text{PC}} = 23.9$, C⁵), 123.2 (d, $J_{\text{PC}} = 6.3$, C⁶ or C⁷), 126.4 (d, $^2J_{\text{PC}} = 2.5$, C¹), 128.0 (s, C⁸ or C⁹ or C¹⁰), 128.0 (s, C⁸ or C⁹ or C¹⁰),

132.4 (s, C^8 or C^9 or C^{10}), 134.6 (d, $J_{PC} = 15.1$, C^6 or C^7). $^{31}P \{^1H\}$ NMR (80.95 MHz, CD_2Cl_2) δ : + 46.6 (s). *Anal.* Found: C, 66.71; H, 9.53; N, 11.58 %. Calc. C, 66.91; H, 9.57; N, 11.56 %.

Reaction of dimethylacetylene dicarboxylate (DMAD) with **13c/13o**: **17**



To a Young's NMR tube was added **13c/13o** (38 mg, 0.092 mmol), dimethylacetylene dicarboxylate (13 mg, 0.092 mmol) and CD_2Cl_2 (0.8 mL). After 24 h the reaction was found to be complete by ^{31}P NMR spectroscopy with 95 % conversion to **17**.

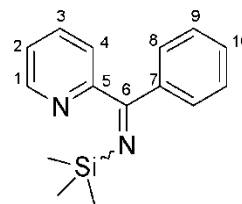
1H NMR (499.77 MHz, CD_2Cl_2) δ : 1.12 (6H, d, $^3J_{HH} = 6.8$, $CHCH_3$), 1.15 (6H, d, $^3J_{HH} = 6.8$, $CHCH_3'$), 1.21 (6H, d, $^3J_{HH} = 6.8$, $CHCH_3''$), 1.37 (6H, d, $^3J_{HH} = 6.8$, $CHCH_3'''$), 3.53 (3H, s, CO_2CH_3), 3.56 - 3.70 (5H, m, $CHCH_3$ and C^3H), 3.73 (3H, s, CO_2CH_3'), 4.53 (1H, dd, $J = 4.5$, C^4H), 5.03 (1H, dd, $^3J_{HH} = 8.1$ $J = 3.8$, C^2H), 6.10 - 6.15 (1H, m, C^1H), 7.13 (1H, t, $^3J_{HH} = 7.2$, $C^{10}H$), 7.26 (2H, t, $^3J_{HH} = 7.9$, C^9H), 7.26 (2H, d, $^3J_{HH} = 7.6$, C^8H). $^1H \{^{31}P\}$ NMR (499.77 MHz, CD_2Cl_2) δ : 1.12 (6H, d, $^3J_{HH} = 6.8$, $CHCH_3$), 1.15 (6H, d, $^3J_{HH} = 6.8$, $CHCH_3'$), 1.21 (6H, d, $^3J_{HH} = 6.8$, $CHCH_3''$), 1.37 (6H, d, $^3J_{HH} = 6.8$, $CHCH_3'''$), 3.53 (3H, s, CO_2CH_3), 3.56-3.70 (5H, m, $CHCH_3$ and C^3H), 3.73 (3H, s, CO_2CH_3'), 4.53 (1H, dd, $J = 4.5$, C^4H), 5.03 (1H, dd, $^3J_{HH} = 8.1$ $J = 3.8$, C^2H), 6.13 (1H, d, $^3J_{HH} = 8.2$, C^1H), 7.13 (1H, t, $^3J_{HH} = 7.2$, $C^{10}H$), 7.26 (2H, t, $^3J_{HH} = 7.9$, C^9H), 7.26 (2H, d, $^3J_{HH} = 7.6$, C^8H). $^{13}C \{^1H\}$ NMR (100.62 MHz, CD_2Cl_2) δ : 22.6 (d, $^3J_{PC} = 1.6$, $CHCH_3$), 23.3 (d, $^3J_{PC} = 1.8$, $CHCH_3'$), 23.5 (d, $^3J_{PC} = 1.6$, $CHCH_3''$), 23.8 (d, $^3J_{PC} = 2.6$, $CHCH_3'''$), 39.3 (d, $^4J_{PC} = 2.0$, C^3), 39.9 (d, $^3J_{PC} = 11.0$, C^4), 47.6 (d, $^2J_{PC} = 4.0$, $CHCH_3$), 48.1 (d, $^2J_{PC} = 4.0$, C^1HCH_3), 51.7 (s, CO_2CH_3), 52.2 (s, $CO_2C^1H_3$), 100.5 (d, $^3J_{PC} = 7.0$, C^2),

109.8 (d, $^3J_{PC} = 33.0$, C^5), 126.5 (s, C^{10}), 126.1 (s, C^1), 127.8 (d, $^4J_{PC} = 1.0$, C^8), 128.1 (s, C^9), 138.3 (d, $^2J_{PC} = 4.0$, C^6), 139.6 (d, $^3J_{PC} = 26.0$, C^7), 144.6 (s, CCO_2CH_3), 149.4 (s, $C'CO_2CH_3$), 161.9 (s, CO_2CH_3), 163.1 (s, $C'O_2CH_3$). $^{31}P \{^1H\}$ NMR (161.91 MHz, CD_2Cl_2) δ : + 46.6 (s). MS (El^+) m/z : 554 (M^+).

Reaction of **13o/13c** with BF_3

To a cooled ($-78\text{ }^\circ\text{C}$) solution of **13o/13c** (298 mg, 0.721 mmol) in hexane (40 mL) was added dropwise boron trifluoride (0.9 M diethyl ether solution of BF_3 , 0.80 mL, 0.721 mmol). The solution was allowed to warm to room temperature and a yellow solid precipitated after 15 minutes leaving a colourless solution. The solid was isolated by filtration and washed with hexane. The $^{31}P \{^1H\}$ NMR spectrum of the solid showed a mixture of peaks at 32 ppm (minor) and 40 ppm (major). No single product was isolated.

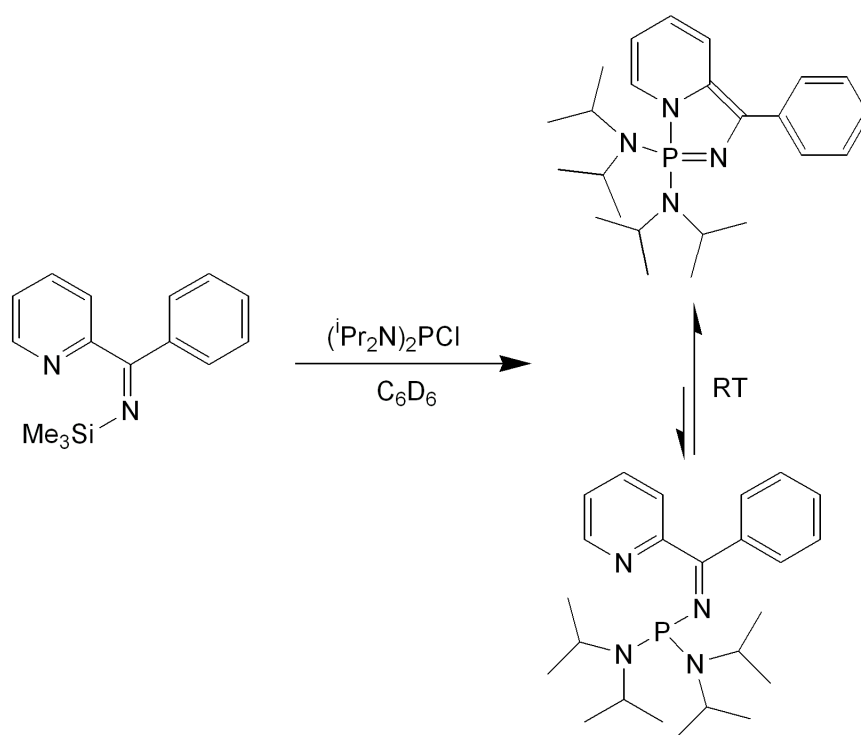
Trimethylsilyl(phenyl pyridin-2-yl methylene)amine



2-Cyanopyridine (0.45 g, 4.32 mmol) was dissolved in diethyl ether (40 mL), cooled to $-78\text{ }^\circ\text{C}$ and phenyllithium (1.8 M in dibutylether, 2.39 mL, 4.32 mmol) added dropwise. The mixture was stirred for 4 h, after which the mixture was warmed to room temperature. The volatile components were removed *in vacuo* and DME (30 mL) added followed by addition of Me_3SiCl (0.55 mL). After 5 minutes a light yellow solution above a white precipitate was observed. The mixture was stirred for a further hour before the removal of the volatile components, under reduced pressure, gave a light yellow solid. The desired product was extracted with CH_2Cl_2 (1 x 50 mL, 2 x 15 mL) as a yellow solution. Removal of the CH_2Cl_2 *in vacuo* gave a yellow oil (713 mg, 65 %).

^1H NMR (400.13 MHz, C_6D_6) δ : 0.18 (9H, s + satellites, CH_3), 6.61 (1H, ddd, $^3J_{\text{HH}} = 7.5$, $J_{\text{HH}} = 5.0$, $^4J_{\text{HH}} = 1.2$, C^2H), 7.00 (1H, td, $^3J_{\text{HH}} = 7.8$, $^4J_{\text{HH}} = 1.8$, C^3H), 7.08 - 7.12 (m, 3H, C^9H + C^{10}H), 7.27 (1H, dt, $^3J_{\text{HH}} = 8.0$, $^4J_{\text{HH}} = 1.1$, C^4H), 7.66 - 7.70 (2H, m, C^8H), 8.38 (1H, ddd, $J_{\text{HH}} = 4.8$, $^4J_{\text{HH}} = 1.8$, $^4J_{\text{HH}} = 1.1$, C^1H). ^{13}C $\{^1\text{H}\}$ NMR (50.28 MHz, C_6D_6) δ : 1.5 (s + satellites, CH_3), 122.9 (s, C^4), 124.0 (s, C^2), 129.0 (s, C^9 or C^{10}), 129.6 (s, C^8), 130.5 (s, C^9 or C^{10}), 136.2 (s, C^3), 141.8 (s, C^7), 149.8 (s, C^1), 159.6 (s, C^5), 174.5 (s, C^6).

Reaction of trimethylsilyl(phenyl pyridin-2-yl methylene)amine with $(i\text{-Pr}_2\text{N})_2\text{PCl}$



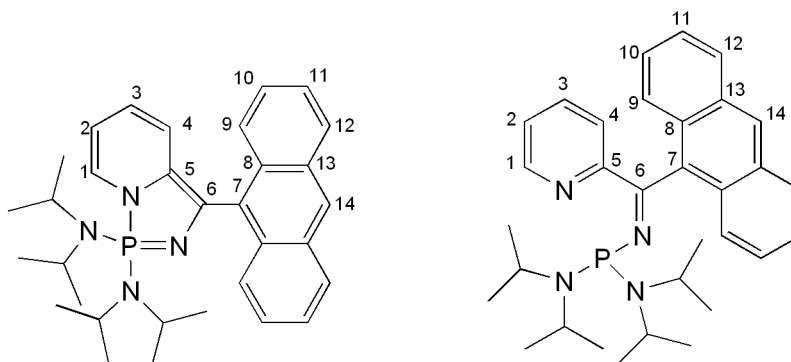
Trimethylsilyl(phenyl pyridin-2-yl methylene)amine (28 mg, 0.11 mmol) and $(i\text{-Pr}_2\text{N})_2\text{PCl}$ (29.4 mg, 0.11 mmol) were dissolved in deuterated benzene (0.8 mL) and added to a Young's NMR tube. The reaction was observed, by ^{31}P NMR spectroscopy, to proceed slowly at room temperature with 60 % conversion to **13o/13c** after 17 h. Complete conversion of the chlorophosphine occurred within two weeks.

Attempted reaction of 13c/13o with diphenylacetylene

To a Young's tap NMR tube **13c/13o** (35 mg, 0.084 mmol), diphenylacetylene (15 mg, 0.084 mmol) and deuterated benzene (0.8 mL) were added and the resultant solution heated for 15 h at 70 °C. Both ^{31}P NMR and ^1H NMR spectroscopies revealed no change and the reaction was discontinued.

7.5. Further reactions exploring the open P^N ligand / closed diazaphosphole equilibrium

1,1-Bis(diisopropylamino)-3-anthracenyl-1 λ^5 -[1,3,2]diazaphospholo [1,5- α]pyridine and bis(Diisopropylamino)phosphino(anthracenyl pyridin-2-yl methylene)amine: 18c and 18o respectively



9-Bromoanthracene (644 mg, 94 % purity, 2.35 mmol) was dissolved in diethyl ether (40 mL) and slowly added to n-BuLi (1.6 M in hexanes, 1.47 mL, 2.35 mmol) at - 30 °C producing an ethereal suspension of anthracenyllithium.¹ The suspension was subsequently added by cannula to a stirred solution of 2-cyanopyridine (245 mg, 2.35 mmol) in diethyl ether (30 mL) at -78 °C and the mixture stirred for 1 h, then (i-Pr₂N)₂PCl (628 mg, 2.35 mmol) was added directly as a solid and stirred for a further hour. After allowing to warm to room temperature, the volatile components were removed under reduced pressure, dimethoxyethane (25 mL) added and the purple suspension stirred for 16 h. The volatile components were removed *in vacuo*, hexane (200 mL) added and

the resulting solution filtered. Concentration of the solution led to the formation of a grey precipitate (699 mg, 58 %).

Purple single crystals of the *closed* isomer, suitable for an X-ray diffraction study, were grown by addition of hexane to a concentrated ethereal solution of **18**. A semi-crystalline yellow solid was obtained by slow evaporation of a saturated benzene solution of **18** over a period of 4 d and was demonstrated by solid state ^{31}P NMR spectroscopy to be exclusively the 'open' isomer.

18c/18o:

^{31}P NMR (499.77 MHz, $\text{C}_6\text{D}_5\text{CD}_3$) (297 K) δ : 40.5 (s, 64 %), 68.9 (s, 36 %). (303 K) δ : 40.5 (s, 69 %), 68.9 (s, 31 %). (333 K) δ : 40.5 (s, 75 %), 68.9 (s, 25 %). (363 K) δ : 40.5 (s, 82 %), 68.9 (s, 18 %).

18c: 'Closed' isomer (*less prevalent isomer at room temperature*)

^1H NMR (499.77 MHz, $\text{C}_6\text{D}_5\text{CD}_3$) δ : 1.14 (12H, d, $J = 6.8$, CHCH_3), 1.29 (12H, d, $J = 6.8$, CHCH_3'), 3.51 - 3.64 (4H, m, CHCH_3), 5.13 (1H, dd, $J = 9.6$, $J = 5.7$, $\text{C}^2\text{H}/\text{C}^3\text{H}$), 5.25 - 5.30 (1H, m, $\text{C}^2\text{H}/\text{C}^3\text{H}$), 5.92 (1H, d, $J = 9.8$, C^4H), 6.22 - 6.27 (1H, m, C^1H), 7.14 - 7.24 (2H, m, aromatic protons), ** 7.28 - 7.36 (2H, m, aromatic protons), 7.86 (2H, d, $J = 8.5$, aromatic protons), 8.13 (1H, s, C^{14}H), 9.06 (2H, d, $J = 8.9$, aromatic protons). $^1\text{H} \{^{31}\text{P}\}$ NMR (499.77 MHz, $\text{C}_6\text{D}_5\text{CD}_3$) δ : 1.14 (12H, d, $J = 6.8$, CHCH_3), 1.29 (12H, d, $J = 6.8$, CHCH_3'), 3.57 (4H, septet, CHCH_3), 5.13 (1H, dd, $J = 9.6$, $J = 5.7$, $\text{C}^2\text{H}/\text{C}^3\text{H}$), 5.25 - 5.30 (1H, m, $\text{C}^2\text{H}/\text{C}^3\text{H}$), 5.92 (1H, d, $J = 9.8$, C^4H), 6.24 (1H, d, $J = 7.6$, C^1H), 7.14 - 7.24 (2H, m, aromatic protons), ** 7.28 - 7.36 (2H, m, aromatic protons), 7.86 (2H, d, $J = 8.5$, aromatic protons), 8.13 (1H, s, C^{14}H), 9.06 (2H, d, $J = 8.9$, aromatic protons). $^{31}\text{P} \{^1\text{H}\}$ NMR (202.31 MHz, $\text{C}_6\text{D}_5\text{CD}_3$) δ : + 40.5. ^{31}P CP MAS NMR (161.88 MHz) δ : + 39.5.

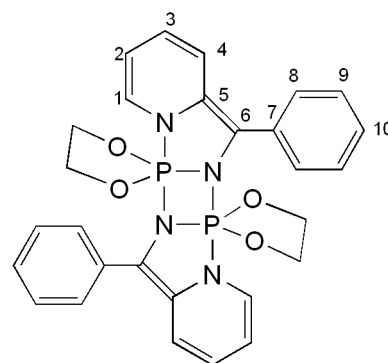
** Overlapping signals.

18o: 'Open' isomer

^1H NMR (499.77 MHz, $\text{C}_6\text{D}_5\text{CD}_3$) δ : 0.95 (12H, d, $J = 6.8$, CHCH_3), 1.16 (12H, d, $J = 6.8$, CHCH_3'), 3.94 - 4.06 (4H, m, CHCH_3), 6.56 - 6.61 (1H, m, aromatic proton), 7.14 - 7.24 (2H, m, aromatic protons), ** 7.27 - 7.34 (2H, m, aromatic protons), 7.79 (2H, d, $J = 8.5$, aromatic protons), 7.96 (2H, d, $J = 8.5$, aromatic protons), 7.99 (1H, d, $J = 5.0$, pyridyl proton), 8.11 (1H, s, C^{14}H), 8.52 (2H, d, $J = 7.8$, aromatic protons). ^{31}P $\{^1\text{H}\}$ NMR (202.31 MHz, $\text{C}_6\text{D}_5\text{CD}_3$) δ : + 68.9. ^{31}P CP MAS NMR (161.88 MHz) δ : + 62.6. $^{++}$

Anal. Found: C, 74.75; H, 7.94; N, 11.17 %. Calc. C, 74.97; H, 8.06; N, 10.93 %.

The diazadiphosphetane, 20, that corresponds to the cyclodimerisation of the proposed species 3-phenyl-*spiro*-[1 λ^5 -(1,3,2)diazaphospholo[1,5-*a*] pyridine-1,2'-[1,3,2]dioxaphospholane]



To a stirred, cooled ($-78\text{ }^\circ\text{C}$) solution of dried 2-cyanopyridine (0.50 g, 4.8 mmol) in dimethoxyethane (40 mL) was added dropwise phenyllithium (2.0 M in dibutylether, 2.4 mL, 4.8 mmol) and the mixture stirred for an hour, giving a dark red solution. Dropwise addition of $(\text{OCH}_2\text{CH}_2\text{O})\text{PCl}$ (0.42 mL, 4.8 mmol) gave a yellow brown solution. The mixture was allowed to warm to room temperature and stirred for 16 h. Volatile components were removed under reduced pressure, CH_2Cl_2 (40 mL) added and the

$^{++}$ The mass spectrometry techniques EI and CI were unsuccessful for this compound.

resulting solution filtered. Layering with hexane gave orange crystals which were isolated by filtration and washed with hexane (744 mg, 57 %).

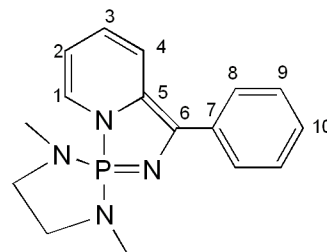
Both components of **20**:

^{31}P { ^1H } NMR (161.91 MHz, CD_2Cl_2) δ : - 37.8 (89 %), - 43.2 (11 %).

Predominant component of **20**:

^1H NMR (399.96 MHz, CD_2Cl_2) δ : 3.03 - 3.16 (1H, m, OCH), 3.36-3.47 (1H, m, OCH'), 3.66 - 3.76 (1H, m, OCH''), 3.80 - 3.91 (1H, m, OCH'''), 5.30 - 5.37 (1H, m, $\text{C}^1\text{H}/\text{C}^2\text{H}/\text{C}^3\text{H}/\text{C}^4\text{H}$), 5.88 (1H, m, $\text{C}^1\text{H}/\text{C}^2\text{H}/\text{C}^3\text{H}/\text{C}^4\text{H}$), 6.53 (1H, d, $J = 8.6$, $\text{C}^1\text{H}/\text{C}^2\text{H}/\text{C}^3\text{H}/\text{C}^4\text{H}$), 6.83 (1H, m, $\text{C}^1\text{H}/\text{C}^2\text{H}/\text{C}^3\text{H}/\text{C}^4\text{H}$), 7.11 (1H, t, $J = 8.0$, C^{10}H), 7.26 (2H, t, $J = 7.4$, C^9H), 7.32 (2H, d, $J = 7.9$, C^8H). ^{13}C { ^1H } NMR (175.95 MHz, CD_2Cl_2) δ : 60.5 (s, CH_2), 63.2 (s, $\text{C}'\text{H}_2$), 106.7 (t, $J = 1.8$, $\text{C}^1/\text{C}^2/\text{C}^3/\text{C}^4$), 113.2 (s, $\text{C}^5/\text{C}^6/\text{C}^7$), 119.8 (s, $\text{C}^1/\text{C}^2/\text{C}^3/\text{C}^4$), 123.5 (s, $\text{C}^1/\text{C}^2/\text{C}^3/\text{C}^4$), 125.6 (s, C^{10}), 127.9 (s, C^8/C^9), 128.1 (s, C^8/C^9), 129.2 (t, $J = 15.7$, $\text{C}^5/\text{C}^6/\text{C}^7$), 132.7 (s, $\text{C}^1/\text{C}^2/\text{C}^3/\text{C}^4$), 134.9 (t, $J = 2.7$, $\text{C}^5/\text{C}^6/\text{C}^7$). MS (EI^+) m/z : 544 (M^+). *Anal.* Found: C, 61.51; H, 4.83; N, 10.17 %. Calc. C, 61.77; H, 4.81; N, 10.29 %.

1',3'-dimethyl-3-phenyl-*spiro*-[1 λ^5 -[1,3,2]diazaphospholo[1,5-a]pyridine-1,2'-[1,3,2]diazaphospholane], 21c



To a stirred, cooled ($-78\text{ }^\circ\text{C}$) solution of dried 2-cyanopyridine (0.50 g, 4.8 mmol) in dimethoxyethane (40 mL) was added dropwise phenyllithium (1.8 M in dibutylether, 2.67 mL, 4.8 mmol) and the mixture stirred for an hour, giving a dark red solution. A

solution of (MeNCH₂CH₂NMe)PCl¹¹ (0.73 g, 4.8 mmol) in dimethoxyethane (10 mL) was added slowly by cannula. The mixture was allowed to warm to room temperature and stirred for 16 h. Volatile components were removed under reduced pressure, CH₂Cl₂ (40 mL) added and the resulting solution filtered. The volatile components were removed under reduced pressure and the resulting dark red solid washed with hexane (3 x 10 mL), (1.150 g, 81 %).

¹H NMR (699.73 MHz, C₆D₆) δ: 2.02 (6H, d, ³J_{PH} = 10.5, NCH₃), 2.40 (4H, m, NCH₂), 5.36 (1H, t, J = 6.2, C²H), 5.57 (1H, dd, J = 6.2, C³H), 6.14 (1H, m, C¹H), 7.06 (1H, tt, J = 7.3, 1.0, C¹⁰H), 7.17 (1H, d, J = 9.6, C⁴H), 7.32 (2H, t, J = 8.1, C⁹H), 8.17 (2H, d, J = 8.4, C⁸H). ¹³C {¹H} NMR (175.95 MHz, C₆D₆) δ: 31.4 (d, J = 6.1, NCH₃), 46.4 (d, J = 12.7, NCH₂), 108.5 (d, J = 6.2, C²), 114.9 (s, C³), 122.7 (d, J = 9.9, C⁴), 123.1 (d, J = 34.2, C⁵), 124.7 (s, C¹), 125.1 (s, C¹⁰), 127.2 (s, C⁸), 129.0 (s, C⁹), 140.3 (d, J = 26.0, C⁷).^{††} ³¹P {¹H} NMR (80.96 MHz, C₆D₆) δ: + 40.6. MS (EI⁺) *m/z*: 298 (M⁺). *Anal.* Found: C, 64.22; H, 6.43; N, 18.59 %. Calc. C, 64.42; H, 6.42; N, 18.78 %.

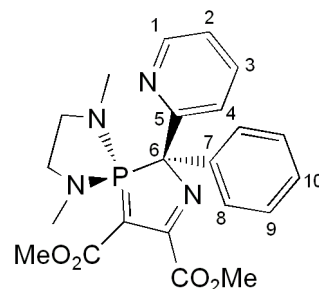
Reaction of **21c** with Se to form **21o.Se**

To a solution of **21c/21o** (30 mg, 0.10 mmol) in C₆D₆ (0.8 mL) in a Young's NMR tube was added grey selenium (96 mg, 1.21 mmol) giving a red solution above a black solid. After heating at 50 °C for 96 h complete conversion to the selenide derivative was confirmed by ³¹P NMR spectroscopy.

³¹P {¹H} NMR (80.96 MHz, CDCl₃) δ: + 66.7 (s + satellites, ¹J_{SeP} = 842).

^{††} Carbon-6 was not detected and this is proposed to be because of the longer relaxation times of quaternary carbons, relative to protonated carbons, giving rise to a much lower intensity signal.

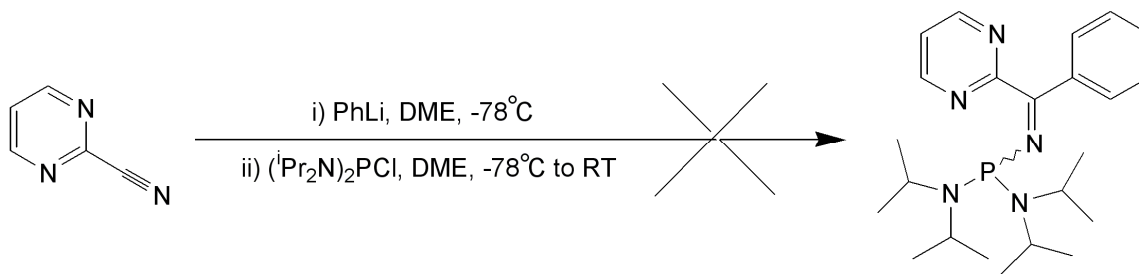
Reaction of 21c/21o with DMAD: 22



To a Young's NMR tube was added **21** (30 mg, 0.1 mmol), DMAD (14 mg, 0.1 mmol) and CD₂Cl₂. After 4 h the reaction was found to be complete by ³¹P {¹H} NMR spectroscopy.

¹H NMR (699.73 MHz, CD₂Cl₂) δ: 1.71 (3H, d, ³J_{PH} = 10.8, NCH₃), 1.81 (3H, d, ³J_{PH} = 10.8, NCH'₃), 3.07 - 3.19 (1H, m, NCH_a), 3.25 - 3.31 (2H, m, NCH_b and NCH_c), 3.50 (3H, s, CO₂CH₃), 3.55 - 3.61 (1H, m, NCH_d), 3.93 (3H, s, CO₂CH₃), 7.18 - 7.23 (1H, m, C²H + C¹⁰H), 7.26 (2H, t, ³J_{HH} = 7.4, C⁹H), 7.65 (1H, t, ³J_{HH} = 8.2, C³H), 7.75 (2H, d, ³J_{HH} = 7.9, C⁸H), 7.82 (1H, d, ³J_{HH} = 7.9, C⁴H), 8.64 (1H, d, ³J_{HH} = 4.6, C¹H). ¹³C {¹H} NMR (175.95 MHz, CD₂Cl₂) δ: 30.8 (d, J = 7.4, NC'H₃), 32.6 (d, J = 4.0, NCH₃), 48.5 (d, J = 7.6, NC'H₂), 50.0 (d, J = 6.9, NCH₂), 50.6 (s, CO₂Me), 52.7 (s, CO₂Me), 59.3 (d, J = 140.4, P=CCO₂Me), 76.3 (d, J = 65.5, C⁶), 122.7 (s, C²), 123.1 (d, J = 4.2, C⁴), 127.8 (d, J = 2.6, C¹⁰), 128.2 (d, J = 3.3, C⁸), 128.5 (d, J = 2.1, C⁹), 137.6 (s, C³), 138.0 (s, C⁷), 148.4 (d, C¹), 160.4 (s, C⁵), 165.9 (d, J = 10.9, COO), 167.8 (d, J = 11.6, C'OO), 170.3 (d, J = 53.1, N=CCO₂Me). ³¹P {¹H} NMR (80.96 MHz, CD₂Cl₂) δ: + 84.3.

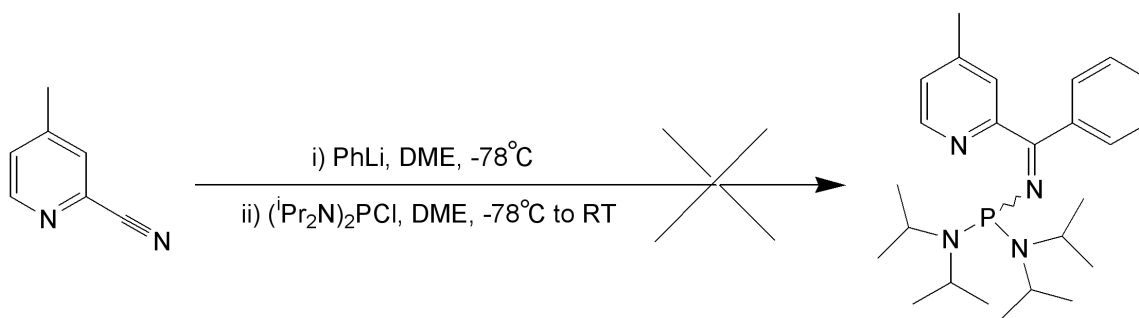
Attempted synthesis of a pyrimidyl-*N*-iminophosphine



To a cooled (-78 °C) solution of 2-cyanopyrimidine (500 mg, 4.8 mmol) in DME (40 mL) was added phenyllithium (1.8 M, 2.67 mL, 4.8 mmol) with stirring. After 1 h (i-Pr₂N)₂PCl was added, the mixture allowed to stir to room temperature for 16 h. The ³¹P NMR spectrum showed signals at 31.2, 35.4, 35.7, 101.7 and 102.4 ppm with all of (i-Pr₂N)₂PCl consumed.

Attempted synthesis of bis(diisopropylamino)phosphino(phenyl *para*-methylpyridin-2-yl methylene)amine

1st attempt:



To a stirred, cooled (-78 °C) solution of dried 2-cyano-4-methylpyridine (0.49 g, 4.15 mmol) in dimethoxyethane (50 mL) was added dropwise phenyllithium (1.8 M in dibutylether, 2.31 mL, 4.15 mmol) and the mixture stirred for an hour, giving a dark red solution. Solid (i-Pr₂N)₂PCl (1.11 g, 4.15 mmol) was added direct and the reaction allowed to warm to room temperature. After stirring for 22 h the ³¹P {¹H} NMR spectrum

was recorded showing signals at 51 (2 peaks, ~50 %), 44 (~25 %) and 37 (~25 %) ppm. Attempts to separate these products were unsuccessful.

2nd attempt:

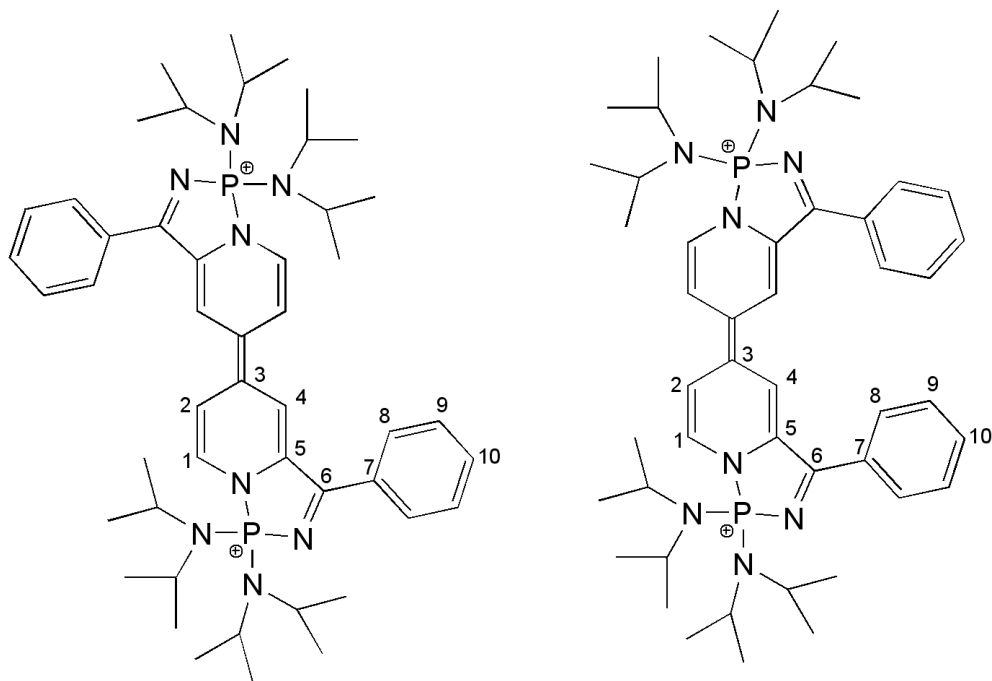
To a stirred, cooled (-116 °C) solution of dried 2-cyano-4-methylpyridine (0.245 g, 2.08 mmol) in diethylether (50 mL) was added dropwise phenyllithium (1.8 M in dibutylether, 1.16 mL, 2.08 mmol) and the mixture stirred for an hour, giving a dark red solution. The mixture was warmed to room temperature, the volatile components removed under reduced pressure and solid (i-Pr₂N)₂PCl (0.56 g, 2.08 mmol) added. Addition of dimethoxyethane (40 mL) produced an instant colour change from pink to dark brown. Stirring overnight gave a deep red solution. ³¹P {¹H} NMR spectroscopy revealed a mixture of signals at 42 (55 %), 48 (20 %) and 56 (25 %) ppm. The reaction was discontinued.

7.6. Investigations into the 'Scholl-like' coupling of **13o**/**13c**

Synthesis of (*E*)- and (*Z*)- 1,1,1',1'-tetrakis(diisopropylamino)-3,3'-diphenyl-1*H*,1'*H*-[5,5'-bi-1 λ^5 -[1,3,2]diazaphospholo[1,5-*a*]pyridinylidene]-1,1'-dium, *trans*-**23** and *cis*-**23**

1) By use of (i-Pr₂N)₂POTf

Figure 1: The triflate counter anions are omitted for clarity.



A solution of **13o**/**13c** (207 mg, 0.50 mmol) in CH₂Cl₂ (5 mL) was added slowly to a solution of (i-Pr₂N)₂POTf (190 mg, 0.50 mmol) in CH₂Cl₂ (5 mL). After 7 days the solution was layered with hexane and a green semi-crystalline solid was slowly precipitated. The solid was isolated by filtration, washed with Et₂O (3 x 3 mL), H₂O (3 x 3 mL) and dried *in vacuo* (171 mg, 61 %). Single crystals of *trans*-**23** suitable for an X-ray structure determination were grown by cooling (- 30 °C) of a saturated solution of **23** in CH₂Cl₂/hexane over a period of 3 d.

^1H NMR (699.74 MHz, CD_2Cl_2) δ : 1.24 - 1.31 (48H, m, CH_3^{cis} + $\text{CH}_3^{\text{trans}}$), 3.89 (8H, m, $\text{CH}_3\text{CH}^{\text{cis}}$ + $\text{CH}_3\text{CH}^{\text{trans}}$), 6.58 (1H, $^3J_{\text{HH}} = 7.6$, $\text{C}^2\text{H}^{\text{trans}}$), 6.64 (1H, $^3J_{\text{HH}} = 7.6$, $\text{C}^2\text{H}^{\text{cis}}$), 7.03 (1H, m, $\text{C}^1\text{H}^{\text{cis}}$), 7.16 (1H, m, $\text{C}^1\text{H}^{\text{trans}}$), 7.32 (1H, s, $\text{C}^4\text{H}^{\text{cis}}$), 7.46 (1H, s, $\text{C}^4\text{H}^{\text{trans}}$), 7.61 (2H, t, $^3J_{\text{HH}} = 7.2$, $\text{C}^9\text{H}^{\text{cis}}$), 7.68 (2H, t, $^3J_{\text{HH}} = 7.2$, $\text{C}^9\text{H}^{\text{trans}}$), 7.73 - 7.79 (2H, m, $\text{C}^{10}\text{H}^{\text{cis}}$ + $\text{C}^{10}\text{H}^{\text{trans}}$), 7.85-7.91 (2H, m, $\text{C}^8\text{H}^{\text{cis}}$ + $\text{C}^8\text{H}^{\text{trans}}$). $^{\S\S} \text{}^{31}\text{P}$ $\{^1\text{H}\}$ NMR (161.91 MHz, CD_2Cl_2) δ : + 51.4 (s, *trans*), 51.9 (s, *cis*). ^{19}F NMR (376.34 MHz, CD_2Cl_2) δ : - 79.2 (s). MS (nano-ESI $^+$) m/z : 1121 (MH^+). *Anal.* Found: C, 53.71; H, 6.50; N, 9.88 %. Calc. C, 53.56; H, 6.47; N, 9.99 %. $\lambda_{\text{max}}(\text{CH}_2\text{Cl}_2)/\text{nm}$ 325 ($\epsilon/\text{dm}^3 \text{mol}^{-1} \text{cm}^{-1}$ 11800), 392 (9190), 740 (20200).

2) By use of ferrocenium triflate

To a solution of **13o/13c** (140 mg, 0.34 mmol) in CH_2Cl_2 (5 mL) was added ferrocenium triflate²⁰ (114 mg, 0.34 mmol) and the suspension stirred for 1 h. The resultant dark green solution was filtered, layered with hexane and a green semi-crystalline solid was slowly precipitated. The solid was isolated by filtration, washed with Et_2O (3 x 3 mL), H_2O (3 x 3 mL) and dried *in vacuo* (74 mg, 39 %). Analysis confirmed the formation of *trans*-**23** and *cis*-**23** in an approximate ratio of 1:1.

Reduction of **23** by metallic sodium to give **25**

A solution of **23** (50 mg, 0.02 mmol) in THF-d_8 (0.5 mL) was treated with excess finely divided Na metal (250 mg) and the reaction allowed to stand for 2 d at ambient temperature.^{***} ^{31}P NMR spectroscopy revealed 90 % conversion to a species at 39.1 ppm.

^{\S\S} The compound was found to be insufficiently soluble for analysis by ^{13}C $\{^1\text{H}\}$ NMR spectroscopy

^{***} It should be noted that, in the presence of excess sodium, over a period of a further 10 d the compound was observed to undergo an, as yet, unidentified degradation reaction.

^1H NMR (400 MHz, THF- d_8) δ : 1.18 (24H, d, $^3J_{\text{HH}} = 6.8$, CH_3), 1.31 (24H, d, $^3J_{\text{HH}} = 6.8$, CH_3), 3.65 – 3.86 (8H, m, CHCH_3), 5.67 (2H, d, $^3J_{\text{HH}} = 8.1$, C^1H or C^2H or C^4H), 6.44 (2H, dd, $J = 7.7$, $J = 4.8$, C^1H or C^2H or C^4H), 6.91 - 7.00 (4H, m, $\text{C}^{10}\text{H} + \text{C}^1\text{H}$ or C^2H or C^4H), 7.17 (4H, t, $^3J_{\text{HH}} = 7.6$, C^9H), 7.64 (4H, d, $^3J_{\text{HH}} = 6.9$, C^8H). ^{31}P NMR (161 MHz, THF- d_8) δ : + 39.1.

Reaction of **14o** with [(i-Pr₂N)₂P][OTf] in a Young's NMR tube

To a mixture of **14o** (21 mg, 0.05 mmol) and [(i-Pr₂N)₂P][OTf] (19 mg, 0.05 mmol) was added CD₂Cl₂ (0.8 mL). ^{31}P NMR spectroscopy showed signals at 140 and 61 ppm.

Attempted reaction of **13o/13c** and TEMPO

TEMPO (10 mg, 0.064 mmol) was added to a solution of **13o/13c** (26 mg, 0.064 mmol) in C₆D₆ (0.8 mL) in a Young's NMR tube. The mixture was heated to 70 °C for 18 h. No change was observed in colour or by ^{31}P NMR spectroscopy.

Reaction of [Fc][PF₆] and **13o/13c** in a Young's NMR tube

[Fc][PF₆] (15 mg, 0.045 mmol) was added to a solution of **13o/13c** (19 mg, 0.045 mmol) in CD₂Cl₂ (0.8 mL) in a Young's NMR tube. The addition produced a green solution and precipitate. ^{31}P NMR spectroscopy showed peaks at 52 (80 %) and 33 (20 %) ppm in addition to hexafluorophosphate signals. After 24 h standing the peak at 33 ppm was observed to increase in magnitude (to 50 %).

Reaction of **16** with phenyliodine bis(trifluoroacetate) (PIFA) in a Young's NMR tube

A Young's NMR tube was charged with PIFA (14 mg, 0.032 mmol), **16** (31.5 mg, 0.065 mmol), CH₂Cl₂ (0.8 mL) and a C₆D₆ lock tube. Analysis by ^{31}P NMR spectroscopy, after 1 h

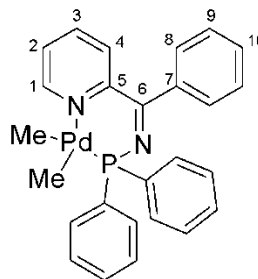
standing, revealed a peak at 52.3 ppm (80 %) with minor peaks between 40 and 60 ppm. After 4 d the ^{31}P NMR spectrum showed the reaction had progressed, showing two major peaks at 206.8 ppm (50 %) and 46.3 ppm (30 %).

Reaction of **13o/13c** with two equivalents of **[Fc][OTf]**

To a solution of **13o/13c** (70 mg, 0.34 mmol) and lutidine (20 mg, 0.34 mmol) was added **[Fc][OTf]** (114 mg, 0.70 mmol). A rapid colour change to green was observed. Removal of the volatile components under reduced pressure gave a dark precipitate, which was washed with Et_2O and then H_2O . The black residue was dissolved in CH_2Cl_2 but attempts to detect a signal by ^{31}P NMR spectroscopy were unsuccessful.

7.7. Synthesis and reactivity of palladium dimethyl and palladium(0) species

Diphenylphosphino (phenyl pyridin-2-yl methylene) amine palladium dimethyl: **[PdMe₂(2IP-PPh₂)]**: **26**



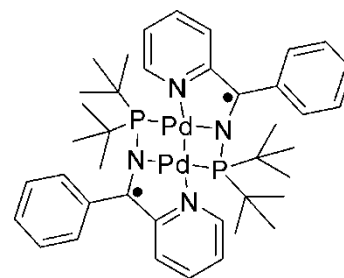
The compounds **2IP-PPh₂** (217 mg, 0.595 mmol) and **[PdMe₂(TMEDA)]** (150 mg, 0.595 mmol) were each dissolved in the minimum of toluene and combined. The resulting reddish-orange solution precipitated an orange solid on standing. The toluene solution was removed by filtration and the solid washed with cold toluene before drying *in vacuo*

(305 mg, 61 %). Orange crystals suitable for an X-ray structure determination were grown by cooling a saturated toluene solution to -30 °C.

NB: The complex is only stable for a few hours in solution at ambient temperature.

^1H NMR (399.97 MHz, C_6D_6) δ : 1.22 (3H, d, $^3J_{\text{PH}} = 8.8$, Pd-CH₃ {*cis*}), 1.44 (3H, d, $^3J_{\text{PH}} = 7.2$, Pd-CH₃ {*trans*}), 6.13 (1H, d, 7.6, C⁴H), 6.36 (1H, m, C²H), 6.43 (1H, td, $J_{\text{HH}} = 7.6$, $J_{\text{HH}} = 2.0$, C³H), 6.95 (8H, m, aromatic protons), 7.08 (1H, tt, $^3J_{\text{HH}} = 7.6$, $J_{\text{HH}} = 1.2$, C¹⁰H), 7.42 (2H, d, 8.5, aromatic proton), 7.68 (4H, t, 9.0, {*m*-C₆H₅}₂P), 9.13 (1H, dd, $^3J_{\text{HH}} = 5.2$, $^4J_{\text{HH}} = 1.2$, C¹H). ^{13}C { ^1H } NMR (175.95 MHz, CD_2Cl_2) δ : -8.9 (d, $^2J_{\text{PC}} = 5.5$, Pd-CH₃ {*cis*}), 7.2 (d, $^2J_{\text{PC}} = 115.2$, Pd-CH₃ {*trans*}), 125.9 (s, C⁴), 127.0 (s, C²), 128.7 (d, $J = 9.0$, aromatic carbon), 128.9 (s, aromatic carbon), 129.9 (s, aromatic carbon), 130.3 (d, $J = 2.1$, aromatic carbon), 132.2 (s, C¹⁰), 132.7 (d, $J = 14.4$, {*o*-C₆H₅}₂P), 136.1 (d, 31.3, {*i*-C₆H₅}₂P), 138.2 (s, C³), 140.1 (d, $^3J_{\text{PC}} = 12.3$, C⁵ or C⁷), 151.0 (d, $^3J_{\text{PC}} = 11.6$, C⁵ or C⁷), 152.1 (s, C¹), 174.7 (d, $J = 2.0$, C⁶). ^{31}P { ^1H } NMR (161.91 MHz, C_6D_6) δ : + 63.4 (s). MS (FAB⁺) m/z : 487 (M-Me)⁺. *Anal.* Found: C, 61.92; H, 5.06; N, 5.49 %. Calc. C, 62.10; H, 5.01; N, 5.57 %.

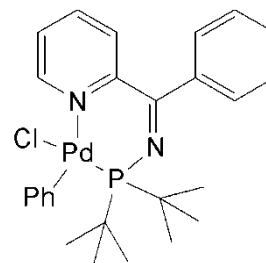
Synthesis of complex [$\{\kappa^2\text{-}N,N\text{-}\kappa^1\text{-}P\text{-}2\text{o-Pd}\}_2$], 27



To [PdMe₂(TMEDA)] (173 mg, 0.69 mmol) was added **2o** (224 mg, 0.69 mmol) and C_6D_6 (10 mL) and the dissolved mixture allowed to stand for 19 d. Dark crystals formed which were isolated by filtration, washed with benzene (3 x 2 mL) and dried *in vacuo* (24 h), giving a dark solid (217 mg, 73 %). Single crystals suitable for an X-ray structure determination study were grown using this technique.

^{31}P Direct Polarisation MAS NMR (161.83 MHz) δ : - 338.2 *Anal.* Found: C, 55.70; H, 6.24; N, 6.47 % Calc. C, 55.50; H, 6.29; N, 6.61 %.⁺⁺⁺

Ditertiarybutylphosphino(phenyl pyridin-2-yl methylene) amine)palladium phenyl chloride: 28

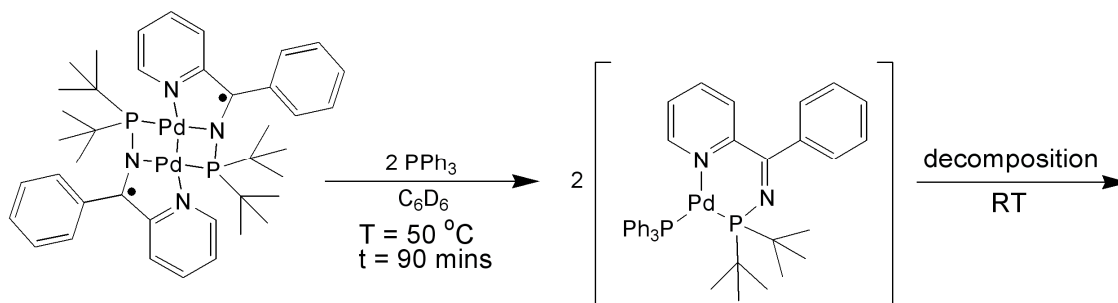


A Young's tap NMR tube was charged with **17** (18 mg, 0.021 mmol) and chlorobenzene (1 mL) added. The tube was warmed to 50 °C for 2 h during which time a colour change from a brown suspension to a light yellow solution was observed. The solvent was removed under reduced pressure and dried *in vacuo* for 12 h.

^1H NMR (699.73 MHz, CDCl_3) δ : 1.09 (18H, d, $^3J_{\text{PH}} = 14.7$, CH_3), 6.87 (1H, t, $^3J_{\text{HH}} = 6.8$, aromatic proton), 7.00 (2H, t, $^3J_{\text{HH}} = 7.3$, aromatic protons), 7.44 - 7.50 (4H, m, aromatic protons), 7.53 (1H, d, $^3J_{\text{HH}} = 7.0$, C^4H), 7.56 - 7.62 (2H, m, aromatic protons), 7.67 (2H, d, $^3J_{\text{HH}} = 7.0$, C^8H), 7.90 (1H, td, $^3J_{\text{HH}} = 7.6$, $^4J_{\text{HH}} = 1.7$, C^3H), 10.25 (1H, d, $^3J_{\text{HH}} = 5.6$, $^4J_{\text{HH}} = 1.3$, C^1H). ^{13}C $\{^1\text{H}\}$ NMR (175.95 MHz, CDCl_3) δ : 28.9 (d, $^2J_{\text{PC}} = 3.8$, CH_3), 40.8 (d, $^1J_{\text{PC}} = 22.6$, CCH_3), 123.5 (s, aromatic carbon), 127.3 (s, aromatic carbon), 127.5 (d, $J = 1.4$, aromatic carbon), 127.6 (s, aromatic carbon), 128.9 (s, aromatic carbon), 129.9 (s, C^8), 131.4 (d, $^2J_{\text{PC}} = 42.6$, $\text{Pd}(i\text{-C}_6\text{H}_5)$), 132.1 (s, C^{10}), 138.7 (s, C^3), 139.9 (d, $^3J_{\text{PC}} = 13.3$, C^7), 140.5 (s, aromatic carbon), 146.6 (d, $^3J_{\text{PC}} = 8.9$, C^5), 155.9 (s, C^1), 175.7 (d, $^2J_{\text{PC}} = 6.9$, C^6). ^{31}P $\{^1\text{H}\}$ NMR (80.96 MHz, CDCl_3) δ : + 97.3 (s). MS (EI^+) m/z : 469 (M-Ph^+), 432 (M-Ph-Cl^+).

⁺⁺⁺ Attempts to characterise this compound by mass spectrometry were unsuccessful

Reaction of **27 with two equivalents of PPh₃ to give the unstable species [(Ph₃P)Pd(κ^2 -P,N-2o)], **29****



A Young's NMR tube was charged with **27** (10 mg, 0.012 mmol), PPh₃ (6 mg, 0.024 mmol) and C₆D₆ (0.8 mL). The tube was warmed at 50 °C for 30 minutes giving a brown solution.

³¹P {¹H} NMR (161.91 MHz, C₆D₆) δ: 26.7 (1P, d, ²J_{PP} = 140), 106.6 (1P, d, ²J_{PP} = 140) 80%, 97.4 (s) 7%, 23.8 (s) 13%.

Reaction of **27 with CH₂Cl₂**

Compound **27** (15 mg, 0.018 mmol) and CH₂Cl₂ (1 mL) were added to a Young's NMR tube and the mixture heated to 50 °C for 1 h. The ³¹P {¹H} NMR spectrum showed a single peak at 111.5 ppm, which has been attributed to the possible formation of **8**. Attempts to grow crystals from the solution were unsuccessful.

Thermolysis of **27 in C₆D₆**

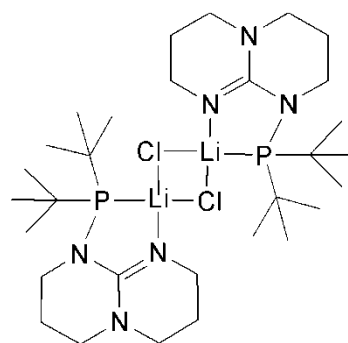
A Young's tap NMR tube was charged with **27** (10 mg, 0.011 mmol) in deuterated benzene (0.8 mL) and placed in an oil-bath pre-heated to 80 °C. After 3 h ³¹P {¹H} NMR spectroscopy revealed the formation of **29** with no residual solid **27** observed. A further 6 h of heating yielded deposition of palladium black and ³¹P {¹H} spectroscopy showed the only phosphorus containing compound to be free ligand.

Reaction of [PdMe₂(TMEDA)], **2o** and PhCl

[PdMe₂(TMEDA)] (216 mg, 0.856 mmol) and **2o** (280 mg, 0.856 mmol) were combined in a dry box and chlorobenzene (5 mL) added. Heating at 50 °C for 2 h yielded an orange solution, which ³¹P {¹H} NMR spectroscopy revealed to comprise two phosphorus environments at 104.2 ppm (55 %) and 96.4 ppm (45 %). Continued heating, for a further 2 h, caused the precipitation of a yellow solid, which dissolved following addition of further chlorobenzene (15 mL). ³¹P {¹H} NMR spectroscopy showed the ratio of products unchanged by the additional warming. Concentration of the solution gave a crystalline solid which was found to be unsuitable for X-ray structure determination. The reaction was discontinued as the products were believed to be **8** and **28**, better described as [PdCl₂(**2o**)] and [PdCl(Ph)(**2o**)] respectively, that have been previously characterised.

7.8. Additional reactions

Synthesis of [{κ²-*N,P*-hppP(*t*-Bu₂)}{LiCl}]₂

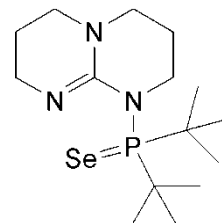


To a cooled (-78 °C) suspension of hppH (1.00 g, 7.18 mmol) in Et₂O (40 mL) was added *n*-BuLi (1.6 M, 4.49 mL, 7.18 mmol) and allowed to warm to room temperature with stirring. After recooling (-78 °C) a solution of *t*-Bu₂PCl (1.30 g, 7.18 mmol) in DME (10 mL) was added and the mixture stirred overnight. The volatile components were removed under reduced pressure and 1,4-dioxane added and the suspension heated (100 °C) for 90 h. Evaporation of the volatile components under reduced pressure gave a

solid which was washed with hexane (80 mL) before addition of CH_2Cl_2 (60 mL). The solution was filtered, the volatile components removed under reduced pressure and the residue recrystallised from MeCN/Et₂O (351 mg, 15 %).

Anal. Found: C, 55.21; H, 9.26; N, 12.95 %. Calc. C, 55.30; H, 9.28; N, 12.90 %.

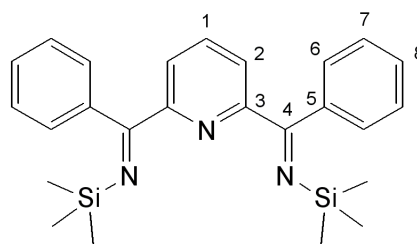
hppP(=Se)t-Bu₂



A Youngs NMR tube was charged with grey Se (58 mg, 0.73 mmol) and a solution of [{hppP(t-Bu)₂}{LiCl}]₂ (29 mg, 0.10 mmol) in CDCl₃ (0.8 mL) added to give a light yellow solution above a black solid. After standing for 24 h complete conversion to the selenide derivative was confirmed by ³¹P NMR spectroscopy.

³¹P {¹H} NMR (80.96 MHz, CDCl₃) δ : + 123.5 (s + satellites, ¹J_{SeP} = 715)

2,6-Bis(trimethylsilyl iminophenyl)pyridine



To a stirred, cooled (-78 °C) solution of dried 2,6-dicyanopyridine (400 mg, 3.1 mmol) in dimethoxyethane (40 mL) was added dropwise phenyllithium (1.8 M in dibutylether, 3.43 mL, 6.2 mmol) and the mixture stirred for 1 h, giving a dark red solution. Trimethylsilyl chloride (0.79 mL, 6.2 mmol) was added dropwise and the mixture allowed to warm to room temperature and stirred for 22 h. The volatile components were removed under reduced pressure, hexane (400 mL) added and the resulting

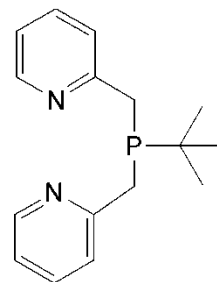
solution filtered. Removal of the solvent under reduced pressure gave a yellow oil (1.076 g, 85 %).

^1H NMR (400.13 MHz, C_6D_6) δ : 0.11 (18H, s, CH_3), 7.04 - 7.10 (7H, m, aromatic protons), 7.40 (2H, d, $^3J_{\text{HH}} = 7.6$, aromatic protons), 7.56 - 7.60 (4H, m, aromatic protons). ^{13}C $\{^1\text{H}\}$ NMR (100.61 MHz, C_6D_6) δ : 1.5 (s, CH_3), 123.0 (s, aromatic carbon), 128.5 (s, aromatic carbon), 129.5 (s, aromatic carbon), 130.3 (s, aromatic carbon), 136.7 (s, aromatic carbon), 141.7 (s, C^5), 158.7 (s, C^3), 174.0 (s, C^4).

Reaction of 2,5-bis(2-pyridyl)phosphole with $[\text{PdMe}_2(\text{TMEDA})]$

2,5-Bis(2-pyridyl)phosphole^{†††} (30 mg, 0.081 mmol) was dissolved in deuterated benzene (0.8 mL) and was added to Young's tap NMR tube. $[\text{PdMe}_2(\text{TMEDA})]$ (21 mg, 0.081 mmol) was added to the tube and the reaction monitored by ^{31}P $\{^1\text{H}\}$ NMR spectroscopy. Within 3 h a single peak at 42 ppm was observed which transformed over 72 h to give a brown precipitate and a major peak at 11.2 ppm (indicative of free ligand) and two minor peaks at 52.3 and 52.8 ppm. Attempts to recrystallise the brown precipitate were unsuccessful.

Synthesis of dipicolyltertiarybutylphosphane: $(\text{pyCH}_2)_2\text{P}(\text{t-Bu})$



The reagent t-BuPCl_2 (2.07 g, 13 mmol) is dissolved in diethyl ether (50 mL) and added dropwise to a stirred suspension of $[\text{PyCH}_2\text{Li.PyCH}_3]$ (5.0 g, 26 mmol) in diethyl ether

^{†††} Synthesised by the group of Prof. R. Réau using the method reported; C. Hay, D. Le Vilain, V. Deborde, L. Toupet, R. Réau, *Chem. Commun.*, **1999**, 345.

(100 mL) at -78 °C. The mixture stirred for an hour before warming to room temperature. The volatile components were removed under reduced pressure, CH₂Cl₂ (60 mL) added and the resultant mixture filtered to give a light orange solution. The CH₂Cl₂ was removed by reduced pressure to yield an orange viscous liquid (2.3 g, 65 %).

¹H NMR (400 MHz, C₆D₆) δ: 1.03 (9H, d, ³J_{PH} = 11.4, CH₃), 3.10 (2H, d, ²J_{PH} = 13.2, PCH₂), 3.33 (2H, d, ²J_{PH} = 12.8, PCH₂'), 6.50-6.56 (2H, m, C⁴H), 6.94-6.96 (4H, m, C⁴H + C³H), 8.51 (2H, d, ³J_{HH} = 4.8, C⁶H). ¹³C {¹H} NMR (100 MHz, C₆D₆) δ: 28.1 (d, ²J = 14.0, CH₃), 29.7 (d, ¹J = 17.0, CCH₃), 35.2 (d, ¹J = 24.9, CH₂), 121.1 (d, ⁴J_{PC} = 1.5, C⁴), 124.4 (d, ³J_{PC} = 6.6, C³), 136.3 (s, C⁵), 150.1 (s, C⁶), 161.5 (d, ²J_{PC} = 9.8, C²). ³¹P {¹H} NMR (202.31 MHz, C₆D₆) δ: + 15.3.

[Ni₂{κ³-N,P,N-(pyCH₂)₂P(t-Bu)}₂Br₆]₂⁺[NiBr₄]₂²⁻

A solution of dipicolyl-t-butylphosphane (328 mg, 1.21 mmol) in CH₂Cl₂ (5 mL) is added to a suspension of [NiBr₂(DME)] (373 mg, 1.21 mmol) and stirred for 2 d. Additional CH₂Cl₂ (10 mL) was added, the solution filtered and the volatiles removed under reduced pressure. The residue was washed with hexane to give a grey solid. Recrystallisation from MeCN gave a green microcrystalline solid (232 mg, 44 %). Single crystals suitable for an X-ray diffraction study were grown by cooling a saturated MeCN solution. Although the data from the X-ray diffraction study was poor, it did allow the connectivity to be established as [Ni₂{κ³-N,P,N-(pyCH₂)₂P(t-Bu)}₂Br₆]₂⁺[NiBr₄]₂²⁻ with seven accompanying molecules of MeCN. MS (nano-ESI⁺) m/z: 901 ([Ni₂{κ³-N,P,N-(pyCH₂)₂P(t-Bu)}₂Br₆]⁺).

¹ J. Wesemann, P. G. Jones, D. Schomburg, L. Heuer, R. Schmutzler, *Chem. Ber.*, 1992, **125**, 2187.

² J. J. H. Edema, W. Stauthamer, F. van Bolhuis, S. Gambarotta, W. J. J. Smeets, A. L. Speks, *Inorg. Chem.*, 1990, **29**, 1302.

-
- ³ J. A. McCleverty, G. Wilkinson, *Inorg. Synth.*, 1966, **8**, 211.
- ⁴ S. Komiya, "Synthesis of Organometallic Compounds – A Practical Guide", Wiley-Interscience, New York, 1998.
- ⁵ W. de Graaf, J. Boersma, W. J. J. Smeets, A. L. Speck, G. van Koten, *Organometallics*, 1989, **8**, 2907.
- ⁶ W. Kaschube, K. R. Pörschke, G. Wilke, *J. Organomet. Chem.*, 1988, **355**, 525.
- ⁷ G. E. Coates, J. A. Heslop, *J. Chem. Soc. (A)*, 1966, 26.
- ⁸ P. W. Dyer, J. Fawcett, M. J. Hanton, *J. Organomet. Chem.*, 2005, **690**, 5264.
- ⁹ M. R. Mazieres, C. Roques, M. Sanchez, J. P. Majoral, R. Wolf, *Tetrahedron*, 1987, **43**, 2109.
- ¹⁰ B. L. Small, M. Brookhart, A. M. A. Bennett, *J. Am. Chem. Soc.*, 1998, **120**, 4049.
- ¹¹ M. S. Anson, C. McGuigan, *Perkin Trans.*, 1989, 715.
- ¹² From J. M. Kliegman and R. K. Barnes, *J. Org. Chem.*, 1970, **35**, 3140.
- ¹³ H. Gilman, S. M. Spatz, *J. Org. Chem.*, 1951, **16**, 1485.
- ¹⁴ R. Fischer, B. Nestler, H. Schütz, *Z. anorg. allg. Chem.*, 1989, **577**, 111.
- ¹⁵ J. Langer, R. Fischer, H. Görls, D. Walther, *J. Organomet. Chem.*, 2004, **689**, 2952.
- ¹⁶ H. Werner, W. Bertleff, U. Schubert, *Inorg. Chim. Acta.*, 1980, **43**, 199.
- ¹⁷ Y. H. Kim, T. H. Kim, N. Y. Kim, E. S. Cho, B. Y. Lee, D. M. Shin, Y. K. Chung, *Organometallics*, 2003, **22**, 1503.
- ¹⁸ M. Kawatsura, J. F. Hartwig, *Organometallics*, 2001, **20**, 1960.
- ¹⁹ R. B. King, N. D. Sadanani, P. M. Sundaram, *Chem. Commun.*, 1983, 477.
- ²⁰ Z-W. Li, A. Yeh, H. Taube, *Inorg. Chem.*, 1994, **33**, 2874.
- ²¹ J. R. Doyle, D. Drew, *Inorg. Synth.*, 1966, **8**, 211.
- ²² S. Budavari, M. J. O'Neil, A. Smith, P. E. Heckelman, *The Merck Index*, an Encyclopedia of Chemicals, Drugs, and Biologicals - Eleventh Edition, Merck Co., Inc. Rahway, NJ, 1989.
- ²³ N. G. Connelly, W. E. Geiger, *Chem. Rev.*, 1996, **96**, 877
- ²⁴ S. Rigaut, J. Perruchon, S. Guesmi, C. Fave, D. Touchard, P. H. Dixneuf, *Eur. J. Inorg. Chem.*, 2005, 447.
- ²⁵ M. Krejčík, M. Daněk, F. Hartl, *J. Electroanal. Chem.*, 1991, **317**, 179.
- ²⁶ M. A. Fox, R. L. Roberts, W. M. Khairul, F. Hartl, P. J. Low, *J. Organomet. Chem.*, 2007, **692**, 3277.

Appendix I: Crystallographic data

X-ray diffraction experiments were carried out by Dr A. Batsanov (Durham University) on Bruker 3-circle diffractometers with CCD area detectors SMART 1K (**13c**), SMART 6K (**10**, **11**, **12**, **15**, **16**, **18c**, *trans*-**20**, *trans*-**23**, **26**, **27**) or a Siemens 3-circle diffractometers with CCD area detector SMART 1K (**7**) using graphite-monochromated Mo- K_α radiation ($\lambda = 0.71073 \text{ \AA}$) and Cryostream (Oxford Cryosystems) open-flow N₂ cryostats. A full sphere of the reciprocal space was covered with narrow-frame (0.3°) ω scans. Absorption corrections by numerical integration based on crystal face-indexing were applied for **13c**.¹ The structures were solved by direct methods and refined by full-matrix least squares against F^2 of all reflections, using SHELXTL software.² The absolute structure of **16** was determined from anomalous scattering by the Flack method.³

¹ G. M. Sheldrick, *SADABS* 2006/1, AXS, Madison WI, USA.

² G. M. Sheldrick, *SHELXTL*, version 6.14, Bruker AXS, Madison WI, USA, 2003.

³ H. D. Flack, *Acta Crystallogr. Sect. A*, **1983**, 39, 876.

Compound	7	10	11
CCDC dep. No.	n/a	n/a	n/a
Empirical formula	C _{28.5} H ₂₁ Cl _{12.5} D _{3.5} N ₂ PPd	C ₂₅ H ₃₃ Cl ₄ N ₂ PPd	C ₃₅ H ₂₃ Cl ₁₁ D ₃ N ₂ PPd
Formula weight	979.02	640.70	1004.92
T, K	120	120	120
Crystal system	Monoclinic	Monoclinic	Triclinic
Space group (No.)	<i>P</i> 2 ₁ / <i>c</i>	<i>P</i> 2 ₁ / <i>c</i>	<i>P</i> -1
<i>a</i> , Å	11.2142(13)	9.0547(6)	9.389(1)
<i>b</i> , Å	13.0562(15)	23.1623(18)	12.511(1)
<i>c</i> , Å	26.365(3)	12.9068(10)	17.570(2)
α , °	90	90	75.33(1)
β , °	98.66(1)	98.60(3)	88.80(1)
γ , °	90	90	86.76(1)
<i>V</i> , Å ³	3816.2(8)	2676.5(3)	1993.4(3)
<i>Z</i>	4	4	2
ρ (calc.), g/cm ³	1.704	1.590	1.674
μ (Mo- <i>K</i> α), mm ⁻¹	1.428	1.170	1.273
Reflections collected	46169	43025	31150
Independent reflections	10877	7795	13743
<i>R</i> (int)	0.034	0.050	0.051
<i>R</i> [<i>I</i> > 2 σ (<i>I</i>)]	0.028	0.031	0.040
w <i>R</i> (<i>F</i> ²) [all data]	0.063	0.069	0.098

Compound	12	13c	15
CCDC dep. No.	n/a	686754	686755
Empirical formula	C _{33.5} H ₃₈ Cl ₉ N ₂ PPd	C ₂₄ H ₃₇ N ₄ P	C ₃₁ H ₄₃ ClN ₄ OPRh
Formula weight	925.08	412.55	657.02
T, K	120	120	120
Crystal system	Monoclinic	Monoclinic	Monoclinic
Space group (No.)	<i>I</i> -2/a	<i>P</i> 2 ₁ / <i>c</i> (#14)	<i>P</i> 2 ₁ / <i>c</i> (#14)
<i>a</i> , Å	15.6325(8)	9.819(1)	16.015(1)
<i>b</i> , Å	21.7026(11)	15.814(2)	12.313(1)
<i>c</i> , Å	23.7451(13)	15.434(2)	16.129(1)
α , °	90	90	90
β , °	98.05(3)	103.25(1)	98.26(1)
γ , °	90	90	90
<i>V</i> , Å ³	7976.5(7)	2332.7(4)	3147.5(4)
<i>Z</i>	8	4	4
ρ (calc.), g/cm ³	1.541	1.175	1.387
μ (Mo-K α), mm ⁻¹	1.14	0.14	0.71
Reflections collected	50414	19524	31940
Independent reflections	10630	5350	9186
R(int)	0.063	0.136	0.049
R [<i>I</i> > 2 σ (<i>I</i>)]	0.057	0.081	0.036
wR(<i>F</i> ²) [all data]	0.168	0.142	0.084

Compound	16	18c	<i>trans</i> - 20
CCDC dep. No.	686756	n/a	n/a
Empirical formula	C ₂₇ H ₄₆ AlN ₄ P	C ₃₈ H ₅₅ N ₄ P	C ₁₄ H ₁₃ N ₂ O ₂ P
Formula weight	484.63	598.83	272.23
T, K	120	120	120
Crystal system	Orthorhombic	Rhombohedral	Monoclinic
Space group (No.)	<i>P</i> 2 ₁ 2 ₁ 2 ₁ (#19)	<i>R</i> -3	<i>P</i> 2 ₁ /n
<i>a</i> , Å	9.797(1)	27.065(3)	10.6599(6)
<i>b</i> , Å	16.105(1)	27.065(3)	9.6642(5)
<i>c</i> , Å	17.788(2)	24.318(3)	12.2985(7)
α , °	90	90	90
β , °	90	90	100.34(1)
γ , °	90	120	90
<i>V</i> , Å ³	2806.7(5)	15427(3)	1246.41(12)
<i>Z</i>	4	18	4
ρ (calc.), g/cm ³	1.147	1.160	1.451
μ (Mo- <i>K</i> α), mm ⁻¹	0.15	0.11	0.22
Reflections collected	38836	31694	22264
Independent reflections	8202	6050	3637
R(int)	0.025	0.108	0.022
R [<i>I</i> > 2 σ (<i>I</i>)]	0.028	0.045	0.033
wR(<i>F</i> ²) [all data]	0.076	0.101	0.096

Compound	<i>trans</i> - 23	26	27
CCDC dep. No.	686757	723960	723961
Empirical formula	C ₅₂ H ₇₆ Cl ₄ F ₆ N ₈ O ₆ P ₂ S ₂	C ₃₃ H ₃₃ N ₂ PPd	C ₆₄ H ₅₄ D ₂₄ N ₄ PPd ₂
Formula weight	1291.07	594.98	1202.19
T, K	120	120	120
Crystal system	Monoclinic	Monoclinic	Triclinic
Space group (No.)	<i>P</i> 2 ₁ / <i>c</i>	<i>P</i> 2 ₁ / <i>n</i>	<i>P</i> -1
<i>a</i> , Å	9.6074(15)	11.566(1)	9.8593(5)
<i>b</i> , Å	17.592(3)	12.739(1)	10.9831(6)
<i>c</i> , Å	18.132(3)	19.727(3)	15.2350(8)
α , °	90	90	73.152(2)
β , °	90.94(2)	106.30(1)	78.824(2)
γ , °	90	90	63.602(3)
<i>V</i> , Å ³	3064.1(8)	2789.7(5)	1410.22(13)
<i>Z</i>	2	4	1
ρ (calc.), g/cm ³	1.399	1.417	1.416
μ (Mo- <i>K</i> α), mm ⁻¹	0.385	0.747	0.738
Reflections collected	35703	36010	24536
Independent reflections	5392	8136	11518
R(int)	0.069	0.057	0.061
R [<i>I</i> > 2 σ (<i>I</i>)]	0.051	0.032	0.041
wR(<i>F</i> ²) [all data]	0.147	0.074	0.080

Appendix II: Postgraduate first year modules

PhD students are required to pass an academic lecture-based module in their first year.

Macromolecular chemistry: 76 % - pass

Appendix III: Colloquia attended

Prof. John Kelly, Trinity College Dublin,

"Photochemical and Photophysical probes for DNA"

Prof. Harry Anderson, University of Oxford,

"Some Recent Experiments with Molecular Wires - Organic Synthesis to Photophysics"

Prof. Odile Eisenstein, University of Montpellier, France,

"Simple Ideas for d(0) Olefin Metathesis Catalyst Design from a DFT Perspective"

Prof. Michael Bruce, University of Adelaide,

"Carbon-rich Complexes—Some Recent Results"

Prof. Mike Turner, University of Manchester,

"Organic Materials for Electronics - ROMP as a route to polyphenylvinylenes"

Prof. Guy Lloyd-Jones, Bristol University,

"Mechanistic studies of metal-mediated processes"

Prof. Dame Louise Johnson, University of Oxford and Diamond Light Source,
"The Diamond Light Source: Implications for UK research and some recent results on structural studies on cell cycle regulatory proteins"

Prof. Donna Blackmond, Imperial College,
"Exploring the Origin of Biological Homochirality: How Catalysis May Have Played a Role"

Dr. Michael Whittlesey, University of Bath,
"N-Heterocyclic carbenes: far from inert ligands"

Prof. Richard Catlow, The Royal Institution of Great Britain,
"Computer Modelling and Synchrotron Radiation Studies of Complex Materials"

Prof. Guy Bertrand, UCR-CNRS Joint Research Laboratory, University of California, Riverside, USA
"New Families of Stable Cyclic Carbenes for the Preparation of Low Ligated Transition Metals, and Highly Active Catalysts. Can a Carbene do the Job of a Metal?"

Dr. Ian Lennon, Dow Pharma, Chirotech Technology Ltd.,
"Pharmaceutical Applications of Asymmetric Hydrogenation."

Prof. C. N. R. Rao, Jawaharlal Nehru Centre for Advanced Scientific Research, Bangalore, India,
"New Chemistry with Nanomaterials"

Prof. Régis Réau, Université de Rennes 1, France,
"Organophosphorus pi-conjugated systems: From model molecules to functional materials"

Prof. Régis Réau, Université de Rennes 1, France,
"Controlled organisation of pi-conjugated systems using coordination chemistry"

Prof. Martin Bryce, Durham University,

"New Functional π -Electron Systems and their Optoelectronic Applications"

Prof. Malcolm Chisholm, Ohio State University, USA

"Linking MM Quadruple Bonds (M = Mo or W) with Organic π -Systems: Studies of Mixed Valency and $M_2\delta$ - π Conjugation"

Prof. Jonathan Clayden, University of Manchester,

"Flat-Packed Stereochemistry: Aromatic Compounds in Three Dimensions"

Dr. Richard Layfield, University of Manchester,

"Organometallic Chemistry with Manganese(II): a Transition Metal Masquerading as a Main Group Element"

Dr. Stuart Mackenzie, Cambridge University,

"Shining Light on the Effects of Geometrical Structure on the Reactivity of Small Transition Metal Clusters"

Prof. Kalman Szabo, Stockholm University, Sweden

"One-Pot Transformations Involving Catalytic Generation of Allyl Boronates"

Prof. Uwe Bunz, Department of Chemistry, Georgia Tech, USA,

"Cruciform Fluorophores"

Prof. Dr. Manfred Scheer, University of Regensburg, Germany,

"Complexed Main Group-Congeners of Hydrocarbons in Molecular and Supramolecular Environments"

Dr. Chris Russell, Bristol University,

"Novel Structure, Bonding and Reactivity for Pnictogens in Low Coordinate Environments ? Is Phosphorus a Carbon Copy?"

Prof. Todd Marder, University of Durham,

"Metal Catalysed Synthesis of Retinoids for Stem Cell Differentiation Including Applications of Novel C-H Bond Functionalisation Processes"

Prof. Stuart Macgregor, Heriot Watt University,

"Computational studies on bond activation reactions at transition metal centres"

Prof. Penny Brothers, University of Auckland, New Zealand,

"Diboron Porphyrins and Corroles: Unexpected Chemistry for Both Boron and the Ligands"

Prof. T. Don Tilley, University of California, Berkeley, USA,

"New Bond Activations at Transition Metal Centres: Fundamental Studies and Applications to Catalysis"

Dr. Polly Arnold, University of Edinburgh,

"Controlled Reduction and Activation Reactions in Organometallic f-block Complexes"

Appendix IV: Presentations and publications

Presentations at external conferences

Confused P-N Heterocycles: 5th European Workshop on Phosphorus Chemistry, March 10 - 11th, 2008 at University of Regensburg, Regensburg, Germany. Award for Presentation.

Confused P-N Compounds: Universities of Scotland Inorganic Chemistry Conference, September 11 - 12th, 2008 at University of Strathclyde, Glasgow, UK.

From Inorganic Heterocycles To Organophosphorus-based π -Conjugated Systems: 6th European Workshop on Phosphorus Chemistry, March 26 - 27th, 2009 at University of Florence, Florence, Italy.

N-Phosphino-pyridyl Imines: Flexible, Multi-functional Reagents: 6th Main Group Chemistry, A Royal Society of Chemistry Dalton Division Meeting, September 11th 2009, University of Manchester, Manchester, UK. Award for presentation.

Poster presentations at external conferences

Confused P-N Heterocycles : 23rd ICOMC, July 13 - 18th, at University of Rennes 1, Rennes, France. Poster prize awarded by the "Royal Australian Chemical Institute in recognition of innovative work at the Interface of Transition Metal and Main Group Organometallic Chemistries"

Publications

A Truly Multifunctional Heterocycle: Iminophosphorane, N,P Chelate, and Dihyrdopyridine : Dan A. Smith, Andrei S. Batsanov, Karinne Miqueu, Jean-Marc Sotiropoulos, David C. Apperley, Judith A. K. Howard and Philip W. Dyer, *Angewandte Chemie International Edition*, 2008, **47**, 8674.

From Cyclic Iminophosphoranes to π -Conjugated Materials :

Dan A. Smith, Andrei S. Batsanov, Mark A. Fox, Andrew Beeby, David C. Apperley, Judith A. K. Howard and Philip W. Dyer, *Angewandte Chemie International Edition*, in the press, DOI: 10.1002/anie.200904219.

Appendix V: Magnetic susceptibility measurements and analyses

All magnetic data were recorded on a Johnson-Matthey-Evans magnetic susceptibility balance with data for complex **27** recorded under an inert atmosphere.

Table 1: Recorded masses

	Mass (g)
Tube	1.4450
Tube + parafilm	1.5036
Tube + parafilm + standard	1.6713
Tube + standard	1.6129
Tube + complex 27 + parafilm	1.5498
Standard	0.1679
Complex 27	0.0462

Table 2: Johnson-Matthey-Evans magnetic susceptibility balance readings

	Magnetic reading	Length of sample in tube (metres)
Tube	- 40	N/A
Tube + standard	1038	0.035
Tube + Complex 27	- 33	0.019

χ_g for the standard = $4.059 \times 10^{-7} \text{ m}^3 \text{ mol}^{-1}$ where the standard is $[(\text{NH}_4)_2\text{Fe}(\text{SO}_4)_2 \cdot 6\text{H}_2\text{O}]$

Equation (1)
$$\chi_g = \frac{C \cdot L \cdot (R - R_0)}{m \cdot 10^{-7}}$$

Equation (2)
$$C = \frac{\chi_g \cdot m \cdot 10^7}{L \cdot (R - R_0)}$$
 Equation (3)

$$\chi_m = \chi_g \cdot \text{MW}$$

χ_g = mass susceptibility ($\text{m}^3 \text{ Kg}^{-1}$)

C = calibration factor

L = length of sample in tube (metres)

χ_m = molar susceptibility ($\text{m}^3 \text{ mol}^{-1}$)

m = mass of sample (Kg)

R = magnetic reading of sample and tube

R_0 = magnetic reading of tube

MW = molecular weight of complex **27** (Kg)

By use of equations (1), (2) and (3) the calibration factor, the observed mass susceptibility and the observed molar susceptibility for complex **27** could be calculated.

$$C = 1.81 \times 10^{-5}$$

$$\chi_g \text{ for complex } \mathbf{27} = 5.20 \times 10^{-9} \text{ m}^3 \text{ Kg}^{-1}$$

$$\chi_m \text{ for complex } \mathbf{27} = 4.50 \times 10^{-9} \text{ m}^3 \text{ mol}^{-1}$$

The observed molar susceptibility is a measure of the magnetism of a sample but arises from paramagnetic and diamagnetic contributions.[§] Therefore, to obtain an estimated magnitude of the paramagnetic component a correction of the observed molar susceptibility is necessary and is possible by the subtraction of diamagnetic correction factors. For complex **27** an estimate of the diamagnetism is presented in the table below, calculated from readily available diamagnetic correction factors for individual atoms (and cations). In absence of data for a palladium(I) cation the use of the correction factor for a palladium(II) cation has been judged to be a reasonable substitution.

*Table 3: Diamagnetic correction factors for complex **27**[§]*

	Diamagnetic correction factors ($\text{m}^3 \text{ mol}^{-1}$)
2 x P(C ₄ H ₉) ₂	- 3.19 x 10 ⁻⁹
2 x Pyridine	- 1.23 x 10 ⁻⁹
2 x Pd ²⁺	- 6.28 x 10 ⁻¹⁰
2 x C ₆ H ₅ ring	- 9.40 x 10 ⁻¹⁰
2 x NC	- 2.90 x 10 ⁻¹⁰
χ_d	- 1.26 x 10 ⁻⁸

Subtraction of the sum of the diamagnetic correction factors (χ_d) from χ_m gives a corrected molar susceptibility (χ_c) of $1.71 \times 10^{-8} \text{ m}^3 \text{ mol}^{-1}$ and by use of equation (4) the corrected value for μ_{eff} (spin-only) is calculated to be $1.80 \mu_B$. This spin only μ_{eff} value is intermediate in magnitude for that expected for zero and two unpaired electrons (Table 4), which indicates neither ferromagnetic or anti-ferromagnetic coupling is predominant and that there is no

[§] G. A. Bain, J. F. Berry, *J. Chem. Ed.*, 2008, **85**, 532.

overall magnetic communication between molecules of complex **27**. Instead, the value of corrected μ_{eff} is representative of a mixture of high and low spin states for complex **27** which are likely to be temperature dependent.

$$\text{Equation (4) } \mu_{\text{eff}} = 797.8(\chi_{\text{C}} * T)^{1/2}$$

μ_{eff} = effective magnetic moment (μ_{B}) T = temperature (K)

χ_{C} = corrected molar susceptibility ($\text{m}^3 \text{mol}^{-1}$)

$$\text{Equation (5) } \mu_{\text{eff}} = g_e[S(S + 1)]^{1/2}$$

$g_e = 2$

S = total spin

Table 4: Calculation of the corrected μ_{eff} for a system with two unpaired electrons showing ferromagnetic coupling or anti-ferromagnetic coupling

s (spin of an electron) = 0.5		
For 2 unpaired electrons	S	μ_{eff} (spin only) (μ_{B})
Ferromagnetic coupling ($S = s + s$)	1	2.83
Anti-ferromagnetic coupling ($S = s - s$)	0	0.00

Appendix VI: Molecular orbital nature of the UV/visible light transitions for compound *cis*-**23** and *trans*-**23**

cis-**23**:

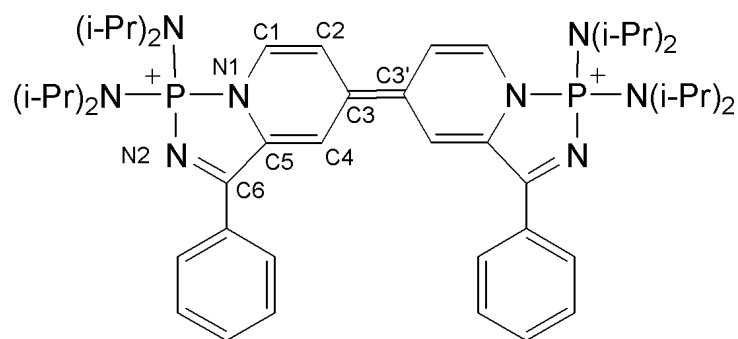
Percentage contribution to the Molecular Orbitals

	MO	eV	Ph	i-Pr ₂ N	C6=N2	C1=C2	C3=C3'	C4=C5	P-N1
225	LUMO+2	-5.30	8	3	7	46	19	9	8
224	LUMO+1	-6.64	13	2	35	9	7	30	3
223	LUMO	-7.41	13	4	37	6	9	20	10
222	HOMO	-9.18	4	5	8	24	21	15	22
221	HOMO-1	-11.12	80	9	9	1	0	0	2

UV/vis transition at 717 nm

Energy (cm ⁻¹)	Wavelength (nm)	Osc. Strength	Major contributions
13941	717	0.6502	HOMO->LUMO (64%)

Ph	i-Pr ₂ N	C6=N2	C1=C2	C3=C3'	C4=C5	P-N1
4-->12	5-->4	8-->35	24-->9	21-->10	15-->20	22-->10
(8)	(-1)	(27)	(-15)	(-11)	(5)	(-12)



cis-**23**

trans-23:

Table 5: Percentage composition of selected molecular orbitals of trans-23

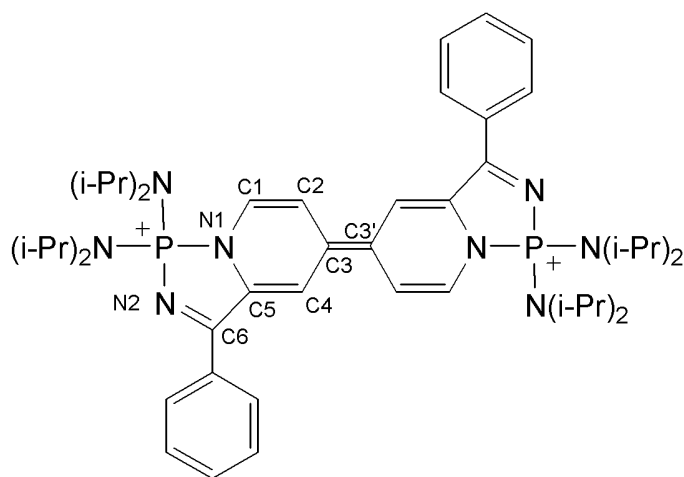
MO		eV	Ph	N(i-Pr) ₂	C6=N2	C1=C2	C3=C3'	C4=C5	P-N1
225	LUMO+2	−5.53	1	3	2	61	14	13	6
224	LUMO+1	−6.45	17	2	40	5	7	25	3
223	LUMO	−7.41	12	4	37	4	8	24	9
222	HOMO	−9.17	4	5	7	25	21	15	22
221	HOMO−1	−11.07	83	6	8	0	0	0	2

Table 6: MO contribution to electronic transition at 402 nm of trans-23

Energy (cm ⁻¹)	Wavelength (nm)	Osc. Strength	Major contribution
24900	402	0.472	HOMO->LUMO+2 (73 %)

Table 7: Percentage change in terms of molecular orbital density between the ground state and excited state for the electronic transition at 402 nm of trans-23

Ph	NiPr	C6=N2	C1=C2	C3=C3'	C4=C5	P-N1
9→6	5→3	7→4	23→53	20→13	14→14	21→6
(-3)	(-2)	(-3)	(30)	(-7)	(0)	(-15)



trans-23